The role of cytochrome b5 and P450 oxidoreductase in the cytochrome P450 mediated activation of the carcinogenic compounds benzo[a]pyrene and ellipticine

Reed, Lindsay Eleanor

Awarding institution:
King's College London

The role of cytochrome b_5 and P450 oxidoreductase in the cytochrome P450 mediated activation of the carcinogenic compounds benzo[*a*]pyrene and ellipticine

Lindsay Eleanor Reed

Thesis submitted to King's College London for the degree of Doctor of Philosophy

September 2018

Acknowledgements

I would like to extend a massive thank you to my supervisors Dr Volker Arlt and Professor David Phillips for their support, encouragement and patience during the course of my Ph.D. I was not always the easiest of students, and no words will ever express how grateful I am for you pushing me when I needed it. A very special thank you also goes to Ian Jarvis. You didn't need to take me under your wing, but you did.

I am incredibly grateful to everyone at Charles University Prague, in particular Iveta Mrizova, Radek Indra, Michaela Moserova and Frantisek Barta, who not only helped me with their technical expertise and time, but gave me a home from home that will be held dear in my heart forevermore. A special thank you also goes to Marie Stiborova who hosted me year after year and provided ongoing support with manuscript writing.

A massive thank you also goes to the members of the Environmental Carcinogenesis Group, past and present, in particular Eszter Nagy, Louisa Lee, George Preston, Osman Sozeri, Jill Kucab, Mateja Sborchia and Lisa Hölzl-Armstrong. You have all provided constant support over the past four years, whether it be helping me solve a problem or just making me laugh when needed. I would especially like to thank Sana Al-Saleh, I am honoured to have gone on this journey with you and would likely not have made it without your endless support and the happiness you brought to my heart. I could not have asked for a better person to have shared the last four years with.

Thank you to my friends, particularly Alix and Dilwyn for providing respite and escape. A special thank you also goes to Hugo. Your constant love and support has gotten me through some of my most challenging moments. You gave me dreams to keep me going through the tough times and was there by my side to celebrate the good times.

Finally, I am eternally grateful to my family. Your constant support over my entire academic career has made me who I am today. Everything I have achieved is because of everything you have given me throughout my life. Thank you.

Abstract

Benzo[*a*]pyrene (BaP), an environmental pollutant, and ellipticine, an anticancer drug, are carcinogens that exert genotoxic effects after metabolic activation by cytochrome P450 enzymes. In the present study two mouse models, the Hepatic Reductase Null (HRN) and Hepatic Cytochrome b_5/P450 Reductase Null (HBRN) and the cancer cell lines Hepa-1c1c7 and HepG2 have been used to study the role of P450-mediated metabolism and disposition of BaP and ellipticine. In HRN mice cytochrome P450 oxidoreductase (POR), the electron donor to P450 enzymes, is deleted specifically in hepatocytes. In HBRN mice the microsomal haemoprotein cytochrome b_5 (Cyb5), which can also act as an electron donor from cytochrome b_5 reductase to P450 enzymes, is also deleted in the liver. HRN and HBRN mice were treated once with BaP or ellipticine for 24 hours. DNA adduct levels were measured by ^{32}P-postlabelling analysis. Mice treated with ellipticine had significantly fewer DNA-adducts in the livers on HRN and HBRN mice compared to WT, with no significant difference between HRN and HBRN. In the mice treated with BaP, however, there were significantly higher levels of DNA adducts in the livers of HRN mice than wild-type (WT) mice while no significant difference in adduct formation was observed in liver between HBRN and WT mice. Hepatic microsomal fractions were also incubated with BaP/ellipticine and DNA in the presence of NAD(P)H *in vitro* which showed as electron donors were lost, adduct formation decreased. This correlated with incubations carried out with BaP or ellipticine which measured formation of metabolites which decreased as electron donors were lost. The results from the incubations also correlated with measured enzyme activity. In order to model the paradoxical phenomenon seen in the HRN mice, Hepa-1c1c7 and HepG2 cells that do not express POR were exposed to BaP. In the Hepa-1c1c7 cells, despite the absence of POR expression, both formation of metabolites, DNA damage (comet assay) and adduct formation was increased compared to WT cells. The HepG2 cell line showed decreased levels of DNA damage (comet assay) in the absence of POR compared to WT cells. Whilst formation of metabolite and adduct formation was reduced compared to WT HepG2 cells 24 hours after treatment with BaP, metabolite and adduct formation was higher in POR KO HepG2 cells compared to WT cells after 48 hours.

Declaration

I hereby declare that all the work presented in this thesis has not been submitted for a degree or other qualification in this or any other university. All of the work described in this thesis has been carried out by me except for the ^{32}P-postlabelling which was carried out by Dr Volker Arlt. All animal treatments were performed at the University of Dundee.

Abbreviations

XME	Xenobiotic-metabolising enzyme
P450	Cytochrome P450
AKR	Aldo-keto reductase
mEH	Microsomal epoxide hydrolase
PTGS	Prostaglandin H synthase
GST	Glutathione *S*-transferase
POR	NADPH:cytochrome P450 oxidoreductase
Cyb5R	NADH:cytochrome b_5 reductase
Cyb5	Cytochrome b_5
AHR	Aryl hydrocarbon receptor
PXR	Pregnane X receptor
CAR	Constitutive androstane receptor
TCDD	2,3,7,8-tetrachlorodibenzo-*p*-dioxin
PAH	Polycyclic aromatic hydrocarbon

BaP	Benzo[*a*]pyrene
HAA	Heterocyclic aromatic amine
PhIP	2-Amino-1-methyl-6-phenylimidazo[4,5-*b*]pyridine
4-ABP	4-Aminobiphenyl
A*a*C	2-Amino-alpha-carboline
NNK	Nicotine-derived nitrosamine ketone
SSB	Single strand break
DSB	Double strand break
CRISPR	Clustered Regularly Interspaced Short Palindromic Repeats
CAS9	CRISPR associated protein 9
ES	Embryonic Stem Cells
WT	Wild-type
HRN	Hepatic Reductase Null
HBRN	Hepatic Cytochrome b_5/P450 Reductase Null
SD	Standard deviation

Table of Contents

List of Figures

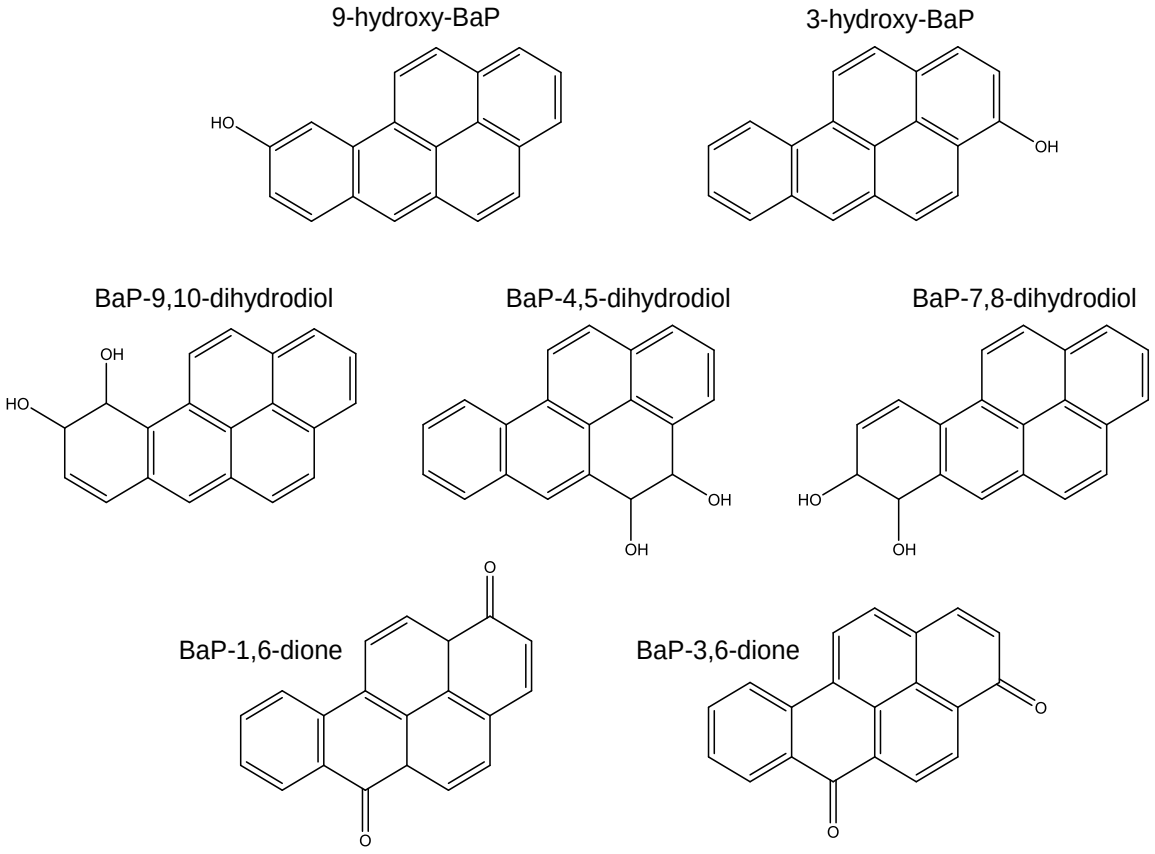

mice. (B) Cyp1a1 activity was determined by the oxidation of Sudan I to hydroxylated metabolites with activity being observed as nmol of total C-hydroxylated metabolites/mg protein/min. (C) Cyp1a2 activity was determined using the MROD assay with activity being observed as pmol of resorufin/mg protein/min. (D) Cyp1a activity was determined using the EROD assay with activity being observed as pmol of resorufin/mg protein/min. (E) Cyp3a activity was determined by the oxidation of testosterone to hydroxylated metabolites with activity being observed as nmol of total C-hydroxylated metabolites/mg protein/min. Values are given as ± SD (n=3). Statistical analysis was performed by one-way Anova with Tukey's multiple comparison test (* = compared to WT; # = compared to HRN. * $^{(\#)}$ $P \leq 0.05$ ** $^{(\#\#)}$ $P \leq 0.01$ *** $^{(\#\#\#)}$ $P \leq 0.001$**** $^{(\#\#\#\#)}$ $P \leq 0.0001$). 114

Figure 4.4: Enzyme activity in the pooled hepatic fractions of ellipticine-treated WT, HRN and HBRN mice using either NADPH or NADH as the enzymatic cofactor. (A) POR activity was observed as nmol of cytochrome *c*/mg/min and was only detected in microsomal fractions from WT mice. (B) Cyp1a1 activity was determined by the oxidation of Sudan I to hydroxylated metabolites with activity being observed as nmol of total C-hydroxylated metabolites/mg protein/min. (C) Cyp1a2 activity was determined using the MROD assay with activity being observed as pmol of resorufin/mg protein/min. (D) Cyp1a activity was determined using the EROD assay with activity being observed as pmol of resorufin/mg protein/min. (E) Cyp3a activity was determined by the oxidation of testosterone to hydroxylated metabolites with activity being observed as nmol of total C-hydroxylated metabolites/mg protein/min. Values are given as ± SD (n=3). Statistical analysis was performed by one-way Anova with Tukey's multiple comparison test (* = compared to WT; # = compared to HRN. * $^{(\#)}$ $P \leq 0.05$ ** $^{(\#\#)}$ $P \leq 0.01$ *** $^{(\#\#\#)}$ $P \leq 0.001$**** $^{(\#\#\#\#)}$ $P \leq 0.0001$). 115

In the *in vitro* experiments carried out in hepatic microsomal fractions from untreated mice, POR activity was detected in both the HRN and HBRN fractions. It was postulated that this could be due to contamination from a WT liver sample; however, no Cyb5 was detected, which would have been present in this case. Genotyping was carried out on retained liver samples from the untreated mice. Although both *Por* and *Cyb5* appeared to be excised, a very faint *Cre* band was detected in one of the untreated HRN and one of the untreated HBRN mice (see **Figure 4.12**). One potential explanation as to why some POR expression and activity was detectable in the hepatic microsomal fractions could be due to Cre mosaicism, whereby there is variable or inconsistent Cre expression in different cells within the liver (Heffner et al., 2012). However the successful knockout of Cyb5 in the hepatocytes further complicates the results. Despite the presence of POR, enzyme activity was reduced in the microsomal fractions

List of Tables

1 Introduction

1.1 Xenobiotic metabolism

Humans are constantly exposed, unavoidably, to a myriad of environmental chemical substances. Xenobiotics, any exogenous chemical, can be natural or synthetic and include dietary toxins, pollutants and drugs. They are able to enter the body through a variety of routes, predominantly the digestive system although this route may be bypassed by absorption via the lungs and skin. Cell membranes are able to prevent the entry and exit of many xenobiotics but are, however, susceptible to lipophilic molecules that are able to diffuse through into the organism. Living organisms have therefore evolved enzyme systems to detoxify these xenobiotics to prevent accumulation of harmful toxins. These enzymes are termed biotransforming enzymes and play a key role in the process of xenobiotic metabolism. Although the gut is capable of metabolising many xenobiotics, the main site of biotransformation is the liver with many xenobiotic-metabolising enzymes (XMEs) residing in the hepatocytes. The primary function of these enzymes is to convert a lipophilic xenobiotic to a more hydrophilic metabolite, promoting a decline in its reabsorption by kidney tubules allowing it to be easily cleared by the kidneys into the aqueous urine where it can be eliminated from the body (Croom, 2012).

The stages of biotransformation are traditionally described as phases I, II and III. Phase I reactions are thought to prepare the xenobiotic for the conjugative reactions of phase II metabolism by making them more reactive. Although predominantly oxidative, phase I reactions also include hydroxylation and reduction. These reactions are catalysed by XMEs such as cytochrome P450 (P450), aldo-keto reductases (AKRs),

microsomal epoxide hydrolase (mEH), prostaglandin H synthase (PTGS), NAD(P)H:quinone oxidoreducatse (NQO1), NAD(P)-dependent alcohol dehydrogenases (ADHs) and microsomal flavin-containing monooxygenases (FMOs). Phase II metabolism conjugates small molecules in the form of polar endogenous sugars, salts or amino acids, to functional groups resulting from phase I metabolism in order to further increase the polarity of the molecule, making it more hydrophilic for excretion. Although phase II metabolism often proceeds a phase I reaction conjugation can also occur directly without preparation by oxidative processes (Croom, 2012). Phase II XMEs include sulfotransferases (SULTs), *N*,*O*-acetyltransferases (NATs), methyltransferases such as catechol-*O*-methyltransferase (COMT), glutathione *S*-transferases (GSTs) and uridine diphosphate glucuronosyltransferases (UGTs) (Rendic and Guengerich, 2012). Phase III metabolism has been defined more recently and describes the system of efflux pumps that exclude water soluble products from the cell to the interstitial fluid, blood and finally the kidneys. The hydrophilic metabolites resulting from the metabolism process are shuttled through cellular lipid bilayer membranes, facilitated by transporter proteins of the ATP-binding cassette (ABC) or solute carrier (SLC) families (Omiecinski et al., 2011). It is noteworthy that whilst separating the stages of biotransformation into phases is convenient, this system has been argued against due to grouping mechanistically unrelated reactions together and dividing related ones, and can be misleading due to phase I and II metabolism not always occurring sequentially (Josephy et al., 2005).

1.2 Cytochrome P450s

P450 enzymes belong to a ubiquitous superfamily of haemoproteins which all have similar core structures and modes of operation and play a central role in the metabolism of a wide variety of substrates (Guengerich, 2008). There are 57 putatively functional human P450s and of these only about a dozen enzymes are responsible for the biotransformation of most foreign substances (Zanger and Schwab, 2013). P450s are generally classified using a systematic nomenclature scheme with current guidelines suggesting that members of new CYP families share at least 40% and members of subfamilies share 55% amino acid identity. Each P450 enzyme is designated the abbreviation CYP to denote the superfamily (Cytochrome P450), followed by a number for the gene family, a capital letter showing the subfamily and a final numeral assigning the individual gene (Sim and Ingelman-Sundberg, 2010).

Mammalian P450s play a multitude of roles within the body, with a set of P450s (e.g. families 5, 8, 11, 17, 19, 21, 24, 26 and 27) responsible for the synthesis of important steroids and eicosanoids from ω-3 and ω-6 polyunsaturated fatty acids such as arachidonic acid or eicosapentaenoic acid (Nebert and Karp, 2008) as well as the catabolism of natural products. Out of the remaining mammalian P450s a small set (i.e. CYP1A2, 2C9, 2C19, 2D6 and 3A4) accounts for most of the metabolism of drugs (Guengerich, 2001). P450s play a major role in phase I metabolism with 70-80% of all phase I XMEs comprising P450 enzymes (Evans and Relling, 1999). This makes them the focus of pharmacological and toxicological research as oxidation reactions catalysed by P450s can result in poor drug bioavailability, leading to acute and chronic toxicities with adverse drug interactions and subsequently cancer susceptibility (Guengerich, 2001). P450 enzymes make up part of a mixed-function oxidase system,

along with other enzymes including NADPH:cytochrome P450 oxidoreductase (POR) (Riddick et al., 2013), NADH:cytochrome b_5 reductase (Cyb5R) and the haemoprotein cytochrome b_5 (Cyb5) (Porter, 2002), bound to the membrane of the endoplasmic reticulum (ER). The most common reaction catalysed by P450 enzymes are mono-oxygenase reactions that require two electrons and involve the insertion of one oxygen atom into the substrate, whilst reducing the other oxygen atom to water:

$$R\text{-}H + O_2 + NADPH + H^+ \rightarrow R\text{-}OH + H_2O + NADP^+$$

1.2.1 Catalytic cycle

Despite the vast array of CYP family members, their activity is reliant on the P450 catalytic cycle. Although the cycle is a complex process with many steps, there are five main features of the process: (*i*) substrate binding, (*ii*) oxygen binding, (*iii*) oxygen splitting, (*iv*) insertion of oxygen into substrate and (*v*) release of product. A simplified diagram of the catalytic cycle for P450 enzymes is shown in **Figure 1.1**. The iron is usually, but not always, in the ferric form (Fe^{3+}-RH) at the start of the cycle. (*i*) The first step in the cycle is the P450 substrate binding that must be oriented in such a way that it is in proximity to the heme iron, on the side opposite to the axial thiolate of the cysteine (Cys) residue in the active site of the enzyme. Substrate binding brings about a conformational change of the active site, often displacing a water molecule from the distal axial coordination position of the heme iron from low-spin to high-spin (Guengerich, 2001, Meunier et al., 2004, Poulos et al., 1987). (*ii*) The first of two electrons is then received from the REDOX partners, reducing the iron (Fe^{2+}-RH) (Sligar et al., 1979). Molecular oxygen sourced from the lungs binds to the iron/substrate complex at the ferrous heme centre at the distal axial coordination

position, initially giving a dioxygen adduct (Fe-O_2). (*iii*) The second electron is transferred from REDOX partners reducing the Fe-O_2 adduct resulting in a short-lived peroxo state. The peroxo group reacts with two protons from the surrounding solvent, breaking the O-O bond. The process is so rapid it has not yet been detected experimentally, therefore the most likely pathway has been proposed whereby the oxygen atom with two spare electrons forms water with two hydrogen atoms leaving a single oxygen atom bound to the iron of the enzyme (Coleman, 2010). A highly reactive intermediate, referred to as P450 compound I, is also formed (Rittle and Green, 2010).

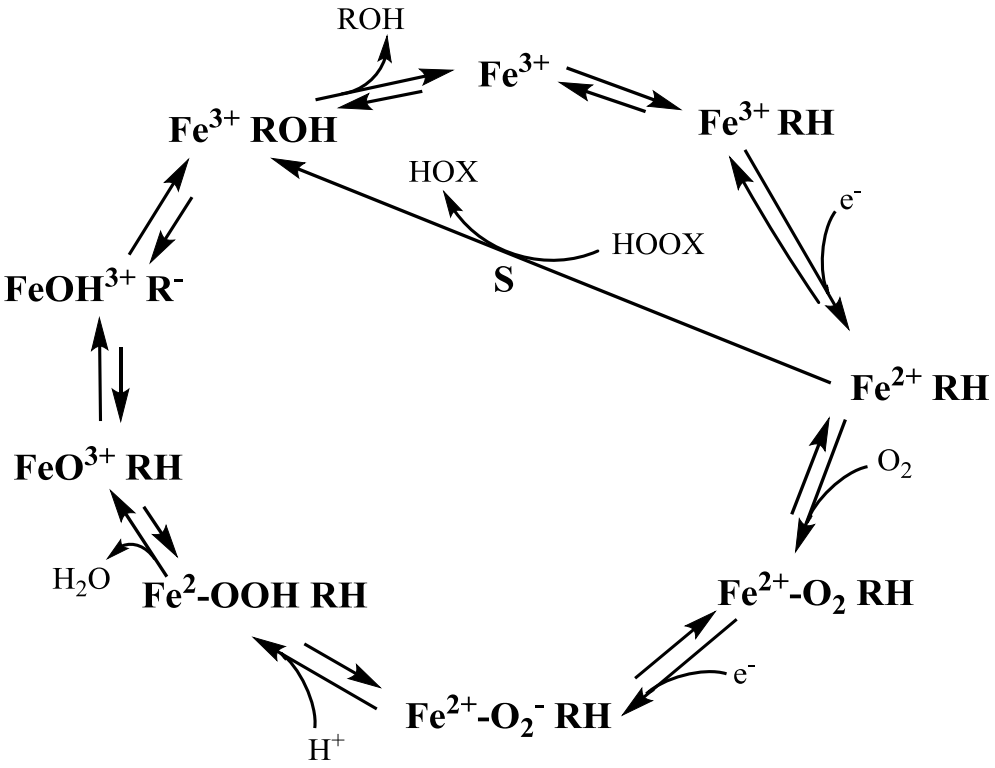

Figure 1.1: Basic reaction cycle of the P450 monoxygenase system. See text for details Adapted from Guengerich 2008.

This P450 protein-bound porphyrin complex with the iron-coordinated active oxygen atom is the proposed intermediate species which hydroxylates inert carbon-hydrogen bonds of substrates (Jung, 2011). (*iv*) The oxygen atom ligated to the iron is transferred to the substrate forming a hydroxyl group. The hydroxyl group and the P450

compound I react, yielding an alcohol (Fe^{2+} and ROH). (*v*) The metabolite is released from the active site of the enzyme which returns to its initial state with a water molecule returning to occupy the distal coordination of the iron nucleus. An alternative pathway for the P450 mono-oxygenation reaction is via the 'peroxide shunt' (path 'S' in **Figure 1.1**). This enables oxidation of the ferric-substrate complex with oxygen donors such as peroxides (Guengerich, 2008, Guengerich, 2001). A hypothetical peroxide 'XOOH' is shown in **Figure 1.1**. Whilst it is possible to simplify this process, and has proven useful in rationalising most oxidation reactions, the cycle is dynamic with steps not necessarily proceeding in a linear order. Substrate binding and release can occur at other steps along the cycle (Guengerich, 2008).

1.2.2 P450 oxidoreductase (POR)

P450 REDOX partners are essential to the P450 catalytic cycle, donating the electrons needed for the oxidative reactions to be catalysed. POR is an NADPH reductase that, although a separate entity from P450s, is indispensable to them. POR is found in most tissues but particularly in the liver, and systemic deletion of POR results in embryonic lethality, demonstrating its necessity to life (Shen et al., 2002, Otto et al., 2003). The reductase is a membrane anchored diflavin protein complex with its catalytic site at the surface of the endoplasmic reticulum, binding the electron carrier flavin adenine dinucleotide (FAD) and flavin mononucleotide (FMN) in distinct globular domains connected by a flexible hinge region (Murataliev et al., 2004, Wang et al., 1997). FAD has evolved to discriminate strongly in favour of NADPH over NADH, fuelling reductive reactions. Electrons are transferred from NADPH through FAD producing NADP+. FAD transports two electrons as $FADH_2$ that are passed on to FMN, forming

$FMNH_2$ which in turn passes the electrons to the iron atom in the prosthetic haem group of P450s (**Figure 1.2**) (Laursen et al., 2011).

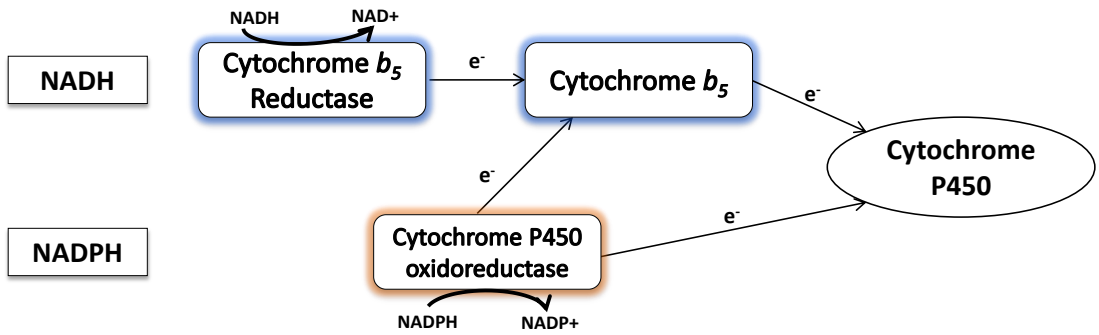

Figure 1.2: Transfer of electrons from the electron donor proteins POR and Cyb5 to the P450 enzyme in the presence of the enzymatic cofactor NADPH and NADH, respectively.

1.2.3 Cytochrome b_5 (Cyb5)

For many years it was widely believed that POR was the sole electron donor to P450 enzymes. However, microsomal Cyb5 in conjunction with Cyb5R can also be important electron donors in the P450 catalytic cycle (Finn et al., 2008). Cyb5 is an electron transport haemoprotein that is ubiquitous in nature and strongly resembles the active site of P450s due to them being built around a central F-9 haem group. Cyb5 is anchored by a helix which is deeply embedded in the membrane of the smooth endoplasmic reticulum (SER) with its haem structure standing clear of the SER membrane in the cytosol (Sergeev et al., 2014). Unlike POR, Cyb5 does not possess enzymatic activity and is dependent on the enzymatic cofactor NADH in conjunction with Cyb5R. The transfer of two electrons during the catalytic cycle are essential and the rate of transfer of the second electron is considered a rate-limiting step in the P450 reaction (Guengerich and Johnson, 1997). Cyb5 can modulate P450 activity in three ways: (*i*) by direct transfer of both electrons via Cyb5R in a pathway independent of POR (Yamazaki et al., 1996a, Yamazaki et al., 1996c); (*ii*) by the transfer of the

second, and rate limiting, electron from either POR or Cyb5R (**Figure 1.2**) (Hildebrandt and Estabrook, 1971); or (*iii*) by acting as an allosteric modifier of the enzyme in a non-catalytic role that can enhance reactions for many, but not all, P450 enzymes (Yamazaki et al., 2002). Cyb5 is both substrate and enzyme specific, and has been shown to both stimulate and inhibit P450 reactions. The P450-mediated metabolism of methoxyflurane, 7-ethoxycoumarin and *p*-nitroanisole demonstrates an absolute requirement for Cyb5 (Canova-Davis et al., 1985, Sugiyama et al., 1980, Sugiyama et al., 1982, Yamazaki et al., 1996b). The P450-mediated metabolism of benzphetamine, a central nerve system stimulant, however, is NADPH-supported and the presence of Cyb5 inhibits the reaction (Morgan and Coon, 1984). Therefore, it is difficult to predict the contribution of Cyb5 to xenobiotic metabolism.

1.2.4 Induction of cytochrome P450

Not all XMEs are constitutively expressed; very often their expression will be induced by the presence of a xenobiotic. The process of enzyme induction has three main requirements (*i*) the cell must detect the presence of particular persistent lipophilic xenobiotics and correctly sense their concentration, (*ii*) the process of detection is translated into an increase in the capability of the appropriate metabolic systems to allow the xenobiotic to be cleared as efficiently as possible and (*iii*) the detection and action system needs to be reversible to allow it to be sensitive to further changes in xenobiotic concentration. The inducible P450s make up a large percentage of the P450s in the human liver and in most cases, induction of P450s occurs by a process involving *de novo* RNA and protein synthesis that has been demonstrated in studies using transcription and translation inhibitors (Daujat et al., 1991). The main inducible P450s, CYP1A1/1A2, CYP2C8/9 and CYP3A4, have a similar induction mechanism,

where ligand activation of key receptor transcription factors including the aryl hydrocarbon receptor (AHR), pregnane X receptor (PXR) and the constitutive androstane receptor (CAR) leads to increased transcription (**Figure 1.3**). The induction of P450s is highly conserved and is found not only in humans but also in many other species including rodents (Tompkins and Wallace, 2007). Another mechanism of P450 induction involves compounds that either stabilise translation or inhibit the protein degradation pathway, e.g. ethanol and CYP2E1 (Woodcroft and Novak, 1998).

The AHR receptor complex is located in the cytoplasm of most cells and consists of four components: (*i*) the AHR, (*ii*) heat shock protein (Hsp90), (*iii)* co-chaperone p23 and (*iv*) an immunophilin called XAP2 (**Figure 1.3a**) (Kewley et al., 2004). The ligand, e.g. 2,3,7,8-tetrachlorodibenzo-p-dioxin (TCDD), binds to the AHR complex which then migrates towards the nucleus (Mimura and Fujii-Kuriyama, 2003). The AHR/ligand complex then breaks away from the Hsp90, p23 and XAP2 and enters the nucleus alone where it heterodimerises with the nuclear protein aryl hydrocarbon nuclear receptor translocator (ARNT) and this new complex binds to specific DNA sequences, termed xenobiotic responsive elements (XRE), upstream of the *CYP1A1/1A2* and *1B1* genes (Tsuji et al., 2014).

Like the AHR, CAR is also found in the cytoplasm complexed with Hsp90 and p23 (**Figure 1.3b**). The CAR retention protein (CCRP) is also part of the complex. As the name suggests, CAR is constitutively expressed so does not necessarily require a ligand to induce its activity, but the presence of inducers, e.g. phenobarbital (PB), will hasten the rate of enzyme induction (Kretschmer and Baldwin, 2005). Upon binding of the ligand, cytoplasmic CAR dissociates from the Hsp90, p23 and CCRP and enters

the nucleus alone where it first forms a heterodimer with the retinoid X receptor (RXR) followed by association with the co-activator SRC-1 to form a complex. The CAR/RXR/SRC-1 complex binds to DNA at the phenobarbitone-responsive enhancer module (PBREM) in the *CYP2B* gene and to the Everted repeat 6 (ER6) element of the *CYP3A4* and *CYP2C9* genes.

This triggers transcriptional activation leading to an induction of the particular P450s (Timsit and Negishi, 2007). Alongside CAR, PXR is also heavily involved in *CYP3A* regulation. PXR is considered highly promiscuous as it has a wide range of substrate structures and, as with AHR, PXR lies dormant in the absence of any ligands. PXR is sequestered in the cytosol, like CAR and AHR, by Hsp90 or CCRP (**Figure 1.3c**). Upon binding of a ligand to the receptor, PXR dissociates from Hsp90 or CCRP and translocates to the nucleus where a heterodimer is formed with RXR (Squires et al., 2004). Binding occurs at the *CYP3A* gene in two separate areas, an ER6 in the proximal promoter of the gene and at the same time the PXR complex binds to a second area called the xenobiotic responsive element (XREM). Both the proximal promoter and the XREM must be bound by the PXR complex before induction can proceed (Chen et al., 2012).

1.3 Chemical carcinogenesis

Associations between cancer and occupational exposures can be dated back to the 16th century when Paracelsus proposed that exposure to natural ores such as arsenic sulphide may have been causing the ‘wasting disease of miners’ in 1567; making Paracelsus the first to consider a chemical compound as an occupational carcinogen. A while later a systematic account of ‘peculiar diseases’ in several different

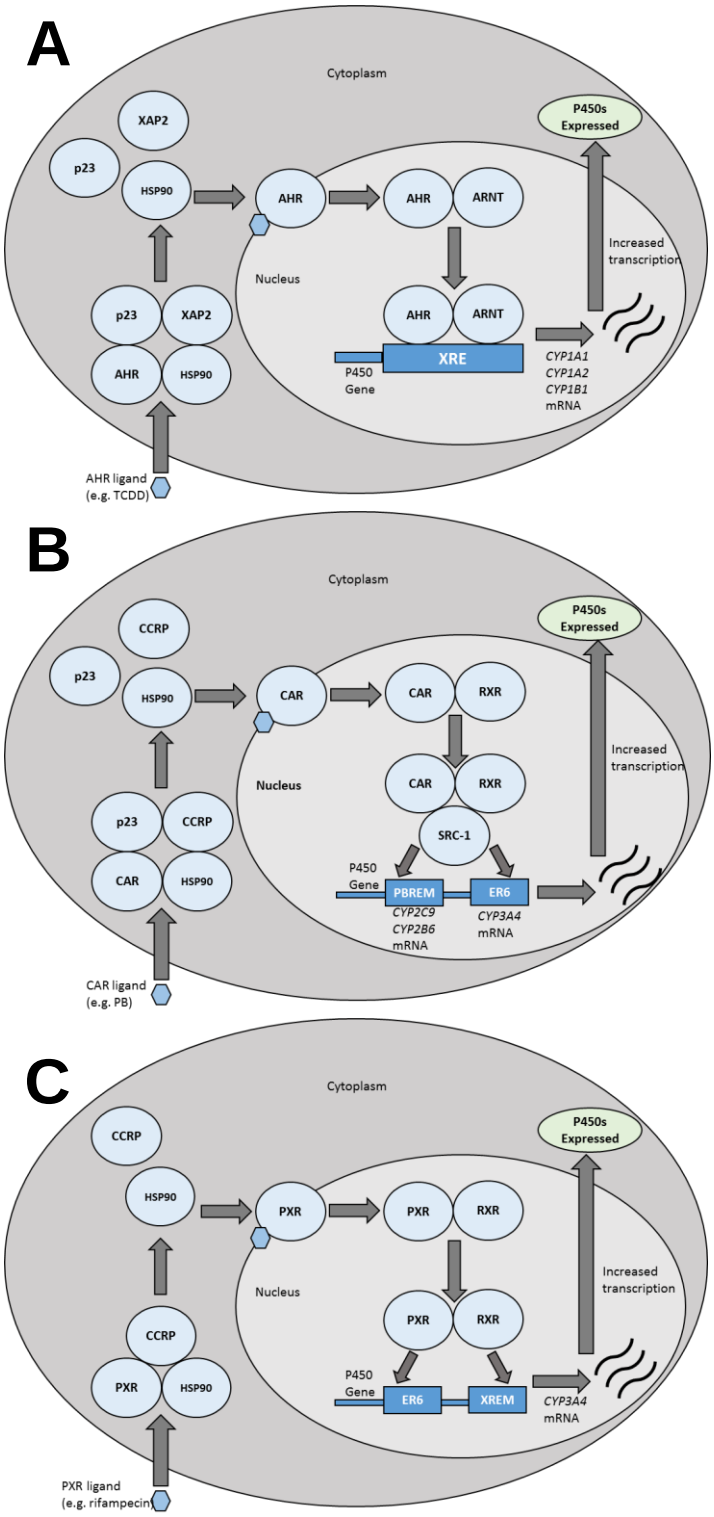

Figure 1.3: Mechanisms of P450 induction. (a) AHR-mediated control of CYP1A1/2 and 1B1, (b) CAR-mediated control of CYP2B6/2C9 and CYP3A4, (c) PXR-mediated control of CYP3A4. See text for details. Image modified from Coleman 2010.

occupational fields was published by Bernadini Ramazzini in 1700. In 1761 John Hill traced cancerous alterations in the nasal mucosa to long term exposure to tobacco snuff. A few years later in 1775 Percival Pott attributed the onset of scrotal cancer in chimney sweeps to repetitive local contamination by soot. The occurrence of scrotal cancer in workers was also linked to arsenic fumes in the copper-smelting works of Cornwall and Wales in 1822 by John Ayrton Paris. By the end of the 19th century it was evident that the occupational exposure to certain chemicals or mixtures of chemicals resulted in carcinogenic effects (Luch, 2005). The field of chemical carcinogenesis came to the fore in the twentieth century when malignant epithelial tumours were experimentally produced for the first time when coal tar was applied to the ears of rabbits; marking the transition into the modern era of experimental cancer research (Yamagiwa and Ichikawa, 1915). Identifying the compounds responsible for carcinogenesis was difficult due to the complex nature of the mixtures, however Sir Ernest Kennaway and his colleagues at the Royal Cancer Hospital in London demonstrated that single polycyclic aromatic hydrocarbons (PAHs) such as dibenz[*a*,*h*]anthracene were tumourigenic in mouse skin (Kennaway and Hieger, 1930, Cook et al., 1937). During this time benzo[*a*]pyrene (BaP) was isolated and found to be the highly carcinogenic compound from coal tar pitch (Cook et al., 1933). By the 1940s chemical carcinogens were shown to be able to bind covalently to cellular macromolecules such as proteins (Miller and Miller, 1947) and following the discovery of the structure of DNA by Watson and Crick in 1953 it was later demonstrated that the carcinogenicity of compounds such as PAHs correlated with the extent of their binding to DNA in mouse skin, but not to RNA or protein (Brookes and Lawley, 1964). Over the course of the latter half of the 20th century, epidemiological

and experimental evidence continued to both compliment and support each other, ever strengthening the link between environmental agents and cancer (Wogan et al., 2004).

1.3.1 Environmental Carcinogens

Around 200 different chemical compounds and mixtures are known or suspected to be environmental carcinogens. Some known human carcinogens are shown in **Table 1.1**. Environmental carcinogens can be divided into 4 categories: organics, inorganics, fibres and particulates and hormones. The largest category of these is the organics (Gooderham and Carmichael, 2007). The International Agency for Research on Cancer (IARC) (http://monographs.iarc.fr/) has developed the classification of carcinogens by evaluation of their carcinogenicity:

Group 1 Carcinogenic to humans (108 agents)

Group 2A Probably carcinogenic to humans (64 agents)

Group 2B Possibly carcinogenic to humans (272 agents)

Group 3 Not classifiable as to its carcinogenicity to humans (508 agents)

Group 4 Probably not carcinogenic to humans (1 agent)

One of the most widely studied groups of carcinogens is the PAHs. They are ubiquitous in the environment as a result of their formation by the incomplete combustion of organic matter (IARC, 2010b, Baird et al., 2005). BaP is the most commonly studied and measured of the PAHs (Arlt et al., 2015b, Krais et al., 2016, Labib et al., 2016, Labib et al., 2012, Siddens et al., 2012, Wohak et al., 2016) and it

Table 1.1: Examples of human chemical carcinogens, their sources of exposure and the target organs. Adapted from Luch 2005.

Compounds	**Main sources/uses**	**Target organ**
Aminoazo dyes		
o-Aminoazotoluene	Pigments; colouring oils; immunosuppressant	Liver, lung, bladder
N,*N*-dimethyl-4-aminoazobenzene	Colour polishes; waxes	Lung. liver
Aromatic amines/amides		
2-Naphthylamine	Dyes; antioxidant	Bladder
Aromatic hydrocarbons		
Benzo[*a*]pyrene	Coal tar; roofing; cigarette smoke	Skin, lung, stomach
Polychlorinated biphenyls	Flame retardants; hydraulic fluids	Liver, skin
Metals (and compounds)		
Arsenic	Natural ores; alloys; pharmaceutical agent	Skin, liver, lung
Cadmium	Natural ores; pigments; batteries; ceramics	Lung, prostate, kidney
Natural carcinogens		
Aflatoxin B_1	Mycotoxin (found in contaminated food)	Liver
Asbestos	Thermal insulation; gaskets	Lung
***N*-nitroso compounds**		
N-Nitrosodimethylamine	Polymers; batteries; nematocides (no longer in use)	Liver, lung, kidney
4-(Methylnitrosamino)-1-(3-pyridyl)-1-butanone	Research tool; cigarette smoke	Lung, liver
Olefins		
Vinyl chloride (VC)	Plastics (PVC); co-polymers	Liver
Trichloroethylene	Degreasing operations; adhesives; lubricants	Liver, kidney
Paraffins/ethers		
1,2-Dichloroethane	Vinyl chloride production; solvent	Liver, lung, breast
Mustard gas (sulphur mustard)	Chemical warfare; research	Lung

is classified by the IARC as a Group 1 human carcinogen. The unavoidable exposure of the human race to PAHs makes a substantial contribution to the overall burden of cancer in humans (Baird et al., 2005, IARC, 2010a, Phillips and Venitt, 2012). A major source of exposure to BaP is tobacco smoke (Alexandrov et al., 2016). However for non-smokers the principal sources can be the diet (Phillips, 1999) and from exposure to air pollution (IARC, 2016). Nitro-PAHs are also widespread environmental contaminants found in grilled food, river sediments, on the surface of ambient air particulate matter and in extracts from diesel and petrol engine emissions (Tokiwa et al., 1986, INCHEM, 2003, Möller, 1994, Purohit and Basu, 2000). Nitro-PAHs have been detected in the lungs of non-smokers with lung cancer leading to increased interest in assessing their potential risk to humans (Tokiwa et al., 1993). Heterocyclic aromatic amines (HAAs) are another class of environmental carcinogens formed from heated products which contain sources of nitrogenous compounds, mainly heated foods of animal origin (Skog et al., 1998). They have also been detected in rain water and cigarette smoke condensate as well as in particles from diesel exhaust fumes (Kataoka, 1997, Liu et al., 2013, Zhang et al., 2011). Originally developed as pesticides, 2-aminofluorene (AF) and *N*-acetyl-2-aminofluorene (AAF) are among the most well-studied of the aromatic amines (Kriek, 1992). Their use as pesticides was, however, ceased due to the discovery that they were animal carcinogens (Clayson, 1981). They have since served as a foundation of knowledge for the development of human biomarkers towards aromatic amines as well as HAAs (Turesky and Le Marchand, 2011). Not all environmental carcinogens are derived from anthropogenic activity; aristolochic acid I (8-methoxy-6-nitro-phenanthro-(3,4-*d*)-1,3-dioxolo-5-carboxylic acid, AAI) is a major component of the natural plant extract aristolochic acid (AA) (Stiborova et al., 2013b, Stiborova et al., 2014b, Arlt et al., 2002). AA and

herbal remedies containing AA have been classed as Group I human carcinogens by IARC (IARC, 2012) as they have been shown to be the cause of Chinese herb nephropathy , now referred to as aristolochic acid nephropathy (AAN), and associated malignancies (Vanherweghem et al., 1993, Debelle et al., 2008). AAN is a rapidly progressive renal fibrosis with a high risk of developing upper urothelial tract carcinoma leading to bladder urothelial carcinoma (Gokmen et al., 2013, Nortier et al., 2000). Aflatoxins are a family of mycotoxins produced by *Aspergillus* fungi found on agricultural crops. Of the four main aflatoxins, aflatoxin B_1 (AFB_1) is the most commonly occurring and the most toxic. Chronic exposure causes liver cancer and individuals with hepatitis B are at a much greater risk (Kew, 2013). *Aspergillus spp.* are abundant in warm, humid regions of the world with many people in sub-Saharan Africa, Latin America and Asia at risk of exposure (IARC, 2015, McMillan et al., 2018).

1.3.2 Metabolic activation

Some highly reactive carcinogens are considered 'direct carcinogens' that are reactive and electrophilic enough to bind covalently to cellular proteins and DNA, e.g. alkylating agents such as mustard gas or ethylene oxide. These compounds, however, are only a small proportion of known human carcinogens. The great majority of carcinogens are nucleophilic or chemically inert, e.g. PAHs, aromatic and heterocyclic amines, aminoazo dyes and *N*-nitrosamines, and are termed procarcinogens (Luch, 2005). Procarcinogens go through the detoxication process, as with all xenobiotics, however they are often activated by XMEs (**Table 1.2**) producing reactive metabolites that are electrophilic and are able to react with nucleophilic sites in cellular

Table 1.2: Examples of individual P450 enzymes involved in the metabolism of carcinogens.

CYP family member	Organ	Carcinogenic substrates
CYP1A1	Many, particularly after induction	• Polycyclic aromatic hydrocarbons • Heterocyclic amines • Aromatic amines • Nitroarenes • Aristolochic acid I • Ellipticine
CYP1A2	Liver	• Aromatic amines • Heterocyclic amines • Polycyclic aromatic hydrocarbons • Aristolochic acid I • Estragole • Aflatoxin B_1
CYP1B1	Extrahepatic organs	• Polycyclic aromatic hydrocarbons • Nitroarenes • Aromatic amines
CYP2A6	Liver	• Nitrosamines • Estragole • Aflatoxin B_1
CYP2E1	Liver, GI tract	• 1,3-butadiene • Carbon tetrachloride • Chloroform • Ethanol • Acrylamide
CYP3A4	Liver, small intestine	• Aflatoxin B_1 • Aromatic amines • Cyclophosphamide • Ellipticine • Tamoxifen

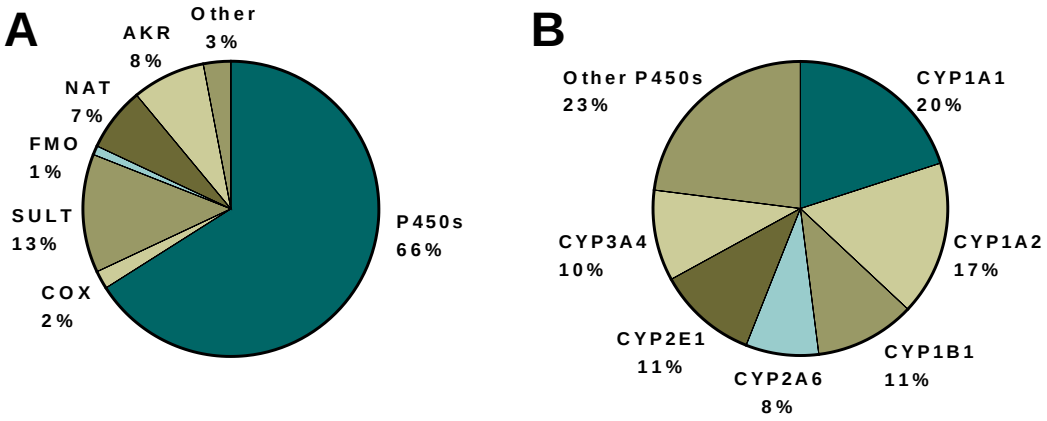

Figure 1.4: Contribution of (a) human XMEs and (b) the individual cytochrome P450s to carcinogen activation according to Rendic and Guengerich 2012. (AKR – aldoketoreductases, NAT – *N*-acetyltransferases, FMO – flavin monooxygenases, SULT – sulfotransferases, COX – cyclooxygenases)

macromolecules such as proteins and nucleic acids. Cytochrome P450s play an important role in the bioactivation of many carcinogens with CYP1A1/1A2/1B1/2A6/2E1 and 3A4 being implicated in ~80% of carcinogen bioactivation reactions (Rendic and Guengerich, 2012) (**Figure 1.4**). CYP1A1/1A2/1B1 play a major role in the bioactivation of PAHs (Baird et al., 2005), aromatic amines (Besaratinia and Tommasi, 2013) and HAAs (Turesky and Le Marchand, 2011). BaP is considered a procarcinogen as it is chemically inert and requires activation via P450-dependent monooxygenases, with CYP1A1 and CYP1B1 playing major roles in the bioactivation pathway, before exerting its genotoxic effects (Hamouchene et al., 2011, Shimada and Fujii-Kuriyama, 2004, Stiborova et al., 2017). The two enzymes catalyse the initial oxidation of BaP to form BaP-7,8-epoxide, which is then converted to BaP-7,8-dihydrodiol by epoxide hydrolase. BaP-7,8-dihydrodiol then undergoes further bioactivation by CYP1A1 and CYP1B1 to form the ultimately reactive species, BaP-7,8-dihydrodiol-9,10-epoxide (BPDE) (Baird et al., 2005, Luch and Baird, 2005) (**Figure 1.5**). BPDE is able to react with DNA, preferentially at guanine residues, to form primarily the pre-mutagenic adduct 10-(deoxyguanosin-N^2-

yl)-7,8,9-trihydroxy-7,8,9,10-tetrahydro-BaP (dG-N^2-BPDE) (Arlt et al., 2008, Kucab et al., 2015, Long et al., 2017, Long et al., 2000). 4-Aminobiphenyl (4-ABP) is an aromatic amine that is metabolised primarily in the liver to *N*-hydroxy-4-ABP, the precursor to 4-ABP-derived DNA adduct formation (**Figure 1.6a**) (Yoshihara and Tatsumi, 1995). The primary step in the activation pathway is *N*-hydroxylation catalysed by CYP1A2, (Yoshihara and Tatsumi, 1995, Turesky et al., 1991, Butler et al., 1989a, Butler et al., 1989b, Hammons et al., 1991, Landi et al., 1996). Metabolic activation of *N*-hydroxy-4-ABP is by esterification mediated by phase II enzymes such sulfotransferases (SULTs) or *N*-acetyltransferases (NATs) (Probst-Hensch et al., 2000, Turesky et al., 1991). PhIP is one of the most abundantly formed carcinogenic HAAs in cooked meat and it is also present in tobacco smoke (Gooderham et al., 2002). Evidence primarily from *in vitro* studies has demonstrated

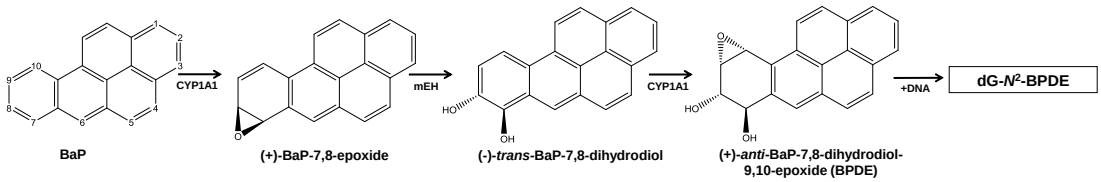

Figure 1.5: P450-mediated bioactivation pathway of BaP producing reactive metabolites that bind to DNA resulting in the dG-N^2-BPDE adduct.

that P450 enzymes are the most important enzymes involved in the initial oxidation of PhIP to form the intermediate *N*-OH-PhIP with CYP1A2 as the predominant P450 enzyme in the activation of PhIP followed by CYP1A1 and 1B1 (Edwards et al., 1994, Shimada et al., 1996) (**Figure 1.6b**). 2-Amino-alpha-carboline (A*a*C) is another carcinogenic heterocyclic amine present in cooked meat and tobacco smoke. The first step of A*a*C metabolism has been demonstrated in rodent and human liver microsomes to be the *N*-oxidation by P450s to form 2-hydroxy-amino-9H-pyrido[2,3-*b*]indole

(HO-NH-A*a*C) that then undergoes conjugation by SULTs or NATs (**Figure 1.6c**) (Niwa et al., 1982, Raza et al., 1996, King et al., 2000). Nicotine-derived nitrosamine ketone (NNK), a nitrosamine, is one of the most potent carcinogens present in tobacco smoke. Carcinogenesis occurs with P450-mediated α-hydroxylation producing reactive metabolites that form pyridyloxobutyl (POB)- and methyl-DNA adducts such as O^6-methylguanine (O^6-mG) (Hecht, 1998, Jalas et al., 2003, Lao et al., 2006) (**Figure 1.6d**). In some cases a bioactivation pathway is not mediated by a single P450 or P450 subfamily but can be more complex and involve other XMEs. An example of this is ellipticine (5,11-dimethyl-6*H*-pyrido[4,5-*b*]carbazole), a cytotoxic alkaloid isolated from the *Apocynaceae* family of plants.

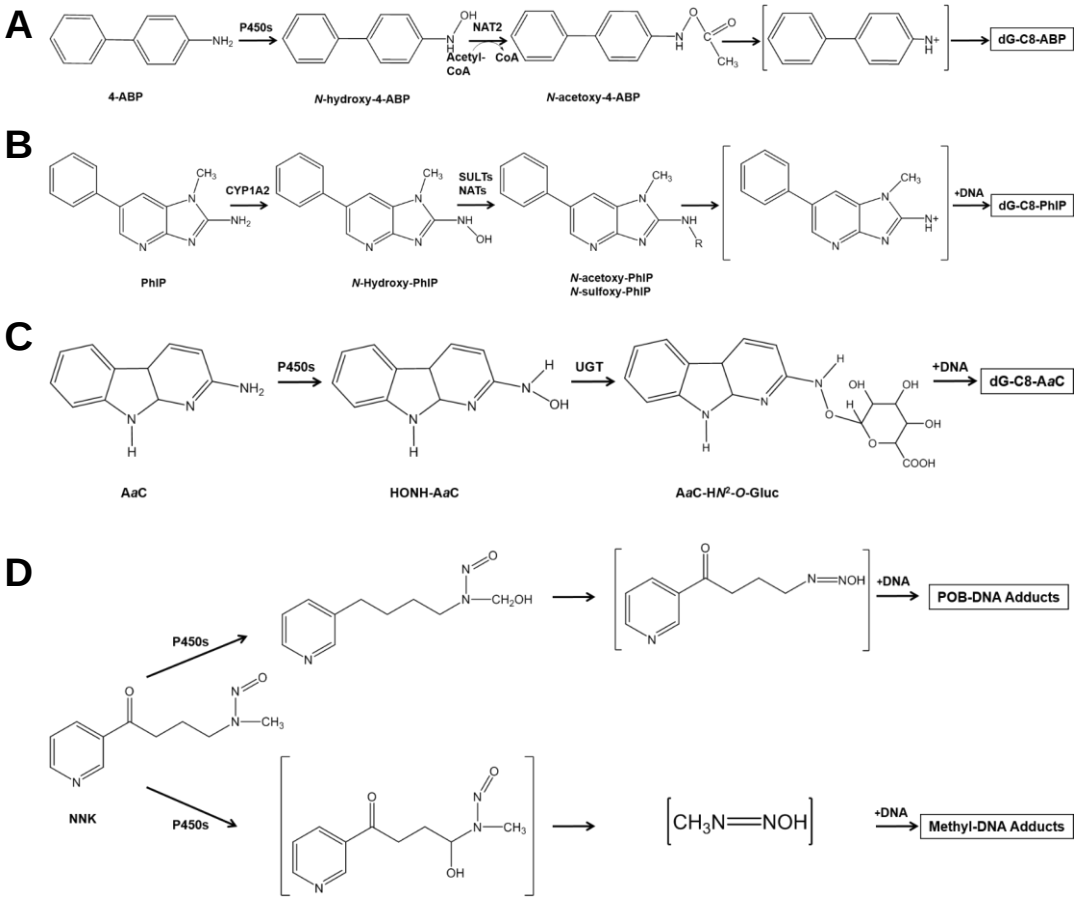

Figure 1.6: P450-mediated bioactivation pathway of (a) 4-ABP, (b) PhIP, (c) A*a*C and (d) NNK.

Activation of ellipticine is catalysed by P450 enzymes and peroxidases, which generate reactive intermediates capable of damaging DNA by forming covalent adducts (Stiborová et al., 2001, Arlt et al., 2003, Stiborova et al., 2003a, Stiborova et al., 2003b, Stiborova et al., 2007, Stiborová et al., 2007, Stiborova et al., 2008, Kizek et al., 2012, Stiborova et al., 2012a, Stiborová et al., 2012). As shown in **Figure 1.7**, ellipticine is oxidised by P450 enzymes and peroxidases to form five metabolites, including the reactive metabolites 12-hydroxy- and 13-hydroxy-ellipticine which dissociate to ellipticine-12-ylium and ellipticine-13-ylium and bind to DNA (Aimová et al., 2008, Stiborova et al., 2015, Stiborova et al., 2014a, Stiborova and Frei, 2014, Stiborová et al., 2011, Stiborova et al., 2004, Tmejova et al., 2014). The N^2-oxide is also considered an active ellipticine metabolite as it converts to 12-hydroxy-ellipticine by the Polonowski rearrangement (Stiborova et al., 2004, Kotrbova et al., 2006). 7-Hydroxy-ellipticine and 9-hydroxy-ellipticine are considered detoxication metabolites (Stiborova et al., 2011, Stiborova et al., 2012a, Stiborová et al., 2012).

1.3.3 Induction of DNA damage

Many carcinogens, whether bioactivated procarcinogens or direct-acting carcinogens, are DNA reactive. Covalent binding of the carcinogen to DNA results in the formation of DNA adducts that are generally formed at purine or pyrimidine bases, with guanine being the most commonly modified base. It is possible for carcinogens to bind to phosphate groups in the nucleic acid but this mechanism is far less common (Phillips, 2007). The resulting DNA adduct can be stable and persist or unstable depending on position of modification within the DNA base. An unstable DNA adduct can lead to

the destabilisation of the sugar-base bond which results in the loss of the adducted base (depurination or depyrimidation) (Phillips and Arlt, 2008). DNA adducts can also

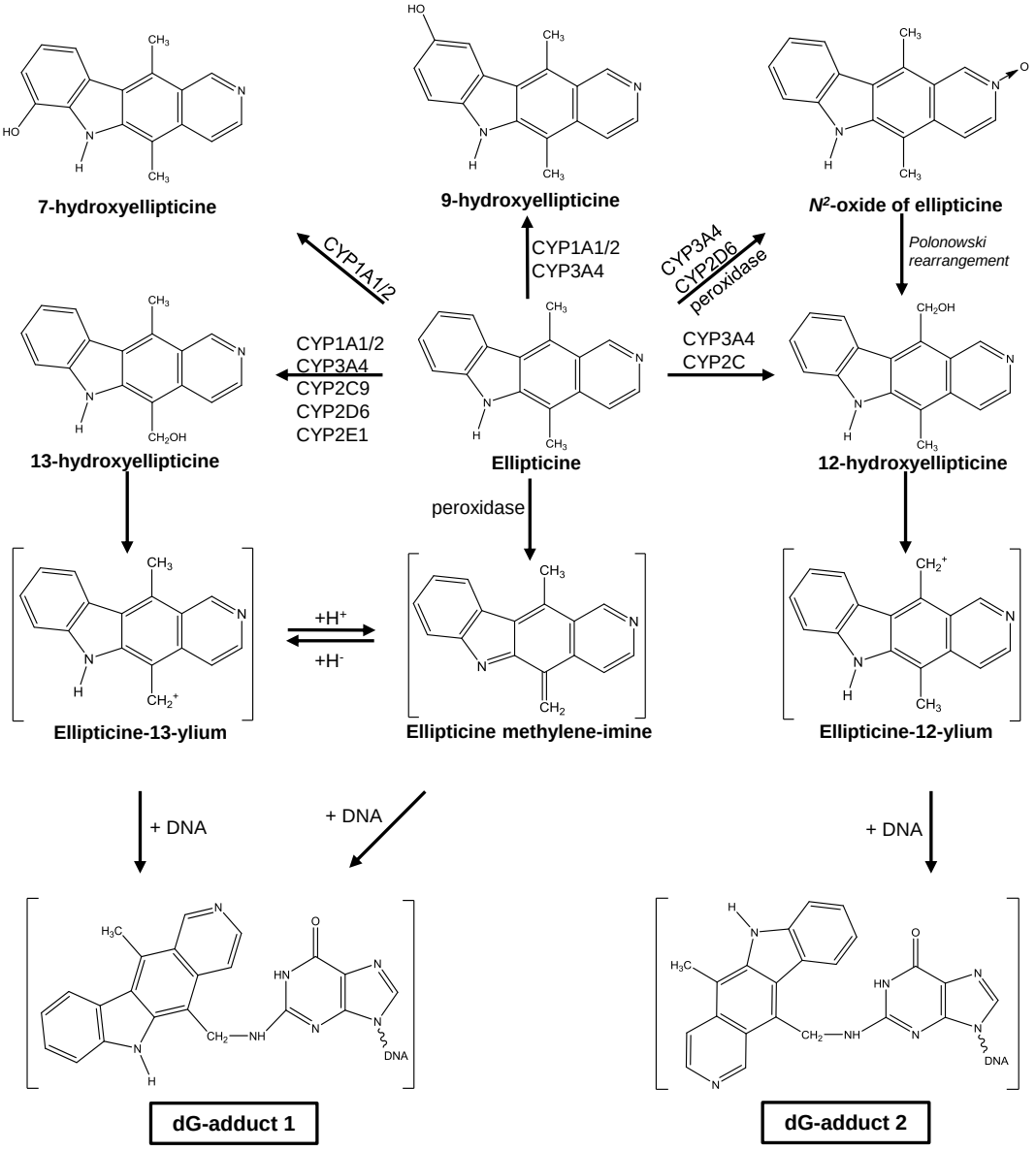

Figure 1.7: P450- and peroxidase-mediated bioactivation pathway of ellipticine.

arise from endogenous processes, including chronic inflammation, oxidative stress and normal metabolism. The most common oxidation lesion in DNA is 8-oxo-2'-deoxyguanosine (8-oxo-dG) which can be formed either through free radical attack on DNA or normal aerobic metabolism and is considered a biomarker of inflammation

induced carcinogenesis (Liguori et al., 2018). Experimental studies have shown a linear relationship between dose, tumour outcome and DNA adduct levels; however this is not always the case at higher doses and several studies have found that whilst tumours do not arise in the absence of DNA adducts, DNA adducts can be formed without necessarily giving rise to tumour formation (Poirier, 2016). The formation of bulky DNA adducts can result in breaks in the sugar-phosphate backbone of the molecule, either in one of the strands of the double helix (single strand breaks; SSB) or in both strands of the double helix (double strand breaks; DSB) (Phillips and Arlt, 2008). Some carcinogens, particularly cancer drugs such as cisplatin, intercalate into DNA to generate inter- or intra-strand crosslinks (Enoiu et al., 2012). These DNA crosslinks block DNA strand separation therefore interrupting essential DNA metabolic processes such as replication and transcription and can also prevent DNA replication leading to cell death (Huang and Li, 2013). Exposure to ultraviolet and other types of radiation can result in the production of pyrimidine dimers, where covalent crosslinks occur in cytosine and thymine residues (Douki et al., 2017).

Upon damage of DNA, there are a number of potential outcomes. Firstly, DNA repair mechanisms within mammalian cells detect the damage and restore the DNA sequence to its original state. Secondly, the DNA damage may trigger mechanisms that lead to programmed cell death (apoptosis). The third outcome is that DNA repair or apoptosis does not occur and the damaged DNA template is replicated incorrectly potentially resulting in mutations (Phillips and Venitt, 2012). Mutagen-mediated DNA damage results in nucleotide mutations (such as A > C, A > G, A > T, C > A). Compounds that form adducts on guanine residues often lead to G > T mutations as is the case with aflatoxin B_1 and BaP (Poon et al., 2014, O'Brien et al., 2016). If these mutations affect the functionality of genes critical for cellular homeostasis (*e.g.* tumour suppressor

genes, mismatch repair genes and proto-oncogenes) then the likelihood of the mutation giving rise to malignancy increases.

1.4 Methods of investigating contribution of XMEs to carcinogen activation

There are a variety of experimental tools that allow the assessment of the contribution of XMEs to the activation of carcinogens both *in vitro* and *in vivo*. The development of targeted gene disruption methodologies have also allowed the investigation into the role of single or multiple enzymes in bioactivation pathways through knocking out enzymes or enzyme activity in *in vitro* or *in vivo* systems.

1.4.1 Gene targeted disruption methodologies

1.4.1.1 Homologous recombination in embryonic stem cells

The method is based upon homologous recombination between a targeting vector and the gene of interest and was developed in the late 1980s (Capecchi, 1989, Smithies et al., 1985). The selection for the appropriate gene targeting event is carried out in petri dishes as opposed to whole organisms, making the process more efficient. The selection process is divided into two steps; the first step identifies embryonic stem (ES) cells cultured from the inner cell mass of mouse blastocycts, whose genome contained the incorporated targeting vector. An engineered neomycin resistance-conferring cassette was incorporated into the homology region of the targeting vector, generally into the region that would correspond to an important and upstream exon of the targeted gene (Cheah and Behringer, 2000). In order to ensure that the incorporation of the targeting vector happened via homologous recombination by

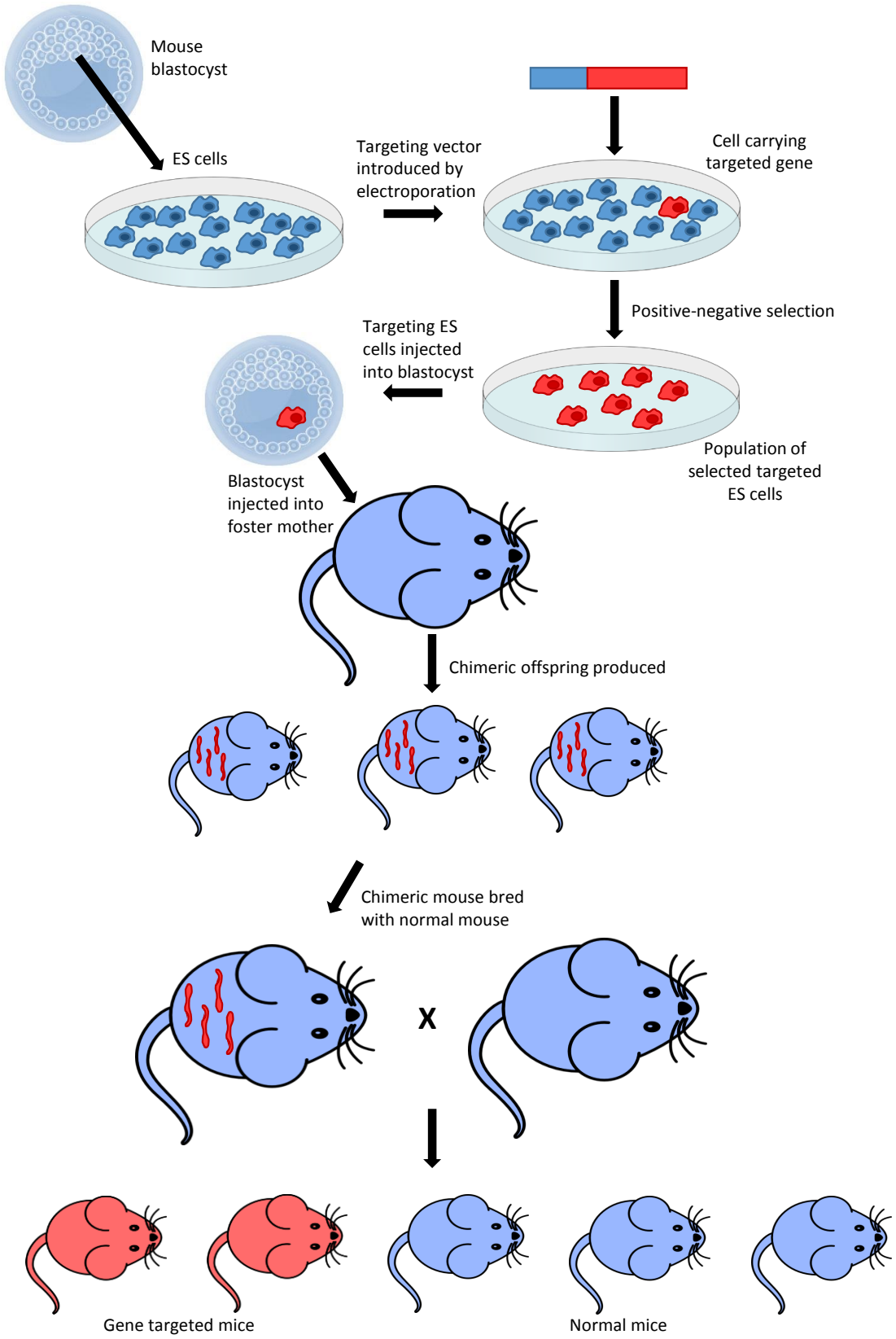

Figure 1.8: The homologous recombination in embryonic cells method of producing knockout mice. See text for details.

replacing the endogenous gene as opposed to insertion into a random locus an additional step was added. This was achieved by the inclusion of the thymidine kinase cassette downstream of the homology region of the construct as a negative selectable marker (Mansour et al., 1988). Once successful selection of gene-targeted ES cells has been carried out they are injected into the cavity of blastocysts to produce embryos containing the disrupted gene. These embryos are implanted into foster mothers who go on to give birth to chimeric offspring. These offspring are then test bred to identify germline chimeras where some of the progeny result from ES cell-derived gametes (**Figure 1.8)** (Melton, 1994). Due to the insertion of a non-native sequence, e.g., the neomycin cassette, in the middle of an important exon of the gene of interest or a stop codon upstream of coding regions, or both, the endogenous gene was ultimately disrupted. Therefore, there was either no protein expression from it, or the translated protein was structurally so abnormal that it could not serve the original biological function. Thus, the mutation induced with this technology was called null mutation, and the transgenic mouse carrying such a mutation, the knock-out or null mutant mouse (Gerlai, 2016).

1.4.1.2 The Cre-lox system

Early gene targeting technology was limited to relatively simple genetic manipulations, *i.e.* introducing a mutation into a gene, or globally deleting the function of a single gene. With the introduction of site-specific recombination strategies came with the possibility of gene deletion in a spatially (with a tissue- or cell- specific promoter) and/or temporally (with an inducible system) controlled fashion, helping to circumvent the problem of embryonic lethality (Arlt et al., 2015a). One of the most commonly used systems in the Cre-lox system (Le and Sauer, 2001). It allows DNA

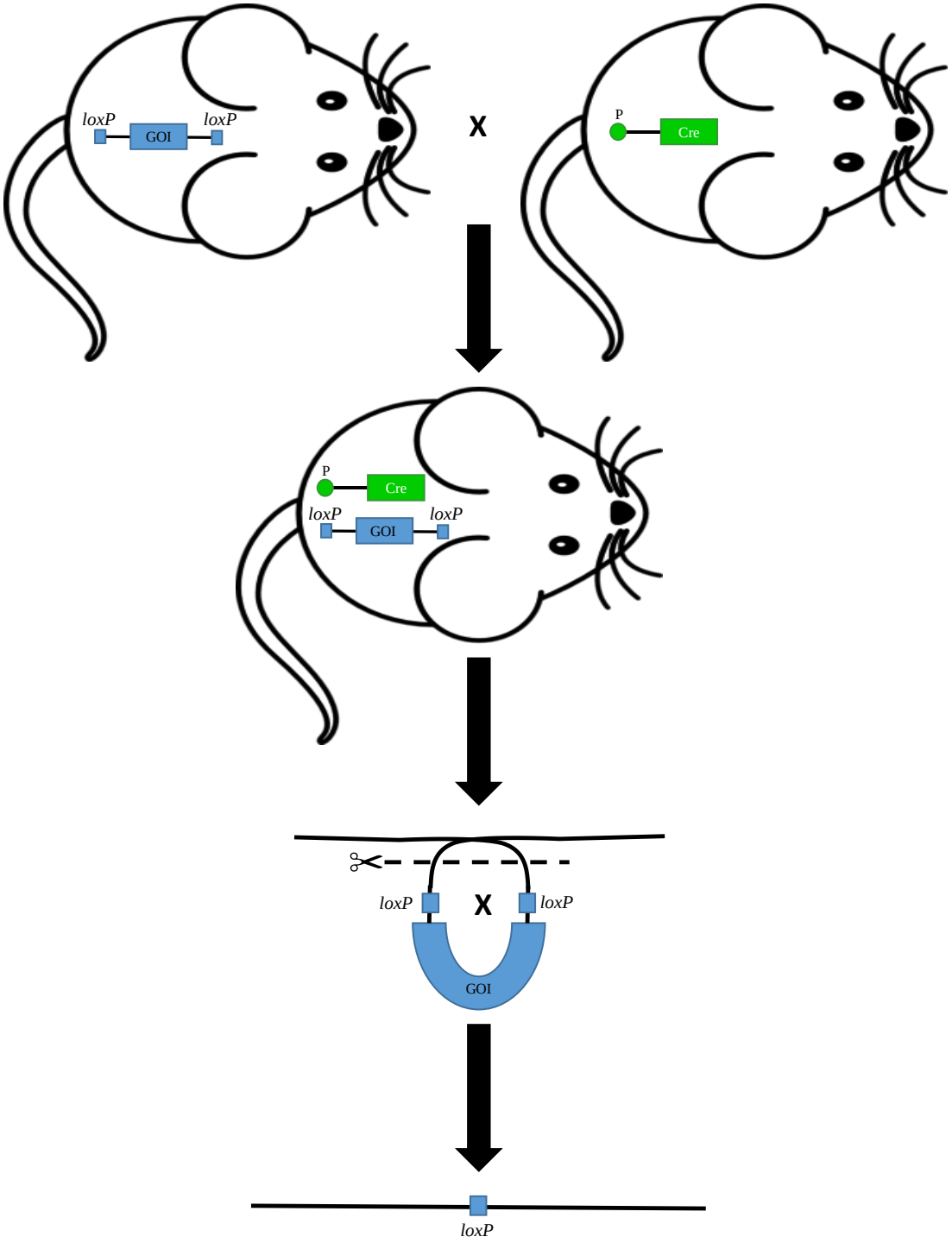

Figure 1.9: The Cre-lox system being utilised in mice to delete a gene of interest (GOI). See text for details.

modification to be targeted to a specific cell type or be triggered by a specific external stimulus and can be utilised in both prokaryotic and eukaryotic systems. Cre is the 38-kDa product of the *cre* gene of bacteriophage P1 and is a site-specific DNA recombinase. Cre recognises a 34-bp site on the P1 genome called *loxP* (locus of X-over of P1) and is able to efficiently catalyse reciprocal conservative DNA recombination between pairs of *loxP* sites. The gene of interest that is flanked by *loxP* sites is considered to be 'floxed'. The *loxP* site consists of two 13-bp inverted repeats flanking an 8-bp nonpalindromic core region. These regions give the *loxP* sites directionality and, depending on the orientation of these sites, Cre either inverts the fragment in between the two *loxP* sites or expels it as a circular fragment. Excision of the DNA as a covalently closed circle results from Cre-mediated recombination between two directly repeated *loxP* sites (reviewed by: (Sauer, 1998)). This system can be utilised in mice to generate knockout models. In order to do this, two mouse lines are needed. One mouse line contains the two *loxP* sites flanking the gene of interest that needs to be deleted. The other line expresses the Cre recombinase, either in the whole organism or a target tissue. By crossing the two mouse lines the *loxP* sites and the Cre are combined, activating the recombination system and deleting the gene of interest (GOI) (**Figure 1.9**). Inducible Cre recombinases have also been developed that are fusion proteins that contain the original Cre recombinase and a specific ligand binding domain that is activated by an exogenous ligand (Jaisser, 2000). Binding of the ligand is thought to produce conformational changes in the fusion protein and/or changes in the intracellular localisation associated with targeting of the recombinase to the nucleus (Metzger and Feil, 1999, Sauer, 1998).

1.4.1.3 CRISPR/Cas9

Archea and bacteria are able to develop future resistance to bacteriophage invasion by integrating short fragments of the viral nucleic acid into clusters of regularly interspaced short palindromic repeats (CRISPRs) (van der Oost et al., 2014). Three types (I-III) of CRISPR systems have been identified, with each system consisting of a cluster of CRISPR-associated (*Cas*) genes, non-coding RNAs and a distinctive array of repetitive elements (direct repeats). These repeats are interspaced by the short fragments derived from foreign DNA targets known as protospacers (Makarova et al., 2011). Together, the protospacers and the direct repeats make up the CRISPR RNA (crRNA) array. Out of the CRISPR systems, the type II CRISPR system is one of the best understood and possesses the CRISPR-associated protein 9 (Cas9) nuclease. Cas9 has an RNA binding domain, an alpha helix recognition lobe (REC), a nuclease lobe that includes the RuvC and HNH nuclease domains for DNA cleavage, and a protospacer adjacent motif (PAM) interacting site. Cas9 binds to the crRNA, creating a complex, causing conformational changes that create a channel that allows for DNA binding (Brouns et al., 2008). The Cas9/crRNA complex scans the DNA searching for the DNA target for a PAM, a 2-6 base pair DNA sequence (5'NGG) immediately following the target DNA sequence. Cas9 will not successfully bind or cleave the target DNA if it is not followed by the PAM sequence (Mojica et al., 2009). Recognition of a PAM site by the Cas9/crRNA complex leads to unwinding of the DNA allowing the crRNA to check the adjacent DNA via complementary base pairing (Sternberg et al., 2014). If the crRNA is not complementary the Cas9 releases, if it is the bridge helix within the REC lobe creates an RNA-DNA heteroduplex with the target DNA (Nishimasu et al., 2014). The PAM site recognition activates the nucleolytic HNH and RuvC domains that create a DSB in the target DNA. These DSBs

are repaired via the non-homologous end joining (NHEJ) repair pathway, which often creates errors by introducing insertion or deletions, or the homology directed repair (HDR) pathway.

The CRISPR system has been adapted for use within the laboratory by using synthetic, easily designed single guide RNAs (gRNA) instead of crRNAs. CRISPR/Cas9 plasmids allow an efficient gene targeted disruption method (**Figure 1.10**). The plasmids encode the 20 nucleotide non-coding gRNA sequence alongside the gRNA scaffold that helps Cas9 bind to target DNA. A marker for successful transfection is also expressed in the plasmid, in most cases this is red or green fluorescent protein to allow visual verification of transfection. A second plasmid is often present in transfection mixtures that still encodes for the gRNA and Cas9, but contains a gene that confers resistance to an antibiotic, *i.e.* puromycin, to allow selection of successfully transfected cells (Ran et al., 2013b). Whilst the CRISPR-Cas9 system is highly efficient, a considerable disadvantage is the number of off-target effects which reduces the specificity of CRISPR/Cas9 editing. This has been overcome with the development of a CRISPR double nickase system whereby a pair of plasmids encode a Cas9 (D10A) nickase mutant (Cas9n). Each plasmid also encodes a gRNA and each Cas9n/gRNA complex creates only one nick in the DNA strand that is complementary to the gRNA. Each pair of gRNAs is offset by around 20 base pairs and recognise target sequences on opposite strands of the target DNA. The resulting double nick created by the pair of Cas9n/gRNA complexes mimics a DSB and DNA repair by NHEJ lead to errors from insertions, deletions or frameshifts that act to disrupt the gene (**Figure 1.11**) (Ran et al., 2013a).

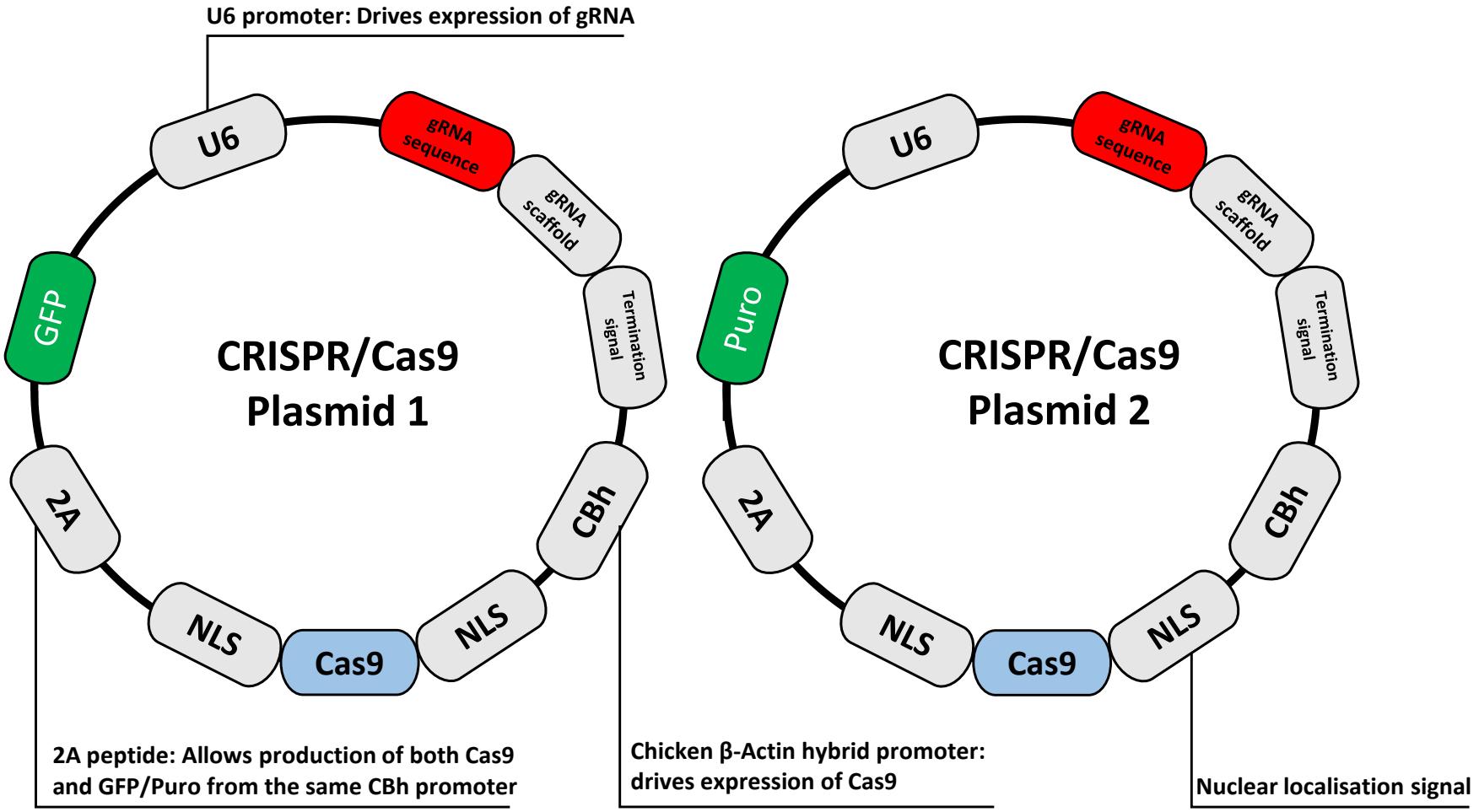

Figure 1.10: Schematic of the CRISPR/Cas9 plasmids and the genes encoded upon successful transfection for gene targeted disruption. See text for details.

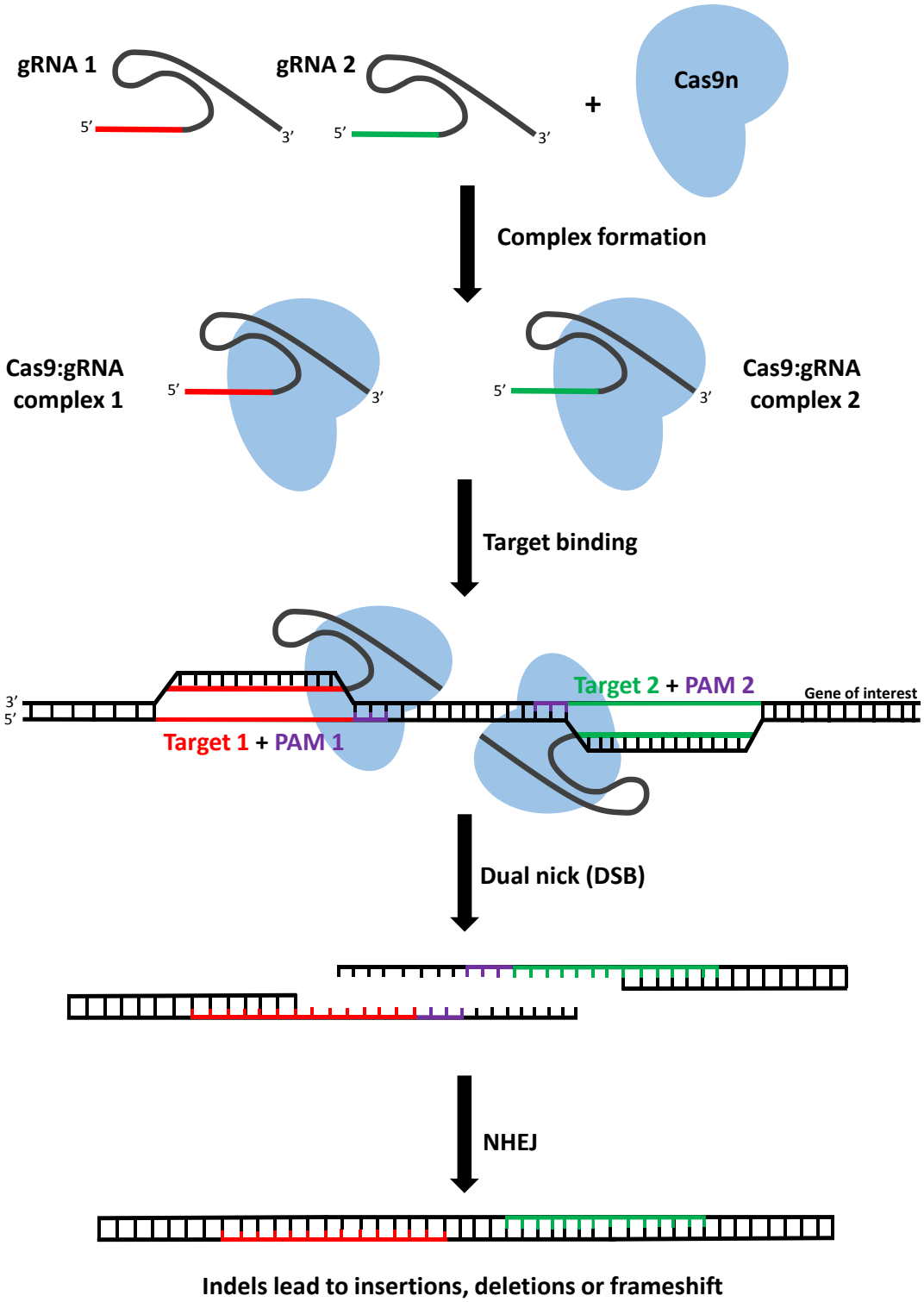

Figure 1.11: Schematic of the double nickase CRISPR/Cas9 plasmid method of gene disruption. See text for details.

1.4.2 *In vitro* systems

1.4.2.1 Cell-free systems

In order to study the reactions catalysed by a single cytochrome P450 experimentally that protein be isolated from animal and plant tissues or large volumes of biological fluids, with kilograms being needed to yield a small amount of a given protein. In the late 1980s and early 1990s the technology for the excision of complete cytochrome P450 genes as well as their reductases and insertion into bacterial, eukaryotic or viral vectors was developed, *E. coli* often the vector of choice, bringing forth a new experimental tool in carcinogenesis studies (Rosano and Ceccarelli, 2014, Stringer et al., 2009). The purified P450s can be used to reconstitute catalytic activities when mixed with redox partners such as POR, with both recombinant proteins purified from bacterial sources. Bacteria are normally devoid of redox partners such as POR so a *tac/tac* promoter is used to produce a single RNA containing both the P450 and reductase messages, each with an independent site for ribosome binding. Such systems yield cytochrome P450 and redox proteins in ~1:1 ratio (Parikh et al., 1997, Guengerich et al., 1997)

Microsomes are comprised of fragments of the ER that form micelles rich in ER-bound enzymes. These microsomal fractions are isolated by centrifugation of homogenised organs, predominantly the liver, at around 10,000 *g* to remove cellular and nuclear membranes, as well as larger cellular organelles. The supernatant is then centrifuged at around 100,000 *g* to provide a pellet that contains the smooth ER, and thus the membrane bound XMEs associated with it. The microsomal fractions can be isolated from a range of tissues (Scotcher et al., 2017, Heilmann et al., 2012, Asha and Vidyavathi, 2010) and incubated in the presence of an NADPH-regenerating system

in the form of enzymatic cofactors. This reaction mixture can be used for the evaluation of phase I oxidative reactions and, with the use of inhibitors, the influence of specific isozymes on the *in vitro* activation of procarcinogens (Nirogi et al., 2015). Microsomal fractions are widely used as an experimental tool in xenobiotic metabolism and have been utilised for chemical carcinogenesis studies since 1948 when it was discovered that the biotransformation of *N*,*N*-dimethyl-4-aminoazobenzene could be catalysed in a cell free system using rat hepatic microsomes (Mueller and Miller, 1948). At that time the enzymes present in microsomal fractions were known as mixed function oxidases until the 1960s when the cytochrome P450 nomenclature was developed (Brodie et al., 1955, Omura and Sato, 1962). Due to microsomes being an isolated part of the cell and the enrichment of P450s in the fractions, it is difficult to extrapolate to *in vivo* metabolism as the absence of competing enzymes and cytosolic cofactors can leave some metabolic outcomes unnoticed (Brandon et al., 2003).

Supersomes are microsomes prepared from insect cells containing cDNA of a single cytochrome P450. They are also a valuable experimental tool as insect cells lack endogenous cytochrome P450 activity, allowing transfection and subsequent activity of the selected P450 to be assessed without competition from endogenous enzymes. They can also be referred to as baculosomes due to the infection of the insect cells by baculo virus (Chen et al., 1997). Supersomes are used as tools in biotransformation studies as they have the added advantage of unique specification by expressing enzyme activity of one single CYP isoform and also find a solution to the problem of limited tissue availability needed to harvest microsomes. As with microsomes, an NADPH-regenerating system needs to be provided (Huang et al., 2000, Rendic et al., 1999).

1.4.2.2 Cell culture

In vitro cell-free systems are very useful for identifying substrates and reactions catalysed by individual P450 enzymes, however they do not represent the cell as a whole in metabolism. *In vitro* models cannot replicate the complex interactions that occur *in vivo;* however they are valuable in providing a quick insight into the metabolism of a large number of compounds (White, 2000). Intact primary hepatocytes represent a strong option as a compromise between an isolated system and the necessity to be as close as possible to the *in vivo* situation. There is evidence that for the study of toxicological endpoints other than metabolism, a typical freshly isolated suspension is an incomplete model, as non-parenchymal cells are very poorly represented (<1%) whilst in the intact organ they account for 20-40% of the total cell number (Ammann and Maier, 1997). Primary cultures can be isolated from tissues of humans or animals, but they require access to donors, can be difficult to handle and can be short lived due to expression of specialised features of the cells being gradually lost once separated from the organism (Coleman, 2010). Immortalised cell lines that originate from tumours were introduced as an alternative to overcome the limitations of primary cells. With advances in biochemistry, molecular biology and cell biology, it became possible to introduce new techniques that enable the production of different cell lines and the characterisation and differentiation of them in order to better understand intracellular processes. Animal cell culture technology is now generally considered a reliable, robust and relatively mature technology (Li et al., 2010). Due to their origins, cell lines often display abnormal characteristics of their parent tumour, e.g. resistance to toxicity, overexpression of detoxification and transport systems and rapid and continuous growth. These abnormalities, however, can be exploited for experimental xenobiotic metabolism focussing on activation or detoxification

mechanisms. Cell lines have an unlimited lifespan, high reproducibility and are much easier to standardise making them an advantageous *in vitro* tool (Jennings, 2015).

Culturing cells within a 2D model as a monolayer or within a suspension is the predominant method *in vitro*. In order to make the model more representative of *in vivo* conditions, cells can be cultured in 3D culture systems. In conventional 2D conditions the extracellular matrix components, cell-to-cell and cell-to-matrix interactions that are important for differentiation, proliferation and cellular functions *in vivo* are lost (Mazzoleni et al., 2009). Cells are cultured on a 3D scaffold that can be generated using various natural and synthetic polymers, *i.e.* collagen, gelatin and elastin). These composites mimic the native extracellular matrix by porosity, fibrous, permeability and mechanical stability and enhances the biophysical and biochemical interaction of the adhered cells. This in turn provides a biologically active environment for the cells to proliferate and differentiate (Ravi et al., 2015). Cells cultured in a 3D environment also differ in gene, protein and cell receptor expression from 2D-cultured cells with various cancer cell lines displaying different gene expression profiles depending on the culture method (Baharvand et al., 2006). Cells are commonly cultured as aggregates, grown on 3D scaffold materials, or are embedded in gels (Lin and Chang, 2008, Moroni et al., 2008, Slaughter et al., 2009). Aggregates are commonly referred to as spheroids (Kunz-Schughart et al., 2004) but alternative names include micromass and microfabricated tissues (Greco et al., 2011, Rivron et al., 2009). Whilst a single cell type can be cultured in a 3D system, studies have also been carried out that co-culture two or more different cell types in order to better mimic an *in vivo* system. (Campbell et al., 2011, Leisten et al., 2012, Susewind et al., 2016). Co-culturing cells has also been shown to overcome the limitations of primary

hepatocytes as co-culturing with endothelial cells in order to preserve their normal function (Kim et al., 2012).

A recent advance in 3D cell culturing is the development of organoids. Pluripotent stem cells (PSCs) and adult stem cells (ASCs), have been shown to assemble into complex structures that contain organised clusters of cells when placed within a hydrogel and in the presence of suitable exogenous factors (Lancaster and Knoblich, 2014). Organoids exhibit the spatial organisation of heterogeneous tissue-specific cells, cell-cell interactions, cell-matrix interactions and certain physiological functions generated by tissue-specific cells within the organoid. This means they provide a stable system allowing extended cultivation and manipulation, a limitation of spheroids (Yin et al., 2016). If provided with the appropriate 3D scaffold and biochemical factors differentiated PSCs are able to self-organise to form tissue specific organoids including the liver (Takebe et al., 2013), kidney (Takasato et al., 2014), brain (Lancaster et al., 2013), intestine (Spence et al., 2011) and optic cup (Eiraku et al., 2011). Many tissues are maintained *in vivo* by tissue-specific ASCs through self-renewal and differentiation followed by self-organisation. This process has been reproduced *in vitro* under specific culture conditions to produce self-organised tissue organoids including pancreas (Huch et al., 2013), stomach (Barker et al., 2010), intestine (Sato et al., 2009) and liver (Huch et al., 2013). Hepatic organoids have been shown to be capable of expressing constitutive and induced cytochrome P450s involved in carcinogen bioactivation, *i.e.* CYP1A1/2, CYP3A and CYP2E (Miyamoto et al., 2005) making organoids a potentially important *in vitro* tool for future chemical carcinogenesis studies.

1.4.3 *In vivo*: mouse models

The development of targeted gene disruption methodologies (Capecchi, 1989, Le and Sauer, 2001) has given rise to numerous transgenic mouse lines (e.g. *CYP*-knockout or *CYP*-humanised) that allow investigation into the contribution of individual cytochrome P450s to chemical-induced genotoxicity and carcinogenesis. A number of knockout and humanised mouse lines have been developed to study the role of P450 enzymes in metabolism (Arlt et al., 2011, Buters et al., 1999, Kimura et al., 1999, Kimura et al., 2003, Uno et al., 2004).

1.4.3.1 P450 null mice

Mice lacking an individual P450 have been widely utilised in metabolism studies. Using the Cre-*lox* system, *Cyp1a1(–/–)* knockout mice on a C57BL/6J and 129/J background were developed through the deletion of the *Cyp1a1* gene (Dalton et al., 2000). These mice are described as being viable and show no obvious phenotype compared to WT littermates. ES cells have also been used to develop P450 null mice. *Cyp3a(–/–)* mice developed using this technology were expected to possess marked physiological changes due to the deletion of *Cyp3a*, however, the mice were shown to be viable and fertile. Haematological, plasma clinical chemistry and pathological examination of male and female mice at approximately 12 weeks of age did not reveal any marked abnormalities, nor did pathological examination between 67 and 84 weeks of age (van Herwaarden, 2007). *Cyp1b1(–/–)* mice were also shown to be indistinguishable from their WT and heterozygous littermates, and gross pathological examination revealed no apparent abnormalities. The mice were also fertile and produced normal-sized litters (Buters et al., 1999). *Cyp1a2(–/–)* mice produced by homologous recombination in ES cells were also shown to have no developmental

issues despite lacking Cyp1a2 activity (Liang et al., 1996). Once these stable P450 knockout mice have been attained it is possible to crossbreed them to create double-knockout lines. Thus *Cyp1a1/1b1(–/–)* and *Cyp1a2/1b1(–/–)* mice have been bred successfully, although simple genetic crosses were not initially able to produce *Cyp1a1/1a2(–/–)* mice due to the genes being located only 13.3 kilobases apart on mouse chromosome 9 (Uno et al., 2006). However, use of the Cre-lox system via two *loxP* sites situated 26 kilobase pairs apart proved to be successful, resulting not only in double knockout *Cyp1a1/1a2(–/–)* mice but also in a *Cyp1a1/1a2/1b1(–/–)* triple knockout line (Dragin et al., 2008).

Disruption of *Cyp* genes encoding for P450 enzymes in mice can result in models with no developmental abnormalities or deleterious phenotype (Gonzalez, 2003). However, this disruption can be problematic in the study of BaP metabolism as *Cyp1a1(–/–)* mice were found to die within approximately 28 days due to immunosuppression when administered repeated oral doses of BaP whereas WT mice remained healthy for at least one year (Uno et al., 2004). Another limitation of knocking out an individual P450 is the substrate overlap seen in this class of enzymes where loss of a single P450 enzyme can be compensated for by remaining P450 enzymes (Henderson et al., 2006).

1.4.3.2 Electron donor null mice

A new approach to investigating the role of P450s in *in vivo* metabolism is to delete the electron donors to P450s, rather than the XMEs themselves. In the absence of the electron donors, P450s cannot complete the catalytic cycle and therefore activity is lost. Global deletion of POR in mice was found to lead to embryonic lethality; however, knocking out POR activity in a single organ creates a much more stable

mouse model (Otto et al., 2003). By utilising inducible Cre recombinases, the *Cpr*^{lox} allele can be deleted resulting in the *Cpr*^{null} allele in a variety of cells and organs via Cre-mediated recombination, following intercrosses between the *Cpr*-lox mouse and a Cre-transgenic mouse. Mice with tissue-specific *Cpr* deletion have been generated, with *Cpr*-lox as a parental strain, for many organs, including the liver (Gu et al., 2003), lung (Weng et al., 2007), heart (Fang et al., 2008), intestine (Zhang et al., 2009), brain (Conroy et al., 2010), mammary gland (Lin et al., 2012), and bone (Panda et al., 2012). The Hepatic Reductase Null (HRN) mouse model (**Table 1.3**) was produced by crossing floxed POR mice with a line carrying Cre recombinase under the control of the hepatocyte-specific albumin promoter (Postic et al., 1999). In these mice POR is deleted specifically in the hepatocytes (Henderson et al., 2003). The HRN mouse is crossed onto a C57BL/6 background and displays no overtly changed phenotype aside from steatotic livers, significantly lowered blood lipids and virtually no bile acid production as a consequence of non-functioning P450-housekeeping activity involved in cholesterol metabolism (Henderson et al., 2003). By preventing the transfer of electrons to the P450 catalytic cycle, the liver is practically devoid of P450 enzyme activity despite having substantially elevated levels of P450s (Henderson et al., 2006).

The use of the albumin promoter in HRN mice to drive Cre expression does however have limitations. The albumin promoter switches on soon after birth, and in the case of HRN mice, drives POR deletion to completion by adulthood. This results in a great inability to control or regulate gene deletion. The Reductase Conditional Null (RCN) mouse (**Table 1.3**) was developed to overcome this limitation. The RCN mouse is a variant on the HRN mouse line *(Por*$^{lox/lox}$*/Cre*^{CYP1A1}*)* whereby POR can be deleted conditionally in the liver and gastrointestinal tract using the rat *CYP1A1* promoter to drive Cre recombinase expression (Finn et al., 2007). Administration of the CYP1A1

inducers TCDD or β-naphthoflavone results in deletion of both hepatic and gastrointestinal POR, whereas administration of 3-methylcholanthrene (3MC) results in the loss only of hepatic POR expression, essentially recapitulated the phenotype of the HRN mouse (Finn et al., 2007, Arlt et al., 2011). POR is not the only electron donor to cytochrome P450s. In order to investigate the role of Cyb5 in P450 metabolism *in vivo,* two mouse models were developed. The first of these was developed using the ES homologous recombination method to produce the Hepatic Cytochrome b_5 null (HBN) mouse (**Table 1.3**) whereby Cyb5 is conditionally deleted in the hepatocytes (Finn, 2008). The mice developed normally and displayed no overt phenotype when compared with their WT littermates and livers from the adult HBN mice looked similar to those of WT mice, with no gross changes in general morphology or pathology. Unlike the HRN mouse, although some expression of P450s was slightly elevated in HBN mice, the changes were not significantly different (Finn, 2008, Finn et al., 2011). The HBN mouse is a valuable tool for investigating the role of Cyb5 in hepatocytes, however the cytochrome b_5 complete null (BCN) mouse (**Table 1.3**) was later generated, using the same ES system as the HBN mice, which possessed a global Cyb5 knockout. Whereas a global deletion of POR led to embryonic lethality the global deletion of Cyb5 resulted in a viable mouse (McLaughlin et al., 2010). Whilst the HBN and BCN mouse models assess the role of Cyb5 in P450-mediated metabolism, POR is still present and contributing to the catalytic activity of P450s. In order to investigate the role of both electron donors simultaneously the Hepatic Cytochrome b_5/P450 Reductase Null (HBRN) mouse model (**Table 1.3**) was generated by crossing HRN mice with the Hepatic Cytochrome b_5 Null (HBN) mouse. This produced a mouse line that lacks both electron donors POR and Cyb5 and thus the activity of P450 enzymes was further reduced relative to

Table 1.3: Selection of single or double electron donor null mouse models. See text for details.

Mouse model	Phenotype	Reference
Hepatic Reductase Null (HRN)	POR deleted specifically in hepatocytes	(Henderson et al., 2003)
Reductase Conditional Null (RCN)	POR conditionally deleted in hepatocytes upon administration of 3-MC	(Finn et al., 2007)
Hepatic Cytochrome b_5 Null (HBN)	Cyb5 deleted specifically in hepatocytes	(Finn, 2008)
Cytochrome b_5 Complete Null (BCN)	Cyb5 deleted globally	(McLaughlin et al., 2010)
Hepatic Cytochrome b_5/P450 Reductase Null (HBRN)	POR and Cyb5 deleted specifically in hepatocytes	(Henderson et al., 2013)

The HRN and HBN model (Henderson et al., 2013). Collectively, these mouse models are powerful *in vivo* tools of investigating the role of hepatic versus extra-hepatic P450 enzymes in xenobiotic metabolism (Henderson et al., 2013, Arlt et al., 2012, Arlt et al., 2008, Henderson et al., 2003, Arlt et al., 2011).

1.5 Aims of the project

The first part of this project aims to investigate the role of P450 enzymes and the contribution of electron donor proteins in the bioactivation of environmental carcinogens. This project utilises both the HRN and HBRN mouse models to investigate the contribution of the electron donors POR and Cyb5 to the P450-mediated metabolic activation of the environmental carcinogen BaP and the anticancer drug ellipticine both *in vivo* and *in vitro.* BaP and ellipticine have both been studied previously in HRN mice and, although they are both activated via P450-mediated pathways, the experiments with HRN mice yielded contrasting results. Utilising the HBRN mouse in this study will help to assess whether the contrast in results is attributable to the contribution of Cyb5 in one reaction but not the other. The use of the two carcinogens side by side will also provide greater mechanistic insights into host factors regulating P450 catalysed carcinogen metabolism. As BaP and ellipticine are activated by P450-mediated pathways so in the absence of electron donors and P450 activity I hypothesise that activation of these carcinogens to form reactive metabolites and DNA-adducts would be reduced compared to WT mice. In order to assess P450-mediated activation in the mice *in vivo,* DNA adduct formation will be assessed across a range of organs. In order to investigate the *in vitro* activation of BaP and ellipticine, hepatic microsomal fractions will be used in reaction mixtures to assess enzyme activity using both colorimetric assays and HPLC, metabolite formation analysed using HPLC and DNA adduct formation analyse using ^{32}P-postlabelling. Protein expression of electron donors and XMEs in the hepatic microsomal fractions will also be investigated using Western blotting.

The second part of the thesis aims to develop an *in vitro* model of the HRN mouse in order to allow further investigation of the accumulation of BPDE-DNA-adduct formation seen in HRN mouse hepatocytes. This model will be developed in immortalised murine hepatocytes, Hepa-1c1c7, originating from a mouse hepatoma. POR expression will be knocked out of Hepa-1c1c7 cells using CRISPR/Cas9 technology. An attempt to create a new cell line from a single clone, to ensure uniformity and reproducibility, will be done using single cell isolation. This cell line will then utilised to investigate the effect of POR on the P450-mediated bioactivation of BaP *in vitro* by assessing metabolite formation using HPLC, DNA damage using the comet assay and DNA adduct formation using ^{32}P-postlabelling. In order to assess whether the disruption of POR in the Hepa-1c1c7 cells will have an effect of protein expression of electron donors and XMEs in the cells, with or without treatment of BaP, Western blotting will be carried out on cell lysates.

The final part of the thesis attempts to compare the responses of mouse hepatoma Hepa-1c1c7 *POR*-knockout cells with that of human hepatoma HepG2 *POR*-knockout cells to BaP. This will help to provide insight as to whether the unexpected accumulation of BPDE-DNA-adducts in hepatocytes lacking POR is limited to mouse models or is also experienced within a human hepatocyte model. The effect of POR on the P450-mediated bioactivation of BaP *in vitro* will be studied by assessing metabolite formation using HPLC, DNA damage using the comet assay and DNA adduct formation by ^{32}P-postlabelling. In order to compare protein expression of electron donors and XMEs in the cells in the absence of POR with that seen in the HRN and POR KO Hepa-1c1c7 cell line, Western blotting will be carried out on cell lysates.

Whilst it is important to understand the mechanisms of P450-mediated bioactivation of carcinogenic agents into reactive metabolites, there are also wider reaching implications into fields such as epidemiology and drug development. Drug candidates with strong P450-inducing activity have a lower chance of surviving the preclinical and clinical stage testing. The assessment of risk-benefit ratio before determining a molecule's suitability for development shows increasing awareness of chemically reactive metabolites that are able to react with essential cellular components (Mohutsky et al., 2010, Baillie and Rettie, 2011, Guengerich, 2010). P450-mediated bioactivation is also taken into consideration when identifying groups at risk of certain cancers, particularly in the relationship between PAHs and lung cancer (Mollerup et al., 2006, Hara et al., 2009, Hung et al., 2003, Gsur et al., 2001). It is also important to assess how representative animal models are in mirroring P450-mediated bioactivation pathways in humans. If *in vitro-in vivo* models being used to investigate P450-mediated bioactivation pathways are not representative, then the identification and assessment of risk-benefit ratios and risk groups for developing cancer may be inaccurate. The work included within this project will contribute towards the understanding of P450-mediated metabolism in animal and human models.

2 Materials and Methods

2.1 Chemicals

Benzo[*a*]pyrene (BaP; CAS no. 50-32-8; purity >96%), ellipticine (CAS no. 519-23-3; purity >99%), NADH (as disodium salt; purity ~95%), NADPH (as tetrasodium salt; ~98% purity), Sudan I and 7-methoxyresorufin were obtained from Sigma-Aldrich (St Louis, MO, USA). Testosterone and 6β-hydroxytestosterone were purchased from Merck (Darmstadt, Germany). All other chemicals used were analytical grade.

2.2 Animal treatment

All animal experiments were carried out at the University of Dundee under licence in accordance with the Animal (Scientific Procedures) Act (1986), as amended by EU Directive 2010/63/EU, and with local ethical approval. HRN ($Por^{lox/lox}/Cre^{CYP1A1}$) mice and HBRN ($Cytb_5^{lox/lox}/Por^{lox/lox}\pm Cre^{ALB}$) mice on a C57BL/6 background were derived as described previously (Henderson et al. 2003; Henderson et al. 2013). Animals were maintained in open-top cages, with free access to food (RM1 diet, Special Diet Services, Essex, UK) and water, and a 12-hour light/dark cycle. Mice homozygous for the floxed *Por* locus ($Por^{lox/lox}$) were used as WT.

2.2.1 Animal treatment with BaP

For the BaP study, groups of female HRN, HBRN and WT mice (3 months old, 25-30 g) were treated intraperitoneally (i.p.) with 125 mg/kg body wt (n = 3/group) of BaP for 1 day following a treatment protocol used previously to study BaP metabolism in

HRN mice (Arlt et al., 2008; 2012). In the present study, i.p. administration was used such that BaP uptake is directly to the liver via mesenteric veins and the lymphatic system, bypassing the gastrointestinal tract and metabolism by extrahepatic CYPs. BaP was dissolved in corn oil at a concentration of 12.5 mg/mL. Control mice (n = 3) received solvent (corn oil) only. Animals were killed 24 hours after the single dose and their tissues (liver, lung, forestomach, glandular stomach, kidney, spleen, small intestine, bladder and colon) were collected, snap-frozen and stored at –80°C until analysis.

2.2.2 Animal treatment with ellipticine

For the ellipticine study groups of female HRN, HBRN and WT mice (3 months old, 25-30 g) were treated i.p. with 10 mg/kg body wt (n = 4/group) of ellipticine for 1 day following a treatment protocol used previously to study ellipticine metabolism in HRN mice (Stiborova et al., 2008). Ellipticine was administered dissolved in 1% acetic acid at a concentration of 2.5 mg/ml. Control mice (n = 3/group) received the solvent only. Animals were killed 24 hours after the single dose and their tissues (liver, lung, small intestine, kidney, spleen, bladder and colon) were collected, snap-frozen and stored at –80°C until analysis.

2.3 Genotyping

To extract DNA for genotyping, pieces of liver tissue were suspended in 400 µL of 50 mM NaOH and heated to 95°C for 15 minutes, followed by vortexing for 5 seconds at the middle and end of the incubation. Next, 35 µL of 1 M Tris-HCL (pH 8.0) was added to each sample, followed by mixing and centrifugation at 13,000 rpm for 20 minutes. The supernatant was either used immediately or stored at –20°C. The primers

and PCR reaction conditions to genotype for WT, HRN and HBRN mice are described in **Table 2.1**. In the case of WT and HRN mice, PCR was carried out with Illustra PuReTaq PCR beads (27955801, GE Healthcare Life Sciences). To visualise

Table 2.1: Primer sequences and PCR conditions for the PCR reactions for the different genes of interest.

Gene	Primer	Primer sequence	PCR Conditions	
Control	OMIR 15	CAA ATG TTG CTT GTC TGG TG	1: 95°C 5 minutes 2: 95°C 30 seconds 3: 50°C 1 minute 4: 72°C 1 minute 5: steps 2-4: 34 times 6: 72°C 5 minutes 7: 4°C forever	
	OMIR 16	GTC AGT CGA GTG CAC AGT TT		
Cre	Cre 685	ACC TGA AGA TGT TCG CGA TTA TCT	1: 94°C 4 minutes 2: 94°C 30 seconds 3: 53°C 1 minute 4: 72°C 30 seconds 5: steps 2-4: 29 times 6: 4°C forever	
	Cre 1054	ACC GTC AGT ACG TGA GAT ATC TT		
POR	Red 1104	AGG CAG GCT GCT CAG GTC GGC	1: 94°C 3 minutes 2: 94°C 30 seconds 3: 60°C 20 seconds 4: 72°C 45 seconds 5: steps 2-4: 34 times 6: 72°C 5 minutes 7: 4°C forever	
	Red 1105	GAC CCT GAA GAG TAT GAC TTG		
	Red 1184	GCT TCC TCT TGC AAA ACC ACA CTG C		
Cyb5	B100	CCA ATG GTC TCT CCT TGG TC	**<u>WT + HRN mice</u>** 1: 95°C 5 minutes 2: 95°C 1 minute 3: 56°C 1 minute 4: 72°C 1 minute 5: steps 2-4: 39 times 6: 72°C 5 minutes 7: 4°C forever	**<u>HBRN mice</u>** 1: 95°C 5 minutes 2: 95°C 30 seconds 3: 50°C 1 minute 4: 72°C 1 minute 5: steps 2-4: 34 times 6: 72°C 5 minutes 7: 4°C forever
	B102 (WT + HRN)	GAT GGA GTT CCC CGA TGA T		
	B104 (HBRN)	CAA TAG CAG CCA GTC CCT TC		

PCR Reaction Mix (Per reaction)	RedTaq 2X Ready Mix (R2523, Sigma)	12.5 µL
	Primer 1	0.5 µL
	Primer 2	0.5 µL
	DNA	2.0 µL
	Nuclease Free Water	9.5 µL
	(In the case of reactions using 3 primers, 9 µL of water used)	

the PCR products, reactions were resolved on 2% agarose gels containing 0.5 µg/mL ethidium bromide. Band size was monitored by loading 3 µL of Gel Pilot 100 bp Plus marker (239045, Qiagen) onto each gel. Electrophoresis was performed at 140 V in TBE buffer (15581044, ThermoFisher) for 45 minutes, and then gels were exposed to UV light for image capture.

2.4 Preparation of hepatic microsomes

The microsomal fraction of tissues comprises fragments of the ER that form micelle structures called microsomes, which contain XMEs such as those found in the mixed-function oxidase system (e.g. P450 enzymes). Microsomal fractions were isolated from the livers of HRN, HBRN and WT mice using standard differential centrifugation. The livers from each mouse line were pooled for each microsomal preparation. The procedure was carried out in a cold room at 4°C with all buffers and materials being brought down to temperature prior to use. The livers were weighed prior to homogenisation in B1 buffer (0.15 M KCL, 0.05 M Tris/HCL; pH 7.4; 50 µm tocopherol in methanol) in a Potter-Elvehjem glass homogeniser. The volume of B1 buffer was dependent on tissue mass with 4 mL B1 per 1 g of tissue being used. The pooled homogenised livers were centrifuged at 2000 rpm for 10 minutes at 4°C (Janetzi K-23 swing-out rotor 4×70 mL) and the supernatant was then collected.

Pellets were resuspended in 250 µL of B1 buffer per 1 g of tissue and then centrifuged again under the same conditions. Both supernatants collected were pooled and centrifuged at 13,500 rpm for 20 minutes at 4°C (Janetski K-24, fixed-angle rotor 6×35 mL). The supernatants were collected and weighed to balance before being ultracentrifuged at 45,000 rpm for 1 hour at 4°C (Beckman Coulter-Optima LE-80K, fixed angle rotor Ti45, 6×64 mL). The supernatants were discarded. Pellets were resuspended and homogenised in 2 mL of B2 buffer (0.1 M $Na_4P_2O_7.10H_2O$; pH 7.2) per 1 g tissue using a small Elvehjem glass homogeniser. The resuspended pellets were then ultracentrifuged at 60,000 rpm for 1 hour at 4°C (Beckman Coulter-Optima LE-80K, fixed angle rotor Ti70, 8×36 mL). The supernatants were discarded and the final pellets were resuspended in 200 µL B3 buffer (0.15 M KCL, 0.05 M Tris/HCL, 20% (*v*/*v*) glycerol; pH 7.4) per 1 g of tissue. Microsomal fractions were aliquoted, immediately frozen in liquid nitrogen and stored at –80°C (Stiborova et al., 2003b). The protein concentration of the fractions was determined using the bicinchoninic protein assay (BCA) (Wiechelman et al., 1988) with the Thermo Scientific™ Pierce™ BCA Protein Kit and bovine serum albumin as a standard.

2.5 Enzyme activity

2.5.1 Cytochrome *c* reduction

POR is able to reduce cytochrome *c* in the presence of NADPH that can be measured colorimetrically allowing the activity of POR enzymes in a sample to be determined over a set time (**Figure 2.1**). The reaction mixture containing 955 µL of potassium phosphate buffer (0.3 M KH_2PO_4 with 1 mM EDTA; pH 7.5) with 25 µL 20 mg/ml

cytochrome *c* and 10 µL 10 mM NADPH was measured at the wavelength 550 nm as a blank. Ten µL of microsomal fraction was then added, the reaction mixture mixed

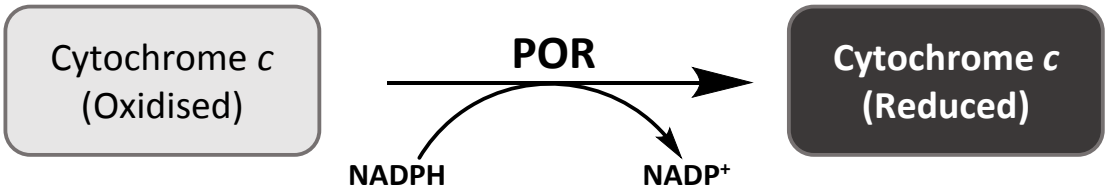

Figure 2.1: Schematic of the reduction of cytochrome *c* by POR in the presence of the enzymatic cofactor NADPH.

slightly and the measurement of $\Delta A_{0\text{-}60}$ at 550 nm was started. The activity of POR was then calculated using the following equation:

$$a = \frac{\Delta A_{0-60}}{\varepsilon \; x \; l \; x \; c_{pr} \; x \; t} \; x \; dilution$$

ε = extinction coefficient (21,010 $dm^3.mol^{-1}.cm^{-1}$, l = length of cuvette, c_{pr} = concentration of protein (mg/ml) , t = time, a = mmol cytochrome *c*/mg_{pr}/min

2.5.2 EROD and MROD

CYP1A1 and CYP1A2 are able to metabolise the substrate 7-ethoxyresorufin (EROD assay) and 7-methoxyresorufin (MROD assay), respectively, by a dealkylation reaction to a fluorescent product, resorufin (**Figure 2.2**). The amount of resorufin produced within a set time can be used to measure CYP1A enzyme activity, with the EROD assay used a measure for

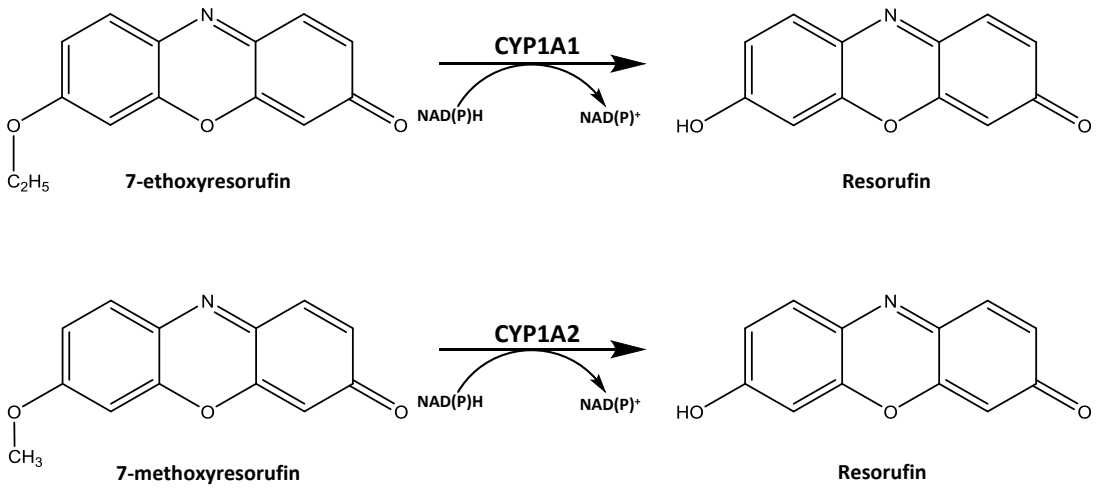

Figure 2.2: Schematic of the dealkylation of 7-ethoxyresorufin and 7-methoxyresorufin by Cyp1a1 and Cyp1a2, respectively, in the presence of the enzymatic cofactors NADPH or NADH.

CYP1A1/2 activity and MROD assay as a measure for CYP1A2 activity (Guengerich and Shimada, 1991). Microsomal fractions (see section 2.3) at a concentration of 0.5 mg/mL of protein were incubated with 2.2 µM of 7-ethoxyresorufin or 7-methoxyresorufin for 2 minutes at room temperature; total incubation volume was 500 µL with potassium phosphate buffer (0.1 M KH_2PO_4; pH 7.4). Aliquots (150 µL) of the reaction mixture were loaded into a 96-well plate and the reaction was initiated with the addition of 17 µL 5 mM NADPH or NADH. The fluorescence was measured for 10 minutes at room temperature on a Luminescence Spectrometer PerkinElmer LS-55 equipped with 96-well plate reader using the excitation wavelengths 530 nm and the emission wavelengths 585 nm. Enzyme activities were quantified using a resorufin standard curve.

2.5.3 Sudan I oxidation

CYP1A1 enzymes are able to metabolise the substrate Sudan I to 4'-hydroxy-, 6'hydroxy-, 3'4-dihydroxy- and 4'6-dihydroxy-Sudan I by hydroxylation (**Figure 2.3**) The amount of hydroxylated metabolites produced within a set time can be used to

measure CYP1A1 activity. Microsomal fractions (see section 2.3) at a concentration of 0.5 mg/ml of protein were preincubated with 100 µM Sudan I for 5 minutes at 37°C; total incubation volume was 500 µL with phosphate buffer (50 mM NaH_2PO_4; pH 7.4). The reaction was initiated with the addition of 50 µL of 10 mM NADPH or NADH. The samples were incubated for 30 minutes at 37°C, shaking at 250 rpm. The reaction was stopped with the addition of 1 mL of ethyl acetate and the metabolites extracted by shaking for 2 minutes at 1400 rpm and centrifuged at 4000 rpm for 5 minutes. The upper layer of ethyl acetate was collected and the process repeated a second time with 750 µL ethyl acetate. The collected ethyl acetate layers were pooled and evaporated to dryness and stored at –20°C. The samples were resuspended in 30 µL of HPLC grade methanol and analysed by HPLC on a Nucleosil® C18 reverse phase column, (250 × 4 mm, 5 µm; Machery-Nagel, Düren, Germany) using a Dionex

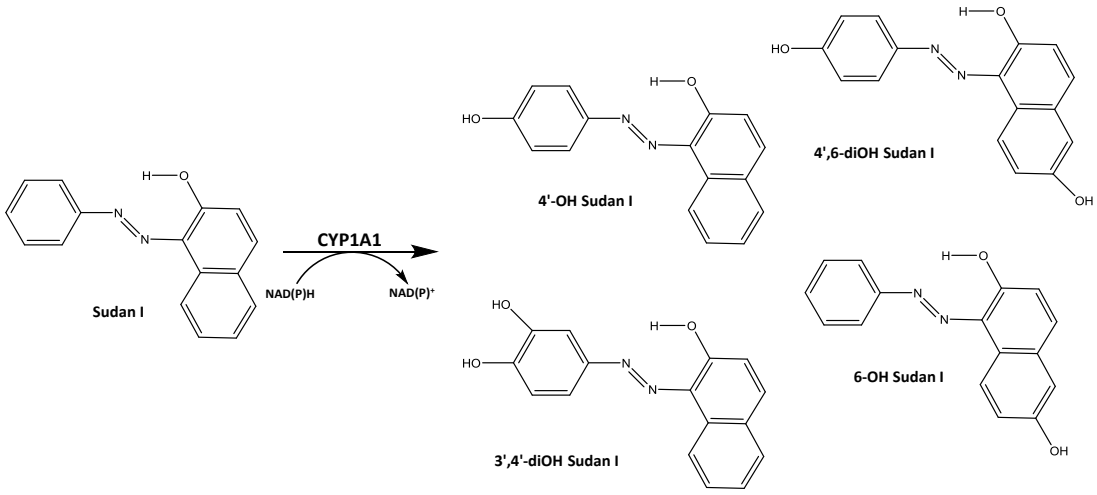

Figure 2.3: Schematic of the hydroxylation of Sudan I by Cyp1a1 to the metabolites 4'-hydroxy-, 6'-hydroxy-, 3',4-dihydroxy- and 4',6-dihydroxy-Sudan I in the presence of the enzymatic cofactors NADPH or NADH.

system consisting of a P580 pump, a UV/VIS Detector UVD 170S/340S, an ASI-100 Automated Sample Injector a thermobox column oven LCO 101 and an In-Line Mobile Phase Degasser Degasys DG-1210 Dionex controlled with Chromeleon™ 6.11

build 490 software. The chromatographic separation of Sudan I metabolites was carried out under the following conditions: 100% 200 mM NH_4HCO_3; pH 8.5 at a flow rate of 0.7 mL/min. Metabolites were detected at 480 nm.

2.5.4 Testosterone hydroxylation

CYP3A4 is able to catalyse the hydroxylation of testosterone in the presence of NADPH and NADH and the resulting metabolites can be measured using HPLC allowing the activity of CYP3A4 enzymes to be determined (**Figure 2.4**). The incubation mixture contained in a final volume of 500 µL: phosphate buffer (100 mM KH_2PO_4; pH 7.4), 50 µM testosterone (10 mM stock in 100% methanol) and 0.5 mg/ml hepatic microsomal protein (see section 2.3). Negative control reactions lacked either microsomal protein, testosterone or enzymatic cofactor. The samples are preincubated for 5 minutes at 37 °C and then the reaction started with the addition of 1 mM NADPH or NADH. The incubation is carried out for 15 minutes at 37°C at 400 rpm. After incubation the reaction was terminated by the addition of 100 µL 1 M aqueous Na_2CO_3 containing 2 M NaCl. Five µL of 1 mM phenacetine (PA) was added as an internal standard. The metabolites were extracted by adding 1 mL of dichloromethane (DCM) to the reaction mixture, shaking for 2 minutes at 1400 rpm before centrifuging for 5 minutes at 13,000 rpm. The DCM layer was removed and collected before the extraction process was repeated. The pooled DCM was then evaporated to dryness using a speedvac evaporator and the samples stored at –20°C. Testosterone and its metabolite 6-β-hydroxytestosterone were separated on Nucleosil (C18) HPLC column (4.6 × 25 mm, 5 µm, Macherey-Nagel, Germany) using a Dionex system consisting of a P580 pump, a UV/VIS Detector UVD 170S/340S, an ASI-100 Automated Sample Injector a thermobox COLUMN OVEN LCO 101 and an In-Line

Mobile Phase Degasser Degasys DG-1210 Dionex controlled with Chromeleon™ 6.11 build 490 software.

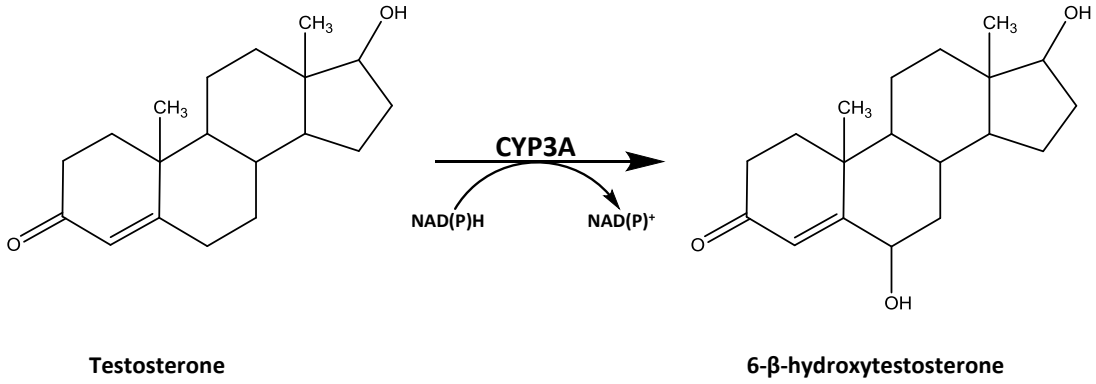

Figure 2.4: Schematic of the hydroxylation of testosterone by Cyp3a in the presence of the enzymatic cofactors NADPH or NADH.

The chromatographic separation of testosterone metabolites was carried out under the following conditions: 75% Methanol (in water) at a flow rate of 0.5 mL/min. Metabolites were detected at 254 nm.

2.6 Microsome *in vitro* incubations

2.6.1 Metabolite formation

2.6.1.1 BaP

Incubation mixtures contained 100 mM potassium phosphate buffer (pH 7.4), NADPH or NADH, pooled hepatic microsomal fraction (0.5 mg protein) and 50 µM BaP (dissolved in 5 µL dimethyl sulfoxide [DMSO]) in a final volume of 500 µL. Control incubations were carried out (*i*) without microsomes; (*ii*) without NADPH or NADH; (*iii*) without BaP. Incubations were carried out at 37°C for 20 minutes. After the incubation, 5 µL of 1 mM PA in methanol was added as an internal standard. BaP

metabolites were extracted twice with ethyl acetate (1 mL), solvent evaporated to dryness and stored at –20°C.

HPLC analysis was performed on the dried ethyl acetate extract of BaP metabolites (see section 3.3) on a Nucleosil® C18 reverse phase column, (250 × 4 mm, 5 µm; Machery-Nagel, Düren, Germany) using a Dionex system consisting of a P580 pump, a UV/VIS Detector UVD 170S/340S, an ASI-100 Automated Sample Injector a termobox column oven LCO 101 and an In-Line Mobile Phase Degasser Degasys DG-1210 Dionex controlled with Chromeleon™ 6.11 build 490 software. The dried samples were resuspended in 25 µL of HPLC-grade methanol and an aliquot of 20 µL was injected onto the HPLC. The chromatographic separation of BaP metabolites were carried out under the following conditions: 50% acetonitrile (aqueous) (*v*/*v*), with a linear gradient of 0-100% of 85% acetonitrile at a flow rate of 0.6 mL/minute. Metabolites were detected by UV absorption at 254 nm and the areas under the curve were calculated relative to the peak area of the internal standard phenacetin and expressed as relative peak areas. Total metabolite values were calculated by combining the values for all peak areas relative to phenacetin for each sample. This approach for measuring metabolite formation does not allow accurate quantification of metabolites, therefore results are expressed as a relative comparison between the different mouse models. BaP metabolite peaks were identified previously through collection of fractions that were analysed by NMR and/or mass spectrometry (Stiborova et al. 2014c). BaP metabolites were identified based on this previous study.

2.6.1.2 Ellipticine

Incubation mixtures contained 100 mM potassium phosphate buffer (pH 7.4), NADPH or NADH (1 mM), 25 µM ellipticine dissolved in 5 µL DMSO and pooled hepatic microsomal fraction (0.5 mg/mL protein) in a final volume of 500 µL. Incubations were carried out at 37°C for 20 minutes. Control incubations were carried out (*i*) without microsomes; (*ii*) without NADPH or NADH; (*iii*) without ellipticine. After incubation, 5 µL of 1 mM PA in methanol was added as an internal standard. Ellipticine metabolites were extracted twice with ethyl acetate (1 mL), solvent evaporated to dryness.

HPLC analysis was performed on the dried ethyl acetate extract of ellipticine metabolites on a Ultrasphere ODS C18 column, (250 × 4.6 mm, 5 µm preceded by a C18 guard column; Beckman) using a Dionex system consisting of a P580 pump, a UV/VIS Detector UVD 170S/340S, an ASI-100 automated sample injector a termobox column oven LCO 101 and an In-Line Mobile Phase Degasser Degasys DG-1210 Dionex controlled with Chromeleon™ 6.11 build 490 software. The eluent was 64% methanol plus 36% of 5 mM heptane sulfonic acid in 32 mM acetic acid in water with a flow rate of 0.8 mL/minute and detection was at 296 nm. Three ellipticine metabolites with the retention times of 6.3, 6.9 and 7.8 minutes were separated and areas under the curve were calculated relative to the peak area of the internal standard phenacetin and expressed as relative peak areas. Total metabolite values were calculated by combining the values for all peak areas relative to phenacetin for each sample. As indicated above, this approach does not allow accurate quantification of metabolites, therefore results are expressed as a relative comparison between the different mouse models. Ellipticine metabolite peaks were previously identified

through collection of fractions that were analysed by NMR and/or mass spectrometry (Stiborova et al. 2004). Ellipticine metabolites were identified based on this study.

2.6.2 DNA adduct formation

2.6.2.1 BaP

Incubation mixtures consisted of 50 mM potassium phosphate buffer (pH 7.4). One mM NADPH or NADH, pooled hepatic microsomal fraction (0.5 mg protein) from HRN, HBRN and WT mice (either untreated or pretreated with BaP), 0.1 mM BaP (dissolved in 7.5 µL DMSO) and calf thymus DNA (0.5 mg) in a final volume of 750 µL. Control incubations were carried out (*i*) without microsomes; (*ii*) without NADPH or NADH; (*iii*) without DNA and (*iv*) without BaP. Incubations were carried out at 37°C for 90 minutes (Arlt et al., 2008). After the incubation, DNA was isolated by a standard phenol-chloroform extraction method as described in section 2.13.1. BaP-DNA adduct formation was determined by ^{32}P-postlabelling as described in section 2.14.

2.6.2.2 Ellipticine

Incubation mixtures consisted of 100 mM potassium phosphate buffer (pH 7.4). NADPH or NADH (10 mM in each case), pooled hepatic microsomal fraction (0.5 mg/mL protein) from ellipticine-pretreated HRN, HBRN and WT mice, 0.1 mM ellipticine dissolved in 7.5 µL methanol and calf thymus DNA (0.5 mg) in a final volume of 750 µL. Incubations were carried out at 37°C for 90 minutes (Stiborova et al., 2008). Control incubations were carried out (*i*) without microsomes; (*ii*) without NADPH or NADH; (*iii*) without DNA and (*iv*) without ellipticine. After incubation, DNA was isolated by a standard phenol-chloroform extraction method. Ellipticine-

DNA adduct formation was determined by ^{32}P-postlabelling as described in section 2.14.

2.7 Cell culture

2.7.1 Cell lines

Mouse hepatoma Hepa-1c1c7 and human hepatocarcinoma HepG2 cells were originally obtained from the American Type Culture Collection (ATCC). HepG2 POR KO cells were obtained from HeraBioLabs, USA. Hepa-1c1c7 cells were cultured in 75-cm^2 flasks (Thermo Scientific) using minimum essential medium (MEM) alpha medium (Life technologies) with 10% foetal bovine serum (FBS; Invitrogen) and 1% penicillin streptomycin (Life technologies). HepG2 cells were cultured in 75-cm^2 flasks (Thermo Scientific) using MEM (Life Technologies) with 10% FBS (Invitrogen), 1% 100 mM sodium pyruvate, 1% 100X non-essential amino acids and 1% penicillin streptomycin (Life Technologies).The cells were grown in a Heraeus HERAcell humidified incubator which was set at 37°C, 5% CO_2 and 95% air.

2.7.2 Maintenance of cell lines

All cell lines were cultured as adherent mono-layers in flasks with the media regularly changed every 2-3 days. When the adherent cells became confluent (~80-90%) they were sub-cultured to maintain continuous growth. To sub-culture all cell lines, media was removed through aspiration and cells washed with 10 mL of phosphate buffer solution (PBS) which was aspirated before 2.5 ml of 0.05% trypsin-ethylenediaminetetraacetic acid (EDTA, Thermo Fisher) was added. The flask was placed into the incubator for 5-10 minutes in order to detach the adherent cells from

the plastic surface. To protect cells, the trypsin was neutralised with 7.5 mL of FBS-containing media and the cell suspension was transferred to a 50-mL conical tube. The tube was centrifuged at 1500 rpm for 5 minutes using an Eppendorf centrifuge 5804 in order to obtain a cell pellet. The supernatant was removed and the cell pellet resuspended in 5 mL of media. An appropriate volume of the cell suspension was added to a new flask and fresh culture media to reach a total volume of 12 mL.

2.7.3 Counting cells

For seeding cells, cells were counted after detachment with trypsin and subsequent centrifugation. Cell pellets were resuspended in an appropriate amount of fresh cell media. Ten µL of the cell suspension was added to 10 µL of trypan blue stain 0.4% (Life technologies) and the cell number was counted using the Countess™ II automated cell counter (Life Technologies) to give total, live and dead cells per mL. For cell seeding calculations the live count was used.

2.7.4 Preparation of frozen stocks and resurrection for cell culture

For the storage of cell lines, cells were harvested using trypsin-EDTA and collected by centrifugation as described in section 2.4.2. Excess media was aspirated and cell pellets were resuspended in a freezing solution consisting of cell media with 10% (*v*/*v*) DMSO. Aliquots (1 mL) of the cell suspension were transferred into cryovials and frozen for 24 hours at –80°C in a Thermo Scientific™ Mr. Frosty™ Freezing Container to achieve a slow freezing rate. Slow freezing and the presence of DMSO in the freezing solution help to minimise the formation of ice crystals which could potentially damage the cells. After initial freezing the cells were transferred to liquid nitrogen. For the resuscitation of frozen cells, aliquots (1 mL) stored in liquid nitrogen

were thoroughly thawed to 37°C and immediately added to 9 mL of fresh cell culture medium. Cells were washed by centrifugation before being inoculated into tissue culture flasks. Cells were not used for experimentation for at least one week to ensure recovery from the effects of cryopreservation.

2.7.5 Treatment of cells with carcinogens

The day prior to carcinogen treatment, cells were seeded into 6 well plates or T75 cm^2 cell culture flasks so as to be sub-confluent on the day of harvest. Hepa-1c1c7 cells were seeded at approximately 0.48×10^5 cells per well for 6 well plates and treated 48 hours post seeding. HepG2 cells were seeded at approximately 2×10^5 cells per well for 6 well plates and 15×10^5 cells per 75-cm^2 cell culture flask.

As further described in chapter 5, BaP was diluted in complete growth medium to expose Hepa-1c1c7 cells with 0.5 µM BaP (0.1% DMSO final). Cells grown in medium containing 0.1% DMSO alone served as control. Cells were incubated with BaP for 24 hours under standard conditions (37°C, 5% CO_2 and 95% air).

As further described in chapter 6 BaP was diluted in complete growth medium to expose HepG2 cells to 2.5 and 5 µM BaP (0.1% DMSO final). Cells grown in medium containing 0.1% DMSO alone served as control. Cells were incubated with BaP for 24 and 48 hours under standard conditions (37°C, 5% CO_2 and 95% air).

2.8 Generation of CRISPR/Cas9 POR knockout Hepa-1c1c7 cell line

2.8.1 Transfection and selection for genetically modified cells

Hepa-1c1c7 cells were seeded at a density of 1.5×10^5 cells/well. Twenty four hours later they were incubated with 5 µL of transfection reagent (sc-395739; Santa Cruz Biotech) and 1 µg of either the cypor KO (sc-422345; Santa Cruz Biotech) or control double nickase plasmid (sc-418922; Santa Cruz Biotech) that possessed a scrambled guide RNA sequence. The transfection reagent and the plasmid were diluted in Plasmid Transfection Medium (sc-108062; Santa Cruz Biotech) for a total concentration of 300 µL and the solution was left to incubate for 20 minutes at room temperature. The cell medium was aspirated from each of the wells and 3 mL of antibiotic-free medium was added. Transfection solution (300 µL) was added to each well. To confirm successful transfection, cells expressing GFP were visualised using fluorescence microscopy with the Nikon eclipse Te2000-S and the programme NIS Elements D23. The exposure was set at 1 second, the gain at 2.00× and the 4× objective was used. The images were subsequently analysed using NIS Elements D23 to outline and measure the fluorescence of the green areas seen. The background fluorescence of each image was subtracted from each identified fluorescent point which were then summed. Seventy two hours post incubation, successfully transfected cells were selected for using 2.5 µg/mL puromycin (sc-108071; Santa Cruz Biotech) in antibiotic free medium.

2.8.2 Isolation of single cell clones

In order to ensure that a cell line is generated whereby all cells exhibit a uniform level of *Por* disruption, single cells were isolated following successful transfection.

Dilutions of transfected cells potentially consisting of cells not expressing POR were prepared at 5 cells/mL in growth medium and seeded onto 96-well plates (200 µL/well) and the plates were incubated at 37°C, 5% CO_2 and 95% air. The medium was changed every 5 days and within 2 weeks it was possible to visualise expanding populations of single cell clones. Wells that contained none or more than one expanding colony were discarded. Wells containing a single expanding colony were selected, trypsinised and transferred to 24-well plates. As cells approached confluency, they were progressively passaged into larger vessels (24-well to 6-well to 25-cm^2 flask to 75-cm^2 flask). Once cells had reached 80-90% confluency in a 75-cm^2 flask, cells were harvested to produce a frozen stock as described in section 2.4.4 with the reminder of the culture being seeded and harvested for Western blot analysis to confirm the absence of POR protein expression, as described in section 2.8.

2.9 Crystal violet staining assay

The crystal violet (CV) staining assay is a method for determining relative cell survival of a treated population of cells compared to a control population that is inexpensive and rapid (Dooley et al., 1994). Crystal violet (4[(4-dimethylaminophenyl)-phenyl-methyl]-*N*,*N*-dimethyl-aniline) is a dye that stains proteins and DNA. The relative density of an adherent cell culture is a function of the amount of crystal violet staining, measured as absorbance at 595 nm.

Cells were seeded onto 6-well plates and treated, as described in section 2.4.5. Twenty four or 48 hours post exposure, the cell culture media was removed by aspiration and cells were rinsed with PBS and after removal, adherent cells were fixed and stained with 1 mL/well of 0.1% (*w*/*v*) crystal violet (Sigma #C3886) in 10% ethanol for 10

minutes. Cells were washed with PBS to remove excess crystal violet and allowed to dry. For quantification, the dye was resolubilised in 5 mL of 50% ethanol per well and absorbance at 595 nm was determined using an ELx800 plate reader. Data are presented as the amount of absorbance in wells of treated cells relative to that of DMSO-treated cells and are representative of at least three independent experiments.

2.10 Western blot analysis

Following cell harvesting, 300 µL of lysis buffer [62.5 mM tris(hydroxymethyl)aminomethane (Tris, pH 6.8), 1 mM EDTA (pH 8.0), 2% sodium dodecyl sulphate (SDS), 10% sterile glycerol with protease and phosphatase inhibitors (Thermo Scientific)] was added to each of the samples. The samples were sonicated using the Sonic Dismembrator Ultrasonic Processor (Thermo Scientific) at 20% amplitude for 10 seconds. The protein concentration of each sample was determined using the Pierce Bicinchoninic acid (BCA) protein assay (Thermo Scientific), using a ELx800 (BioTek) plate reader. The protein concentration of each sample was normalised to obtain equal concentrations of each sample using lysis buffer, β-mercaptoethanol and bromophenol blue. The samples were heated at 95°C for 10 minutes to denature proteins. Once the samples cooled to room temperature they could then be stored at –20°C for further analysis.

For SDS-polyacrylamide gel electrophoresis (SDS-PAGE) protein separation NuPAGE^{TM}4-12% Bis-Tris Gels (Invitrogen) were used. As running buffer, a 1X solution was made up by diluting the 20X stock solution of 2-(*N*-morpholino) ethanesulfonic acid (MES) (Life Technologies) by adding deionised water. An appropriate volume containing 10 µg of protein per sample was loaded into the wells

of the gel, and 2 µL of the size marker (PageRuler^{TM} Prestained Protein Ladder, Thermo Scientific) was also loaded. The gel was run at 130 V for 1.5 hours. Following this, the proteins were transferred from the gel to a nitrocellulose membrane (Bio-Rad) using 1X transfer buffer prepared from a 20X NuPAGE stock solution (Invitrogen) along with methanol in a 1:2:17 dilution of stock:methanol:water. During the transfer the XCell II Blot Module (Invitrogen) was run at 110 V for 1.5 hours. The protein transfer was checked by staining the membrane with Ponceau S solution (Sigma). The membrane was washed briefly with deionised water and then with 1X TBST made by diluting the 10X TBS stock solution (Alpha Diagnostic Intl) with 0.1% Tween (Sigma). The membrane was left to blot in 3% dry skimmed milk dissolved in TBST for ~1 hour on an orbital mixer (Denley, UK).

The blots were incubated with primary antibodies overnight. These included the primary antibody to the housekeeping gene glyceraldehyde phosphate dehydrogenase (GAPDH; MAB374 Chemicon) in a 1:2500 dilution in 3% TBST milk to be used as a loading control. The antibodies used were all diluted in 3% TBST milk with a dilution factor of 1:1000 for anti-POR (ab39995, abcam), 1:1000 for anti-CYP1A1 (sc-20772 (H-70); Santa Cruz Biotech), 1:500 for anti-Cyb5 (sc-33174 (H-114) Santa Cruz Biotech) and 1:1000 for anti-Cyb5R (ABIN453978, Antibodies-online.com). These antibodies were separately incubated with the membrane at 4°C overnight, with the exception of GAPDH which was incubated at room temperature for 30 min. After incubation, the membranes were washed three times with TBST for 5-10 minutes each time. The membranes were incubated with the corresponding secondary antibody for 1 hour. The secondary antibodies used were diluted 1:10,000 with 3% TBST milk and included the anti-rabbit horse radish peroxidase (HRP)-conjugated secondary antibody

(Cell Signalling Technology), the anti-goat HRP-conjugated antibody (Santa Cruz Biotech), the anti-mouse HRP-conjugated antibody (Cell Signalling Technology). Subsequent to secondary antibody incubation, the membranes were washed for ~10 minutes three times with TBST. To detect the probed proteins, chemiluminescence detection was carried out using the ECL™ Western Blotting reagents (GE Healthcare, Amersham) in accordance with the manufacturer's instructions. Equal volumes of Detection Reagents 1 and 2 were mixed and used to cover the membrane for 3-5 minutes. The membranes were placed in a film cassette, and the films were developed in a dark room using a Konica Minolta SRX-101A processor.

2.11 Detection of metabolites in cell culture

For the analysis of metabolite formation, culture medium (1 mL) from exposed cells were collected and stored at –20°C until further processing. Prior to the extraction of metabolites, 5 µL of 1 mM phenacetine was added to each of the culture medium aliquots and vortexed. Ethyl acetate (900 µL) was then added to each aliquot and shaken at 1400 rpm for 2 minutes before being centrifuged for 5 minutes at 13,000 rpm. The upper ethyl acetate phase was removed and transferred to a new Eppendorf tube. Another 900 µL was added to the culture medium and the process repeated, pooling the ethyl acetate layers from each extraction and discarding the culture medium. The ethyl acetate was then evaporated to dryness using a speedvac evaporator and samples stored at –20°C.

For the analysis of BaP metabolites, extracts were resuspended in 30 µL methanol, of which 25-µL aliquots were injected on HPLC. HPLC analysis was performed using a HPLC Agilent 1100 System (Agilent Technologies) with a SunFire™ C18 reverse

phase column (250 × 4.6 mm, 5 µm with a column guard; Waters). The conditions used for the chromatographic separation of BaP metabolites were as follows: mobile phase A: 100% water, mobile phase B: 100% acetonitrile. The separation started with an isocratic elution of 50% of mobile phase B. Then a linear gradient to 98.5% of mobile phase B in 34.5 minutes was followed by isocratic elution for 6 min, a linear gradient from 98.5% to 1.4% of mobile phase B in 3 minutes, followed by an isocratic elution for 1.5 minutes. Total run time was 45 minutes at a flow rate of 1 mL/minute. The metabolites were analysed by fluorescence detection (0-6 min excitation 341 nm, emission 381 nm and 6-45 minutes excitation 380 nm, emission 431 nm). Areas under the curve were calculated relative to the peak area of the internal standard phenacetin and expressed as relative peak areas. As outlined above, results are expressed as a relative comparison between the different cell models. BaP metabolites were identified as described (Stiborova et al., 2014c).

2.12 Single-cell gel electrophoresis (comet) assay

The alkaline version of the comet assay was used to detect DNA damage including single- and double-strand breaks and alkali-labile (*e.g.* apurinic) sites (Arlt et al., 2004, Dusinska and Collins, 2008). These strand breaks may be induced directly by a reactive compound or caused indirectly during the excision step of base/nucleotide excision repair or by processes such as reactive oxygen species (ROS) generated during metabolism of a compound.

Cells were seeded in a 6-well plate and exposed as described in section 2.4.5. After treatment cells were harvested using trypsin, pelleted and resuspended in PBS. Twenty µL of cell suspension was embedded in 180 µl of 0.6% low melting-point agarose (*w/v*

PBS) at 37°C. Thirty µL of the agarose mixture was transferred to a glass slide pre-coated with 1.5% agarose and allowed to set on a cold plate (4°C). The slides were then immersed in lysis buffer (1% Triton 100-X, 2.5 M NaCl, 10 mM Tris and 0.1 M EDTA, pH 10.0) and kept at 4°C in the dark for 1 hour. DNA was then unwound by immersing the slides in alkaline buffer (0.3 NaOH, 1 mM EDTA, pH 13.0) for 40 minutes at 4°C before electrophoresis in a tank (27.5 × 21.5 cm; Scie-Plas, Warwickshire, UK) fitted with a cooling unit to maintain the buffer temperature of 4°C. Electrophoresis was performed at 0.3 A for 20 minutes. Slides were then neutralised by immersing in PBS for 5 minutes, washed by immersing in distilled water for 5 minutes and fixed by immersion in methanol for 5 minutes before being left to dry at room temperature overnight. Nuclei were stained by immersing the slide in ethidium bromide for 5 minutes and washing in distilled water for 5 minutes (**Figure 2.5**). DNA damage was scored using the Comet IV capture system (version 4.11; Perceptive Instruments, UK). At least 50 nuclei were assessed per slide, and tail intensity (% tail DNA) was used as the measure of DNA damage induced, as recommended (Collins et al., 2008). The average tail intensity of three replicate treatments was calculated.

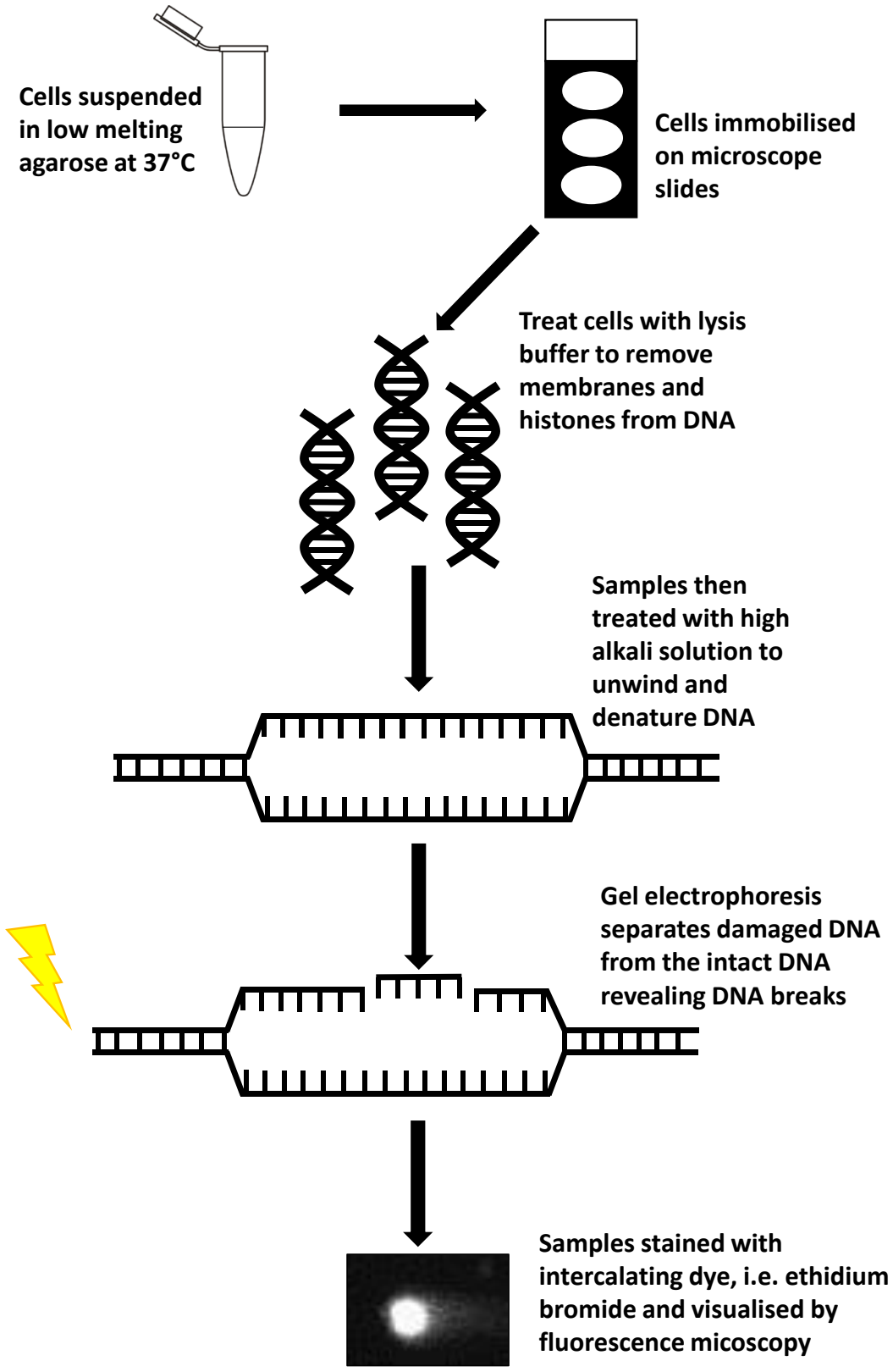

Figure 2.5: Schematic of the single-cell gel electrophoresis (comet) assay.

2.13 DNA isolation using phenol-chloroform extraction

2.13.1 DNA isolation from microsomal incubations

DNA was extracted from incubation mixtures stepwise with equal volumes (400 µL) of phenol (P4557, Sigma), phenol:chloroform:isoamyl alcohol (25:24:1; *v*/*v*) (P2069, Sigma) and chloroform:isoamyl alcohol (24:1; *v*/*v*). DNA was precipitated after adding 1/10th volume NaCl (5 M) and 2 volumes of ice-cold ethanol. The DNA was fished, pelleted and washed with 300 µL 70% ethanol. DNA was resuspended in 100-250 µL TE buffer (10 mM, 1 mM, pH 8.0) and dissolved overnight at 4°C. Finally, samples were incubated at 37°C for 3 hours before DNA concentration and purity were determined spectrophotometrically by measuring UV absorbance at 260, 280 and 230 nm. DNA was stored at –20°C.

2.13.2 DNA isolation from cells

Cell pellets were thawed and resuspended in 400 µL of Tris-EDTA (50 mM, 1 mM, pH 8.0). Each sample was then mixed with 45 µg RNase A (R4875, Sigma) 225 U RNase T1 (R1003, Sigma) and 40 µL 10% SDS in 10 mM EDTA and vortexed and incubated at 37°C for 30 minutes. Next, 40 µL proteinase K (10 mg/mL; P6550, Sigma) was added, resuming incubation at 37°C overnight. Samples were extracted stepwise with equal volumes (400 µL) of phenol, phenol:chloroform:isoamyl alcohol (25:24:1; *v*/*v*) and chloroform:isoamyl alcohol (24:1; *v*/*v*). DNA was precipitated after adding 1/10th volume NaCl (5 M) and 2 volumes of ice-cold ethanol. The DNA was fished, pelleted and washed with 300 µL 70% ethanol. DNA was resuspended in 100-250 µL TE buffer (10 mM, 1 mM, pH 8.0) and dissolved overnight at 4°C. Finally, samples were incubated at 37°C for 3 hours before DNA concentration and purity were

determined spectrophotometrically by measuring UV absorbance at 260, 280 and 230 nm. DNA was stored at –20°C (Arlt et al., 2001).

2.13.3 DNA isolation from animal tissue

Tissue samples (~30 mg) were homogenised in 400 µL of Tris-EDTA buffer (50 mM, 1 mM, pH 8.0). After the addition of 40 µL proteinase K (10 mg/ml) and 40 µL of 10% SDS in 10 mM EDTA samples were vortexed and incubated at 37°C overnight. Samples were extracted stepwise with equal volumes (400 µl) of phenol, phenol:chloroform:isoamyl alcohol (25:24:1; *v*/*v*) and chloroform:isoamyl alcohol (24:1; *v*/*v*). DNA was precipitated after adding $1/10^{th}$ volume NaCl (5 M) and 2 volumes of ice-cold ethanol. The DNA was fished, pelleted and washed with 300 µL 70% ethanol. Pellets were resuspended in 300 µL of Tris-EDTA buffer (50 mM, 1 mM, pH 8.0) and dissolved overnight at 4°C. Subsequently, samples were incubated at 37°C for 2 hours before adding 45 µg RNase A, 225 U RNase T1 and incubating at 37°C for a further 30 min. Residual proteins were removed at 37°C for 2 hours by proteinase K digestion (40 µL; 1 mg/mL) before samples were again extracted with phenol, phenol:chloroform:isoamyl alcohol and chloroform:isoamyl alcohol. After adding $1/10^{th}$ volume NaCl (5 M) and 2 volumes of ice-cold ethanol, the DNA was fished, pelleted and washed with 300 µL 70% ethanol. DNA was resuspended in 100-300 µL TE buffer and dissolved overnight at 4°C. Finally, samples were incubated at 37°C for 3 hours before DNA concentration and purity were determined spectrophotometrically by measuring UV absorbance at 260, 280 and 230 nm. DNA was stored at –20°C.

2.14 DNA adduct analysis

2.14.1 DNA adduct analysis by ^{32}P-postlabelling

The ^{32}P-postlabelling assay provides an ultrasensitive method for the detection of DNA adducts (Phillips and Arlt, 2007).

2.14.2 DNA digestion

DNA samples (4 µg) were evaporated to dryness under vacuum in a speedvac evaporator and digested with 4 µg micrococcal nuclease (30 mU/µL; N3755, Sigma) and calf spleen phosphodiesterase (10 mU/µL; 02100977, MP Biomedical, UK) mixed with 0.8 µL digestion buffer (100 mM sodium succinate, 50 mM $CaCl_2$, pH 6.0) and incubated overnight at 37°C (**Figure 2.6**).

2.14.3 Nuclease P_1 digestion enrichment

Nuclease P_1 digestion was used to enrich for adducted deoxyribonucleoside 3'-monophosphates. This procedure is based on the principle that some bulky adducts, such as those formed by BPDE, create a steric hindrance that inhibits nuclease P_1 binding, thereby leaving the 3'-phosphate group intact in the adducted deoxyribonucleoside 3'monophosphates, while it is cleaved in normal (unmodified) deoxyribonucleoside 3'-monophosphates (Reddy and Randerath, 1986) (**Figure 2.6**). DNA digests (see section 2.12.2) were incubated with 0.96 µL nuclease P_1 (1.25 µg/µL, Sigma #N8639), 1.44 µl zinc chloride (2 mM) and 2.4 µL sodium acetate (0.25 M, pH 5.0) for 1 hour at 37°C. Reactions were terminated by the addition of 1.92 µL Tris base (0.5 M).

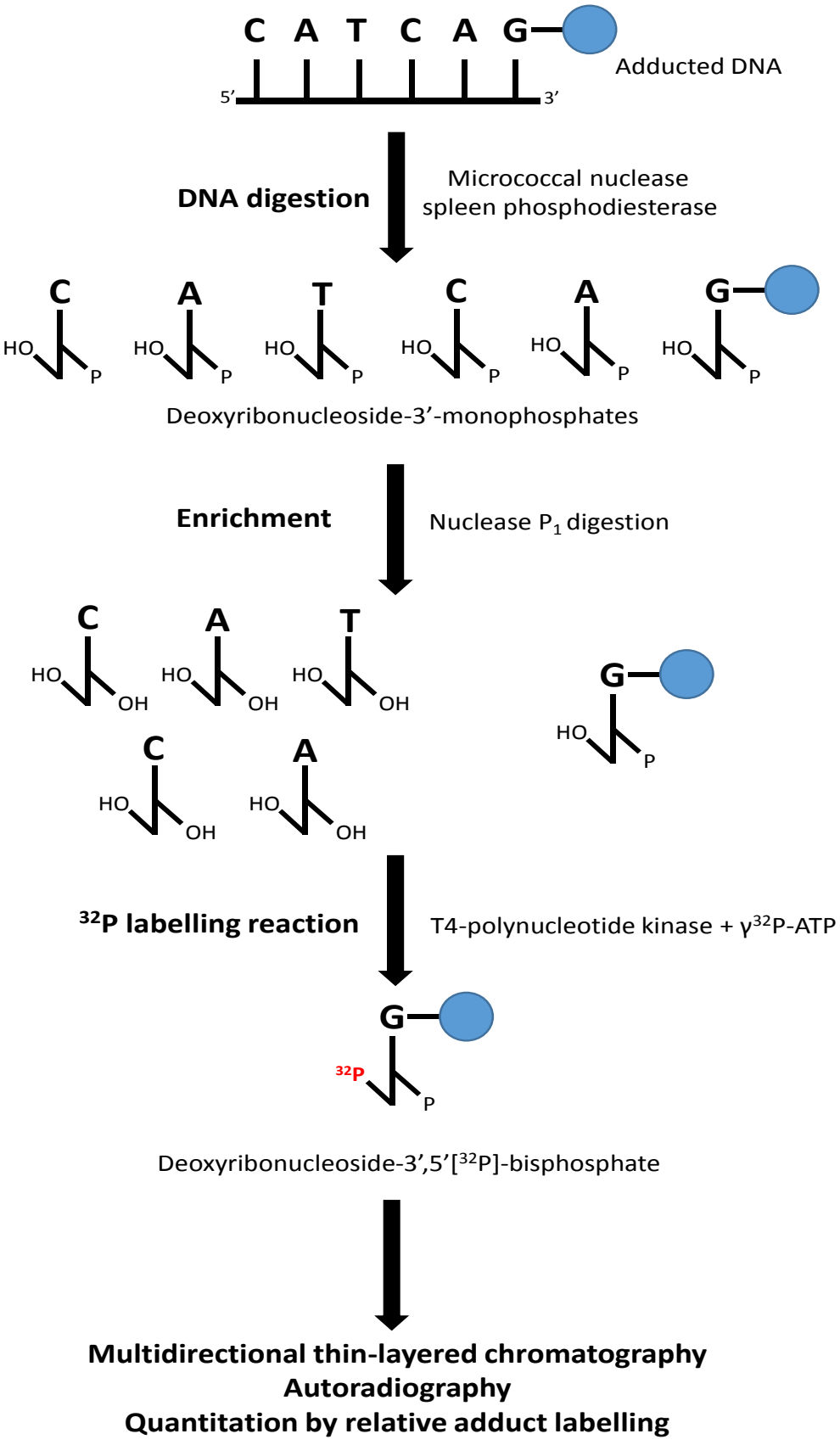

Figure 2.6: Schematic of DNA adduct analysis using the ^{32}P-postlabelling assay.

2.14.4 ^{32}P-postlabelling reaction

In this reaction T4 polynucleotide kinase phosphorylates nucleoside-3'-monophosphates at the 5'-position with ^{32}P-orthophosphate. Enriched samples (see section 2.12.4) were ^{32}P-postlabelled using carrier-free [γ-^{32}P]ATP (50 µCi, ~7000 Ci/mmol, Hartmann Analytic, Braunschweig, Germany) in a mixture consisting of 1 µL 10X digestion buffer (200 mM bicine (pH 9.0), 100 mM $MgCl_2$, 100 mM dithiothreitol (DTT), 10 mM spermidine) and 0.2 µL T4 polynucleotide kinase (30 U/µl, USB, Ohio, USA) for 30 minutes at 37°C.

2.14.5 Thin-layer chromatography

Resolution of ^{32}P-postlabelled adducted deoxyribonucleoside 3'-monophosphates was carried out by multi-directional thin-layer chromatography (TLC) on 10 × 20 cm polyethyleneimine cellulose plates (Macherey-Nagel, Düren, Germany) with a paper wick stapled to the top, as previously described (**Figure 2.7**) (Phillips and Arlt, 2007). The solvent compositions for the resolution of BaP- or BPDE-DNA adducts were D1: 1.0 M sodium phosphate (pH 6.0); D2: 3.5 M lithium formate, 8.5 M urea (pH 3.5); D3: 0.8 M lithium chloride, 0.5 M Tris-HCl, 8.5 M urea (pH 8.0). The solvent compositions for ellipticine-DNA adducts were D1: 1.0 M sodium phosphate, (pH 6.8); D2: 3.5 M lithium formate, 8.5 M urea (pH 4.0); D3: 0.8 M Lithium Chloride, 0.5 M Tris, 8.5 M urea (pH 9.0).

Each labelling reaction mixture was spotted onto a TLC plate at the origin and placed into a glass tank containing 70 mL solvent D1 overnight, with the paper wick hanging over the edge of the tank. The following day the paper wicks were removed and TLC plates cut at the 10-cm centre line, discarding the top half (containing the excess of

unlabelled [γ-^{32}P]ATP). Plates were washed in water and dried. The plates were positioned 180° to the direction of D1 and run in 70 ml of solvent D3 for ~1.5 hr (until the solvent front reached the top of the plate). Plates were again washed in water and dried. Finally, plates were positioned 90° counter clockwise to the direction of D3 and run in 70 mL of solvent D4 as done for D3. Plates were then washed in water and dried prior to quantitation.

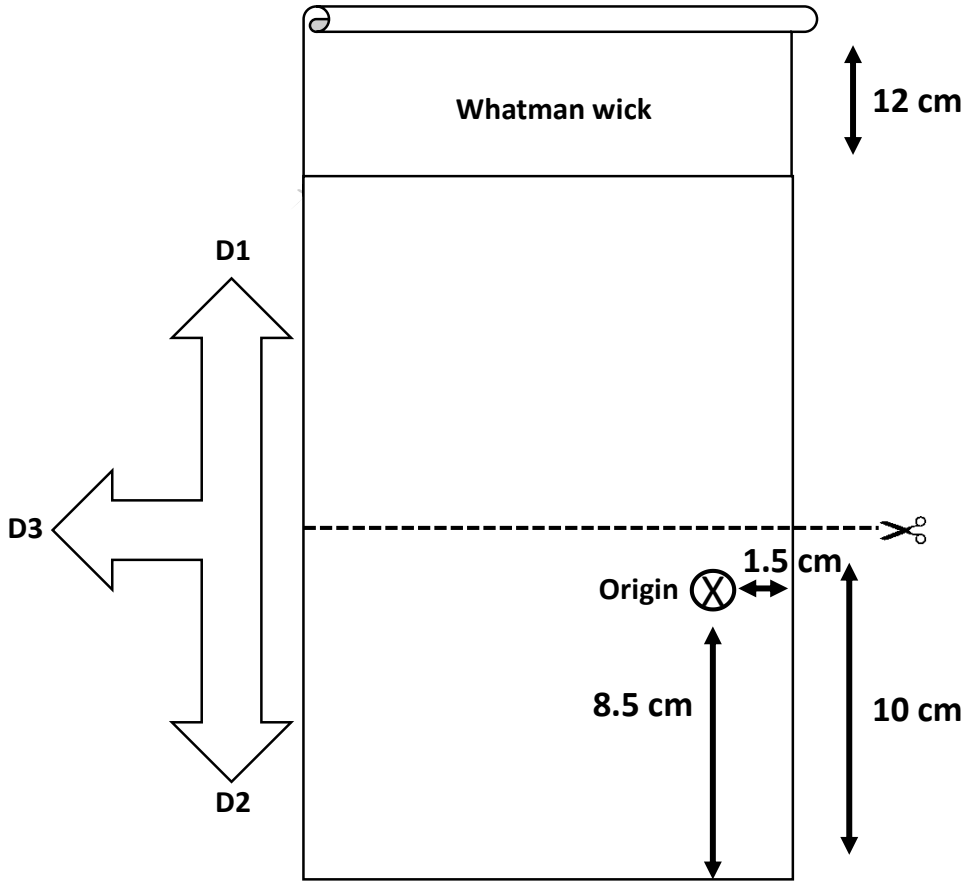

Figure 2.7: Schematic of the multidirectional TLC. Adapted from Phillips et al. 2005.

2.14.6 Quantitation of ^{32}P-postlabelled DNA adducts

After chromatography, TLC plates were scanned using a Packard Instant Imager (Dowers Grove, IL, USA) to image and quantify DNA adduct levels. The imager

measures β particle emission from adduct spots as counts per minute (cpm). Background readings from the TLC plate were subtracted.

DNA adduct levels (RAL, relative adduct labelling) were calculated from adduct cpm, the specific activity of [γ-^{32}P]ATP and the amount of DNA (pmol) used. Results were expressed as DNA adducts/10^8 nucleotides.

3 Cytochrome b_5 impacts on cytochrome P450-mediated metabolism of benzo[*a*]pyrene and its DNA adduct formation: studies in Hepatic Cytochrome b_5/P450 Reductase Null (HBRN) mice

3.1 Introduction

BaP is a procarcinogen that requires metabolic activation via a P450-dependent pathway before reacting with DNA and exerting its genotoxic effects (**Figure 3.1**) (Luch and Baird, 2005, Phillips, 2005). CYP1A1 and CYP1B1 play a major role in this pathway, catalysing the initial oxidation of BaP to BaP-7,8-epoxide, which is then converted to BaP-7,8-dihydrodiol by epoxide hydrolase (Baird et al., 2005, Luch and Baird, 2005). BaP-7,8-dihydrodiol then undergoes further bioactivation by CYP1A1 and CYP1B1 to form the ultimately reactive species, BaP-7,8-dihydrodiol-9,10-epoxide (BPDE). BPDE reacts with DNA to form the pre-mutagenic adduct 10-(deoxyguanosin-N^2-yl)-7,8,9-trihydroxy-7,8,9,10-tetrahydro-BaP (dG-N^2-BPDE) (Arlt et al., 2008, Kucab et al., 2015, Long et al., 2017).

The HRN mouse model has been used previously to investigate the role of hepatic P450 enzymes in the bioactivation of BaP (Arlt et al., 2015a). HRN mice treated with BaP formed up to 13-fold higher levels of BaP-DNA adducts than WT mice indicating that hepatic P450 enzymes play a more important role in the detoxification of BaP *in vivo* despite their importance for BaP activation *in vitro* (Arlt et al., 2008). This result was investigated further by using immunohistochemistry that showed HRN mice have ample capacity for the formation of BaP-DNA adducts (i.e. d-N^2-BPDE) in the liver

and no differences in BaP-DNA adduct formation was observed between hepatocytes (i.e. POR-deficient cells) and non-hepatocytes (i.e. POR-proficient cells) (Arlt et al., 2012).

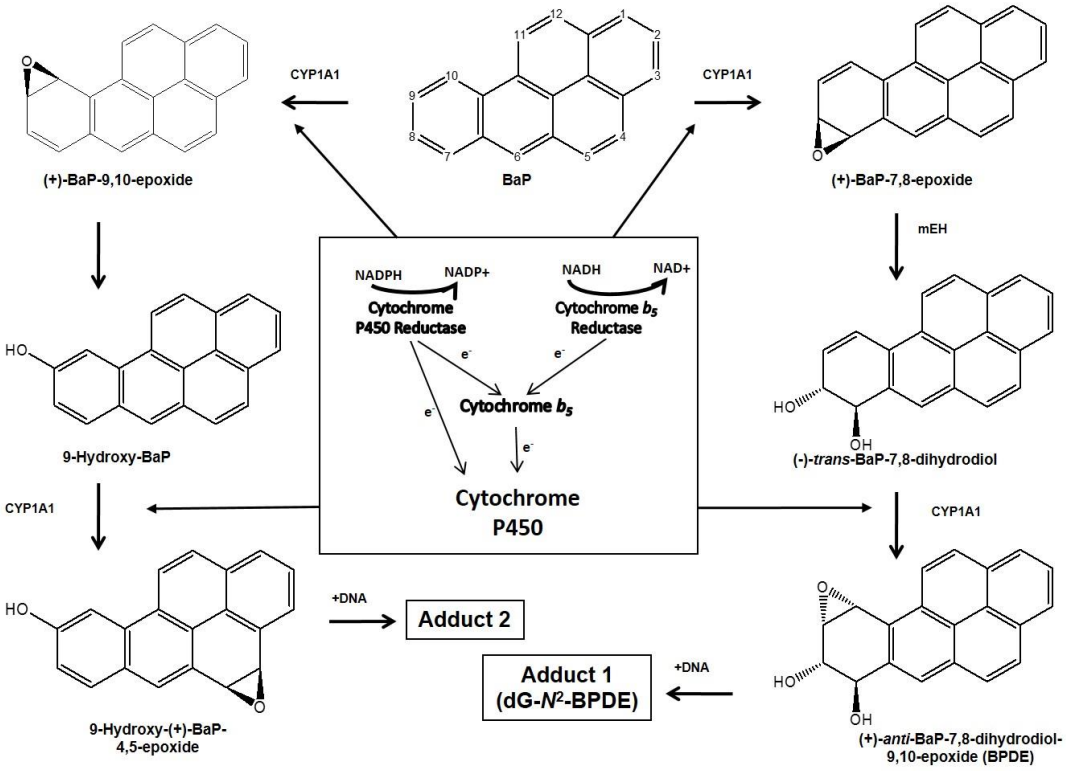

Figure 3.1: Pathways of biotransformation and DNA adduct formation of BaP catalysed by CYP1A1 and mEH. The three-stage pathway, involving mEH, forming the ultimately reactive species BPDE that binds to guanine to form the dG-*N2*-BPDE adduct (adduct 2) is shown on the right. The two-stage pathway that does not involve mEH forms the second adduct that is seen in *in vitro* studies. The diagram in the centre shows the roles of POR, Cyb5R and Cyb5 as electron donors to P450 enzymes such as CYP1A1 that are central to the biotransformation of BaP.

Although the specific enzyme(s) involved in the generation of BaP-DNA-binding species in the liver of HRN mice is not known, it is clear that the process does not produce a different reactive species from that formed in WT mice (Arlt et al., 2008, Arlt et al., 2012). Although POR is deemed to be the predominant electron donor to P450 enzymes (Guengerich, 2008), Cyb5 has also been shown to act as the electron

donor both *in vitro* and *in vivo* (Finn et al., 2008, Yamazaki et al., 2002), and could be contributing to BaP-DNA adduct formation in the livers of HRN mice.

Previously it was found that HRN mice exhibited a higher protein expression of Cyb5 than in WT mice after repeated BaP exposure. Similar results were found for mEH, another important enzyme involved in the formation of the DNA-reactive intermediate BPDE (Arlt et al., 2012). Reconstituted systems utilising CYP1A1, POR, Cyb5, and mEH in different ratios were used to investigate the role of Cyb5 in the metabolic activation of BaP *in vitro.* The results showed that even when levels of POR were low, CYP1A1, Cyb5, and mEH were able to activate BaP into reactive species that bind to DNA (Stiborova et al., 2014c). In addition to this, both the enzymatic cofactors NADPH (cofactor for the POR system) and NADH (cofactor for the Cyb5/Cyb5R system) stimulated CYP1A1-mediated BaP bioactivation *in vitro*, suggesting that the NADH/Cyb5R/Cyb5 system is able to act as sole electron donor to CYP1A1-catalysed BaP bioactivation (Stiborova et al., 2016a, Stiborova et al., 2016b). The findings from the reconstituted systems suggest that even low POR expression in the livers of HRN mice (probably in non-parenchymal cells), in combination with the induction of Cyp1a1, Cyb5 and mEH by BaP, might be sufficient for efficient BaP bioactivation *in vivo*, replacing NADPH-dependent POR in the CYP1A1-catalysed activation of BaP (Stiborova et al., 2014c). Given the increased protein expression of Cyb5 in HRN mice after repeated BaP exposure (Arlt et al., 2012), it is possible that Cyb5 could compensate for the absence of POR in the HRN mice and stimulate P450-mediated BaP bioactivation.

In the present study both the HRN and HBRN mouse models have been used to investigate the contribution of Cyb5 to the metabolic activation of BaP both *in vitro*

and *in vivo* by isolating the hepatic microsomal fractions from WT, HRN and HBRN mice and assessing enzyme activity and BaP-metabolite formation. BaP-DNA adduct formation was analysed to try and elucidate the role of Cyb5 in the activation of BaP both *in vitro* and *in vivo*.

3.2 Materials and Methods

WT, HRN and HBRN mice were treated as described in section 2.2.1 and the hepatic microsomal fractions were isolated according to section 2.4. The Western blotting was carried out on pooled microsomal fractions according to section 2.10. Similarly, for all enzyme activity assays and incubations pooled microsomal fractions were used. It was not possible to carry out biological repeats due to tissue limitations impacting on the yield of microsomal fractions. Enzyme activities were analysed by determining the reduction of cytochrome *c* (i.e. POR), dealkylation of 7-ethoxyresorufin to resorufin (i.e. CYP1A) and the hydroxylation of Sudan I (i.e. CYP1A1), as described in sections 2.5.1, 2.5.2 and 2.5.3, respectively. Microsomal incubations were used to study the formation of BaP metabolites, described in section 2.6.1, and analysed using HPLC as described in section 2.6.1.1. DNA adduct formation *in vitro* was studied using microsomal incubations as described in section 2.6.2.1. DNA was isolated using the phenol-chloroform method described in section 2.13.1 and analysed using ^{32}P-postlabelling as described in section 2.14. *In vivo* DNA adduct formation was studied by isolating DNA from tissues as described in 2.13.3 and analysed using the ^{32}P-postlabelling method as described in section 2.14.

3.3 Results

3.3.1 Protein expression of XMEs

Expression of the electron donor proteins POR, Cyb5 and Cyb5R and the P450 isoenzyme CYP1A1 were probed for in the hepatic microsomal fractions from BaP-treated and untreated WT, HRN and HBRN mice (**Figure 3.2**). POR was expressed only in the WT microsomal fractions and Cyb5 was expressed only in the WT and HRN microsomal fractions, as expected (Henderson et al., 2013, Henderson et al., 2006). Cyb5R was expressed uniformly in all mouse lines and was not altered by treatment with BaP. Treatment with BaP was not also found to alter the levels of POR, Cyb5 and Cyb5R expression relative to controls. Cyp1a1 protein, however, was greatly induced in all mouse lines by BaP treatment and the extent of Cyp1a1 protein induction by BaP was similar in all mouse lines. Whilst a previous study showed increased protein expression of Cyb5 in HRN mice after repeated (i.e. 5 days) BaP treatment (Arlt et al., 2012) there was no observed induction of Cyb5 in HRN microsomal fractions after BaP treatment in this study, probably due to the single 24-hour administration selected here.

3.3.2 Enzyme activity of XMEs

POR activity was detected in the hepatic microsomal fractions from WT mice but not in those from HRN or HBRN mice (**Figure 3.3a** and **3.4a**), as expected (Henderson et al., 2013, Henderson et al., 2006). POR activity in BaP-treated WT mice was slightly lower than in untreated animals.

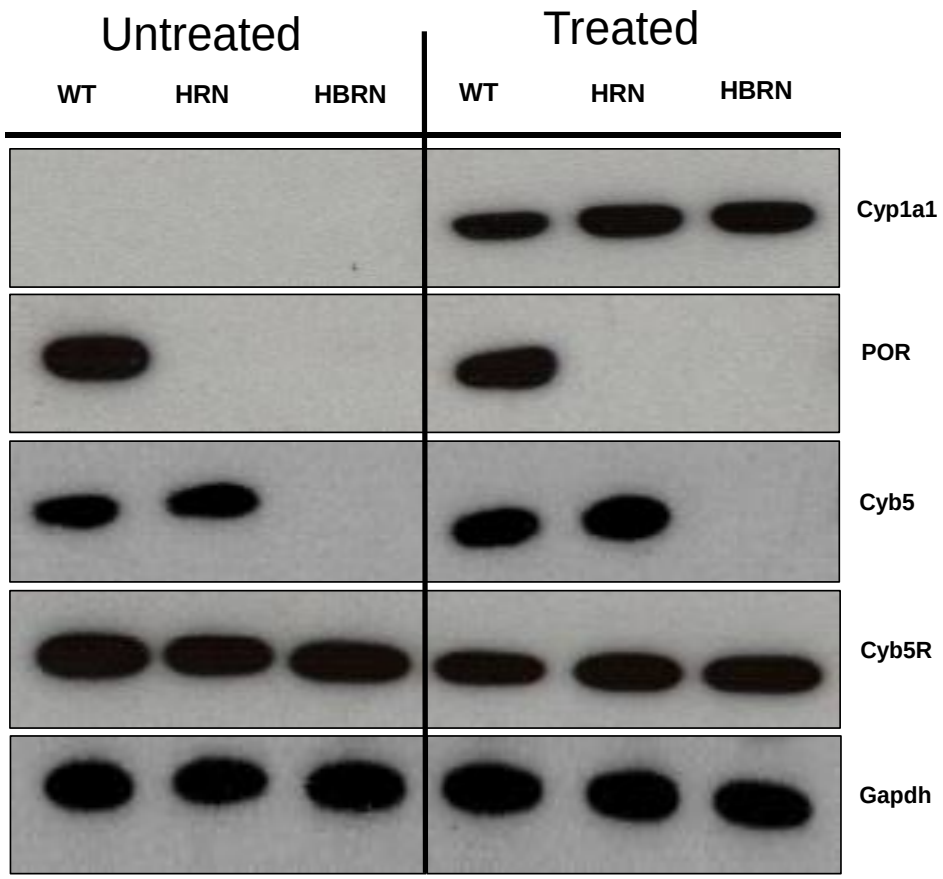

Figure 3.2: Western blot analysis of Cyp1a1, POR, Cyb5 and Cyb5R in the pooled microsomal fractions of untreated (lanes 1-3) and BaP-treated (lanes 4-6) WT, HRN and HBRN mice. Gapdh protein expression was used as a loading control.

Cyp1a (Cyp1a1 and Cyp1a2) activity and Cyp1a1 enzyme activity was measured using EROD (**Figure 3.3b** and **3.4b**) and Sudan I oxidation (**Figure 3.3c** and **3.4c**), respectively. Cyp1a activity was substantially higher in hepatic microsomes from mice treated with BaP than those from untreated mice, regardless of whether NADPH or NADH was used as the enzymatic cofactor in the reaction mixture.

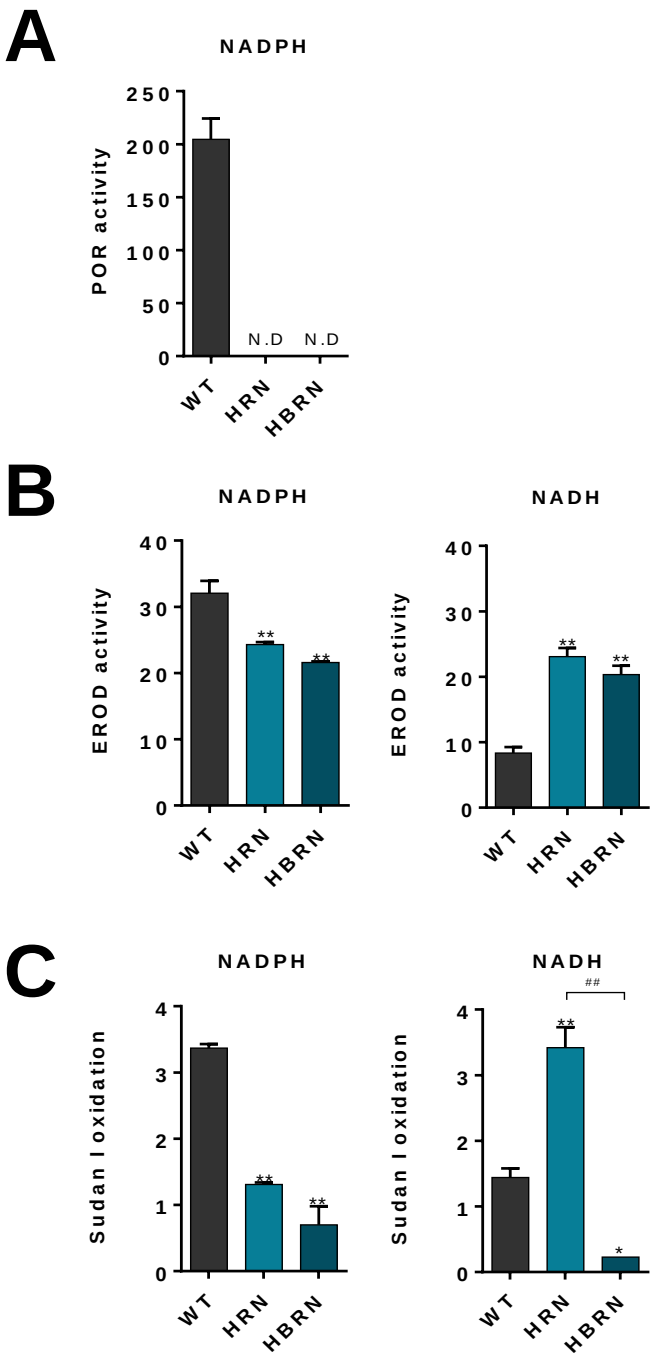

Figure 3.3: Enzyme activity in the pooled hepatic fractions of untreated WT, HRN and HBRN mice using either NADPH or NADH as cofactor. (A) POR activity was measured as nmol of cytochrome *c*/mg/min and was detected only in microsomal fractions from WT mice. (B) Cyp1a enzyme activity was determined using the EROD assay with activity being observed as pmol of resorufin/mg protein/min. (C) Cyp1a1 enzyme activity was determined by the oxidation of Sudan I to hydroxylated metabolites with activity being measured as nmol of total C-hydroxylated metabolites/mg protein/min. Values are given as mean ± SD (*n*=3). Repeat determinations were carried out within the same week. Statistical analysis was performed by one-way Anova with Tukey's multiple comparison test (* = compared to WT; # = compared to HRN. * $P \leq 0.05$ ** $P \leq 0.01$).

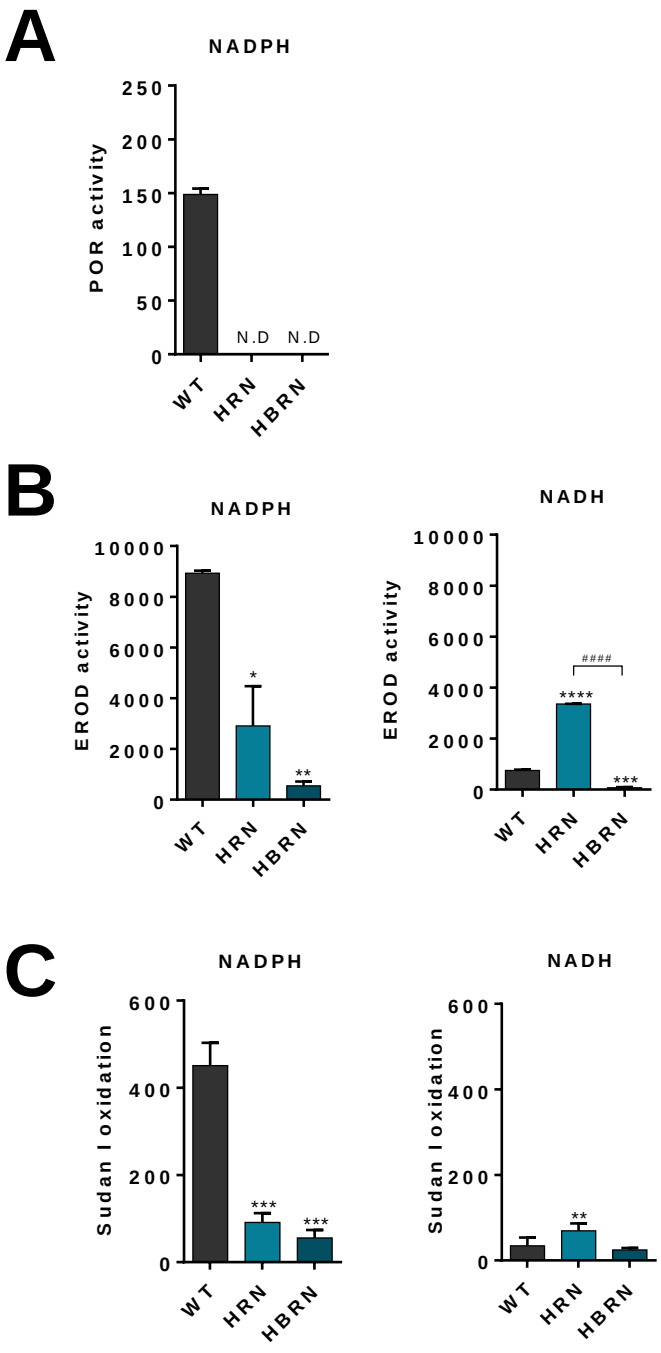

Figure 3.4: Enzyme activity in the pooled hepatic fractions of BaP-treated WT, HRN and HBRN mice using either NADPH or NADH as the enzymatic cofactor. (A) Por activity was observed as nmol of cytochrome *c*/mg/min and was only detected in microsomal fractions from WT mice. (B) CYP1A activity was determined using the EROD assay with activity being observed as pmol of resorufin/mg protein/min. (C) CYP1A1 activity was determined by the oxidation of Sudan I to hydroxylated metabolites with activity being observed as nmol of total C-hydroxylated metabolites/mg protein/min. Values are given as ± SD (*n*=3). Repeat determinations were carried out within the same week. Statistical analysis was performed by one-way Anova with Tukey's multiple comparison test (* = compared to WT; # = compared to HRN. * $P \leq 0.05$ ** $P \leq 0.01$ *** $P \leq 0.001$**** $P \leq 0.0001$).

When NADPH was used in the reaction mixture, hepatic microsomes from BaP-treated WT mice exhibited the highest levels of Cyp1a activity (**Figure 3.4b** and **3.4c**). Cyp1a activity was substantially lower in the hepatic microsomes from BaP-treated HRN mice, correlating with the lack of POR activity in these mice. Cyp1a activity in hepatic microsomes from BaP-treated HBRN mice was significantly lower compared to both BaP-treated WT and HRN mice and showed the lowest level of Cyp1a activity when NADPH was used in the reaction mixture. In the hepatic microsomal fractions from untreated mice Cyp1a activity was also lower in HRN and HBRN mice than in WT mice, but the effect was less pronounced compared with mice treated with BaP (**Figure 3.3b** and **3.3c**).

When EROD was used as a measure of Cyp1a activity and NADH was used in the reaction mixture, hepatic microsomes from BaP-treated HRN mice showed significantly higher Cyp1a activity than the hepatic microsomal fractions from BaP-treated WT and HBRN mice (**Figure 3.4b**). Hepatic microsomes from BaP-treated HBRN mice exhibited the lowest level of Cyp1a activity in the presence of NADH. When Sudan I oxidation was used as a measure for Cyp1a1 activity, BaP-treated WT and HBRN mice showed a similar level of Cyp1a1 activity (**Figure 3.4c**).

In untreated WT, HRN and HBRN mice Cyp1a activity was lower in the absence of the electron donors when NADPH was used in the reaction mixture, with activity highest in WT mice and lowest in HBRN mice. When NADH was used in the reaction mixtures, however, Cyp1a activity was highest in the hepatic microsomal fractions from HRN mice and lowest in those from WT mice. Cyp1a1 activity measured by Sudan I oxidation, however, was lowest in the HBRN mice (**Figure 3.3b** and **3.3c**).

3.3.3 Analysis of BaP metabolites by HPLC

Hepatic microsomes isolated from WT, HRN and HBRN mice were incubated with BaP and either NADPH or NADH before being analysed by HPLC to determine the BaP metabolite profile. The highest level of total metabolite formation *in vitro* was observed in the hepatic microsomal fraction from BaP-pretreated WT mice when NADPH was used as cofactor (**Figure 3.5a**). Total metabolite formation in microsomal fractions from WT mice was around 3-fold lower than when NADH was used. Levels of total metabolite formation in microsomal fractions from untreated mice were lower but followed the same pattern (**Figure 3.5b**).

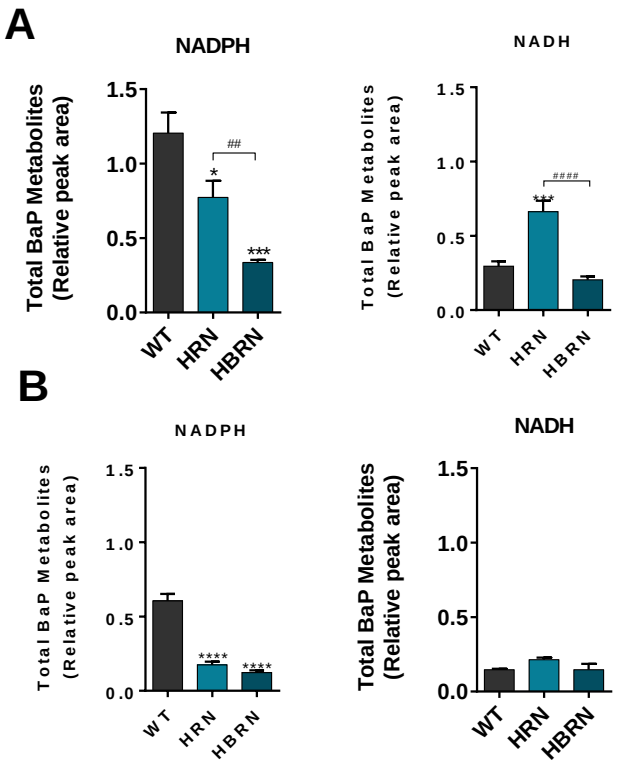

Figure 3.5: Total formation of BaP metabolites during *in vitro* incubations with hepatic microsomal fractions from (A) BaP-pretreated WT HRN and HBRN mice using either NADPH or NADH as cofactor and from (B) untreated WT HRN and HBRN mice using either NADPH or NADH as cofactor. Values are given as mean ± SD (n=3). Repeat incubations were carried out and analysed within the same week. Statistical analysis was performed by one-way Anova with Tukey's multiple comparison test (* = compared to WT; # = compared to HRN. * $P \leq 0.05$ ** $P \leq 0.01$ *** $P \leq 0.001$**** $P \leq 0.0001$).

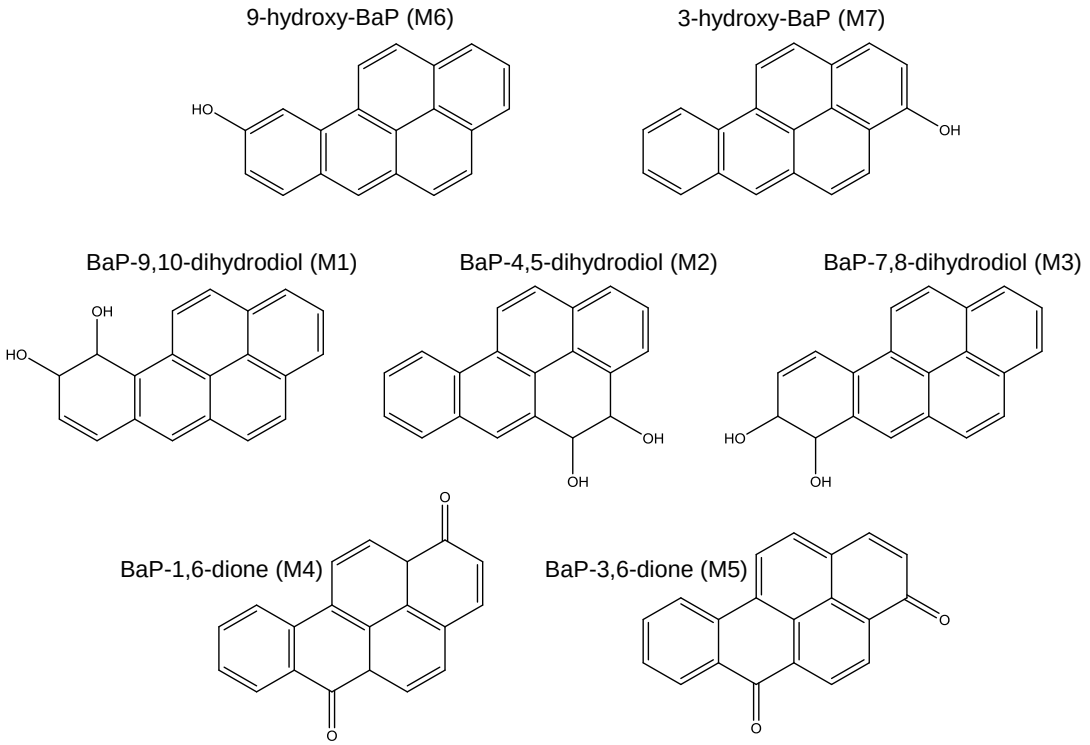

Figure 3.6: Structures of BaP metabolites detected from *in vitro* incubations of BaP with hepatic microsomal fractions.

Hydroxylated BaP metabolites and BaP-dihydrodiols, as well as BaP-diones, were identified (**Figure 3.6**). A metabolite, Mx, whose structure has yet to be elucidated, was detected also. Residual BaP and/or BaP metabolites were not detected in hepatic microsomes isolated from BaP-treated mice. No BaP metabolites were detected by HPLC in control incubations without microsomes, without NADPH/NADH-generating system or without BaP (**Figure 3.7c** and **3.7d**). Representative HPLC chromatograms showing the BaP metabolite profiles are shown in **Figure 3.7a** and **3.7b**.

When incubations were carried out using hepatic microsomal fractions from untreated mice the overall formation of BaP metabolites was highest in WT mice when NADPH was used in the reaction mixture, whereas when NADH was used the highest formation of metabolites was seen in HRN mice (**Figure 3.5b** and **3.8**). Although the

amount of metabolites detected was lower, this pattern is similar to that observed in microsomes from BaP-pretreated mice, again correlating with Cyp1a activity

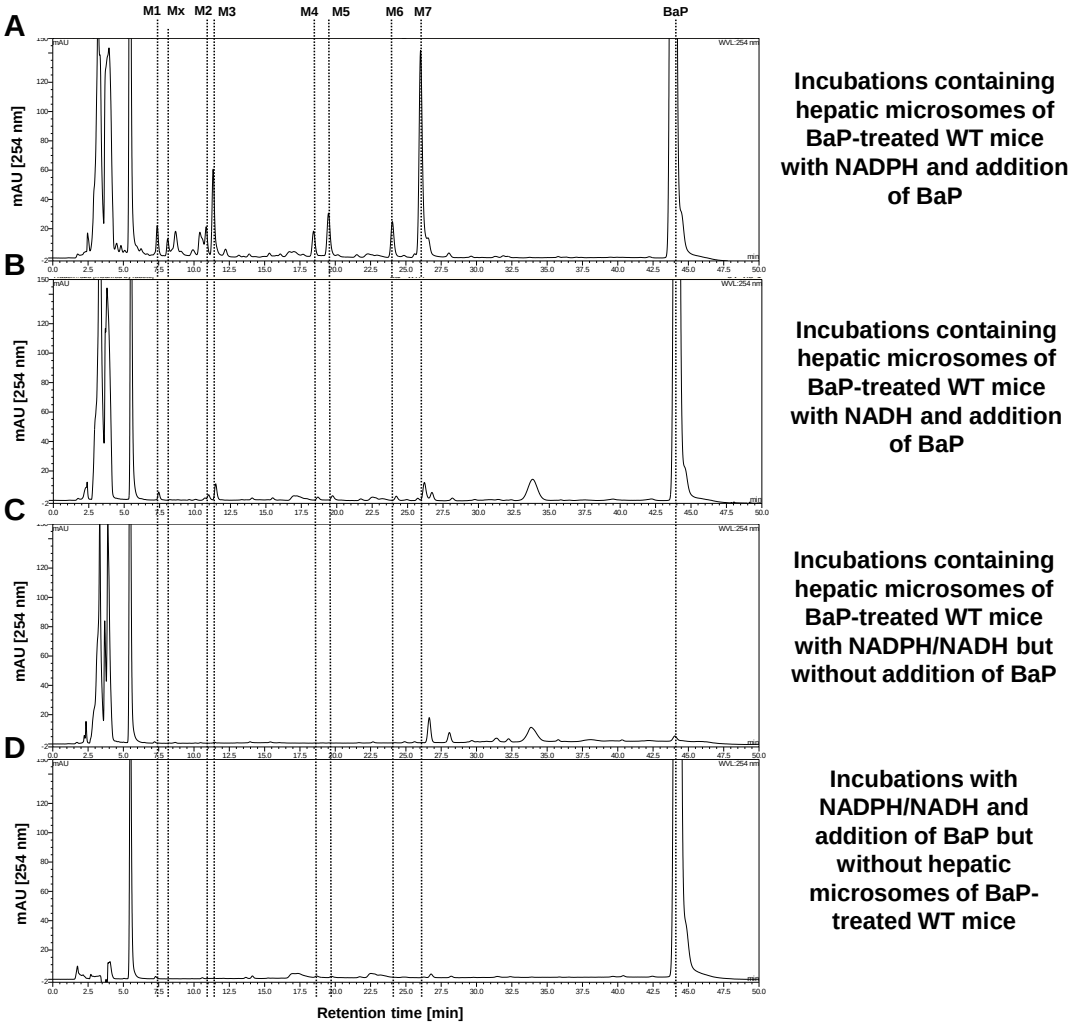

Figure 3.7: Representative HPLC chromatograms from *in vitro* incubations with hepatic microsomal fractions from BaP-pretreated WT mice with BaP and either NADPH or NADH as cofactor. BaP-9,10-dihydrodiol (M1), BaP-4,5-dihydrodiol (M2), BaP-7,8-dihydrodiol (M3), 1,6-BaP-dione (M4), 3,6-BaP-dione (M5), 9-hydroxy BaP (M6), 3-hydroxy BaP (M7) and an unknown BaP metabolite (Mx).

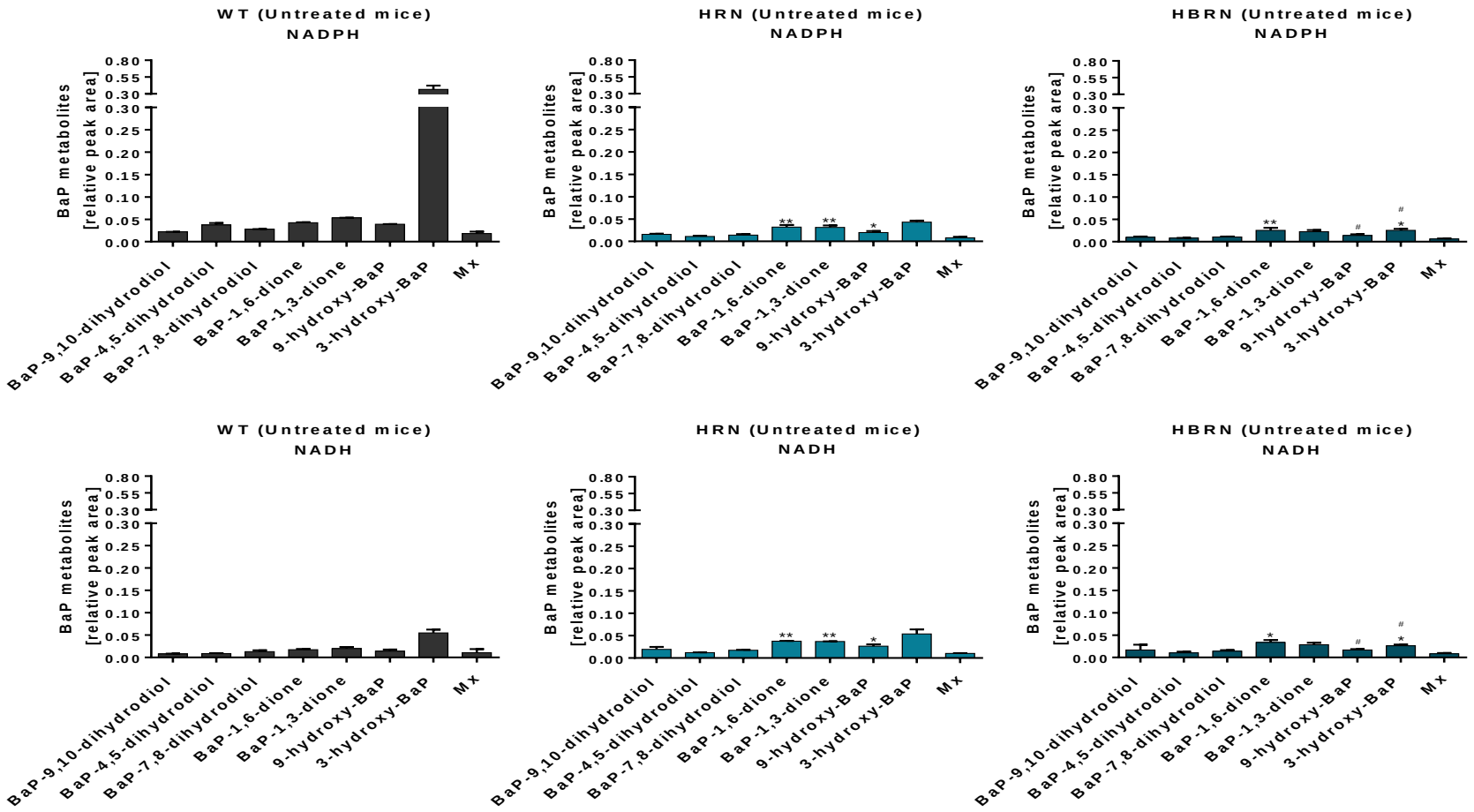

Figure 3.8: Formation of BaP metabolites from *in vitro* incubations with hepatic microsomal fractions from BaP-untreated WT, HRN and HBRN mice with BaP and either NADPH or NADH as cofactor. Values are given as mean ± SD (n=3). Repeat incubations were carried out and analysed within the same week. Statistical analysis was performed by one-way Anova with Tukey's multiple comparison test (* = compared to WT; # = compared to HRN. * $P \leq 0.05$ ** $P \leq 0.01$).

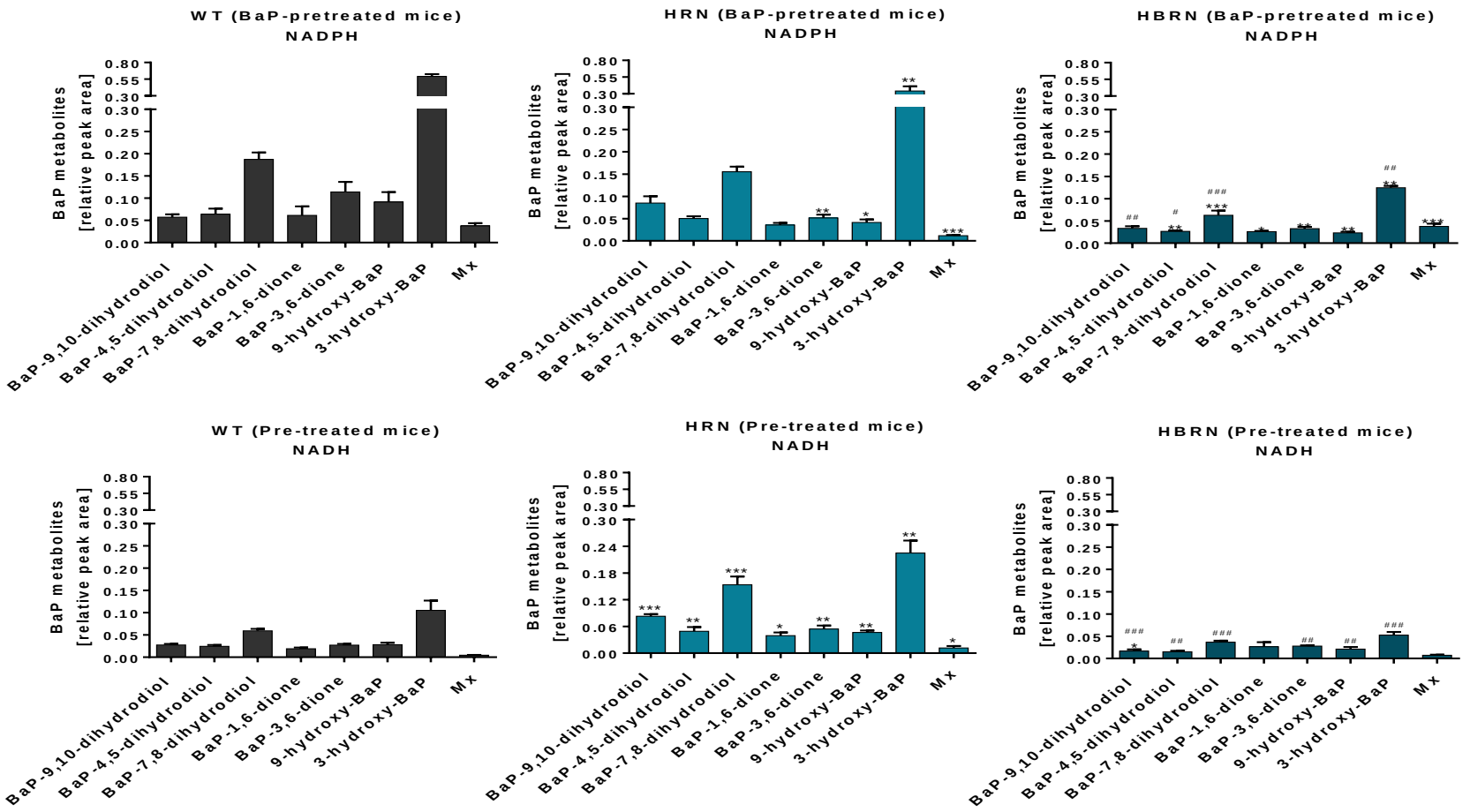

Figure 3.9: Formation of BaP metabolites from *in vitro* incubations with hepatic microsomal fractions from BaP-pretreated WT, HRN and HBRN mice with BaP and either NADPH or NADH as cofactor. Values are given as mean ± SD (*n*=3). Repeat incubations were carried out and analysed within the same week. Statistical analysis was performed by one-way Anova with Tukey's multiple comparison test (* = compared to WT; # = compared to HRN. * $P \leq 0.05$ ** $P \leq 0.01$ *** $P \leq 0.001$).

The two major metabolites formed in all incubations with microsomal fractions from BaP pre-treated mice were 3-hydroxy-BaP and BaP-7,8-dihydrodiol (**Figure 3.9**). With NADPH as the cofactor, the overall formation of BaP metabolites was significantly lower in hepatic microsomal fractions from BaP-pretreated HRN mice with formation of BaP-3,6-dione, 9-hydroxy-BaP, 3-hydroxy-BaP and the unidentified metabolite Mx being significantly lower than with BaP-pretreated WT mice (**Figure 3. 9**).

Except for BaP-9,10-dihydrodiol, all metabolites were detected at significantly lower amounts compared with hepatic microsomes from BaP-pretreated WT mice. Formation of the metabolites BaP-9,10-dihydrodiol, BaP-4,5-dihydrodiol, BaP-7,8-dihydrodiol and 3-hydroxy-BaP were at lower levels than with BaP-pretreated HRN hepatic microsomes (**Figure 3.9**).

When NADH was used as the enzymatic cofactor the overall formation of BaP metabolites in hepatic microsomal fractions from BaP-pretreated HRN mice was higher than with microsomal fractions from BaP-pretreated WT mice with all metabolites being formed in higher quantities. Overall metabolite formation in hepatic fractions from BaP-pretreated WT and HBRN mice was not significantly different with only BaP-9,10-dihydrodiol being significantly lower (**Figure 3.5** and **3.9**). All metabolites except for BaP-1,6-dione and Mx were significantly lower compared with BaP-pretreated HRN hepatic microsomes (**Figure 3.9**). The rate of BaP metabolite formation in the hepatic microsomal fractions correlated with the levels of Cyp1a enzymatic activity and the enzymatic cofactor used (NADPH or NADH).

3.3.4 BaP-DNA adduct formation *in vitro*

The ability of hepatic microsomes isolated from control and BaP-treated WT, HRN and HBRN mice to catalyse BaP-DNA adduct formation *in vitro* was investigated (**Figure 3.10**).

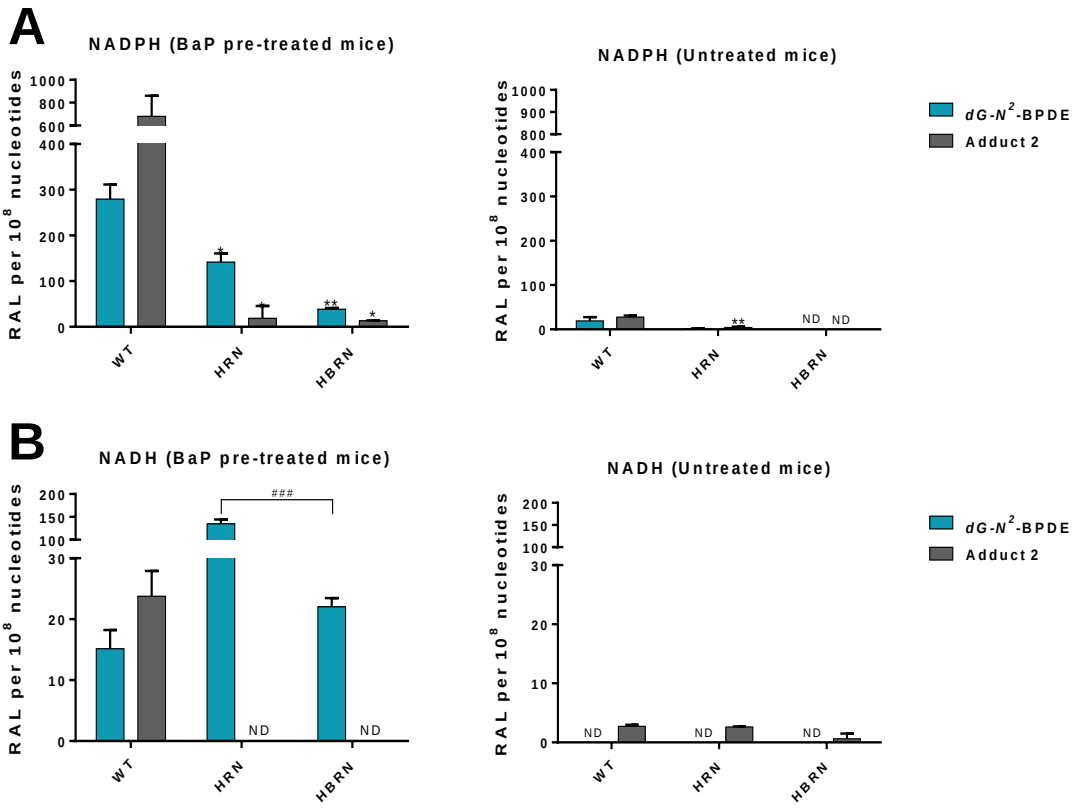

Figure 3.10: Quantitative TLC ^{32}P-postlabelling analysis of dG-N^2-BPDE (adduct 1) and adduct 2 from *in vitro* incubations with DNA, BaP and hepatic microsomal fractions from BaP-pretreated or untreated WT, HRN and HBRN mice using either NADPH (A) or NADH (B) as cofactor. Duplicate incubations were carried out within the same week and DNA stored at –20°C until analysis. Values are given as mean ± SD (n=4); DNA from two separate incubations were measured in duplicate in separate ^{32}P-postlabelling analyses. Statistical analysis was performed by one-way Anova with Tukey's multiple comparison test (* = compared to WT; # = compared to HRN. * $P \leq 0.05$ *** $P \leq 0.001$).

The BaP-DNA adduct pattern obtained by ^{32}P-postlabelling analysis from *in vitro* microsomal incubations consisted of up to two major adduct spots (**Figure 3.11**). One spot (assigned adduct 1) has been previously identified as dG-N^2-BPDE (Arlt et al.,

2008). The other spot (assigned adduct 2), has not yet been fully structurally identified and is likely derived from the reaction of 9-hydroxy-BaP-4,5-epoxide with guanine residues in DNA (Schoket et al., 1989; Nesnow et al., 1993; Fang et al., 2003). These two adducts are the results of the biotransformation pathways illustrated in **Figure 3.1**. Essentially no BaP-DNA adducts were formed in control incubations with microsomes of BaP-pretreated WT mice without BaP, but were detectable in control incubations with microsomes of BaP-pretreated HRN and HRBN mice. These findings indicate that some BaP that was not detectable by HPLC is retained in hepatic microsomes of BaP-pretreated HRN and HRBN mice, and is activated to form BaP-DNA adducts.

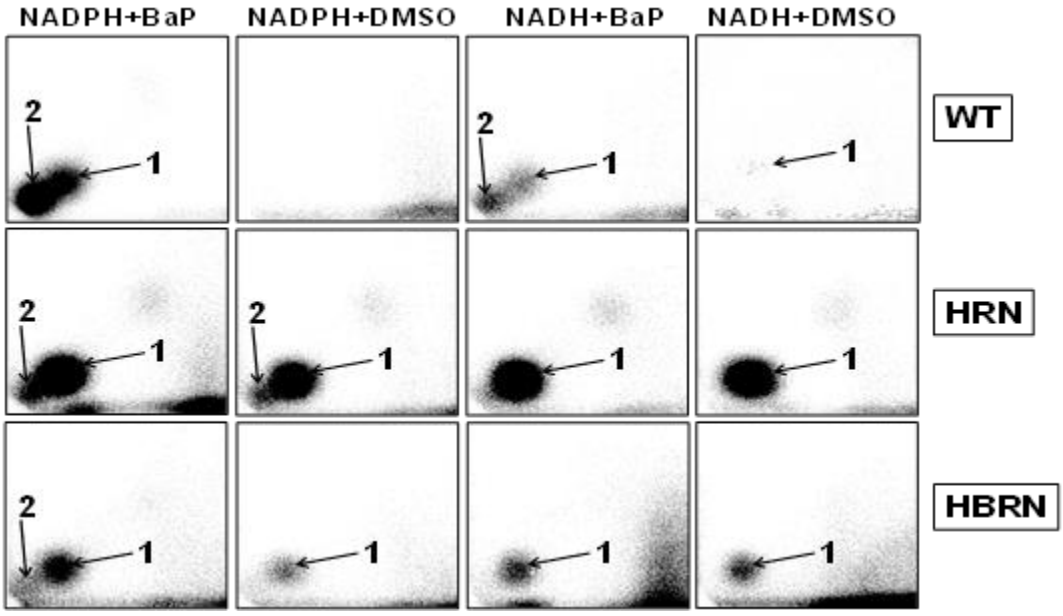

Figure 3.11: Autoradiograms showing adduct profiles by TLC ^{32}P-postlabelling analysis from *in vitro* incubations with hepatic microsomal fractions from BaP-pretreated WT, HRN and HBRN mice, DNA and BaP. The origin on the TLC plate, at the bottom left-hand corners, was cut off before exposure.

During *in vitro* incubations with WT microsomal fractions from BaP-pretreated mice and with NADPH as the enzymatic cofactor, adduct 2 was the predominant DNA adduct formed. Formation of dG-N^2-BPDE (adduct 1) was much lower (**Figure 3.10a**). This was not observed with hepatic microsomal fractions from BaP-pretreated

HRN and HBRN mice, where formation of the dG-N^2-BPDE adduct was greater than adduct 2 when NADPH was used in the reaction mix (**Figure 3.10b**). When NADH was used as the enzymatic cofactor adduct 2 was not detected. When NADPH was used the greatest BaP-DNA adduct formation was seen with microsomal fractions from BaP-pretreated WT mice.

Levels of adduct 1 (dG-N^2-BPDE) *in vitro* strongly correlated with the amounts of BaP-7,8-dihydrodiol formed in hepatic microsomal fractions from BaP-pretreated mice, both with NADPH and NADH as cofactor. When NADPH was used as cofactor, the formation of BaP-7,8-dihydrodiol was lower in HRN microsomal fractions and lowest in HBRN microsomal fractions relative to WT, correlating with dG-N^2-BPDE (adduct 1) formation in these microsomal fractions. The highest levels of BaP-7,8-dihydrodiol were observed in HRN microsomal fractions with NADH as cofactor, with similar amounts being formed in WT and HBRN hepatic microsomal fractions.

When NADPH was used as cofactor the amounts of 9-hydroxy-BaP correlated with the levels of adduct 2 in hepatic microsomal fractions from BaP-pretreated mice. The levels of 9-hydroxy-BaP detected were also the highest in HRN microsomal fractions when NADH was used as cofactor. As adduct 2 was not detectable in microsomal fractions of either HRN or HBRN BaP-pretreated mice there was no correlation found to the amount of 9-hydroxy-BaP formed. Because DNA adduct formation was low in microsomal fractions from untreated mice, no correlation to metabolite formation was attempted.

3.3.5 BaP-DNA adduct formation *in vivo*

The BaP-DNA adduct pattern obtained from *in vivo* treatments consisted of one major adduct spot in all tissues, dG-N^2-BPDE (assigned spot 1), as well as minor adduct spots 2 and 3 in some extrahepatic tissues. Adduct spot 2 was the same as that identified in the *in vitro* incubations (**Figure 3.11**); however adduct 3 has not been structurally identified and it was detected only in colon and small intestine (**Figure 3.12**). No DNA adducts were detected in tissues of untreated mice (data not shown).

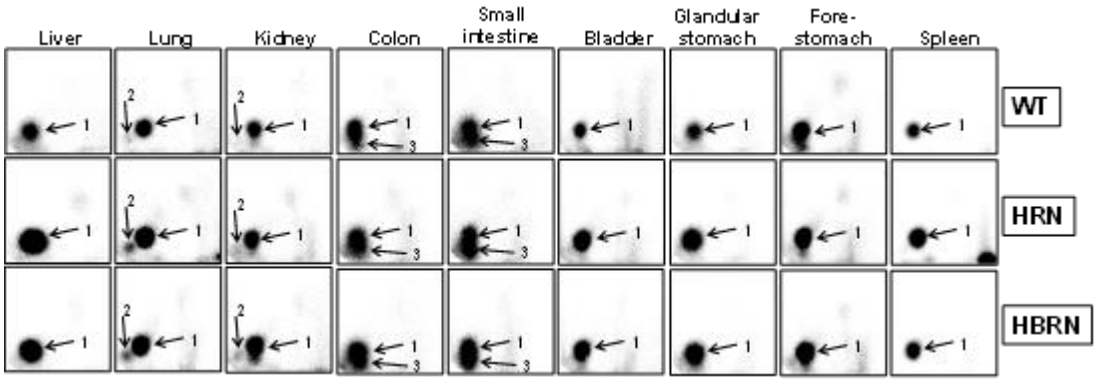

Figure 3.12: Autoradiograms showing adduct profiles by TLC ^{32}P-postlabelling in organs of WT, HRN and HBRN mice treated i.p with 125 mg/kg bw BaP for 24 h. The origin on the TLC plate, at the bottom left-hand corners, was cut off before exposure.

Of the organs tested (liver, lung, small intestine, kidney, spleen, colon, forestomach, glandular stomach and bladder) no significant difference was exhibited between the mouse models with the exception of the small intestine and the liver (**Figure 3.13**). In the small intestines there were significantly higher levels of BaP-DNA adducts in HBRN mice than in WT mice. BaP-DNA adduct formation in the livers of HRN mice was ~7-fold higher than in WT mice. BaP-DNA adduct formation in HBRN mice was significantly lower than that observed in HRN mice, although no significant difference between WT and HBRN mice was found. This supports the results demonstrated in previous studies with BaP-treated HRN mice (Arlt et al., 2012, Arlt et al., 2008). BaP-

DNA adduct formation in the livers of BaP-treated WT, HRN and HBRN mice *in vivo* strongly correlated with the formation of BaP-7,8-dihydrodiol and dG-N^2-BPDE in hepatic microsomal fractions of BaP-pretreated mice. Collectively, these results support the notion that the Cypb5/Cyb5R systems strongly contributes to BaP-DNA adduct formation in HRN mice.

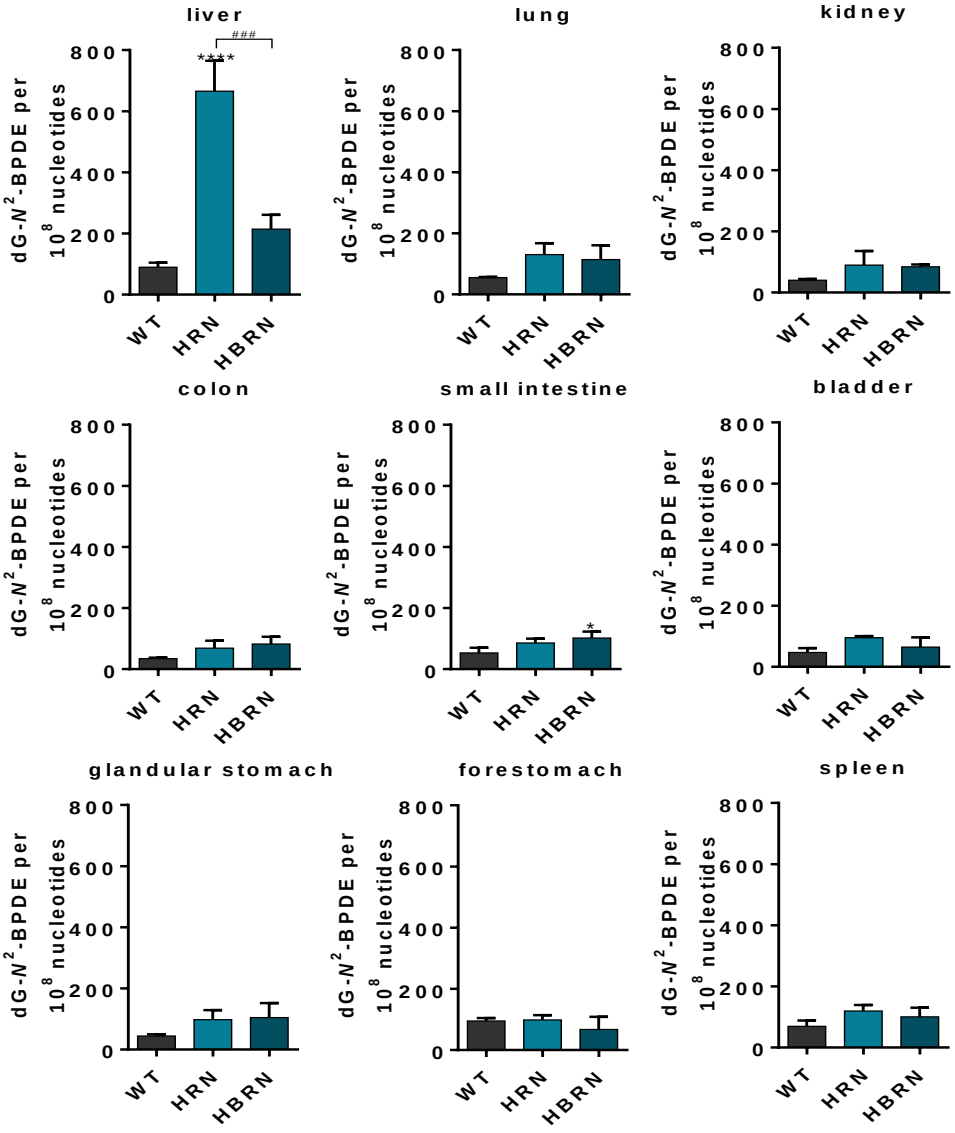

Figure 3.13: Quantitative TLC ^{32}P-postlabelling analysis of dG-*N2*-BPDE adducts in organs of WT, HRN and HBRN mice treated i.p with 125 mg/kg bw BaP for 24 h. Values are given as ± SD (*n*=3); each DNA sample isolated from tissue of individual animals was analysed once. Statistical analysis was performed by one-way anova with Tukey's multiple comparison test (* = compared to WT; # = compared to HRN. * $P \leq 0.05$ *** $P \leq 0.001$**** $P \leq 0.0001$).

3.4 Discussion

The *in vitro* experiments using pooled hepatic microsomal fractions clearly demonstrated that Cyb5 contributes to the bioactivation of BaP. The formation of BaP-DNA adducts and BaP metabolites correlated with Cyp1a enzyme activity, and were lessened by the loss of electron donors when NADPH was used as cofactor to examine the POR-dependent pathway. When the NADH-dependent Cyb5R pathway was investigated, Cyp1a enzyme activity was higher in the hepatic microsomal fractions of HRN mice than in those of WT mice. In the microsomal fractions from HBRN mice the activity was significantly lower relative to WT mice, indicating that the increased expression of Cyb5 is contributing to increased NADH-dependent activity. These results correlate with those from experiments with reconstituted enzyme systems (Stiborova et al., 2016a, Stiborova et al., 2014c) supporting the hypothesis that Cyb5 is contributing to the bioactivation of BaP in the livers of HRN mice in the absence of POR.

The *in vivo* results, however, contrast with the observations from the *in vitro* experiments when NADPH was used as cofactor. Whereas bioactivation of BaP was reduced with the loss of electron donors and P450 activity *in vitro, in vivo* the results were different. HRN mice displayed a 7-fold increase in hepatic DNA adduct formation compared with WT mice, reflecting findings seen in previous studies (Arlt et al., 2012, Arlt et al., 2008). DNA adduct formation in the livers of HBRN mice was significantly lower than in HRN mice, further suggesting a role for Cyb5 in BaP-DNA adduct formation in HRN mice. When NADH was used as cofactor, bioactivation of BaP *in vitro* (i.e. BPDE-DNA adduct formation) correlated with P450 activity and the

formation of BaP-7,8-dihydrodiol (precursor of BPDE) in hepatic microsomal fractions. Levels of BPDE-DNA adduct formation *in vitro* was highest in the hepatic microsomal fraction from BaP-pretreated HRN mice and correlated with hepatic BPDE-DNA adduct formation *in vivo, i.e.* highest levels of dG-N^2-BPDE were seen in the livers of BaP-treated HRN mice. These results again support the conclusion that the Cyb5/Cyb5R system strongly contributes to BPDE-DNA adduct formation in the livers of HRN mice. The level of DNA adducts in the livers of HBRN mice, however, was not significantly different from that observed in the livers of WT mice, which was unexpected.

Both the HRN and HBRN mice display no overt changes in phenotype, except for steatotic livers as a consequence of the loss of P450-housekeeping activity involved in cholesterol metabolism (Henderson et al., 2003). Potentially the high dose of BaP combined with the steatotic livers could mean that some BaP is retained in the livers being released and metabolised over a longer period when normally detoxication mechanisms would have allowed any remaining BaP to be excreted. Treatment of mice with doses of 125 mg/kg bw BaP has been shown to be carcinogenic when administered daily for 5 days (Hakura et al., 1998) and is why this dose was used in the present study. A 10-fold lower dose of BaP has also been shown to result in increased BaP-DNA adduct formation in the livers of HRN mice relative to WT mice (Arlt et al., 2012). Similar models with liver-specific deletion of POR (liver-*Por*-null mouse models) have been developed (Wu et al., 2003). Administration of 40 mg/kg bw to liver-*Por*-null mice did not result in a significant change in liver retention of BaP relative to WT mice (Wang et al., 2017). Furthermore, there was no significant difference in the clearance of BaP in HRN mice compared to WT mice (Arlt et al., 2008). Clearance of BaP in HBRN mice has not been investigated in this study.

The increased formation of hepatic BaP-DNA adducts in the HRN mice indicates that, in accordance with other studies (Uno et al., 2001, Uno et al., 2004, Uno et al., 2006, Shi et al., 2010), P450 activity in hepatocytes *in vivo* is more important for BaP detoxication than bioactivation. Evidence for this hypothesis came from a study of BaP bioactivation in *Cyp1a1(–/–)* mice. Treatment of these mice i.p. with BaP (500 mg/kg bw) resulted in a 4-fold increase in hepatic DNA adduct formation relative to WT mice (Uno et al., 2001). Some WT and *Cyp1a1(–/–)* in the study were pre-treated with 2,3,7,8-tetrachlorodibenzo-*p*-dioxin (TCDD) in order to assess whether any other dioxin-inducible enzymes were able to contribute to BaP activation. These TCDD-pre-treated mice had decreased levels of BaP-DNA adducts and enhanced clearance of BaP from the blood, indicating that the accumulation of BaP-DNA adducts in *Cyp1a1(–/–)* mice could be due to the lack of Cyp1a1-mediated detoxication (Uno et al., 2001). Further studies with *Cyp1a1(–/–), Cyp1a2(–/–)* and *Cyp1b1(–/–)* single-knockout, *Cyp1a1/1b1(–/–)* and *Cyp1a2/1b1(–/–)* double-knockout mice suggested that Cyp1b1 was responsible for the activation of BaP whilst Cyp1a1 was responsible for detoxication (Nebert et al., 2013). Although these studies provide a rationale for the increased BaP-DNA adduct levels in the livers of HRN relative to WT mice, they do not explain the formation of BaP-DNA adducts in the livers of HRBN mice. These findings may suggest that a P450-independent mechanism contributes to the activation of BaP in HBRN mice. It is noteworthy that DNA adduct formation of the dietary carcinogen 2-amino-1-methyl-6-phenylimidazo[4,5-*b*]pyridine (PhIP) was similar in the livers of Reductase Conditional Null (RCN) and WT mice (Arlt et al., 2011) whereas RCN mice treated with BaP formed 5.6-fold higher liver DNA adduct levels than WT mice (Arlt et al., 2012). Like HRN mice, RCN mice have a liver-specific deletion of POR and thus show the same phenotype (Arlt et al., 2015a). Although PhIP

bioactivation is considered to be catalysed by CYP1A2, the results in the RCN model suggested that PhIP may be activated mainly by a non-P450 pathway in the livers or extrahepatic P450s of RCN mice (Arlt et al., 2011).

Previous investigations showed that there was no difference in Ptgs1 and Ptgs2 expression between HRN and WT mice when exposed to BaP (Arlt et al., 2008). Hepatic Ptgs2 expression was also compared between *Cyp1a1(–/–)* and *Cyp1a1(+/+)* mice treated with BaP and no differences were found (Uno et al., 2004). Nevertheless, it may be possible that basal expression of Ptgs/Cox in the livers of HRN and HBRN contributes to the bioactivation of BaP-7,8-dihydrodiol to BPDE, with oxidation of BaP to BaP-7,8-dihydrodiol still needing to be catalysed by a non-P450/non-Ptgs/Cox pathway. AKRs have also been implicated in the formation of BaP-DNA adducts, competing with P450 enzymes to activate dihydrodiols. The products of AKR-catalysed reactions are *o*-quinones that produce BaP-7,8-dione-DNA adducts (Jiang et al., 2005, Jiang et al., 2006, Huang et al., 2013) distinctly different from those detected in this study. The analysis of BaP-7,8-dione-DNA adducts was beyond the scope of the present study. As indicated above AKRs metabolise dihydrodiols, but not BaP itself, which further questions their involvement in the processes observed in the current study.

Wang and colleagues (Wang et al., 2017) have proposed that, besides Ptgs/Cox and Akr, 5-lipoxygenase contribute to the hepatic bioactivation of BaP in liver-*Por*-null mice. These conclusions were based on *in vitro* experiments measuring BPDE-DNA adduct formation (i.e. detection of BaP-tetrols by LC-MS/MS analysis after DNA hydrolysis) using S9 fractions isolated from WT and liver-*Por-null* mice and using inhibitors of these enzymes. Although useful, mimicking *in vivo* phenotypes with

inhibition profiles *in vitro* is not straightforward. Firstly, inhibitors are usually not wholly specific. Secondly, as seen again in this study using hepatic microsomes, extrapolating *in vitro* data to *in vivo* results is often not straightforward. However, it may be appropriate to test some inhibitors of other oxidoreductases (e.g. Ptgs/Cox or Akr) in BaP-treated HBRN mice *in vivo* and determine the subsequent BPDE-DNA adduct formation in the livers of these animals.

Conversely, the results of this study in BaP-treated HBRN mice may suggest a role for systemic transport of reactive BaP intermediates (e.g. BPDE) to the liver. Besides the liver, other organs (e.g. lung) have been shown to mediate CYP-catalysed bioactivation of BaP (Arlt et al., 2015b). Other studies in mice have demonstrated that blood components (i.e. serum) can facilitate the systemic transport of BPDE (Ginsberg and Atherholt, 1989). Thus the livers of BaP-treated HBRN mice, which are considered largely deficient in CYP-mediated BaP activation, may still receive substantial quantities of DNA-reactive BaP intermediates (i.e. BPDE) or the proximate carcinogen (i.e. BaP-7,8-dihydrodiol) that originate from their CYP-mediated formation in extra-hepatic tissues. It is noteworthy that reactive BaP metabolites have been shown to be transferred from an activator cell to another target cell (Sebti et al., 1982), again illustrating efficient transfer of BPDE despite its reactivity. Other studies have shown that hepatocytes and non-parenchymal liver cells have capacity to catalyse BaP-derived DNA adduct formation (Horton et al., 1985). Thus, it is possible that BaP bioactivation in CYP-expressing non-parenchymal liver cells may contribute to BaP-DNA adduct formation the livers of HBRN mice. To investigate this would require isolation and culture of hepatocytes and non-parenchymal liver cells from HBRN mice and exposure of these cells to BaP for subsequent BaP-DNA adduct analysis.

In summary, this study has shown that both Por and Cyb5 contribute to the bioactivation of BaP *in vitro* and that Cyb5 also plays an important role *in vivo* for BaP activation in the HRN mice. The presence of BPDE-DNA adducts in the livers of HBRN mice, however, raises the fundamental question of how BaP is being metabolically activated in the livers of HBRN mice despite the absence of both electron donors. It is clear that HBRN mice possess ample capacity to form hepatic BaP-DNA adducts that arise from BPDE, the same process that occurs in WT mice. The results from this study continue to question the role of P450 enzymes in the bioactivation and detoxication of BaP, as well as to suggest the potential for a P450-independent BaP activation mechanism which will require further investigation. Alternatively, our results may also suggest the systemic circulation of DNA-reactive BaP intermediate (i.e. BPDE) which originate from P450-mediated activation in extra-hepatic tissues contributing to the detection of BaP-DNA adducts in the livers of HBRN mice. Likewise, non-parenchymal liver cells may play a role in catalysing P450-mediated bioactivation of BaP in HBRN mice.

4 Application of hepatic cytochrome b_5/P450 reductase null (HBRN) mice to study the role of cytochrome b_5 in the cytochrome P450-mediated bioactivation of the anticancer drug ellipticine

4.1 Introduction

Ellipticine (5,11-dimethyl-6*H*-pyrido[4,5-*b*]carbazole) is a cytotoxic alkaloid isolated from the *Apocynaceae* family of plants. Both ellipticine and its derivatives possess anti-HIV and anti-tumour properties allowing it to be used against several cancers with limited toxic side effects and no haematological toxicity by functioning through multiple mechanisms that result in cell cycle arrest and initiation of apoptosis (Martinkova et al., 2010, Stiborova et al., 2011, Miller and McCarthy, 2012, Stiborova and Frei, 2014). The main mechanisms by which ellipticine exerts its anti-tumour, cytotoxic and mutagenic effects are inhibition of topoisomerase II, intercalation into DNA and enzyme-mediated formation of covalent ellipticine-derived DNA adducts (Garbett and Graves, 2004, Stiborova and Frei, 2014, Banerjee et al., 2015, Vann et al., 2016). Although ellipticine was initially found to be a promising anticancer drug there were a number of problematic toxic side effects. It has, however, proved to be amenable to systematic structural modification to produce a number of analogues with lower toxicities and improved anticancer activities (Garbett and Graves, 2004).

Activation of ellipticine is catalysed by cytochrome P450 (CYP) enzymes and peroxidases, which generate reactive intermediates capable of damaging DNA by forming covalent adducts (Stiborova et al., 2008, Stiborová et al., 2001, Stiborova et

al., 2003a, Stiborova et al., 2012b, Stiborová et al., 2012, Stiborova et al., 2007, Stiborová et al., 2007, Stiborova et al., 2003b). As shown in **Figure 1.7** (see Introduction), ellipticine is oxidised by cytochrome P450 enzymes to form five metabolites, including the reactive metabolites 12-hydroxy- and 13-hydroxy-ellipticine which dissociate to ellipticine-12-ylium and ellipticine-13-ylium and bind to DNA (Aimová et al., 2008, Stiborova et al., 2015, Stiborova et al., 2014a, Stiborova and Frei, 2014, Stiborova et al., 2004). The N^2-oxide is also considered an active ellipticine metabolite as it converts to 12-hydroxy-ellipticine by the Polonowski rearrangement (Stiborova et al., 2004, Kotrbova et al., 2006). 7-Hydroxy- and 9-hydroxy-ellipticine are considered detoxication metabolites due to their efficient excretion shown in experimental animals (Stiborova et al., 2012a, Stiborová et al., 2012).. Although ellipticine is not currently in use as an anticancer drug, it holds value as a compound for studying P450-mediated activation. Understanding the role of cytochrome P450 enzymes in ellipticine metabolism is important both pharmacologically and toxicologically and may help in the development of clinically useful ellipticine analogues.

Previous studies using reconstituted systems investigated the role of Cyb5 in the metabolic activation of ellipticine *in vitro* showed that the presence of Cyb5 resulted in a considerable increase in the activation metabolites 12-hydroxy- and 13-hydroxyellipticine (Kotrbova et al., 2011, Stiborova et al., 2012a, Stiborová et al., 2012, Stiborová et al., 2017). The formation of ellipticine-DNA adducts was also shown to increase ~6-fold in the case of CYP1A1, ~4-fold for CYP1A2 and ~3-fold for CYP3A4 (Stiborova et al., 2012a, Kotrbova et al., 2011). These findings were supported by studies using human recombinant cytochrome P450s in Supersomes™ with CYP3A4 and 1A1 being the most efficient at forming ellipticine-DNA adduct 1

and with adduct 2 being formed by CYP2C19, 2C9 and 2D6 in the presence of Cyb5 (Stiborová et al., 2012). Rats exposed to ellipticine have also shown a significant increase in the expression of both Cyb5 mRNA and protein, and hepatic microsomes isolated from these rats catalysed ellipticine oxidation more efficiently (Stiborova et al., 2016c). Together these studies provide evidence for the role of Cyb5 in the bioactivation of ellipticine both *in vitro* and *in vivo*.

In the present study we have used both the HRN and HBRN mouse lines to investigate the contribution of Cyb5 to the metabolic activation of ellipticine to form DNA adducts *in vivo* alongside microsomal incubations to investigate metabolite and DNA adduct formation *in vitro.* Hepatic microsomal cytochrome P450 enzyme activity and protein expression have also been assessed.

4.2 Materials and methods

WT, HRN and HBRN mice were treated as described in section 2.2.2 and the hepatic microsomal fractions were isolated according to section 2.4. Western blotting was carried out on pooled microsomal fractions according to section 2.10. Similarly, for all enzyme activity assays and incubations pooled microsomal fractions were used. It was not possible to carry out biological repeats due to tissue limitations impacting on the yield of microsomal fractions. Genotyping of the untreated mice was carried out according to section 2.3. Enzyme activities were analysed by determining the reduction of cytochrome *c* (i.e. POR), dealkylation of 7-ethoxyresorufin/7-methoxyresorufin to resorufin (i.e. CYP1A/1A2), testosterone hydroxylation (i.e. CYP3A), and the hydroxylation of Sudan I (i.e. CYP1A1), respectively and are all described in sections 2.5.1, 2.5.2, 2.5.3 and 2.5.4. Microsomal incubations were used to study the formation of ellipticine metabolites, described in section 2.6.1, and analysed using HPLC as described in section 2.6.1.2. DNA adduct formation *in vitro* was studied using microsomal incubations as described in section 2.6.2 with DNA being isolated using the phenol-chloroform method described in section 2.13.1. *In vivo* DNA adduct formation was studied by isolating DNA from tissues as described in 2.13.3. DNA adduct formation was analysed using the ^{32}P-postlabelling method as described in section 2.14.

4.3 Results

4.3.1 Protein expression of XMEs

Expression of electron donor proteins (i.e. POR, Cyb5, Cyb5R) associated with the mixed-function oxidase system (i.e. cytochrome P450) were probed for in the hepatic microsomal fractions from WT, HRN and HBRN mice exposed to ellipticine (**Figure 4.1**). In the mice exposed to ellipticine POR was expressed in the WT mice only and Cyb5 was expressed only in WT and HRN mice, as expected (Henderson et al., 2013, Reed et al., 2018b). In the untreated mice however, POR was unexpectedly detected in the pooled microsomal fractions of both HRN and HBRN mice. A faint band of Cyb5 was also detectable in the microsomal fraction from the untreated HBRN mice. These findings indicate that, in untreated HRN and HBRN mice used as controls, complete deletion of POR and Cyb5 was not achieved. In order to investigate these findings further the genotype of the control animals was re-analysed (see section 4.3.2) as shown in **Figure 4.2**. Cyb5R was expressed uniformly across all mouse lines. Cyp1a1 expression was greater in HRN and HBRN hepatic microsomal fractions after ellipticine treatment compared to WT. Cyp1a1 protein was not detected in the untreated microsomal fractions across all mouse lines. Cyp3a protein was constitutively expressed across all mouse lines but expression was increased in both treated and untreated HRN and HBRN mice.

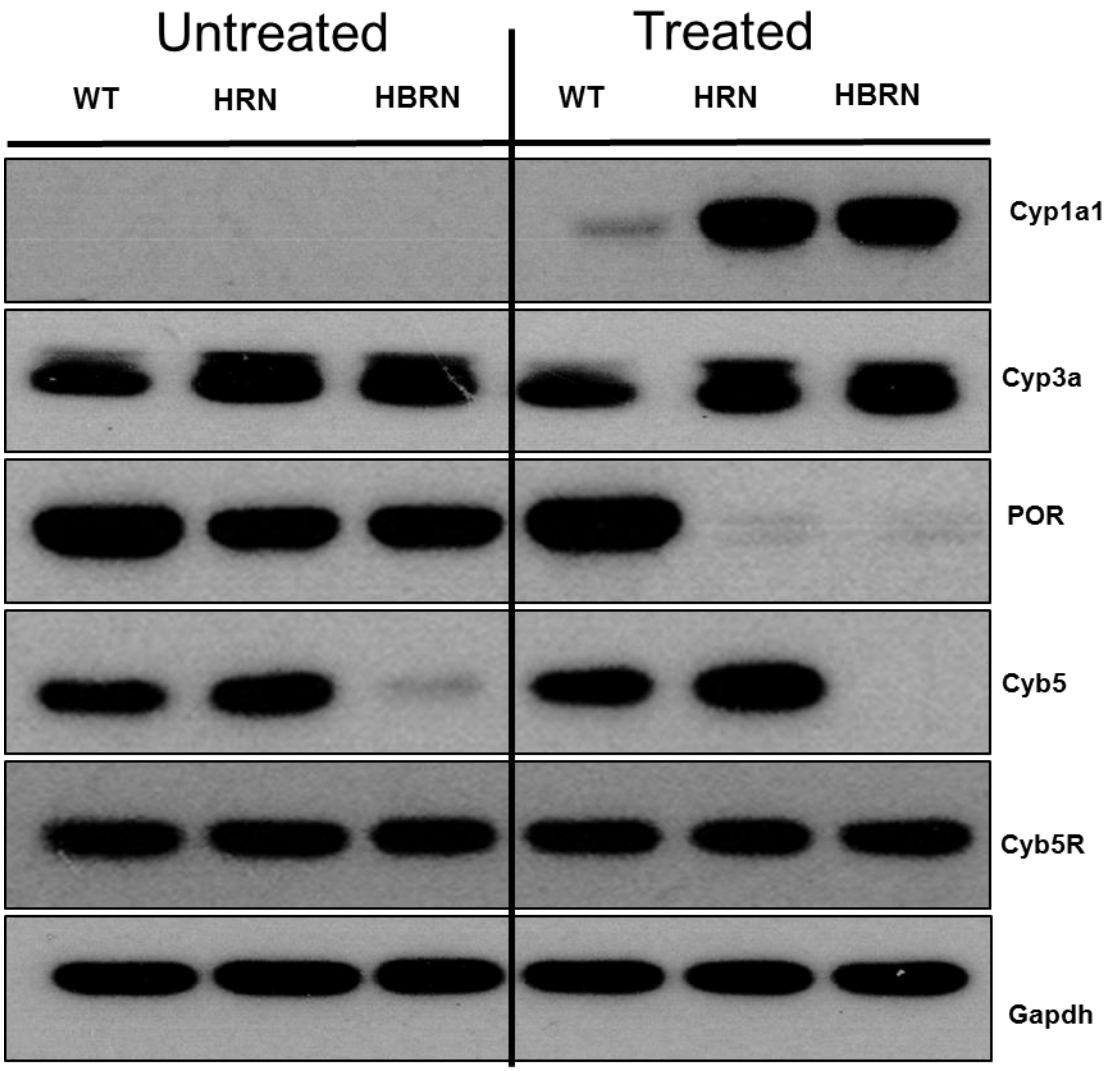

Figure 4.1: Western blot analysis of Cyp1a1, Cyp3a, POR, Cyb5 and Cyb5R in the pooled microsomal fractions of untreated (lanes 1-3) and ellipticine-treated (lanes 4-6) WT, HRN and HBRN mice. Gapdh protein expression was used as a loading control. Representative images of the Western blotting are shown, and at least duplicate analysis was performed in separate experiments.

4.3.2 Genotyping of WT, HRN and HBRN mice

Due to the unexpected detection of POR protein in the pooled hepatic microsomal fractions isolated from HRN and HBRN mice during Western blot analysis (**Figure 4.1**), genotyping was carried out on the livers of the individual untreated mice. The *Por*, *Cyb5* and *Cre* genes were investigated (**Figure 4.2**). Although both *Por* and *Cyb5* appeared to be excised, a very faint *Cre* band was detected in one of the untreated

HRN and one of the untreated HBRN mice (see **Figure 4.2**). Mus musculus adult male thymus sequence was used as control. One potential explanation as to why some POR expression and activity was detectable in the hepatic microsomal fractions could be due to Cre mosaicism, which can arise in one of at least two ways. First, Cre might not be expressed in every cell in the organ of interest. Second, Cre might be expressed but fail to recombine the floxed allele in every cell. However the successful knockout of Cyb5 in the hepatocytes further complicates the results. Due to the schedule of experimental work, ^{32}P-postlabelling was the only experiment carried out after Western blotting had revealed the inconsistencies in POR expression. If time and financial considerations had allowed it, the study would have been repeated. The untreated microsomal fractions were however used for enzyme activity assays and incubations for metabolite formation, but not for ellipticine-DNA adduct formation *in vitro*. Despite the presence of POR, enzyme activity was reduced in the microsomal fractions apart from in the case of Sudan I oxidation where there was no pronounced difference in the levels of activity between the treated and untreated microsomal fractions.

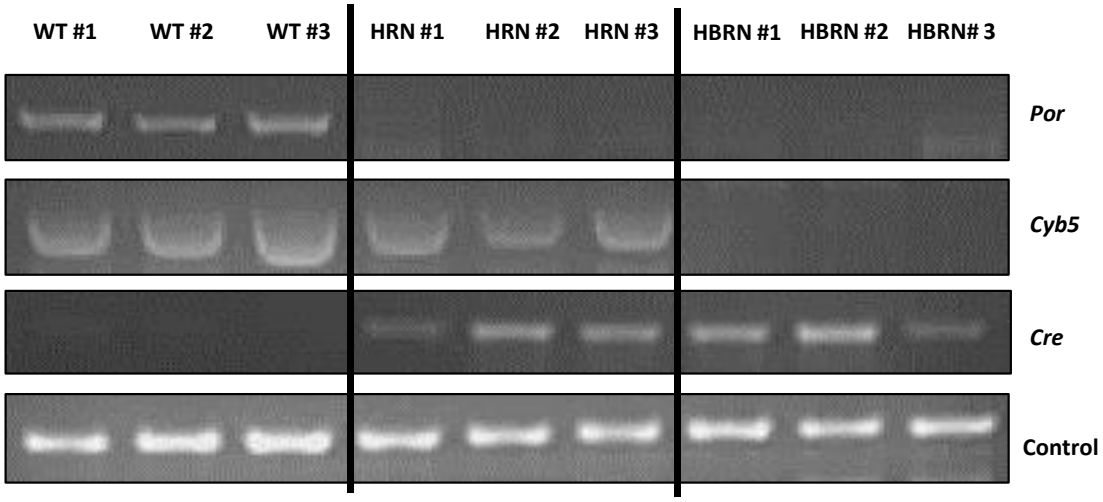

Figure 4.2: Genotyping of the DNA isolated from the livers of untreated WT, HRN and HBRN mice. *Por* gene was not detected in any of the HRN or HBRN mice and *Cyb5* gene was not detected in the HBRN mice. The *Cre* gene was present in only the HRN and HBRN mice however only a faint band was detected for in the HRN #1 mouse and the HBRN #3 mouse.

4.3.3 Enzyme activity of XMEs

POR activity was detected in all hepatic microsomal fractions isolated from untreated mice, with the highest level of activity highest in WT mice (**Figure 4.3a**). In the ellipticine-treated mice, POR activity was detected in the microsomal fractions from WT mice but not in knockout animals (**Figure 4.4a**), which is as expected given the deletion of POR in the hepatocytes of HRN and HBRN mice (Arlt et al., 2015a, Henderson et al., 2013). Sudan I oxidation (**Figure 4.3b** and **4.4b**), MROD activity (**Figure 4.3b** and **4.4c**) and EROD activity (**Figure 4.3d** and **4.4d**) were used as measures of Cyp1a1, Cyp1a2 and Cyp1a enzyme activity, respectively, and testosterone 6βhydroxylation (**Figure 4.3e** and **4.4e**) as a measure of Cyp3a enzyme activity. When the cofactor for POR, NADPH, was used in the reaction mixture, hepatic microsomes from WT mice exhibited the highest levels of Cyp1a activity, except for in EROD where the levels of activity were equal in WT and HRN hepatic microsomal fractions isolated from ellipticine-treated animals (compare **Figure 4.4d**).

According to the Sudan I oxidation and MROD assays (**Figure 4.4b** and **c**) Cyp1a1/2 activity was significantly lower in the hepatic microsomes from HRN mice which correlated with the lack of POR activity in HRN mice relative to WT mice. Cyp1a1/2 activity in hepatic microsomes from HBRN mice was significantly lower compared to WT and HRN mice and showed the lowest level of Cyp1a1/2 activity when NADPH was present. When NADPH was used in the reaction mixture, hepatic microsomes from WT mice exhibited the highest level of Cyp3a activity, with levels being greatly lower than in the HRN and HBRN fractions. In the hepatic microsomal fractions from untreated mice Cyp1a/1a2/3a activity was highest in the WT mice and lowest in the HBRN mice but the effect was less pronounced compared with mice treated with ellipticine (compare **Figure 4.3b, c, d** and **e** and **Figure 4.4b, c, d** and **e**).

When the cofactor for Cyb5R, NADH, was used in the reaction mixture, hepatic microsomes from ellipticine-treated HRN mice showed significantly higher Cyp1a

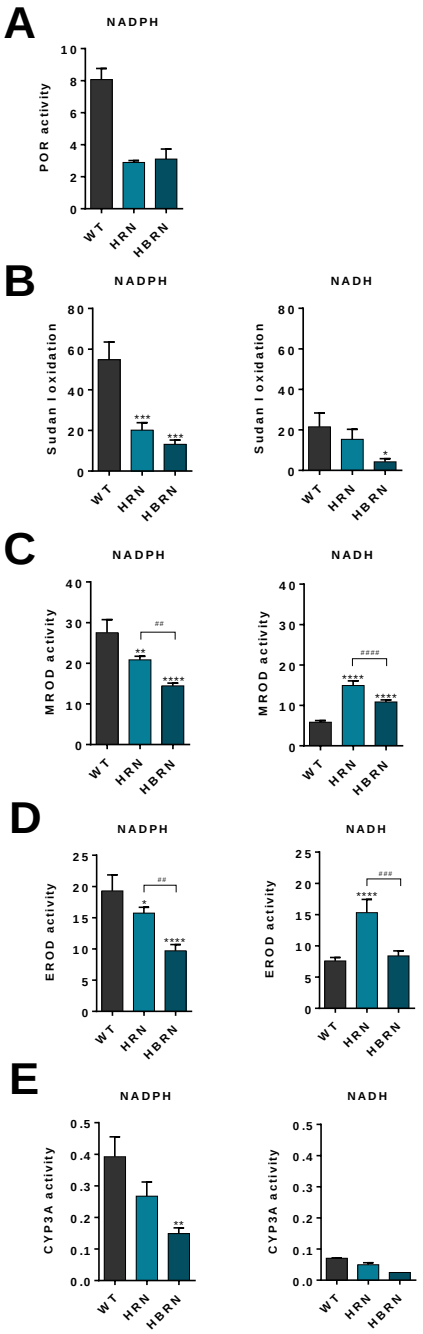

Figure 4.3: Enzyme activity in the pooled hepatic fractions of untreated WT, HRN and HBRN mice using either NADPH or NADH as the enzymatic cofactor. (A) POR activity was observed as nmol of cytochrome *c*/mg/min and was only detected in microsomal fractions from WT mice. (B) Cyp1a1 activity was determined by the oxidation of Sudan I to hydroxylated metabolites with activity being observed as nmol of total C-hydroxylated metabolites/mg protein/min. (C) Cyp1a2 activity was determined using the MROD assay with activity being observed as pmol of resorufin/mg protein/min. (D) Cyp1a activity was determined using the EROD assay with activity being observed as pmol of resorufin/mg protein/min. (E) Cyp3a activity was determined by the oxidation of testosterone to hydroxylated metabolites with activity being observed as nmol of total C-hydroxylated metabolites/mg protein/min. Values are given as ± SD (n=3). Repeat determinations were carried out within the same week.Statistical analysis was performed by one-way Anova with Tukey's multiple comparison test (* = compared to WT; # = compared to HRN. * $^{(\#)}$ $P \leq 0.05$ ** $^{(\#\#)}$ $P \leq 0.01$ *** $^{(\#\#\#)}$ $P \leq 0.001$**** $^{(\#\#\#\#)}$ $P \leq 0.0001$).

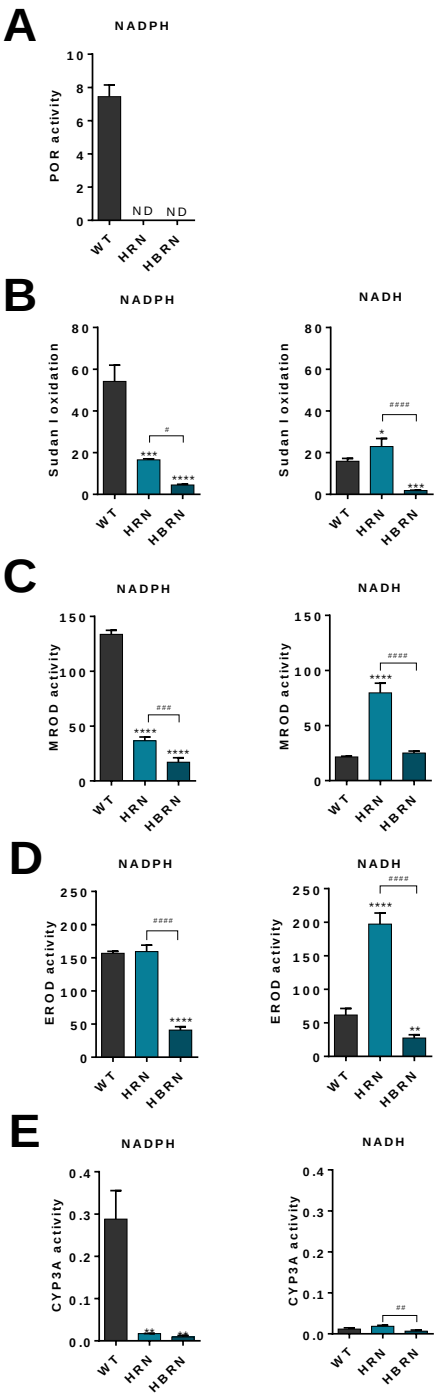

Figure 4.4: Enzyme activity in the pooled hepatic fractions of ellipticine-treated WT, HRN and HBRN mice using either NADPH or NADH as the enzymatic cofactor. (A) POR activity was observed as nmol of cytochrome *c*/mg/min and was only detected in microsomal fractions from WT mice. (B) Cyp1a1 activity was determined by the oxidation of Sudan I to hydroxylated metabolites with activity being observed as nmol of total C-hydroxylated metabolites/mg protein/min. (C) Cyp1a2 activity was determined using the MROD assay with activity being observed as pmol of resorufin/mg protein/min. (D) Cyp1a activity was determined using the EROD assay with activity being observed as pmol of resorufin/mg protein/min. (E) Cyp3a activity was determined by the oxidation of testosterone to hydroxylated metabolites with activity being observed as nmol of total C-hydroxylated metabolites/mg protein/min. Values are given as ± SD (n=3). Repeat determinations were carried out within the same week. Statistical analysis was performed by one-way Anova with Tukey's multiple comparison test (* = compared to WT; # = compared to HRN. * $^{(\#)}$ $P \leq 0.05$ ** $^{(\#\#)}$ $P \leq 0.01$ *** $^{(\#\#\#)}$ $P \leq 0.001$**** $^{(\#\#\#\#)}$ $P \leq 0.0001$).

activity than the hepatic microsomal fractions from ellipticine-treated WT and HBRN mice (**Figure 4.4b, c** and **d**). Using MROD as a measure for Cyp1a2 activity, enzyme activity was similar in ellipticine-treated WT and HBRN mice (**Figure 4.4c**). When EROD and Sudan I oxidation were used as a measure for Cyp1a activity hepatic microsomes from ellipticine-treated HBRN mice exhibited the lowest level of Cyp1a activity in the presence of NADH (**Figure 4.4b** and **d**). When NADH was used in the reaction mixture, hepatic microsomes from ellipticine-treated HRN mice showed significantly higher Cyp3a activity than the hepatic microsomal fractions from HBRN mice but not WT mice treated with ellipticine (**Figure 4.4e**). In the hepatic microsomal fractions from untreated mice Cyp1a/1a2 activity was highest in the HRN mice but was less pronounced compared with ellipticine-treated mice (**Figure 4.3c** and **d**). This pattern was not observed with Cyp1a1/3a activity with hepatic microsomal fractions from WT mice exhibiting higher levels of activity compared to HRN mice and the lowest activity levels in HBRN mice (**Figure 4.3b** and **e**).

4.3.4 Analysis of ellipticine metabolites by HPLC

Hepatic microsomes isolated from WT, HRN and HBRN mice were incubated with ellipticine and subsequently analysed by HPLC to determine the ellipticine metabolite profile. Representative HPLC chromatograms are shown in **Figure 4.5**. Three metabolites were formed in the microsomal incubations; 9-hydroxyellipticine (assigned to peak M1), 12-hydroxyellipticine (assigned to peak M2) and 13-hydroxyellipticine (assigned peak to M3) (**Figure 4.5a** and **b**). No metabolites were detected in control incubations without microsomes, without NADPH/NADH-generating system or without ellipticine (**Figure 4.5c** and **d**). There was still a large amount of unchanged ellipticine detected, indicating that only a small percentage was

metabolised during the incubation. The total formation of metabolites was highest in the hepatic microsomal fraction from WT mice when

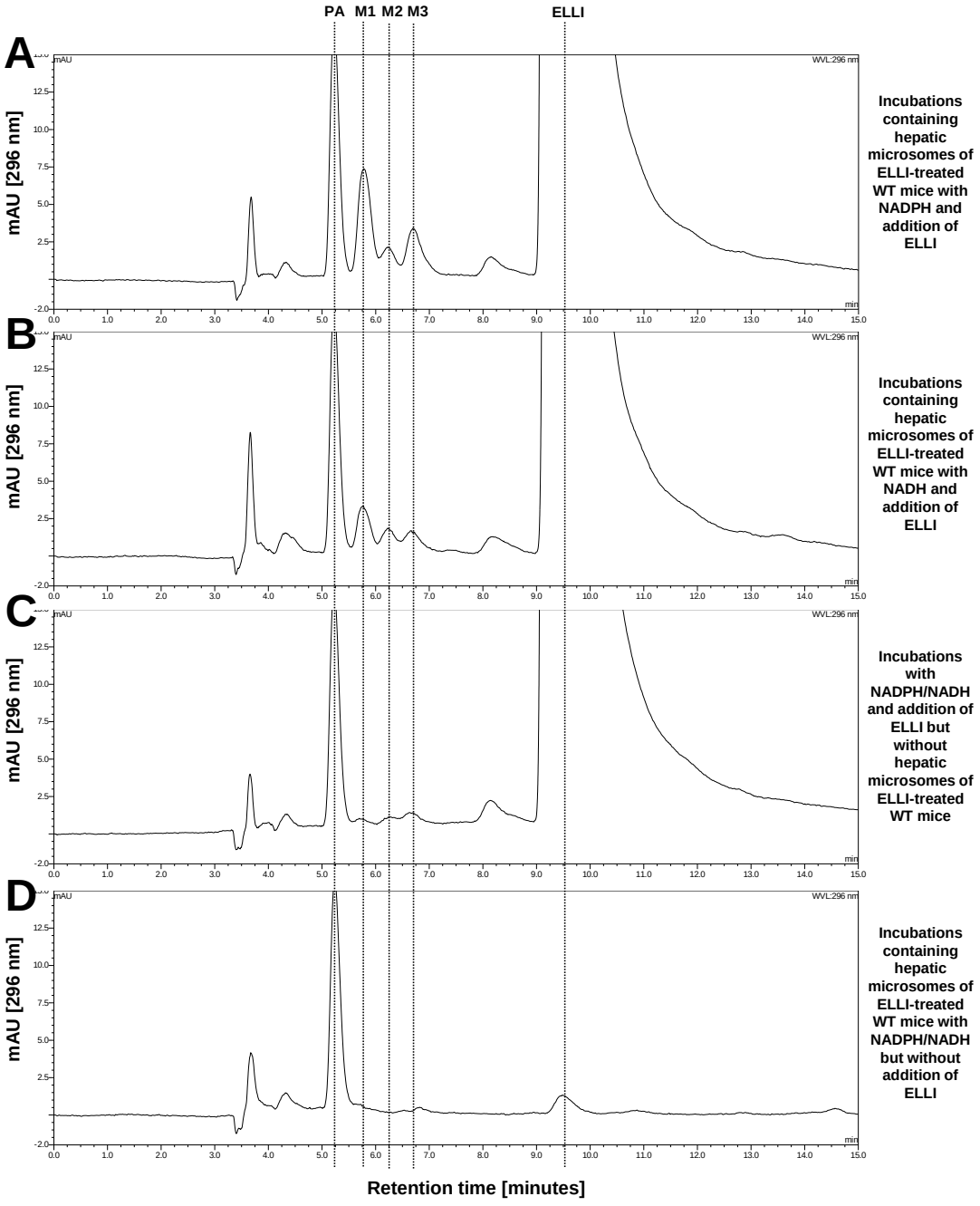

Figure 4.5: Representative HPLC chromatograms from *in vitro* incubations with hepatic microsomal fractions from ellipticine-pretreated WT mice with ellipticine (ELLI) and either NADPH or NADH as cofactor. M1: 9-hydroxyellipticine; M2: 12-hydroxyellipticine; M3: 13-hydroxyellipticine. Phenacetin (PA) was used as internal standard.

NADPH was used in the reaction mix (**Figure 4.5a**). Total ellipticine metabolite formation in hepatic microsomal fractions from WT mice was around 3-fold higher compared to when NADH was used (**Figure 4.5a**). Hydroxylated ellipticine metabolites were identified and the structures are shown in **Figure 1.7**. When NADPH was used as cofactor the overall formation of metabolites was significantly lower in hepatic microsomal fractions from untreated HRN mice with production of 9-hydroxyellipticine and 13-hydroxyellipticine being significantly lower compared with untreated WT, and 12-hydroxyellipticine not being detected (**Figure 4.6**). The lowest level of overall ellipticine metabolite formation was with the hepatic microsomal fractions isolated from untreated HBRN mice (**Figure 4.6a**). All metabolites were detected at significantly lower amounts than with WT hepatic microsomes and 9-

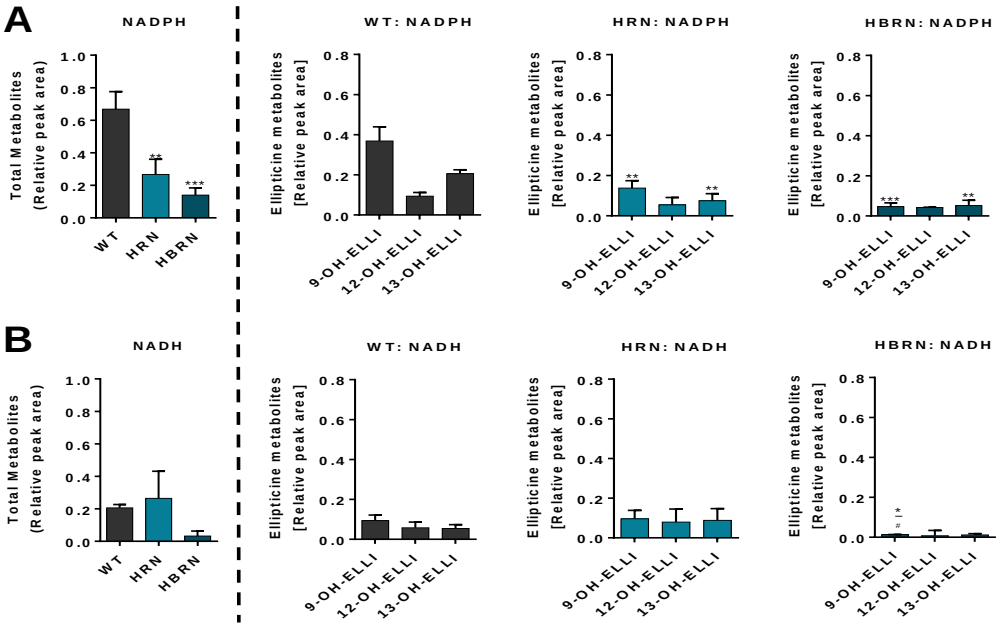

Figure 4.6: Total formation of ellipticine metabolites and formation of individual metabolites during *in vitro* incubations with hepatic microsomal fractions from untreated WT, HRN and HBRN mice using either A, NADPH or B, NADH as an enzymatic cofactor. Values given as ± SD (n=3). Repeat incubations were carried out and analysed within the same week. Statistical analysis was performed by one-way Anova with Tukey's multiple comparison test (* = compared to WT; # = compared to HRN. * $^{(\#)}$ $P \leq 0.05$ ** $^{(\#\#)}$ $P \leq 0.01$ *** $^{(\#\#\#)}$ $P \leq 0.001$). ND, not detected.

hydroxyellipticine was lower compared with HRN hepatic microsomes isolated from control (untreated) animals (**Figure 4.6**).

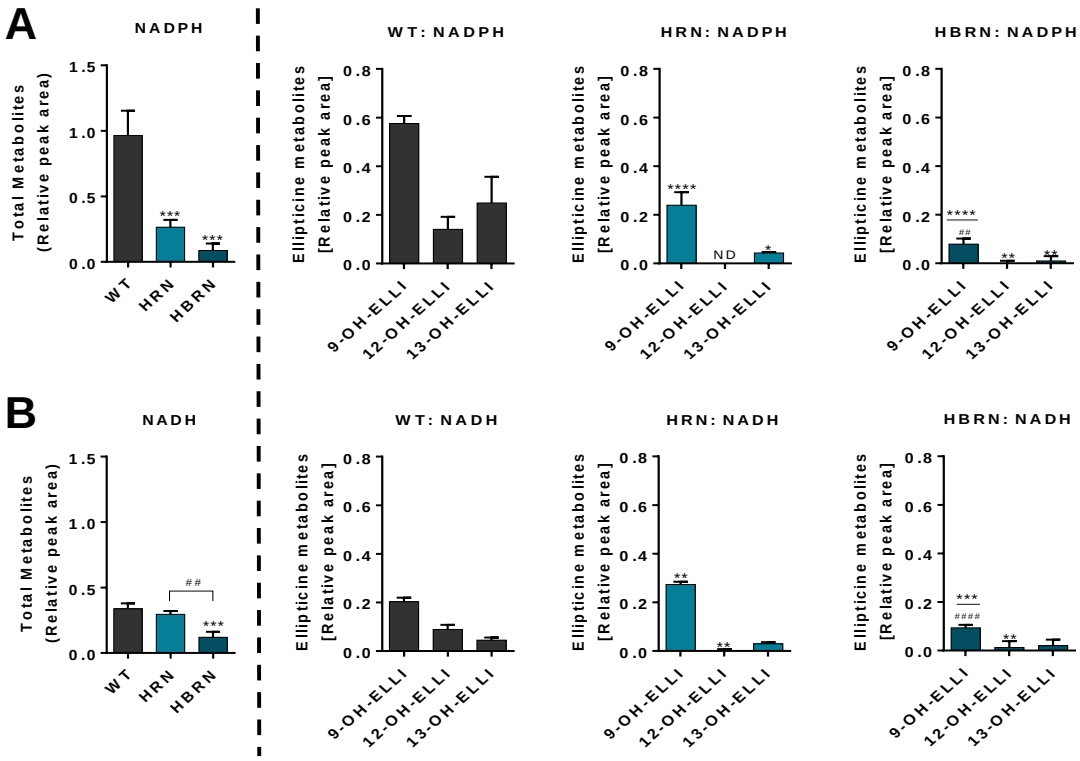

Figure 4.7: Total formation of ellipticine metabolites and formation of individual metabolites during *in vitro* incubations with hepatic microsomal fractions from ellipticine-treated WT, HRN and HBRN mice using either A, NADPH or B, NADH as an enzymatic cofactor. Values given as ± SD (n=3). Repeat incubations were carried out and analysed within the same week. Statistical analysis was performed by one-way Anova with Tukey's multiple comparison test (* = compared to WT; # = compared to HRN. * $^{(\#)}$ $P \leq 0.05$ ** $^{(\#\#)}$ $P \leq 0.01$ *** $^{(\#\#\#)}$ $P \leq 0.001$ **** $^{(\#\#\#\#)}$ $P \leq 0.0001$). ND, not detected.

When NADH was used as cofactor the overall formation of metabolites in hepatic microsomal fractions isolated from untreated HRN mice was not significantly different to fractions from untreated WT with 9-hydroxyellipticine being significantly higher but 12-hydroxyellipticine being significantly lower and no significant difference in the levels of 13-hydroxyellipticine. Overall metabolite formation in hepatic fractions isolated from untreated HBRN mice was significantly lower than with both WT and HRN fractions from control (untreated) animals (**Figure 4.6b**) with

9-hydroxyellipticine being significantly lower compared with both WT and HRN fractions and 12-hydroxyellipticine being significantly lower compared with WT (**Figure 4.6b**). When incubations were carried out using hepatic microsomal fractions from treated mice (**Figure 4.7**), the overall formation of ellipticine metabolites was highest in WT mice when NADPH was used in the reaction mixture (**Figure 4.7a**), whereas when NADH was used the highest formation of metabolites was seen in HRN mice (**Figure 4.7b**). The rate of ellipticine metabolism in the hepatic microsomal fractions correlated with the levels of Cyp1a/3a enzymatic activity and the particular enzymatic cofactor used (compare **Figures 4.4** and **4.6**).

4.3.5 Ellipticine-DNA adduct formation *in vitro*

The ability of hepatic microsomes isolated from WT, HRN and HBRN mice to catalyse ellipticine-DNA adduct formation *in vitro* was investigated (**Figure 4.8a**). The ellipticine-DNA adduct pattern obtained by ^{32}P-postlabelling analysis from microsomal incubations consisted of one major and one minor adduct spot (assigned adduct 1 and 2) previously detected *in vitro* and *in vivo* (Stiborova et al., 2008, Stiborova et al., 2012b, Stiborová et al., 2012). Because the adduct spots were incompletely separated total ellipticine-DNA adduct levels were determined. When NADPH was used the highest ellipticine-DNA adduct formation was seen in microsomal fractions from WT mice. There was significantly less DNA adduct formation with the microsomal fractions isolated from ellipticine-pretreated HRN and HBRN mice (**Figure 4.9**). The degree of total ellipticine-DNA adduct formation in the hepatic microsomal fractions correlated with the amounts of ellipticine metabolites formed (compare **Figure 4.7a**). When NADH was used there was no significant difference in adduct formation between any of the fractions (**Figure 4.9**).

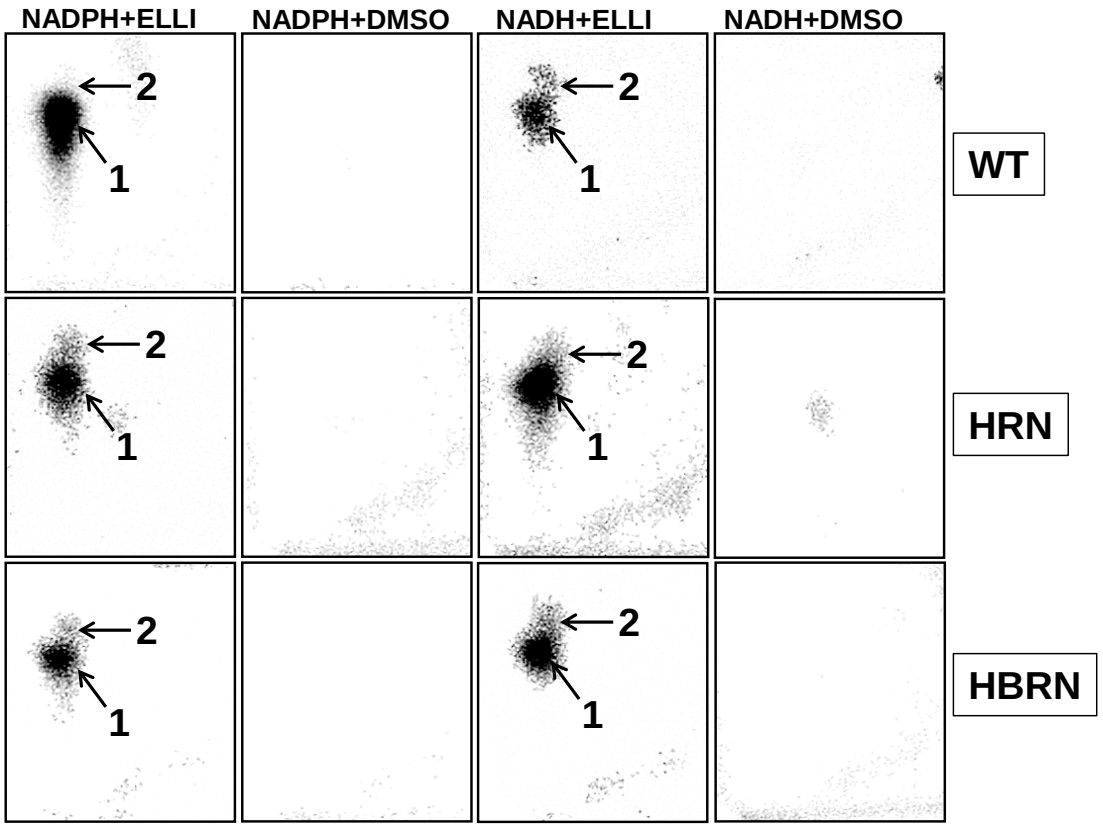

Figure 4.8: Autoradiograms showing adduct profiles by TLC ^{32}P-postlabelling analysis from *in vitro* incubations with hepatic microsomal fractions from ellipticine (ELLI)-pretreated WT, HRN and HBRN mice, DNA and ellipticine. The origin on the TLC plate, at the bottom left-hand corners, was cut off before exposure. See text for details. Adduct spots 1 and 2 are formed in deoxyguanosine residues of DNA by metabolites 13-hydroxyellipticine and 12-hydroxyellipticine, respectively.

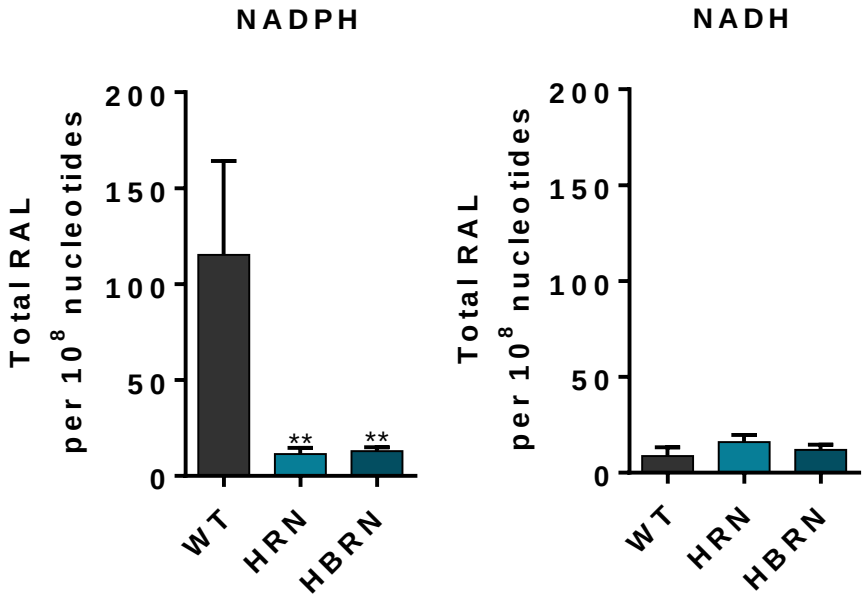

Figure 4.9: Total formation of ellipticine-DNA adducts during *in vitro* incubations with hepatic microsomal fractions from ellipticine-pretreated WT, HRN and HBRN mice using either NADPH or NADH as an enzymatic cofactor. Duplicate incubations were carried out within the same week and DNA stored at –20°C until analysis. Values are given as ± SD (*n*=4); DNA from two separate incubations were measured in duplicate in separate ^{32}P-postlabelling analyses. Statistical analysis was performed by one-way Anova with Tukey's multiple comparison test (* = compared to WT; ** $P \leq$ 0.01).

4.3.6 Ellipticine-DNA adduct formation *in vivo*

The ellipticine-DNA adduct pattern obtained from *in vivo* treatments consisted of one major adduct spot (**Figure 4.10**) previously detected *in vitro* and *in vivo* (Stiborova et al., 2008, Stiborova et al., 2012b, Stiborová et al., 2012). Another adduct, tentative assigned adduct spot 4 (**Figure 4.10**), which was detected previously in ellipticine-treated rats and mice (Stiborova et al., 2008, Stiborova et al., 2003a, Stiborova et al., 2014a, Stiborová et al., 2007), was also formed in WT and HRN mice in selected tissues. As this adduct was detectable in only a few tissues (liver, lung and small intestine) in WT and HRN mice but not HBRN, its level was not quantified when adduct formation was compared between tissues. Of the organs tested (liver, lung, kidney, small intestine, spleen, colon and bladder) only the liver, lung and small

intestine exhibited any significant differences between the mouse models (**Figure 4.11**). In the lung and small intestine the levels of ellipticine-DNA adducts were significantly higher in HRN mice compared with WT mice. DNA adduct formation in the livers of HRN and HBRN mice was significantly lower, by 62% and 73%, respectively, than in WT mice.

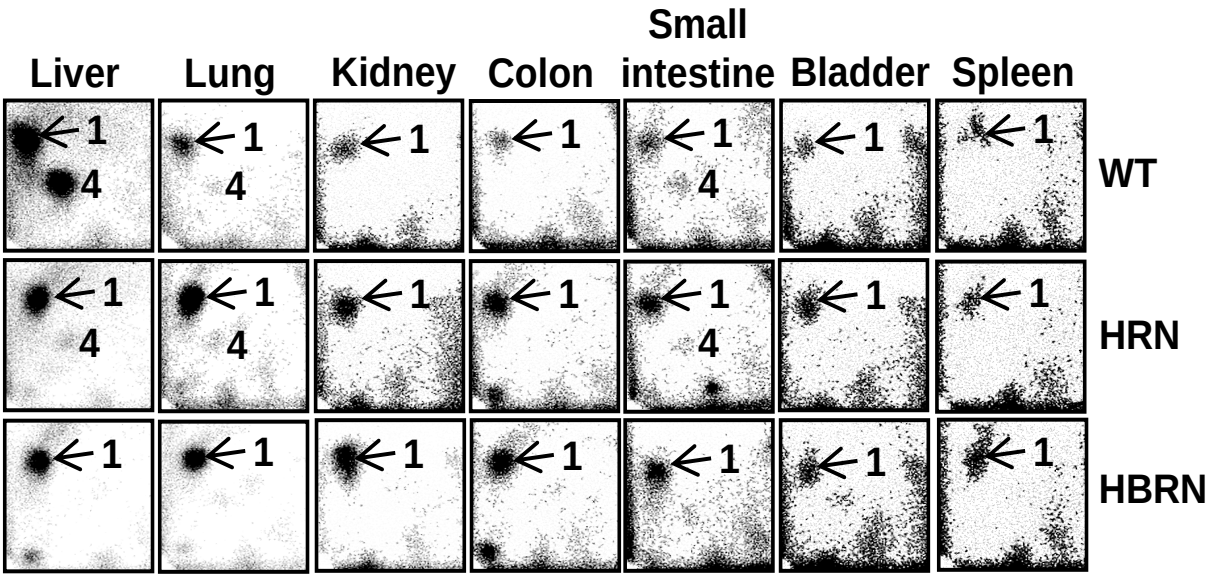

Figure 4.10: Autoradiographs of ellipticine-DNA adducts in liver, lung, kidney, colon, small intestine, bladder and spleen tissues in ellipticine-treated WT, HRN and HBRN mice. The origin on the TLC plate, at the bottom left-hand corners, was cut off before exposure. Adduct spot 1 is formed in deoxyguanosine residues of DNA by the metabolite 13-hydroxyellipticine.

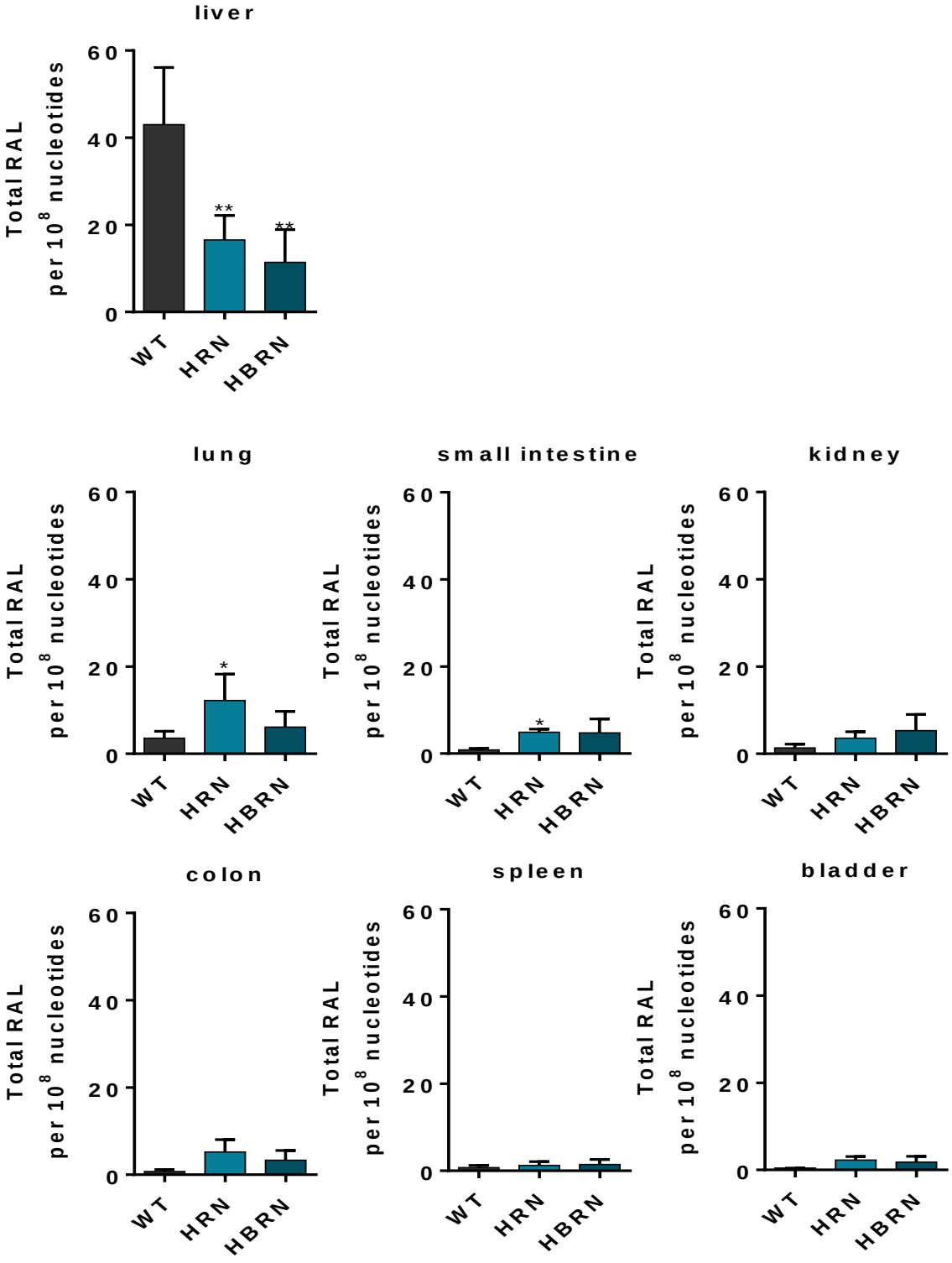

Figure 4.11: Quantitative TLC ^{32}P-postlabelling analysis of ellipticine-DNA adducts in organs of WT, HRN and HBRN mice treated i.p with 10 mg/kg bw ellipticine for 24 h. Values are given as ± SD (*n*=4); each DNA sample isolated from tissue of individual animals was analysed once. Statistical analysis was performed by one-way Anova with Tukey's multiple comparison test (* = compared to WT; * $P \leq 0.05$).

4.4 Discussion

Although the role of the electron donor protein Cyb5 in the metabolic activation of ellipticine has been well characterised *in vitro*, its role *in vivo* is less understood. In the present study both HRN mice, which lack expression of hepatic POR, and HBRN mice, which lack expression of hepatic POR and Cyb5, have been used to investigate the contribution of Cyb5 to the metabolic activation of ellipticine *in vivo* and *in vitro.*

The *in vitro* experiments in this study were carried out using pooled hepatic microsomal fractions. When NADPH was used as cofactor to examine the POR-dependent pathway in hepatic microsomal fractions from ellipticine-treated mice, cytochrome P450 enzyme activity assays clearly showed a reduction in Cyp1a activity as electron donors were lost. However, whilst significant reductions in total ellipticine metabolite and ellipticine-DNA adduct formation were found compared to WT there was no significant difference between HRN and HBRN fractions themselves, correlating with the results from Cyp3a marker activity. When the NADH-dependent Cyb5R pathway was investigated, there was higher Cyp1a enzyme activity in the microsomal fractions of HRN mice than in those of WT mice. In the microsomal fractions from HBRN mice the activity was significantly lower relative to WT mice, indicating that increased NADH-dependent activity is caused by the increased expression of Cyb5. Cyp1a activity did not correlate with total ellipticine metabolite formation as there was no significant difference between the WT and HRN fractions with only HBRN fractions showing significant reductions compared to both WT and HRN. Although this reduction in total metabolite formation would be suggestive of the contribution of Cyb5 to the activation of ellipticine, whilst all metabolites formed by HBRN fractions were reduced compared to WT, the only metabolite significantly

reduced in HBRN fractions compared to HRN fractions was 9-hydroxyellipticine, a detoxication metabolite. This supports previous results in the HRN mouse with 9-hydroxyellipticine being affected by the absence of POR and cytochrome P450 activity more than other metabolites (Stiborova et al., 2008). Total ellipticine-DNA adduct formation *in vitro* in the presence of NADH was lower than when NADPH was present, but not significantly different between the mouse lines.

In the *in vitro* experiments carried out in hepatic microsomal fractions from untreated mice, POR activity was detected in both the HRN and HBRN fractions. It was postulated that this could be due to contamination from a WT liver sample; however, no Cyb5 was detected, which would have been present in this case. Genotyping was carried out on retained liver samples from the untreated mice. Although both *Por* and *Cyb5* appeared to be excised, a very faint *Cre* band was detected in one of the untreated HRN and one of the untreated HBRN mice (see **Figure 4.12**). One potential explanation as to why some POR expression and activity was detectable in the hepatic microsomal fractions could be due to Cre mosaicism, whereby there is variable or inconsistent Cre expression in different cells within the liver (Heffner et al., 2012). However the successful knockout of Cyb5 in the hepatocytes further complicates the results. Despite the presence of POR, enzyme activity was reduced in the microsomal fractions apart from in the case of Sudan I oxidation where there was no pronounced difference in the levels of activity between the treated and untreated microsomal fractions.

Previous studies with reconstituted CYP1A1 and CYP1A2 showed that the presence of Cyb5 in the reaction mixture alters the resulting ellipticine metabolites profiles, with a shift from detoxication metabolites, 9-hydroxyellipticine and/or 7-

hydroxyellipticine, to metabolites that can ultimately form DNA adducts, 12-hydroxyellipticine and/or 13-hydroxyellipticine (Kotrbova et al., 2011). These findings were echoed in studies using human CYP3A4 in Supersomes™, which found that the presence of Cyb5 in the reaction mixture also led to an increase in formation of 12-hydroxyellipticine and 13-hydroxyellipticine (Stiborova et al., 2012a, Stiborová et al., 2012, Stiborová et al., 2017). In hepatic microsomal fractions from HBRN mice that do not possess either electron donor, metabolite formation was significantly lower than with WT fractions regardless of the cofactor used. In the hepatic microsomal fractions from HRN mice in the presence of NADH, however, the formation of 9-hydroxyellipticine was significantly higher than with microsomal fractions from WT mice whilst metabolites associated with metabolic activation were significantly lower (i.e. 12-hydroxyellipticine). The absence of Cyb5 in hepatic microsomal fractions from HBRN mice correlates with the findings from reconstituted P450 enzymes suggesting Cyb5 contributes to the activation of ellipticine *in vitro* (Kotrbova et al., 2011, Stiborová et al., 2017, Stiborova et al., 2012a, Stiborová et al., 2012). This correlation, however, does appear to be limited to ellipticine metabolite formation. Previous studies (Kotrbova et al., 2011, Poljakova et al., 2005, Stiborova et al., 2013a, Stiborová et al., 2017) found that the shift in metabolite production was coupled with an increase in *in vitro* ellipticine-DNA adduct formation. The hepatic microsomal fractions from the present study, however, found no significant difference between DNA adduct formation in HRN or HBRN hepatic microsomal fractions regardless of the enzymatic cofactor used.

The present *in vivo* results correlated with *in vitro* ellipticine-DNA adduct formation when NADPH was used as cofactor. Both HRN and HBRN mice showed significantly lower (~60-70%) hepatic ellipticine-DNA adduct formation than WT mice, but there

was no significant difference between the two knockout lines. The HRN results correlate with a previous study that found a 65% reduction in hepatic DNA-adduct formation in HRN mice (Stiborova et al., 2008) suggesting a greater contribution of the POR-dependent pathway to the bioactivation of ellipticine *in vivo*. *In vitro* experiments carried out in the present study with the cofactor NADH showing Cyb5R-dependent pathways contributing to ellipticine bioactivation in HRN mice correlated with *in vivo* adduct formation in the lungs and small intestine of HRN mice, suggesting that the Cyb5/Cyb5R systems contributes to ellipticine-DNA adduct formation in these extrahepatic organs of HRN mice. Ellipticine-DNA adduct formation in the extrahepatic organs of WT and HRN mice has been observed previously with HRN mice showing higher levels than WT mice, suggesting that ellipticine or its metabolites are being distributed via the bloodstream to organs and tissues with the metabolic capacity to oxidatively activate ellipticine (Stiborova et al., 2008). In the present study there was a trend for ellipticine-DNA adduct levels to be higher in the extrahepatic organs, i.e. kidney, colon and bladder, of both HRN and HBRN mice than of WT mice, with levels of ellipticine-DNA adduct formation being significantly higher in the lungs and small intestines of HRN mice than of WT mice. This could be due to the decreased levels of P450-mediated ellipticine metabolism in the livers of HRN and HBRN mice causing higher amounts of ellipticine to be distributed to extrahepatic organs. Levels of ellipticine-DNA adduct formation were not greatly different in any of the extrahepatic organs of HBRN mice compared to WT mice, suggesting that increased levels of activated ellipticine in the extrahepatic organs could be attributed to Cyb5 activity in the HRN mice.

The significant reduction in DNA adduct formation in the livers of HRN and HBRN mice indicates that P450 enzymes are responsible for the majority of ellipticine

activation, although hepatic DNA adduct formation in HRN and HBRN mice is still detectable. It is possible that ellipticine activation still occurs due to the greater induction of hepatic cytochrome P450 enzymes in HRN and HBRN mice compared to WT mice combined with expression of POR and Cyb5 in the non-parenchymal liver cells. Further investigation of this would require isolation and culture of hepatocytes and non-parenchymal liver cells from HBRN mice and exposure of these cells to ellipticine for subsequent ellipticine-DNA adduct analysis, but this was beyond the scope of the present study. The bioactivation of ellipticine can also be catalysed via cytochrome P450-independent mechanisms that are not dependent on POR or Cyb5. Numerous peroxidases such as bovine LPO, human MPO, ovine COX-2 and plant HRP have previously been shown to activate ellipticine to reactive metabolites, which form two DNA adducts analogous to those generated by the P450-mediated reactions (Stiborova et al., 2007). Of the ellipticine metabolites, peroxidases predominantly form an ellipticine dimer (Stiborova et al., 2007), and generate the reactive intermediate ellipticine-13-ylium that is responsible for formation of adduct 1 (**Figure 1.7**). Another metabolite detected was the N^2-oxide (**Figure 1.7**), interestingly one that is also generated by the oxidation of ellipticine by P450s and forms adduct 2 *in vitro* after the N^2-oxide undergoes the Polonowski re-arrangement to form 12-hydroxyellipticine (Poljakova et al., 2005). In several tissues in ellipticine-treated WT and HRN mice (present study) we detected adduct 4, which has also been observed previously in ellipticine-treated rats (Stiborova et al., 2003a, Stiborova et al., 2014a, Stiborová et al., 2007) and *in vitro* studying ellipticine-DNA adduct formation recombinant human CYP3A4 expressed in Supersomes™ (Stiborova et al., 2011). However, the structure of this adduct has not yet been elucidated. Peroxidase-mediated

ellipticine activation was also shown to generate two additional DNA adducts (Stiborova et al., 2007) that were, however, not detected in this study.

Studies with hepatic microsomal fractions from WT and HRN mice from mice pretreated with BaP were carried out to investigate the effect of enzyme induction on activation of ellipticine *in vitro* (Stiborova et al., 2013a). Microsomal incubations with ellipticine, DNA and arachidonic acid, a cofactor for COX-dependent oxidation, showed DNA adduct formation at a level similar to that when POR, Cyp1a or Cyp3a enzymes were inhibited in hepatic microsomal fractions from untreated mice. In the hepatic microsomal fractions from mice pretreated with BaP, ellipticine-DNA adduct formation with arachidonic acid was higher, very likely due to induction of COX by BaP, with no significant difference between fractions from WT and HRN mice (Stiborova et al., 2013a). This participation of COX in hepatic microsomal fractions from HRN mice suggests that peroxidases could be responsible for the activation of ellipticine in the livers of HRN and HBRN mice.

In summary, this study has shown that whilst POR contributes to the bioactivation of ellipticine *in vitro,* the role of Cyb5 is still rather unclear. The role of Cyb5 in the activation of ellipticine *in vivo* in both HRN and HBRN mice appears to be less important. These findings confirm the importance of P450 enzymes in the bioactivation of ellipticine. Whilst non-parenchymal liver cells may play a role in catalysing P450-mediated bioactivation of ellipticine in HRN and HBRN mice, the presence of ellipticine-DNA adducts in the livers of HRN and HBRN mice suggests the involvement of a P450-independent bioactivation mechanism.

5 The application of a murine cytochrome P450 oxidoreductase null cell line for the assessment of cytochrome P450-mediated metabolism of benzo[*a*]pyrene and its DNA adduct formation *in vitro*

5.1 Introduction

Previous *in vivo* studies using a variety of different cytochrome P450, electron donor, or *Ahr* knockout mice treated with BaP yielded paradoxical results to *in vitro* studies. Whereas *in vitro* studies show that P450s are important for the bioactivation of BaP (Stiborova et al., 2017, Stiborova et al., 2016a, Stiborova et al., 2016b, Stiborova et al., 2014c), *in vivo* studies have demonstrated a more important role for P450s in detoxication (Arlt et al., 2012, Arlt et al., 2008, Sagredo et al., 2009, Sagredo et al., 2006, Uno et al., 2004, Uno et al., 2006, Uno et al., 2001). This was also seen with the results from the study described in Chapter 3. In order for this paradoxical effect to be investigated further without the limitations of working with mouse models, such as limited tissue availability and ethical issues, an *in vitro* model would be required.

Metabolism in a whole organism is complex, and although *in vivo* models are the most relevant, it is costly. The use of *in vivo* models has also come under scrutiny in recent years with schemes such as the 3Rs aiming to replace, reduce, and refine animal models within research. Cell culture models can be alternative experimental tools in understanding the role of enzymes in the bioactivation of carcinogens. A well-studied murine hepatocyte line is the Hepa-1c1c7 line, which was developed from a study that sought to isolate and generate a hepatoma cell line that produced serum albumin, a

characteristic of hepatocytes, at a higher rate than in pre-existing cultured hepatoma cells (Darlington et al., 1980). This cell line was derived from the clonal line Hepa-1 from a hepatoma that arose in a C57L mouse line and propagated in C57L/J mice, and which was found to be stable over an extended period in continuous culture (Bernhard et al., 1973). One characteristic of this line is that it expresses Ahr and has highly inducible Cyp1a1 (Hankinson, 1979, Fong et al., 2005). This makes Hepa-1c1c7 cells suitable for studying BaP metabolism due to the importance of Cyp1a1 in the initial oxidation step of BaP to produce reactive metabolites (Baird et al., 2005). Hepa-1c1c7 cells have been shown previously to be capable of metabolising BaP to numerous metabolites. High levels of 3-hydroxy-BaP formation were observed compared to 9-hydroxy-BaP, which was attributed to Cyp1a1 being the predominant cytochrome P450 in these cells, as the same metabolic profile has been reported using cloned Cyp1a1 in the presence of BaP (Holme et al., 2007, Gautier et al., 1996). Previous studies using Hepa-1c1c7 cells have shown that BaP-induced apoptosis develops over a period of 24 hours with the main apoptotic steps being dependent on Cyp1a1 induction and the formation of the reactive metabolite BPDE (Solhaug et al., 2005, Solhaug et al., 2004a, Solhaug et al., 2004b). The ability of the cells to form reactive metabolites was also demonstrated with the formation of the DNA adduct dG-N^2-BPDE (Holme et al., 2007), the same adduct that is formed *in vivo* (Arlt et al., 2012, Arlt et al., 2008). The importance of P450-mediated BaP activation was demonstrated in Hepa-1c1c7 cells as Cyp1a1 was shown to be accountable for cell cytotoxicity and apoptosis in studies using Cyp1a1 inhibitors α-naphthoflavone and ellipticine (Chung et al., 2007).

The aim of the present study was to create an *in vitro* model that is able to mimic the HRN mouse model, which demonstrated high levels of DNA adduct accumulation in

multiple studies after BaP exposure (Arlt et al., 2012, Arlt et al., 2008, Reed et al., 2018b), in order to investigate the role of cytochrome P450-mediated metabolism in the activation of BaP *in vitro*. POR expression was disrupted in the Hepa-1c1c7 cells using the CRISPR/Cas9 system and a single clone was isolated and expanded to produce a uniform cell line. The response of the cell model to BaP exposure was investigated by analysing the expression of XMEs and cytochrome P450 electron donors, BaP metabolite formation, DNA damage (comet assay) and DNA adduct formation.

5.2 Methods

Hepa-1c1c7 cells were cultured as described in section 2.7. Disruption of the *Por* gene was carried out using the CRIPSR/Cas9 system. Transfection of the cells and selection of transfected cells were carried out according to section 2.8.1. Isolation of single cell clones and the subsequent generation of a cell line were described in section 2.8.2. The response to BaP was investigated in WT cells exposed to a control double nickase plasmid and in the knockout cells from the single cell isolation in order to assess both the contribution of POR to BaP metabolism in the cell and any potential off-target effects of the double nickase plasmid. Hepa-1c1c7 cells were seeded and exposed to BaP according to section 2.7.5. Cytotoxicity to BaP in all three cell lines was assessed using crystal violet staining according to section 2.9. Upon selection of an appropriate concentration of BaP the expression of electron donor proteins and XMEs were investigated by Western blotting as described in section 2.10. Formation of BaP metabolites was investigated by HPLC analysis of metabolites extracted from the cell culture medium as described in section 2.11. DNA damage was investigated in the

cells after exposure to BaP using the comet assay as described in section 2.12. DNA adduct formation in the cells was analysed as described in section 2.14.

5.3 Results

5.3.1 Cell morphology

Cells transfected with control plasmid (C) and POR knockout plasmid (POR KO) did not show any visual differences in cell morphology compared to WT Hepa-1c1c7 cells after having undergone transfection with CRISPR/Cas9 plasmids (**Figure 5.1**).

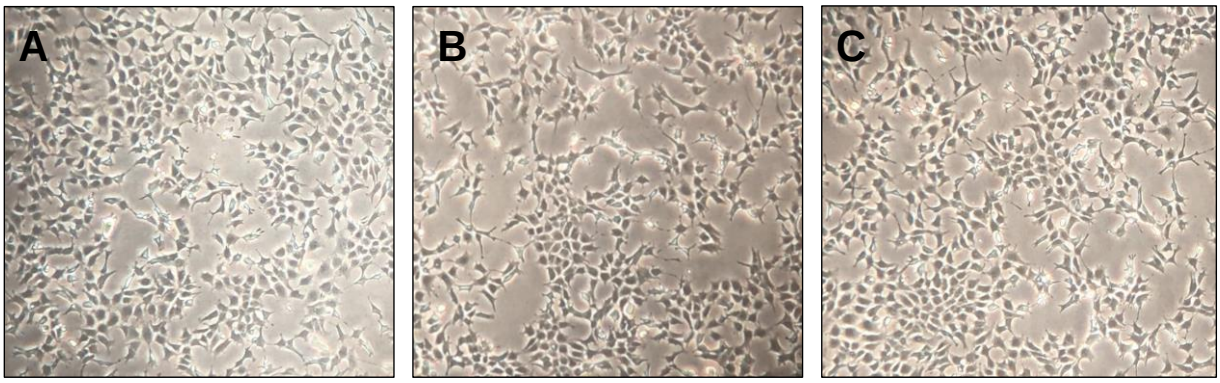

Figure 5.1: Representative images of WT Hepa-1c1c7 cells (A), Hepa-1c1c7 cells transfected with control plasmid (B) and POR KO Hepa-1c1c7 cells (C).

5.3.2 BaP-induced cytotoxicity

WT, C and POR KO cells were treated with a range of concentrations of BaP over a 24- and 48-hour period. WT and C cells displayed no pronounced difference in the threshold of cell viability. Cells lacking POR expression, however, did not display any substantial decrease in the percentage cell viability over 24 or 48 hours (**Figure 5.2**). Based on the cytotoxicity data in WT cells 0.5 µM BaP was selected for further experiments, which led to ~60-70% cell viability over 24 or 48 hours.

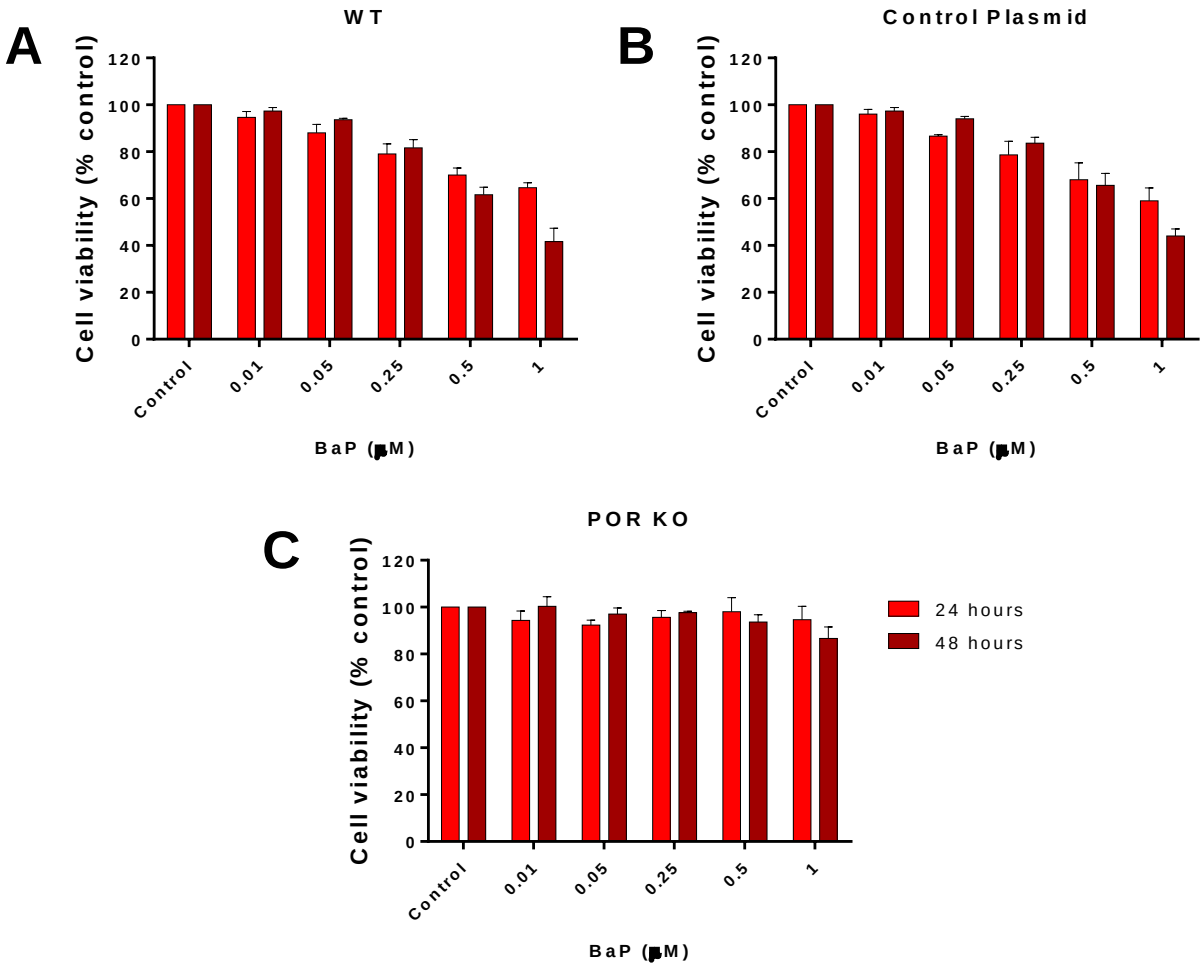

Figure 5.2: Cytotoxicity of WT (a), C (b) and KO (c) Hepa-1c1c7 cell lines after treatment with a range of concentrations of BaP over a 24 and 48 hour period. Values are given as mean ± SD (*n*=3).

5.3.3 Protein expression of XMEs

Expression of POR, Cyb5 and Cyb5R and Cyp1a1 were probed for in BaP-treated (0.5 μM) and untreated WT, C and KO cells (**Fig. 5.3**). POR was expressed in WT and C cells but no expression was observed in the POR KO cells. Cyb5 and Cyb5R were expressed across all cell lines. Treatment with BaP did not alter the levels of POR and Cyb5R expression relative to controls. Cyb5 and Cyp1a1, however, were induced in all cell lines by BaP treatment; and the extent of Cyp1a1 and Cyb5 induction by BaP was similar in all cell lines.

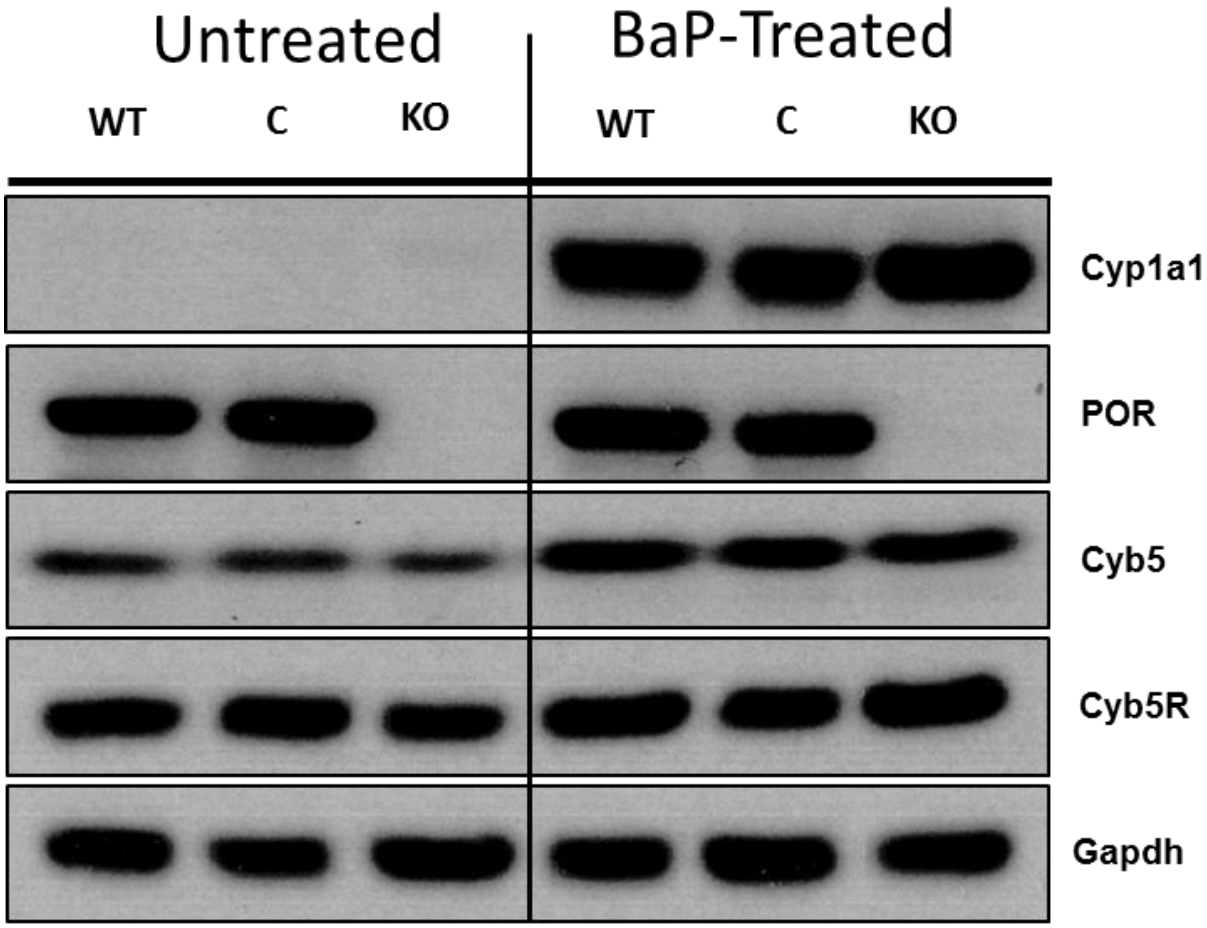

Figure 5.3: Western blot analysis of Cyp1a1, POR, Cyb5 and Cyb5R in untreated (lanes 1-3) and BaP-treated (0.5 µM for 24 hours; lanes 4-6) WT, C and KO Hepa-1c1c7 cells. Representative images of the Western blotting are shown, and at least duplicate analysis was performed from independent experiments. Gapdh protein expression was used as a loading control.

5.3.4 Analysis of BaP metabolites by HPLC

WT, C and KO cells were treated with 0.5 µM BaP for 24 hours before the cell medium was removed and BaP metabolites extracted. Extracts were subsequently analysed by HPLC to determine the BaP metabolite profile. BaP-7,8-dihydrodiol, the precursor to BPDE, and BaP-tetrol-I-1, one hydrolysis product of BPDE, were the two metabolites detected along with unmetabolised BaP. The two BaP metabolites analysed were

identified using authentic standards as described previously (Wohak et al., 2016). The highest level of metabolite formation was seen in the KO cells with formation of both BaP-7,8-dihydrodiol and BaP-tetrol-I-1 being higher than that of WT and C cells (**Figure 5.4**). There was no significant difference in metabolite formation between WT and C cells for either BaP-7,8-dihydrodiol or BaP-tetrol-I-1. The level of unmetabolised BaP was not significantly different across any of the cell lines. No BaP or BaP metabolites were detected in untreated WT, C or KO cells (**Figure 5.5a**). Representative chromatograms showing the BaP metabolite profiles are shown in **Figure 5.5**.

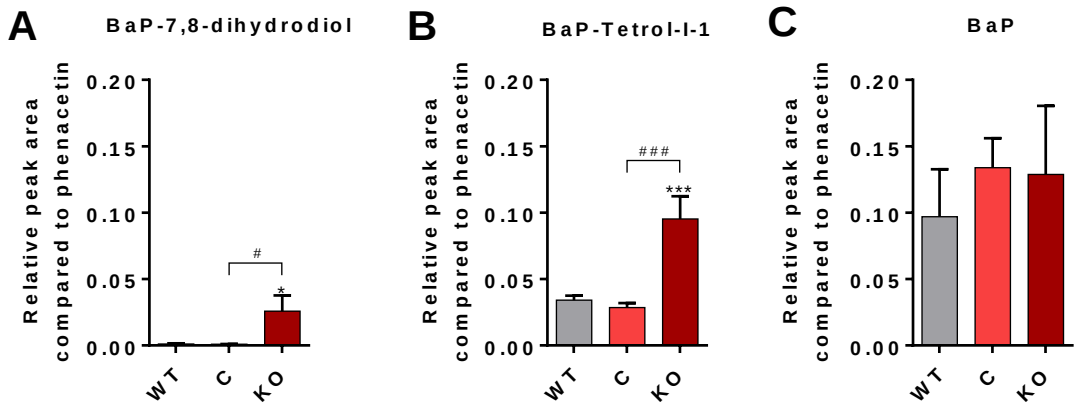

Figure 5.4: Formation of BaP-7,8-dihydrodiol (A), BaP-tetrol-I-1 (B) and BaP (C) in WT, C and POR KO Hepa-1c1c7 cells after treatment with 0.5 µM BaP for 24 hours. Values are given as mean ± SD (*n*=3). Statistical analysis was performed by one-way Anova with Tukey's multiple comparison test (* = compared to WT; # = compared to C. * $P \leq 0.05$ *** $P \leq 0.001$).

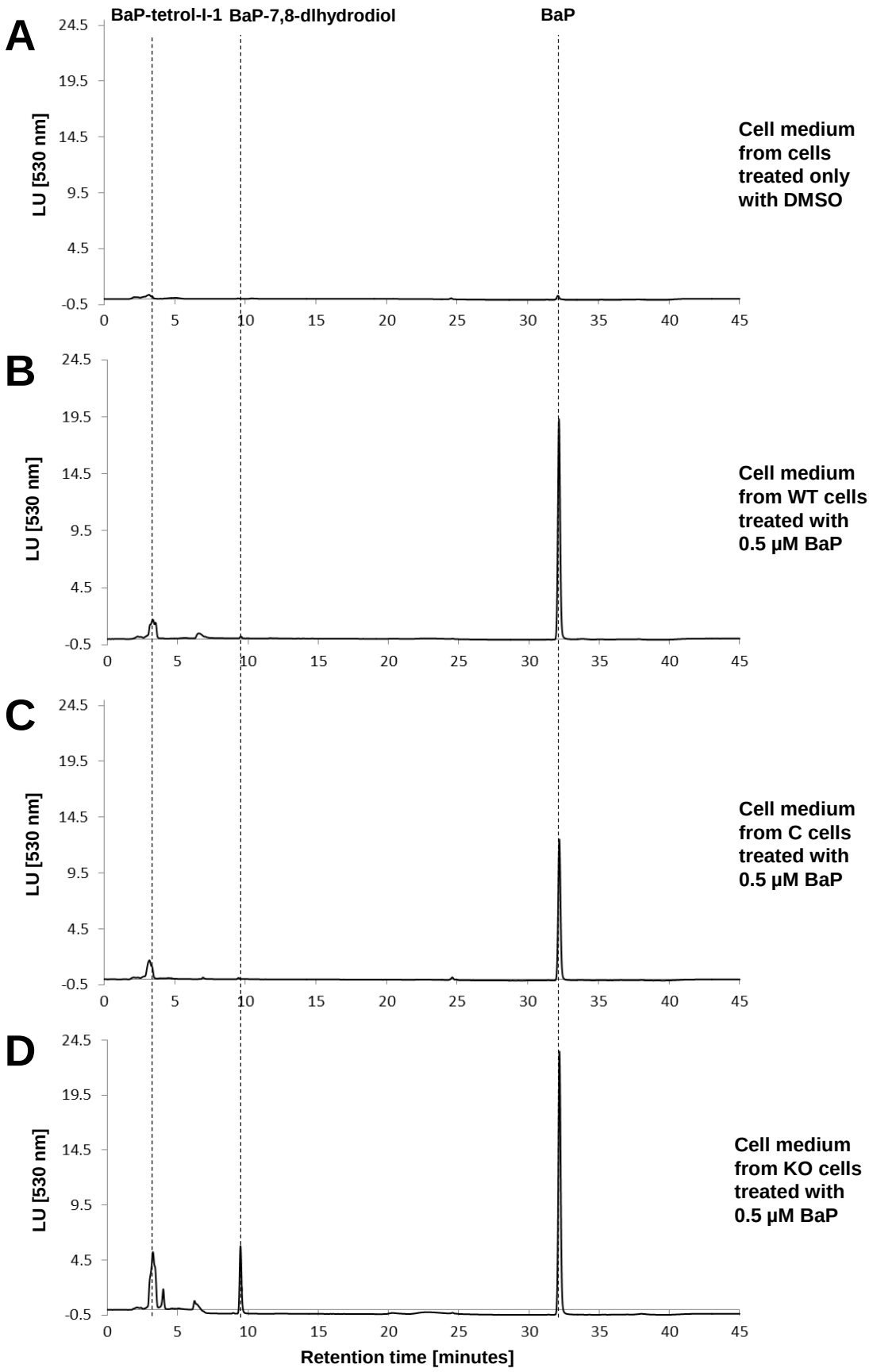

Figure 5.5: Representative HPLC chromatograms from WT, C and KO Hepa-1c1c7 cells treated with 0.5 µM BaP for 24 hours. Phenacetin (PA) was used as internal standard.

5.3.5 Analysis of DNA damage by comet assay

DNA damage caused by exposure to BaP in the different Hepa1c1c7 cell lines was assessed using the comet assay. WT, C and KO cells were treated with 0.25, 0.5 and 1 µM BaP for 24 hours before analysing DNA damage with the comet assay (**Figure 5.6**). In untreated cells, no difference was observed across any of the cell lines. No significant difference was observed in WT and C cells when exposed to any of the BaP concentrations tested. No significant difference was observed in WT, C or POR KO cells when exposed to 0.25 µM BaP. When treated with 0.5 and 1 µM BaP, POR KO cells exhibited significantly higher levels of DNA damage when compared to both WT and C cells.

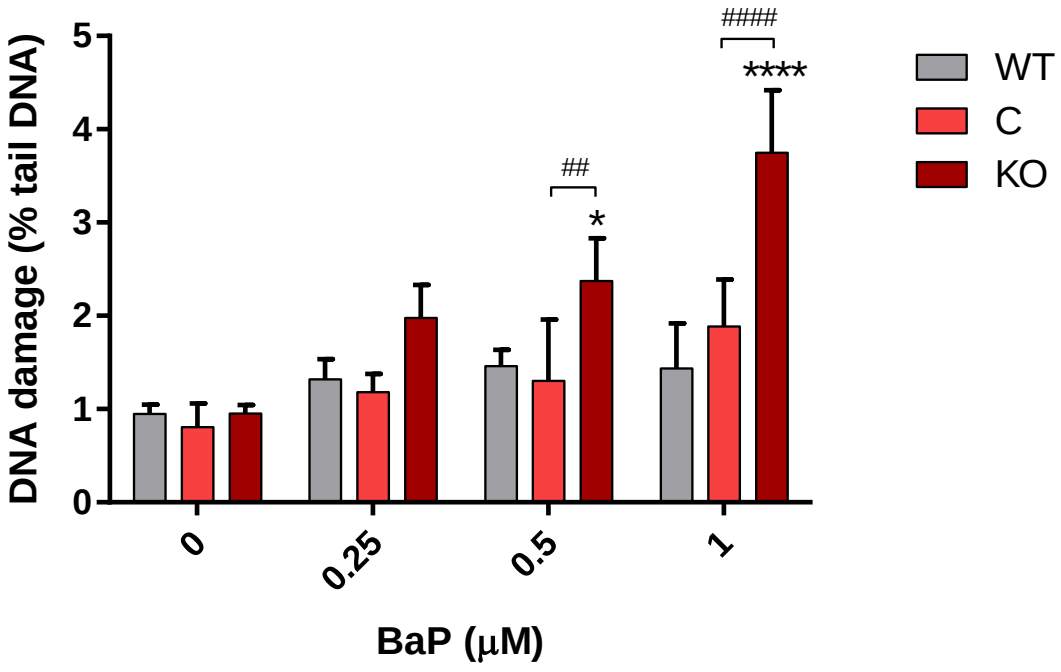

Figure 5.6: Assessment of DNA damage (% tail DNA) in WT, C and POR KO Hepa-1c1c7 cells using the comet assay. Cells were either untreated or treated with 0.25, 0.5 or 1 µM BaP for 24 hours. Values are given as ± SD (*n*=3); 50 nuclei/sample were scored and averaged. Statistical analysis was performed by one-way Anova with Tukey's multiple comparison test (* = compared to WT; # = compared to C. * $P \leq 0.05$, ** $P \leq 0.01$, **** $P \leq 0.0001$).

5.3.6 BaP-DNA adduct formation

The ability of WT, C and KO cells to catalyse BaP-DNA adduct formation was investigated. DNA isolated from untreated cells or those treated with 0.5 µM BaP for 24 hours was analysed using the ^{32}P-postlabelling method. The BaP-DNA adduct pattern obtained by ^{32}P-postlabelling analysis consisted of one adduct spot previously identified as dG-*N*^{2}-BPDE (Arlt et al., 2008) (**Figure 5.7)**. An additional spot was present on the autoradiogram from POR KO Hepa-1c1c7 cells, however the structure has not yet been identified. No DNA adducts were detected in untreated cells (data not shown). BaP-DNA adduct formation was significantly higher in POR KO cells compared to both WT and C cells (**Figure 5.8**). There was no significant difference between WT and C cells. Levels of dG-*N*^{2}-BPDE formation in the POR KO cells correlated with the formation of BaP-7,8-dihydrodiol and BaP-tetrol-I-1 (compare **Figure 5.4** and **Figure 5.8**) and DNA damage as measured by the comet assay (compare **Figure 5.6** and **Figure 5.8**).

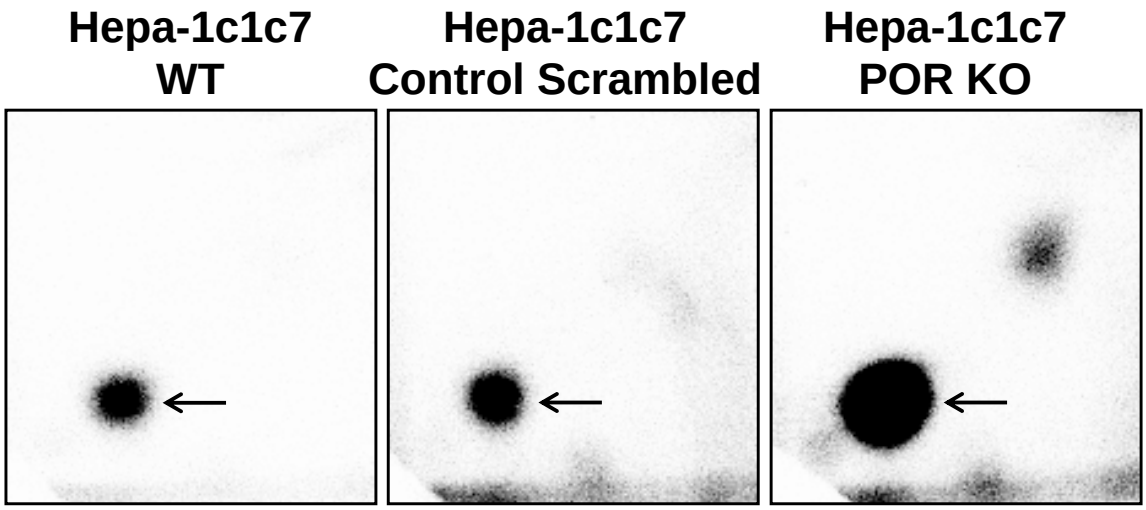

Figure 5.7: Autoradiograms showing adduct profiles by TLC ^{32}P-postlabelling in WT, C and POR KO Hepa-1c1c7 cells treated with 0.5 µM BaP for 24 h. The origin on the TLC plate, at the bottom left-hand corners, was cut off before exposure. The arrow indicates the dG-*N*^{2}-BPDE adduct. See text for details.

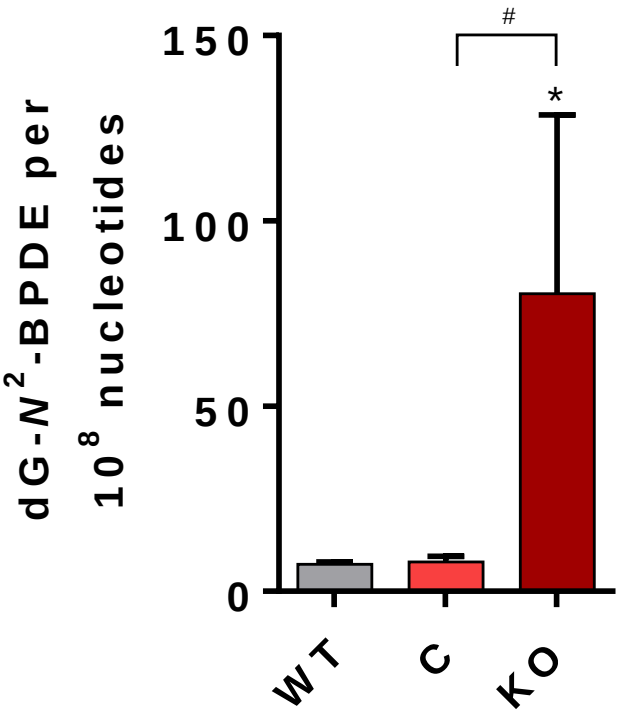

Figure 5.8: Quantitative TLC ^{32}P-postlabelling analysis of dG-N^2-BPDE adducts in WT, C and POR KO Hepa-1c1c7 cells treated with 0.5 µM BaP for 24 h. Values are given as ± SD (n=3). Statistical analysis was performed by one-way Anova with Tukey's multiple comparison test (* = compared to WT; $^{\#}$ = compared to C. * $P \leq 0.05$).

5.4 Discussion

The roles of the electron donors POR and Cyb5 have been investigated *in vivo* in the HRN and HBRN mouse models (see Chapters 3 and 4). Despite the absence of P450 activity in the hepatocytes of the mouse models, HRN mice exhibited significantly higher levels of hepatic DNA formation, whilst HBRN mice showed no significant difference in hepatic DNA formation when compared to WT mice. In order to further investigate the paradoxical result seen in the livers of HRN mice, the *Por* gene was deleted in the murine hepatoma derived cell line Hepa-1c1c7 using CRISPR/Cas9 technology leading to transfected cells not expressing POR. In order to assess any potential off-target effects of the transfection process, WT Hepa-1c1c7 cells were also transfected with a plasmid containing scrambled gRNA. The transfection process with scrambled gRNA did not affect expression of XMEs and electron donor proteins in the cells when compared with WT cells. No significant difference between WT and C cells was observed during metabolite formation, DNA damage (comet assay) and DNA adduct formation analysis. The expression of Cyb5 was induced in all cell lines after BaP treatment, this induction is in line with a higher protein expression of Cyb5 in the livers of HRN mice after repeated BaP exposure. This effect was also seen in WT and C Hepa-1c1c7 cells, however, which was not observed in the livers of BaP-treated WT mice (Arlt et al., 2012). POR KO Hepa-1c1c7 cells exhibited a resistance to BaP toxicity compared to WT and C cells, suggesting that BaP is not being activated to reactive, genotoxic metabolites. However, BaP metabolite formation was significantly higher in POR KO cells compared to both WT and C cells. This result was in contrast to the lower levels of metabolite formation in incubations with hepatic microsomal fractions from HRN mice compared to WT mice when NADPH was used

as cofactor (Reed et al., 2018b). DNA damage (comet assay) in the cells correlated with metabolite formation with significantly higher levels of DNA damage observed in POR KO cells than WT and C cells. This indicated that the BaP metabolites detected in the cell culture medium were exerting genotoxic effects in the cells which was confirmed by the formation of dG-N^2-BPDE adducts, as this adduct is formed via the cytochrome P450-mediated pathway and proceeds via BaP-7,8-dihydrodiol formation. The dG-N^2-BPDE adduct is the same adduct as seen in the HRN mouse model and the accumulation of BaP-DNA adducts in the absence of POR in POR KO cells correlates with previous studies carried out with the HRN mouse (Arlt et al., 2012, Arlt et al., 2008). The second adduct observed in *in vitro* incubations with hepatic microsomal fractions, which is likely derived from the reaction of 9-hydroxy-BaP-4,5-epoxide with guanine (Reed et al., 2018b), was not detected in the Hepa-1c1c7 model.

Due to the Hepa-1c1c7 model expressing Ahr and possessing highly inducible Cyp1a1 (Hankinson, 1979, Fong et al., 2005), Hepa-1c1c7 cells that lack a functional *Cyp1a1* gene or the transcription factors controlling its expression have been developed previously (Hankinson, 1979, Hankinson, 1995, Ma and Whitlock, 1996). Hepa-1c1c7 cells with an Ahr-defective (Ahr-D) phenotype were generated using targeted gene disruption (Ma and Whitlock, 1996). The phenotype of the cells was affected considerably, by the 90% reduction of Ahr expression in the Ahr-D Hepa-1c1c7 cells compared to WT. The Ahr-D Hepa-1c1c7 cells exhibited morphological changes, appearing less well-differentiated, more spindle shaped and failing to form well-organised monolayers at high density. Ahr-D Hepa-1c1c7 cells exhibited decreased rates of proliferation in culture and showed barely detectable levels of albumin. Disruption of the *Por* gene in Hepa-1c1c7 cells in this study, however, contrasted with the Ahr-D Hepa-1c1c7 model as reduction of P450 activity did not noticeably affect

cell morphology in culture, the ability to form well-organised monolayers or cell growth and proliferation. Previous studies that selected BaP resistant clones of Hepa-1c1c7 cells discovered that BaP resistant clones had greatly reduced specific activities of aryl hydrocarbon hydroxylase, now known as Cyp1a1, due to a defective induction mechanism (Hankinson, 1979, Hankinson, 1995). This correlates with the BaP-induced cytotoxicity investigated in this study where cell viability in POR KO cells was higher compared to both WT and C cells.

The POR KO Hepa-1c1c7 model demonstrated a resistance to BaP toxicity, a trait observed in Cyp1a1-defective Hepa1c1c7 cells (Hankinson, 1979, Hankinson, 1995). The ability of Cyp1a1-defective Hepa1c1c7 cells to catalyse BaP into reactive intermediates that form DNA adducts was investigated previously. In the absence of Cyp1a1 activity in these cells, BaP-DNA adducts were virtually undetectable (Uno et al., 2001). These results correlated with the hepatic microsomal fractions from HRN and HBRN mice incubated with BaP *in vitro* that had reduced levels of DNA adduct formation (Reed et al., 2018b). The results obtained from the present study contrast with these previous findings, with DNA adduct formation being greater in POR KO cells than in WT and C cells expressing POR, correlating instead with the findings *in vivo* with HRN mice (Arlt et al., 2012, Arlt et al., 2008, Reed et al., 2018b). Why both Cyp1a1-defective cells and POR KO cells exhibit resistance to BaP cytotoxicity yet demonstrate such substantial differences in levels of DNA adduct formation is not known. It is also unclear why cells that are resistance to BaP toxicity also exhibit increased DNA damage and DNA adduct formation. Tissues are protected from the effects of carcinogens by cell death such as apoptosis due to the removal of cells with extensive DNA damage. DNA damage often initiates various cell signalling pathways related to DNA repair activity, cell cycle arrest and cell survival or cell death

(apoptosis). The relative proportion of the different cell signalling pathways triggered by DNA damage upon exposure will, to a large degree, determine if the compound will give rise to predominantly mutagenic or cytotoxic effects (Holme et al., 2007). It is possible that the absence of POR-mediated P450 activity could alter the cell signalling response in the POR KO Hepa-1c1c7 cells.

The metabolites detected in the cell medium, BaP-7,8-dihydrodiol and BaP-tetrol-I-1, are associated with BaP activation. WT Hepa-1c1c7 cells have previously been shown to form BaP tetrols, the hydrolysis products of BPDE metabolites, a reaction catalysed by Cyp1a1 (Holme et al., 2007, Gautier et al., 1996). However, POR KO Hepa-1c1c7 cells were able to form the BaP-tetrol and dihydrodiol at a greater rate than WT and C Hepa-1c1c7 cells. By disrupting the *Por* gene as opposed to a single cytochrome P450 enzyme, *i.e.* Cyp1a1, it was possible to overcome the issue of substrate overlap in hepatic P450s that could have also been activating BaP (Nebert and Dalton, 2006). Although POR is the predominant electron donor to P450s, Cyb5 is also able to act as the sole electron donor to P450s, enabling some catalytic activity. Reconstituted systems utilising CYP1A1, POR, Cyb5, and mEH in different ratios were used to investigate the role of Cyb5 in the metabolic activation of BaP *in vitro.* The results showed that even when levels of POR were low, CYP1A1, Cyb5, and mEH activated BaP efficiently to reactive species that bind to DNA (Stiborova et al., 2014c). In HBRN mice, the absence of Cyb5 was shown to result in significantly less hepatic DNA adduct formation than in HRN mice (Reed et al., 2018b) and it is possible that expression of Cyb5 is most likely contributing to the formation and accumulation of metabolites and DNA adducts in the POR KO Hepa-1c1c7 cells. HRN and HBRN mice were found to have steatotic livers that could have stored BaP. Lipid content of the Hepa-1c1c7 cells lacking POR was not assessed, however if a similar effect on

lipid metabolism were to occur in POR KO Hepa-1c1c7 cells it could alter the BaP bioavailability, BaP metabolism and elimination. BaP has been shown to be sequestered in Hepa-1c1c7 cells in lipid droplets throughout the intracellular space, with the highest percentage found attached to the ER near the nucleus (Rizwan et al., 2015). In the present study, levels of unmetabolised BaP by HPLC were the same in all the cell lines; however, this only took into account BaP in the cell culture medium, not BaP sequestered in cells.

One proposed explanation for the paradoxical results from previous *in vitro* and *in vivo* studies was the presence of a P450-independent bioactivation mechanism in hepatocytes (Reed et al., 2018a). The metabolites and adducts detected in POR KO Hepa-1c1c7 cells are all derived from the cytochrome P450-mediated pathway. Hepa-1c1c7 cells have been shown to express inducible COX-2 (Puga et al., 1997). BaP is a good substrate for COX-2 as well as Cyp1a1 and Cyp1b1 and is capable of metabolising BaP to reactive intermediates that bind with DNA (Nemoto and Takayama, 1984, Marnett, 1990). Alongside COX-2, AKR and LOX-5 have also been implicated in the activation of BaP (Wang et al., 2017). The results from this study have demonstrated the role of P450 enzymes in the detoxication of BaP and the potential for a P450-independent activation mechanism.

6 The application of a human cytochrome P450 oxidoreductase null cell line for the assessment of cytochrome P450-mediated metabolism of benzo[*a*]pyrene and its DNA adduct formation *in vitro*

6.1 Introduction

Investigations of the role of P450 enzymes in the bioactivation of BaP in mice have yielded paradoxical results in *in vivo* studies to *in vitro* studies. Whereas *in vitro* studies show that P450s are important for the bioactivation of BaP (Stiborova et al., 2017, Stiborova et al., 2016a, Stiborova et al., 2016b, Stiborova et al., 2014c), *in vivo* studies have demonstrated a more important role for P450s in detoxification (Arlt et al., 2012, Arlt et al., 2008, Sagredo et al., 2009, Sagredo et al., 2006, Uno et al., 2004, Uno et al., 2006, Uno et al., 2001). This was also seen with the results from the study described in Chapter 3. The POR KO Hepa-1c1c7 cell line used in Chapter 5 yielded results that correlate with the *in vivo* studies. Whilst these results bring into question the role of P450 enzymes in mice, it is unknown whether this is also observed in human models.

A widely used and well-studied human hepatocyte cell line is HepG2. It is a hepatocellular carcinoma-derived cell line that is frequently used as *in vitro* alternative to primary human hepatocytes (Donato et al., 2015). Although HepG2 cells have reduced levels of some metabolic activities compared to primary human hepatocytes they have been shown to be capable of inducing phase I and phase II enzymes involved in BaP metabolism and DNA adduct formation (Wilkening et al., 2003). Generally,

HepG2 has been described as a sensitive model for identifying and quantifying DNA-damaging properties of environmental and dietary agents (Knasmuller et al., 1998). Several studies have shown that BaP-DNA adduct formation increases in HepG2 cells in a concentration-dependent manner (Naspinski et al., 2008, Shiizaki et al., 2017, Hockley et al., 2006). BaP-DNA-adduct formation has been shown to be less dependent on time as no significant difference was observed within the time points of 6, 25 and 48 hours studied (Hockley et al., 2006). Changes in gene expression, however, were shown to be time- and concentration-dependent with changes observed in genes involved in xenobiotic metabolism, cell cycle regulation, apoptosis/anti-apoptosis, chromatin assembly and oxidative stress response. The overall response to BaP consisted of up-regulation of tumour suppressor genes and down-regulation of oncogenes promoting cell cycle arrest and apoptosis. Anti-apoptotic signalling that may increase cell survival and promote tumourigenesis was also evident (Hockley et al., 2006).

P450 activity has also been shown to play an important role within the metabolism of BaP in HepG2 cells: when cells were pretreated with TCDD and subsequently exposed to BaP had BaP-DNA-adduct formation as well as *HPRT* mutation frequency were reduced through the induction of CYP1A1. These effects were shown to be even more pronounced in cells exposed to BPDE after TCDD pretreatment (Shiizaki et al., 2013), suggesting that increased levels of CYP1A1 are protective against BaP-induced DNA damage. This effect was also seen in HepG2 cells transfected with PXR that lead to increased levels of XME protein expression (e.g CYP1A2, GST and UGT). Levels of BaP-DNA-adducts were significantly reduced compared to WT HepG2 cells with lower levels of XME expression, again demonstrating the protective role of P450 enzymes in the HepG2 model (Naspinski et al., 2008). Although the response of

HepG2 cells with increased levels of XME expression to BaP has been investigated, the response of cells after treatment with BaP in the absence of P450 activity is less well understood.

The aim of the present study was to use a human cell culture model that lacks POR protein expression to investigate whether this human *in vitro* model mimics the results observed in the HRN mouse model *in vivo* (Arlt et al., 2012, Arlt et al., 2008, Reed et al., 2018b) and the POR KO Hepa-1c1c7 mouse model *in vitro* (Chapter 5), which both formed high levels of DNA adducts after BaP exposure. For this approach to examine the role of P450-mediated metabolism in the activation of BaP in a human *in vitro* model, a commercially available POR KO HepG2 cell line was used alongside WT HepG2 cells. The response of the cells to BaP exposure was investigated by analysing the expression of XMEs and P450 electron donors, BaP metabolite formation, DNA damage (comet assay) and DNA adduct formation.

6.2 Materials and Methods

HepG2 cells were cultured as described in section 2.7. The response to BaP was investigated in WT cells and POR KO cells in order to assess both the contribution of POR to BaP metabolism in the cell. HepG2 cells were seeded and exposed to BaP according to section 2.7.5. Cytotoxicity to BaP in both cell lines was assessed using crystal violet staining according to section 2.9. Upon selection of an appropriate concentration of BaP the expression of electron donor proteins and XMEs were investigated using Western blotting as described in section 2.10. Formation of BaP metabolites was investigated by extracting metabolites from cell media and analysed using HPLC as described in section 2.11. DNA damage in the cells after exposure to BaP was investigated using the comet assay as described in section 2.12. DNA adduct formation in the cells was analysed as described in section 2.14.

6.3 Results

6.3.1 BaP-induced cytotoxicity

WT and POR KO cells were treated with a range of BaP concentrations (0.5-10 µM) over a 24- or 48-hour period (**Figure 6.1**). POR KO cells showed a lesser degree of difference between 24- and 48-hour exposure times in the different concentrations when compared to WT cells. POR KO cells also showed less cytotoxicity in the 48-hour exposure time at the higher concentrations of 5 and 10 µM (**Figure 6.1b)**. Based on the cytotoxicity data in the WT cells, 2.5 and 5 µM BaP were selected for further experiments which led to ~70% cell viability over 24 or 48 hours.

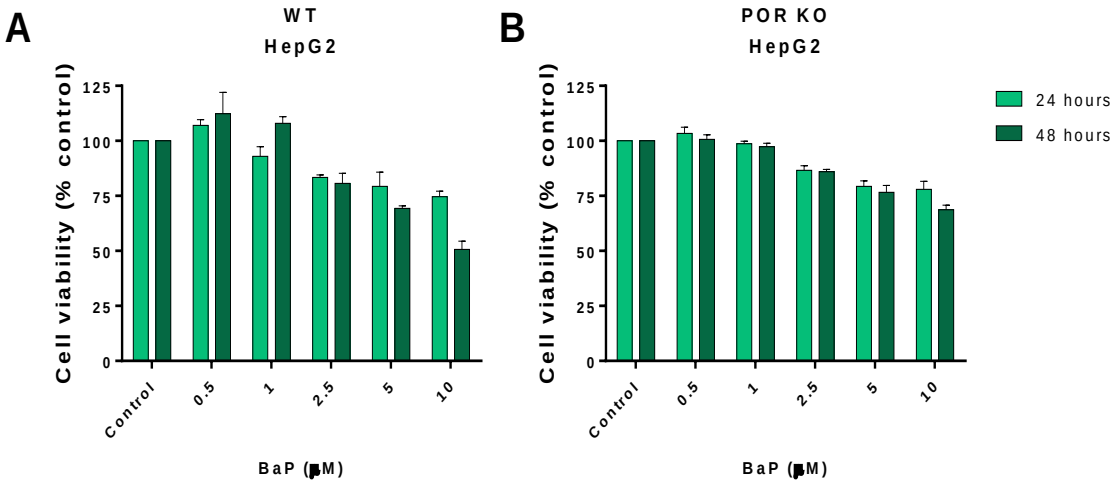

Figure 6.1: Cytotoxicity of WT (A) and POR KO (B) HepG2 cell lines after treatment with a range of BaP concentrations over a 24- and 48-hour period. Values are given as mean ± SD (*n*=3).

6.3.2 Protein expression of XMEs

Expression of the electron donor proteins POR, Cyb5 and Cyb5R and CYP1A1 were probed for in BaP-treated (2.5 and 5 µM) and untreated WT and POR KO HepG2 cells (**Fig. 6.2**). POR was expressed in WT cells but no expression was observed in the POR

KO cells. Cyb5 and Cyb5R were expressed in all cell lines. Treatment with BaP did not alter the levels of POR, Cyb5 and Cyb5R expression relative to controls. CYP1A1 protein, however, was induced in both cell lines by BaP treatment; and the extent of CYP1A1 induction by BaP was greater in the POR KO HepG2 cells.

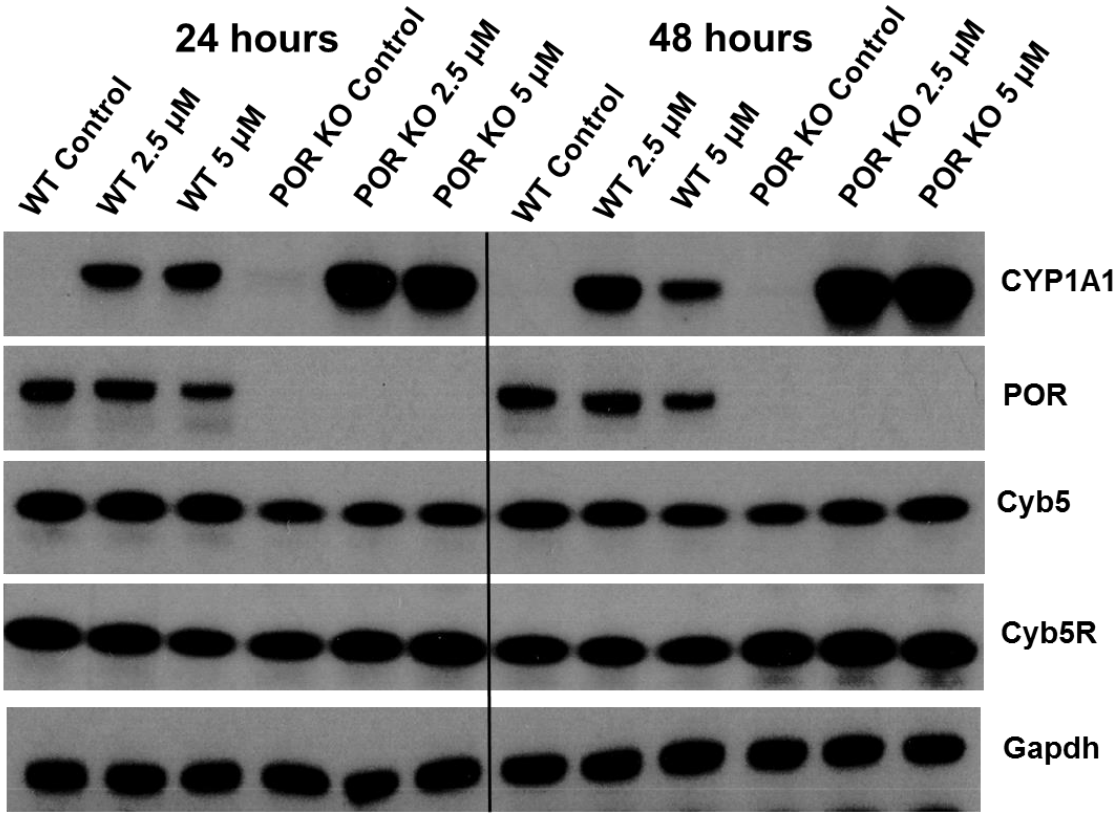

Figure 6.2: Western blot analysis of CYP1A1, POR, Cyb5 and Cyb5R in untreated and BaP-treated (2.5 and 5 µM for 24 or 48 hours) WT and POR KO HepG2 cells. Representative images of the Western blotting are shown, and at least duplicate analysis was performed in independent experiments. Gapdh protein expression was used as a loading control.

6.3.3 Analysis of BaP metabolites by HPLC

WT and POR KO HepG2 cells were treated with 2.5 and 5 µM BaP for 24 and 48 hours before the cell medium was removed and BaP metabolites extracted. Extracts were subsequently analysed by HPLC to determine the BaP metabolite profile. BaP-7,8-dihydrodiol, the precursor to BPDE, and BaP-tetrol-I-1, one hydrolysis product of

BPDE, were the two metabolites detected along with unmetabolised BaP. The two BaP metabolites analysed were identified using authentic standards as described previously (Wohak et al., 2016). Representative chromatograms showing the BaP metabolite profiles are shown in **Figure 6.3** and **Figure 6.4**. The highest level of metabolite formation was seen in the WT cells with formation of both BaP-7,8-dihydrodiol and BaP-tetrol-I-1 being significantly higher than in POR KO cells after exposure to either 2.5 or 5 µM BaP for 24 hours (**Figure 6.5a**). After exposure to 2.5 µM BaP for 48 hours, the levels of BaP-tetrol-I-1 formation was significantly higher in POR KO cells compared to WT cells. Exposure to 5 µM BaP for 48 hours resulted in no significant difference in BaP-tetrol-I-1 formation between the two cell lines. No BaP-7,8-dihydrodiol formation was detected in WT HepG2 cells after exposure to either BaP concentration for 48 hours. In the POR KO HepG2 cells, however, BaP-7,8-dihydrodiol formation was detected (**Figure 6.5b**). Whilst levels of BaP-metabolite formation decline in the WT cells from 24 to 48 hours after treatment with either 2.5 or 5 µM BaP, formation of BaP metabolites increases over the exposure time in the POR KO cells. The level of unmetabolised BaP was significantly higher in the medium from POR KO cell when compared to that of WT cells after exposure to either 2.5 or 5 µM BaP for 24 or 48 hours (**Figure 6.5**). No BaP or BaP metabolites were detected in untreated WT or POR KO cells (**Figure 6.3a and 6.4a**).

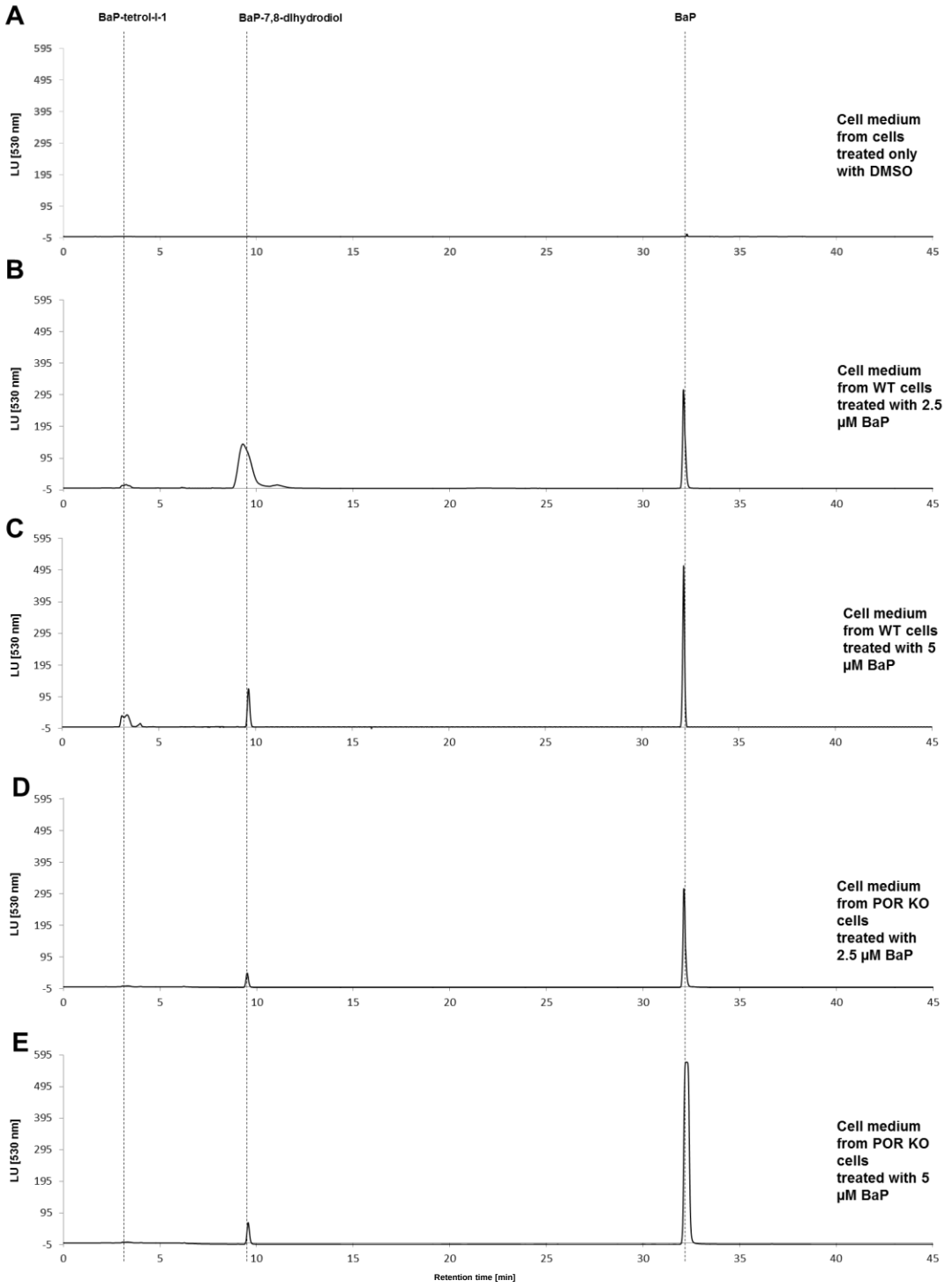

Figure 6.3: Representative HPLC chromatograms from WT and POR KO HepG2 cells treated with 2.5 and 5 µM BaP for 24 hours. Phenacetin (PA) was used as internal standard.

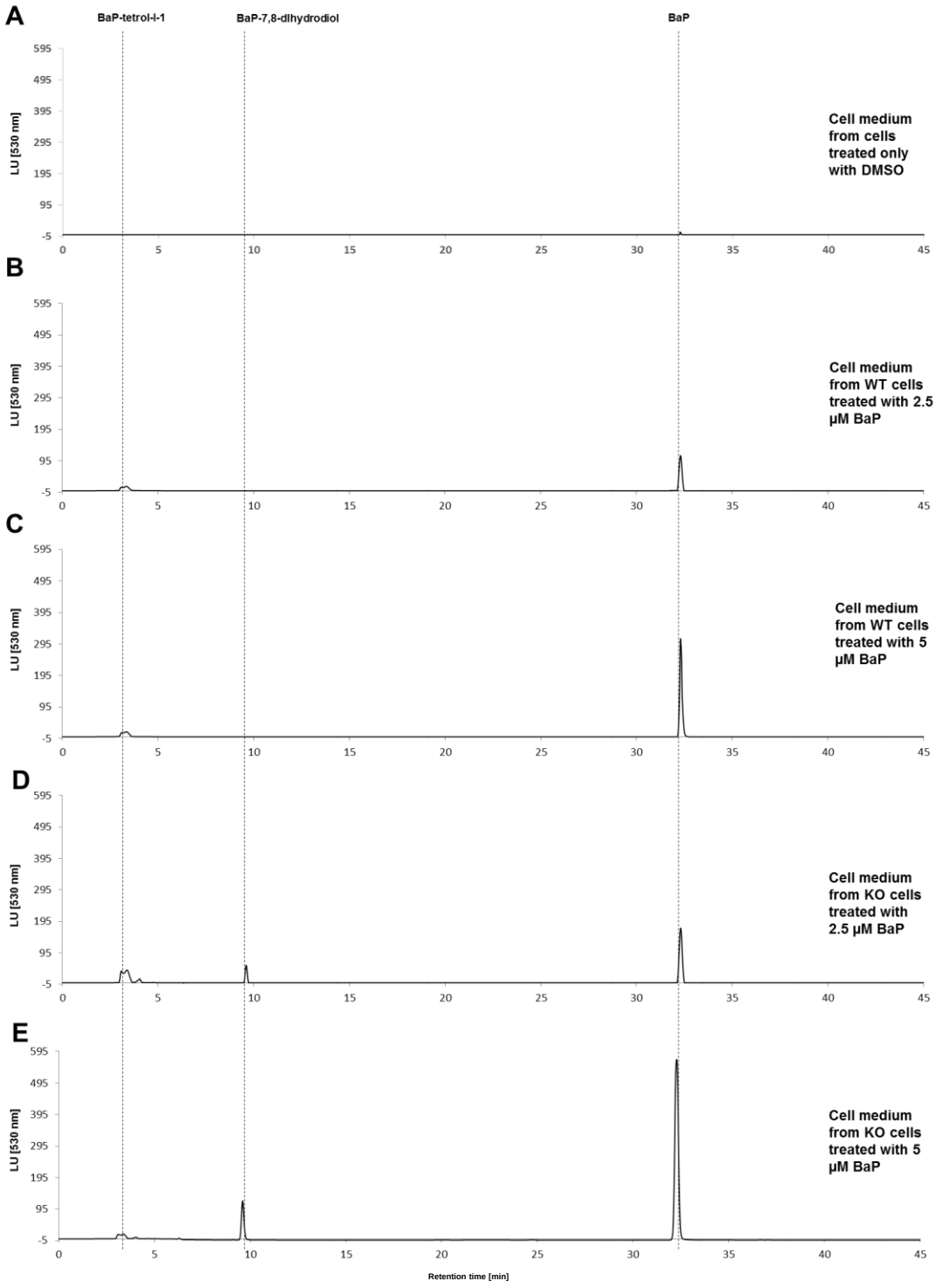

Figure 6.4: Representative HPLC chromatograms from WT and POR KO HepG2 cells treated with 2.5 and 5 µM BaP for 48 hours. Phenacetin (PA) was used as internal standard.

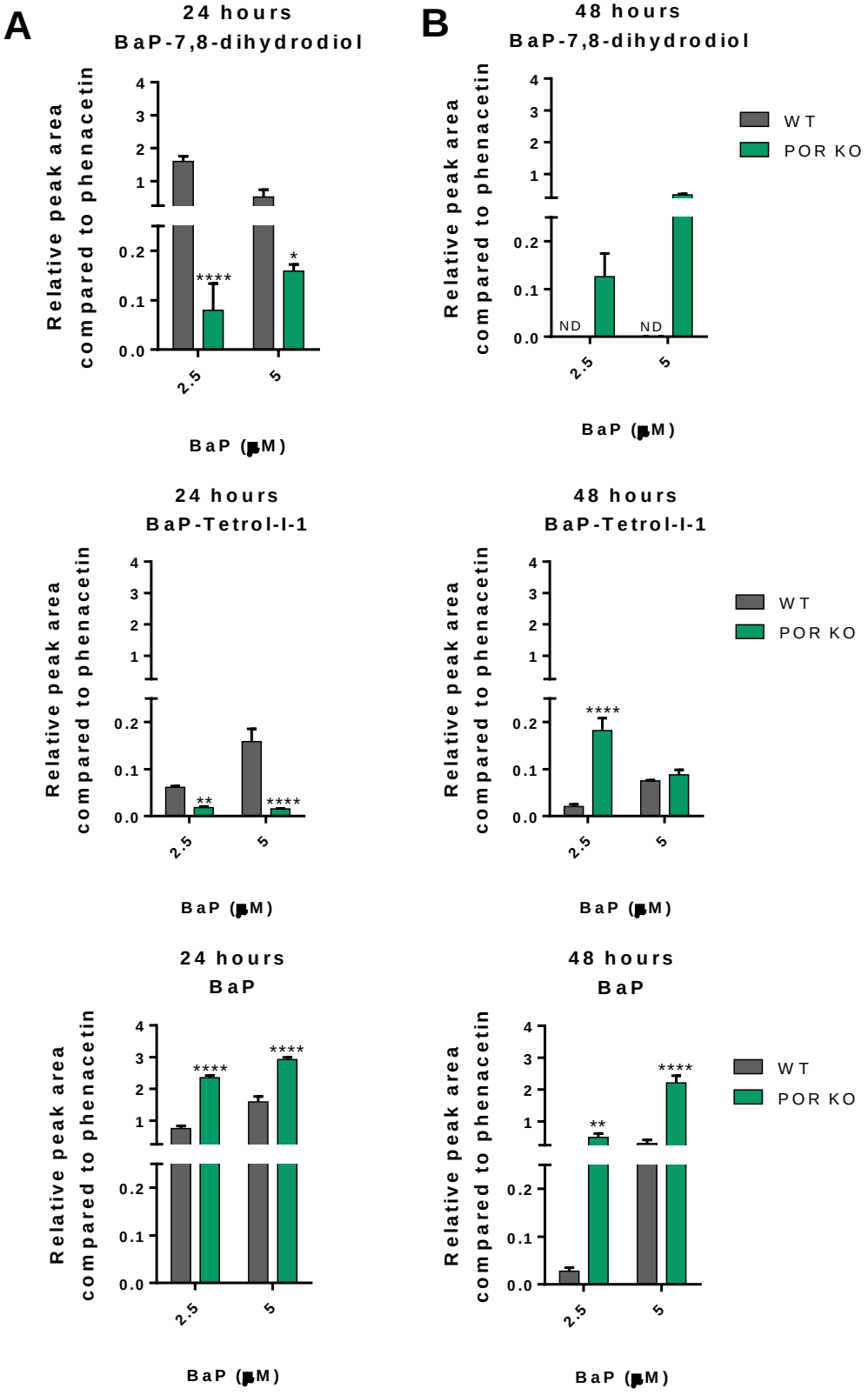

Figure 6.5: Formation of BaP-7,8-dihydrodiol, BaP-tetrol-I-1 and BaP in WT and POR KO HepG2 cells after treatment with 2.5 and 5 µM BaP for 24 (a) and 48 (b) hours. Values are given as mean ± SD (n=3). Statistical analysis was performed by one-way Anova with Tukey's multiple comparison test (* = compared to WT. * $P \leq 0.05$, ** $P \leq 0.01$, **** $P \leq 0.0001$).

6.3.4 Analysis of DNA damage by comet assay

DNA damage caused by exposure to BaP in WT and POR KO HepG2 cells was assessed using the comet assay. WT and POR KO cells were treated with 2.5, 5 and 10 µM BaP for 24 and 48 hours before analysing DNA damage with the comet assay (**Figure 6.6**). In untreated cells, no difference was observed across either of the cell lines. No significant difference was observed in WT or POR KO cells when exposed to 2.5 or 5 µM BaP. When treated with 10 µM BaP, WT cells exhibited significantly higher levels of DNA damage when compared to KO cells at both 24 and 48 hours (**Figure 6.6**).

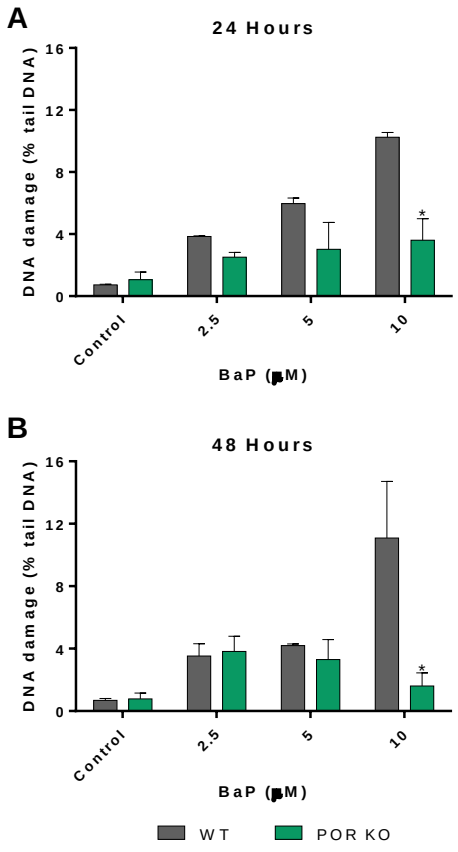

Figure 6.3: Assessment of DNA damage (% tail DNA) in WT and POR KO HepG2 cells using the comet assay. Cells were either untreated or treated with 2.5, 5 or 10 µM BaP for 24 and 48 hours. Values are given as ± SD (*n*=3); 50 nuclei/sample were scored and averaged. Statistical analysis was performed by one-way Anova with Tukey's multiple comparison test (* = compared to WT. * $P \leq 0.05$).

6.3.5 BaP-DNA adduct formation

The ability of WT and POR KO HepG2 cells to catalyse BaP-DNA adduct formation was assessed by ^{32}P-postlabelling. DNA isolated from untreated cells or those treated with 2.5 or 5 µM BaP for 24 and 48 hours was analysed. No DNA adducts were detected in untreated cells (data not shown). One major adduct spot was observed on TLC plates in all BaP-treated cells (**Figure 6.7**) which has previously been identified as dG-N^2-BPDE (Arlt et al., 2008).

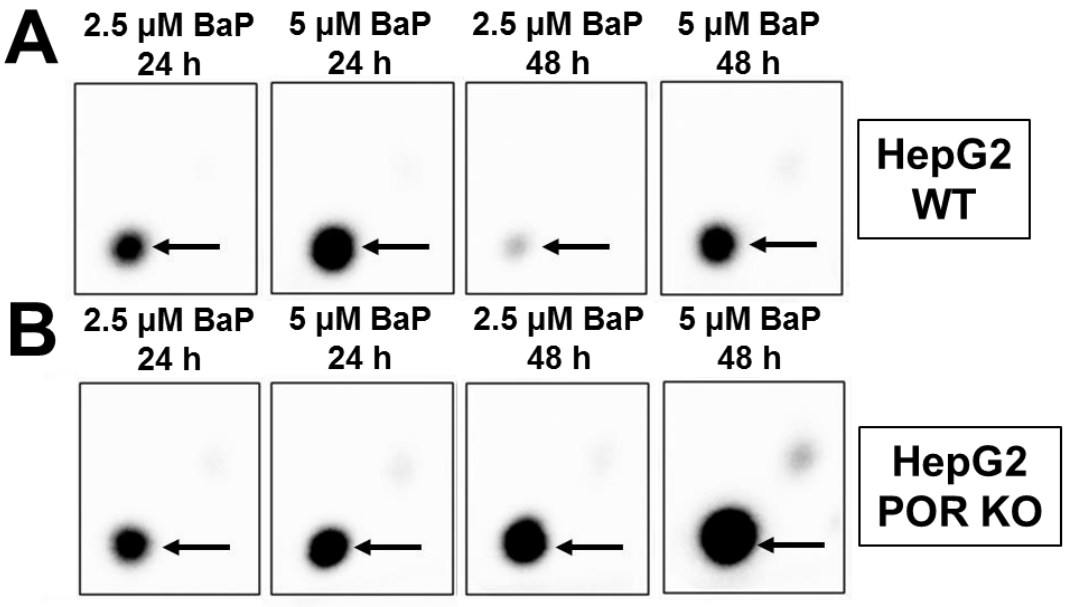

Figure 6.4: Autoradiograms showing adduct profiles by TLC ^{32}P-postlabelling in WT (a) and POR KO (b) HepG2 cells treated with 2.5 or 5 µM BaP for 24 and 48 hours. The origin on the TLC plate, at the bottom left-hand corners, was cut off before exposure. The arrow indicates the dG-N^2-BPDE adduct.

There was no significant difference between WT and POR KO cells in BaP-DNA adduct formation 24 hours after treatment with 2.5 µM BaP; however, BaP-DNA adduct formation was significantly higher in WT cells compared to POR KO cells 24 hours after treatment with 5 µM BaP (**Figure 6.8**). Levels of BaP-DNA adducts were,

however, significantly higher in POR KO cells 48 hours after treatment with 2.5 and 5 µM BaP than in WT cells (**Figure 6.8**). Levels of dG-N^2-BPDE formation in the POR KO cells 24 hours post-exposure correlated with BaP-7,8-dihydrodiol formation (compare **Figure 6.5** and **Figure 6.8**) and DNA damage as measured by the comet assay (compare **Figure 6.6** and **Figure 6.8**). Levels of dG-N^2-BPDE formation in the POR KO cells 48 hours post exposure correlated with the formation of BaP-7,8-dihydrodiol (compare **Figure 6.5** and **Figure 6.8**) but contrasted with DNA damage as measured by the comet assay (compare **Figure 6.6** and **Figure 6.8**).

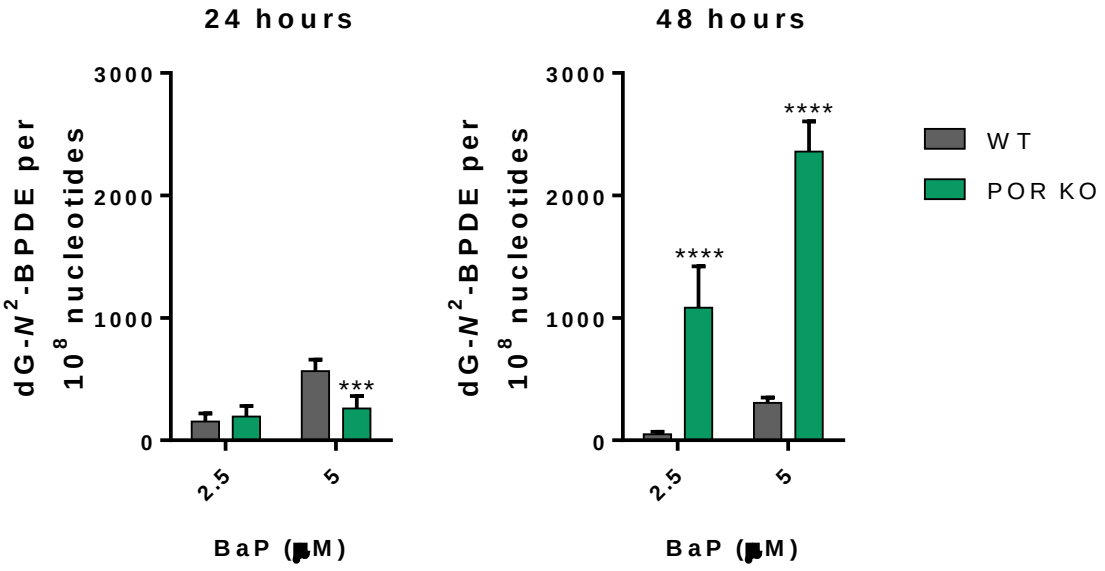

Figure 6.5: Quantitative TLC ^{32}P-postlabelling analysis of dG-N^2-BPDE adducts in WT and POR KO cells treated with 2.5 and 5 µM BaP for 24 and 48 hours. Values are given as ± SD (n=3). Statistical analysis was performed by one-way Anova with Tukey's multiple comparison test (* = compared to WT;* $P \leq 0.05$).

6.4 Discussion

The role of the P450 electron donor POR has been studied in mice, both *in vivo* (Arlt et al., 2012, Arlt et al., 2008) and *in vitro*; in hepatic microsomal fractions (Reed et al., 2018b); in reconstituted systems (Stiborova et al., 2014c); and in cells (see Chapter 5). Collectively these studies have revealed paradoxical results regarding the role of P450 enzymes in the activation or detoxication of BaP. In order to investigate whether or not this extends into a human hepatic model, the human hepatoma cell line HepG2 was used alongside POR KO HepG2 cells. Western blotting confirmed the absence of POR protein in the POR KO HepG2 cells. Expression of other electron donor proteins remained unchanged in both cell lines regardless of concentration or time. This contrasts with results seen with HRN mice and POR KO Hepa-1c1c7 cells, where Cyb5 expression was induced after treatment with BaP (See Chapter 3 and 5). CYP1A1 protein was not detectable in untreated WT and POR KO HepG2 cells under the experimental conditions used but was greatly induced after treatment with BaP. Expression of CYP1A1 was greater in POR KO HepG2 cells than in WT HepG2 cells, with expression of CYP1A1 higher in KO POR cells after 48 hours compared to 24 hours. Despite the absence of POR expression, POR KO HepG2 cells did not exhibit the same degree of resistance to BaP toxicity that was seen in the POR KO Hepa-1c1c7 cells over either a 24- or 48-hour period, which indicates that BaP is being activated into reactive genotoxic metabolites at similar levels as in WT HepG2 cells. However, BaP metabolite formation in POR KO HepG2 cells was significantly lower than in WT cells after exposure to either 2.5 or 5 μM for 24 hours, correlating with BaP metabolite formation in hepatic microsomal fractions from HRN mice (Chapter 3). When cells were exposed to BaP for 48 hours however, BaP metabolite formation was significantly higher in POR KO HepG2 cells compared to WT HepG2 cells,

correlating with results seen in POR KO Hepa-1c1c7 cells (Chapter 5). BaP-tetrol-I-1 levels were significantly higher in POR KO HepG2 cells than in WT HepG2 cells when treated with 2.5 µM BaP whilst no significant difference was observed in formation when treated with 5 µM BaP. No BaP-7,8-dihydrodiol formation was detected in WT HepG2 cells after 48 hours at either concentration of BaP, whilst formation was still detected in POR KO cells. No significant difference was observed in levels of DNA damage in WT and POR KO cells after treatment with 2.5 and 5 µM BaP for 24 or 48 hours. After treatment with 10 µM BaP levels of DNA damage were significantly higher in WT cells than in POR KO cells after both 24 and 48 hours. This correlates with BaP metabolite formation after 24 hours, indicating that not enough BaP is being activated into reactive, genotoxic metabolites to cause DNA damage. Levels of DNA damage after 48 hours however, contrast with levels of BaP metabolite formation in POR KO HepG2 cells. Treatment with 2.5 µM BaP for 24 hours resulted in no significant difference in dG-N^2-BPDE adduct formation in WT and POR KO HepG2 cells. However, after treatment with 5 µM BaP there was significantly higher levels of dG-N^2-BPDE adduct formation in WT cells, correlating with BaP-7,8-dihydrodiol formation and DNA damage (comet assay) after 24 hours. This also correlates with dG-N^2-BPDE adduct formation in hepatic microsomal fractions from HRN mice (Chapter 3). After 48 hours treatment however, regardless of concentration the levels of BaP-DNA adduct formation were significantly higher in the POR KO HepG2 cells compared to WT HepG2 cells. The dG-N^2-BPDE adduct is the same adduct as seen in the HRN mouse model and the accumulation of BaP-DNA adducts in the absence of POR in POR KO HepG2 cells correlates with previous studies carried out with the HRN mouse (Arlt et al., 2012, Arlt et al., 2008) and POR KO Hepa-1c1c7 cells (Chapter 5).

The results of the present study are clearly time-dependent, with POR KO HepG2 cells displaying the greatest levels of BaP metabolite and dG-N^2-BPDE adduct formation being 48 hours after treatment, whereas in WT HepG2 cells this was observed after just 24 hours. BaP-DNA adduct formation has previously been assessed in WT HepG2 cells over a range of BaP concentrations (0.01-5 μM) and time points. Whilst concentration was found to affect levels of DNA adducts, there was no significant difference between the 6, 24 and 48 hour time points for each concentration (Hockley et al., 2006). The time-dependent differences in the POR KO HepG2 cells could be indicative of slower clearance of BaP compared to WT HepG2 cells. Loss of POR in HRN and HBRN mice resulted in steatotic livers that could have stored BaP. Lipid content of the POR KO HepG2 cells was not assessed; however if a similar effect on lipid metabolism was to occur in POR KO HepG2 cells it could alter BaP bioavailability, BaP metabolism and elimination. Levels of unmetabolised BaP in the cell culture media of POR KO HepG2 cells were significantly higher than with WT HepG2 cells regardless of concentration or time, however whether this is because of reduced cellular uptake of BaP due to slower metabolism is unknown. The levels of BaP sequestered in HepG2 cells were not assessed but a combination of slower metabolic clearance of BaP and higher levels of sequestered BaP could offer an explanation for the accumulation of dG-N^2-BPDE adducts in POR KO HepG2 cells. The accumulation of dG-N^2-BPDE adducts in HRN mice (Arlt et al., 2012) and POR KO Hepa-1c1c7 cells (Chapter 5) was associated with increased levels of Cyb5 protein expression, however no difference in Cyb5 expression was observed regardless of concentration or time between POR KO HepG2 and WT HepG2 cells despite the accumulation of dG-N^2-BPDE adduct formation in the POR KO HepG2 cells. Still, it

is probable that Cyb5 compensates for the lack of POR and contributes to increased P450-mediated activation of BaP.

Although HepG2 cells have inducible CYP1A1 (Hockley et al., 2006), they lack PXR expression, which is a low affinity nuclear receptor that transcriptionally regulates many genes associated with xenobiotic metabolism. It plays an important role in detoxication, so much so that PXR is considered to be a xenosensor due to the broad range of xenobiotic substrates including pharmaceuticals, dietary nutrients and environmental contaminants (Kliewer, 2003). In order to assess the role of PXR and the subsequent upregulation of XMEs that metabolise BaP, previous studies used a PXR-transfected HepG2 cell line (Naspinski et al., 2008). Formation of BaP-DNA adducts in PXT-overexpressing HepG2 cells was significantly decreased compared to WT HepG2 cells, suggesting that the presence of PXR reduces the formation of BPDE. These results correlate with findings from *AHR(–/–)* mice in which BaP-DNA adduct formation was greater than in WT mice (Kondraganti et al., 2003). BaP-DNA adduct formation was also significantly reduced in PXR-overexpressing HepG2 cells that had been pretreated with rifampicin, a CYP3A4 inducer, indicating the importance of P450s for detoxication in this model (Naspinski et al., 2008). After exposure to BaP, mRNA levels of *CYP1A2* and *GSTP1* (glutathione *S*-transferase P1) were notably higher in the PXR-overexpressing cells HepG2 compared to WT HepG2 cells. Levels of *CYP1A1* mRNA was also increased in both cell lines after BaP treatment, however this effect was attenuated in PXR-transfected cells (Naspinski et al., 2008). This correlates with results observed in *Cyp1a1(–/–)* mice where absence of Cyp1a1 activity led to increased levels of BaP-DNA adduct formation (Uno et al., 2001, Uno et al., 2004, Uno et al., 2006). The results from the present study also indicate that

P450 enzymes play a more important role in the detoxification of BaP as opposed to bioactivation.

Other XMEs have been implicated in the activation of BaP. BPDE-DNA adduct formation was shown to have reduced levels in the hepatic S9 fractions from *gpt*, >80%, and HRN-*gpt* mice, >50%, in the presence of aldo-keto reductase (AKR), COX1/2 and 5-LOX inhibitors (Wang et al., 2017). HepG2 cells have been shown to have significantly increased levels of AKR gene expression after treatment with BaP (Hockley et al., 2006, Jennen et al., 2010). AKRs have been shown to catalyse the oxidation of BaP-7,8-dihydrodiol to form a ketol, which tautomerises to form the air-sensitive BaP-7,8-catechol. This catechol undergoes one-electron oxidation in air to form an *o*-semiquinone anion radical and a subsequent one-electron oxidation in air to form the fully oxidised BaP-7,8-dione (*o*-quinone) that leads to DNA base oxidation (e.g. 8-oxo-dGuo) (Penning, 2014). Studies with *AKR1A1*-transfected human bronchoalveolar cells showed that AKRs and P450 enzymes compete in the activation of BaP-7,8-dihydrodiol (Jiang et al., 2005). A later study utilising *AKR1A1*-transfected cells found that the same major adduct, dG-N^2-BPDE, was formed as in CYP1A1/1B1-induced cells when treated with BaP-7,8-dihydrodiol. However, *AKR1A1*-transfected cells exhibited a 3-hour lag phase before significant BaP-DNA adduct formation (i.e. dG-N^2-BPDE) was detected (Ruan et al., 2007). In POR KO HepG2 cells therefore, AKRs could potentially contribute to BaP-DNA-adduct formation. On the other hand, previous findings showed that control HepG2 cells exhibited the highest levels of DNA-adduct formation compared to *AKR1A1*-transfected or CYP1A1/1B1-induced HepG2 cells, raising further questions about the roles of P450 and AKR enzymes in BaP bioactivation (Ruan et al., 2007). Whilst COX1/2 has previously been implicated in the activation of BaP, no significant changes in gene expression were seen in HepG2

cells treated with BaP (Hockley et al., 2006, Jennen et al., 2010). Further investigation of these enzymes and the effect of BaP on their expression in the POR KO HepG2 cells as opposed to WT HepG2 cells could offer further insight into enzymes involved in the bioactivation of BaP. This could then help identify potential P450-independent BaP activation pathways in the POR KO cells, this was however beyond the scope of the present study.

7 General Discussion

P450 enzymes have been implicated in the bioactivation of numerous procarcinogens, playing an important role in the process of chemical carcinogenesis (Guengerich, 2008). Since the development of genetically-engineered P450 knockout mouse models, investigations into the role of P450s have shown how complex this process is. In Chapter 3 the results from studies using the pooled hepatic microsomal fractions incubated with NADPH showed that as electron donors were lost, the levels of BaP activation decreased from those seen in hepatic microsomal fractions isolated from WT mice, demonstrating that Cyb5 contributes to the activation of BaP *in vitro*. These results also clearly demonstrated the importance of P450s in the bioactivation of BaP *in vitro.* BaP-DNA adduct formation *in vivo*, however, contrasted with the findings *in vitro*. Hepatic BaP-DNA-adduct formation was significantly higher in HRN mice lacking POR expression in the hepatocytes compared to WT mice and formation in HBRN mice, whilst significantly lower than HRN mice, showed no significant difference compared to WT. These results suggest that P450 enzymes actually play a more important role in the detoxication of BaP *in vivo*.

In Chapter 4 the *in vitro* studies using the pooled hepatic microsomal fractions incubated with NADPH showed that Cyb5 contributes to the activation of ellipticine *in vitro.* As electron donors were lost, the levels of ellipticine activation decreased from those seen in hepatic microsomal fractions isolated from WT mice. These results also clearly demonstrated the importance of P450s in the bioactivation of ellipticine *in vitro.* These results correlated with the *in vitro* studies with hepatic microsomal fractions and BaP from Chapter 3. The results on ellipticine-DNA adduct formation *in vivo* confirmed the importance role of P450 enzymes in the bioactivation of ellipticine.

Ellipticine-DNA adduct formation was significantly reduced in the livers of HRN and HBRN mice compared to WT mice. In contrast to *in vitro* results, however, there was no significant difference between ellipticine-DNA adduct levels in the livers of HRN and HBRN mice, demonstrating that whilst Cyb5 contributes to the activation of ellipticine *in vitro*, this role is not fulfilled *in vivo*. This contrasts with the role of Cyb5 in BaP activation, whereby it was seen to play a role in the livers of HRN mice.

The results from the POR KO Hepa-1c1c7 cells contrasted with the *in vitro* results from the hepatic microsomal fractions in Chapter 3, with BaP metabolite formation being significantly higher in the POR KO Hepa-1c1c7 cells compared to WT Hepa-1c1c7 cells. Levels of BaP-DNA adducts also contrasted with that seen in hepatic microsomal fractions incubated with NADPH and BaP *in vitro*, instead correlating with hepatic microsomal fractions incubated with NADH and *in vivo* results from HRN mice. This suggests that Cyb5 contributes to the bioactivation of BaP in POR KO Hepa-1c1c7 cells. Levels of Cyb5 expression were induced in both the WT and POR KO Hepa-1c1c7 cells exposed to BaP, however the accumulation of BaP-DNA adducts was only observed in the POR KO Hepa-1c1c7 cells. As with the results from Chapter 3, these results are indicative that cytochrome P450s may play a more important role in the detoxication of BaP, as opposed to its bioactivation.

The results from POR KO HepG2 cells showed that levels of BaP activation (i.e. BaP-7,8-dihydrodiol formation) were higher in POR KO cells than WT HepG2 cells which also resulted in substantially higher BaP-DNA adduct formation in POR KO HepG2 cells. These results correlate with those seen in HRN mice and POR KO Hepa-1c1c7 cells, where an absence of POR expression results in higher levels of BaP activation, suggesting P450s play a more important role in the detoxication of BaP as opposed to

activation. Future studies should aim to additionally knockout Cyb5 in both POR KO HepG2 and POR KO Hepa-1c1c7 cells in order to have *in vitro* cell culture models that mimic the HBRN mouse model and to specifically assess the contribution of Cyb5 in the BaP bioactivation in these cells.

The paradoxical results discussed in Chapter 3, and the evidence that cytochrome P450s play a more important role in BaP detoxication as opposed to its activation discussed in Chapter 3, 5 and 6 are not isolated phenomena. Enzyme kinetic studies carried out with liver microsomes from *Cyp1a2(–/–)* and *Cyp2e1(–/–)* mice demonstrated the importance of cytochrome P450s in the *N*-hydroxylation of 4-ABP *in vitro* (Wang et al., 2015). Investigation of 4-ABP metabolism *in vivo*, however, in both *Cyp1a2(–/–)* and *Ahr(–/–)* mice showed that treatment of mice with 4-ABP induced hepatocellular adenoma and liver foci, however there were no differences found in incidence between *Cyp1a2(–/–), Ahr(–/–)* and WT mice (Kimura et al., 1999). Hepatic microsomal fractions isolated from *Cyp1a2(–/–) and Ahr(–/–)* mice exhibited half the microsomal arylamine *N*-hydroxylation activity of that seen with WT hepatic microsomal fractions during incubations with 4-ABP, indicating that only half of the enzymatic activity attributed to 4-ABP activation was due to Cyp1a2 (Kimura et al., 1999). Another study using *Cyp1a2(–/–)* mice, with or without TCDD pretreatment, and measurement of methaemoglobin levels as a biomarker of 4-ABP exposure showed that the presence of Cyp1a2 actually decreased methaemoglobin formation and in fact TCDD pretreatment lowered it further (Shertzer et al., 2002). A third *in-vivo* study using *Cyp1a2(–/–)* mice was carried out with or without TCDD pretreatment, this time focusing on DNA adduct formation (Tsuneoka et al., 2003). *Cyp1a2(–/–)* mice formed similar or higher levels 4-APB-DNA adducts than WT mice in both liver and bladder. When mice were pre-treated with TCDD, hepatic DNA

adduct levels were either lower or similar to the corresponding group of mice that did not receive TCDD, adding further weight to the argument that Cyp1a2 is more important for clearance of 4-ABP than for its activation (Tsuneoka et al., 2003).

Evidence primarily from *in vitro* studies has demonstrated that P450s are the most important enzymes involved in the initial oxidation of PhIP to form the intermediate *N*-OH-PhIP with CYP1A2 as the predominant P450 enzyme in the activation of PhIP followed by CYP1A1 and 1B1 (Edwards et al., 1994, Shimada et al., 1996). Initial studies of PhIP activation in *Cyp1a2(–/–)* mice showed that exposure to PhIP led to significantly lower DNA adduct formation in *Cyp1a2(–/–)* mice compared to WT mice in the mammary gland and colon, and was not detectable in the liver and kidney of *Cyp1a2(–/–)* mice. These findings indicated the importance of the role of Cyp1a2 in the activation of PhIP *in vivo* (Snyderwine et al., 2002). In a later study in which PhIP was administered to *Cyp1a2(–/–)* mice, *N*-hydroxylation of PhIP was ~8-fold higher in microsomal fractions from WT mice than those from *Cyp1a2(–/–)* mice, however, the *Cyp1a2(–/–)* mice had a *higher* incidence of tumours than WT mice (Kimura et al., 2003). Hepatic microsomal fractions incubated with PhIP *in vitro* resulted in 8-fold greater DNA adduct formation with hepatic microsomal fractions from RCN mice without 3MC pretreatment (i.e. mice with active POR) compared to RCN mice with 3MC pretreatment (i.e. mice with inactive POR). These *in-vitro* results do not correlate with the *in-vivo* findings, however as DNA adduct formation in extrahepatic tissues was lower in POR-inactive mice than in POR-active mice and hepatic DNA adduct formation was not different between both mouse lines. These findings suggest that although Cyp1a2 plays a role in the bioactivation of PhIP *in vitro*, another P450-independent mechanism may also contribute to its activation *in vivo* (Arlt et al., 2011).

To investigate the roles of hepatic and intestinal cytochrome P450s in the metabolic activation of A*a*C, two mouse models were employed (Turesky et al., 2015). The first, the liver-specific P450 reductase (*Cpr*)-null (LCN) mouse model (Gu et al., 2003), has POR deleted in the liver whereas the second mouse model, the intestinal epithelium-specific *Cpr*-null (IECN) mouse, has POR deleted specifically in the intestinal epithelium (Zhang et al., 2009). IECN mice exposed to A*a*C did not show any significant differences to WT mice in the pharmacokinetic parameters for A*a*C or its metabolites, demonstrating a lack of contribution by intestinal P450s to first-pass clearance of A*a*C. The formation of DNA adducts in IECN mice was only significantly different from WT mice in the bladder where formation was 1.5-fold higher. On the other hand hepatic microsomal fractions from LCN mice were unable to oxidise A*a*C *in vitro,* whereas DNA adduct formation *in vivo* was found to be not lower in liver than in WT mice and significantly higher in lung (4-fold), bladder (1.2-fold) and colon (4-fold) (Turesky et al., 2015). These findings suggest that P450 enzymes do not contribute significantly to the activation of A*a*C but they may play a greater role in its detoxication (Turesky et al., 2015).

P450-mediated α-hydroxylation of NNK has been demonstrated *in vivo* with the use of P450 inhibitors (Takeuchi et al., 2003, Hecht et al., 1996) and *in vitro* with lung microsomes (Hecht, 1998). Although activation of NNK is carried out in the lungs, hepatic microsomes have been shown to be at least as active as lung microsomes in activating NNK *in vitro* (Jalas et al., 2005). To further elucidate the role of hepatic and pulmonary P450s two mouse models were used, a lung-*Cpr*-null mouse (i.e. POR null). The lung-*Cpr*-null mice had fewer lung tumours than WT mice, implicating the role of pulmonary P450s in the activation of NNK. The liver-*Cpr*-null mice, however, had *higher* levels of lung tumour multiplicity than WT mice (Weng et al., 2007). These

findings were confirmed in a later study using HRN-*gpt* delta mice (Luan et al., 2012). NNK-induced mutation frequency was 3 times higher in the lung of HRN-*gpt* delta mice than in control *gpt* delta mice. Furthermore, pharmacokinetic studies showed significantly higher plasma levels of NNK and significantly lower rates of clearance in HRN-*gpt* delta mice compared to controls, suggesting that although pulmonary P450s play a role in NNK activation, hepatic P450s may in fact play a larger role in detoxification (Luan et al., 2012). However, *in-vitro* studies using recombinant CYP2A5 demonstrated the ability of this CYP enzyme to efficiently activate NNK (Felicia et al., 2000, Jalas et al., 2003) and NNK-induced lung tumorigenesis in mice was found to be reduced when Cyp2a enzymes were inhibited (Miyazaki et al., 2005). *Cyp2a5*-null mice treated with NNK showed there was no change in the systemic clearance of NNK or its major circulating metabolite 4-(methylnitrosamino)-1-(3-pyridyl)-1-butanol (NNAL). Levels of pulmonary O^6-mG adducts were significantly lower in *Cyp2a5*-null mice compared to WT mice. Levels of hepatic O^6-mG adducts however showed no significant differences between *Cyp2a5*-null mice and WT mice at either dose despite previous studies showing that hepatic P450s were protective against NNK-induced lung tumorigenesis (Weng et al., 2007, Zhou et al., 2012). The P450 knockout was extended to *Cyp2abfgs*-null mice, in which all *Cyp2a*, *2b*, *2g*, *2f* and *2s* genes are deleted (Li et al., 2014). Levels of pulmonary O^6-mG adducts were substantially reduced compared to both WT and *Cyp2a5*-null mice. The *Cyp2abfgs*-null mice also demonstrated resistance to NNK-induced lung tumourigenesis, unlike the WT or *Cyp2a5*-null mice. In contrast to the POR knockout mice, these results suggest that there is in fact a contribution from mouse Cyp2a, 2b, 2g, 2f and 2s enzymes toward the bioactivation of NNK *in vivo* (Li et al., 2014).

The role of P450s in the metabolism of environmental carcinogens is complex. Whilst numerous *in-vitro* studies have demonstrated the role of P450s in the activation of carcinogens, the use of *Cyp*-knockout mice or *Por*-knockout mouse models lacking P450 enzyme activity have yielded paradoxical results demonstrating that P450s *in vivo* are in fact more important for detoxification. Although P450s are capable of activating carcinogens to their reactive intermediates, in an *in vivo* situation where myriad more biological factors are at play, this role appears to shift. These results are also not limited to a particular carcinogen or carcinogenic family, or to a particular knockout mouse model. Although the numerous mouse models utilised have been derived by a variety of methods for disrupting P450 expression or activity (Capecchi, 1989, Le and Sauer, 2001), there is the possibility that by disrupting P450 expression or activity, the metabolic balance in tissues is disturbed and alternative contributing factors to activation or detoxication that may have been minor come to the fore. Many of the studies discussed have short exposure times (less than one month) and have focused on short-term markers, e.g. protein or DNA adduct and metabolite formation, which may not reflect the longer term carcinogenic consequences. Nevertheless two of the studies described here have investigated tumour formation with different carcinogens and have yielded the same overall paradoxical outcome as the short-term studies (Kimura et al., 2003, Weng et al., 2007). Whilst *Por*-knockout mouse models lacking P450 enzyme activity are powerful tools for investigations of xenobiotic metabolism, the paradoxical results they yield require further investigations to better understand mechanisms of activation. One possibility that arises from these studies and the work described within this project is the potential for P450-independent activation pathways that are as yet unidentified.

The results from this project, together with the studies of other carcinogens discussed previously, do raise questions about the wider implications of P450-mediated metabolism. If P450s are more important for detoxication than activation of carcinogens it would allow more accurate assessments to be made for risk factors such as *CYP1A1* polymorphisms. If there is an unidentified P450-independent bioactivation pathway for procarcinogens such as BaP then there may be as yet unidentified risk groups for developing cancers associated with these compounds. This could ultimately also affect epidemiological predictions of disease development. Identifying any other P450-independent activation mechanisms would also be of importance in drug development as currently the main focus is on P450-mediated bioactivation pathways as the mechanism for reactive metabolite formation. Awareness of other potential pathways could help improve preclinical toxicity assessments and ensure that financial investments are not lost at later stages of drug development. This project has also added to the body of evidence regarding the *in vitro* and *in vivo* paradox that should be considered when using subcellular fractions to assess the potential of compounds being activated to reactive metabolites. By increasing understanding of the bioactivation mechanisms, both P450-dependent and P450-independent, the risk assessment of procarcinogens in the environment could be improved.

8 References

AIMOVÁ, D., POLJAKOVÁ, J., KOTRBOVÁ, V., MOSEROVÁ, M., FREI, E., ARLT, V. M. & STIBOROVÁ, M. 2008. Ellipticine and benzo(a)pyrene increase their own metabolic activation via modulation of expression and enzymatic activity of cytochromes P450 1A1 and 1A2. *Interdiscip Toxicol,* 1**,** 160-8.

ALEXANDROV, L. B., JU, Y. S., HAASE, K., VAN LOO, P., MARTINCORENA, I., NIK-ZAINAL, S., TOTOKI, Y., FUJIMOTO, A., NAKAGAWA, H., SHIBATA, T., CAMPBELL, P. J., VINEIS, P., PHILLIPS, D. H. & STRATTON, M. R. 2016. Mutational signatures associated with tobacco smoking in human cancer. *Science,* 354**,** 618-622.

AMMANN, P. & MAIER, P. 1997. Preservation and inducibility of xenobiotic metabolism in long-term cultures of adult rat liver cell aggregates. *Toxicol in Vitro,* 11**,** 43-56.

ARLT, V. M., COLE, K. J. & PHILLIPS, D. H. 2004. Activation of 3-nitrobenzanthrone and its metabolites to DNA-damaging species in human B lymphoblastoid MCL-5 cells. *Mutagenesis,* 19**,** 149-56.

ARLT, V. M., HENDERSON, C. J., WOLF, C. R., STIBOROVA, M. & PHILLIPS, D. H. 2015a. The Hepatic Reductase Null (HRN[trade mark sign]) and Reductase Conditional Null (RCN) mouse models as suitable tools to study metabolism, toxicity and carcinogenicity of environmental pollutants. *Toxicol Res,* 4**,** 548-562.

ARLT, V. M., KRAIS, A. M., GODSCHALK, R. W., RIFFO-VASQUEZ, Y., MRIZOVA, I., ROUFOSSE, C. A., CORBIN, C., SHI, Q., FREI, E., STIBOROVA, M., VAN SCHOOTEN, F. J., PHILLIPS, D. H. & SPINA, D. 2015b. Pulmonary inflammation impacts on CYP1A1-mediated respiratory tract DNA damage induced by the carcinogenic air pollutant benzo[a]pyrene. *Toxicol Sci,* 146**,** 213-25.

ARLT, V. M., POIRIER, M. C., SYKES, S. E., JOHN, K., MOSEROVA, M., STIBOROVA, M., WOLF, C. R., HENDERSON, C. J. & PHILLIPS, D. H. 2012. Exposure to benzo[a]pyrene of Hepatic Cytochrome P450 Reductase Null (HRN) and P450 Reductase Conditional Null (RCN) mice: Detection of benzo[a]pyrene diol epoxide-DNA adducts by immunohistochemistry and 32P-postlabelling. *Toxicol Lett,* 213**,** 160-6.

ARLT, V. M., SCHMEISER, H. H. & PFEIFER, G. P. 2001. Sequence-specific detection of aristolochic acid-DNA adducts in the human p53 gene by terminal transferase-dependent PCR. *Carcinogenesis,* 22**,** 133-40.

ARLT, V. M., SINGH, R., STIBOROVA, M., GAMBOA DA COSTA, G., FREI, E., EVANS, J. D., FARMER, P. B., WOLF, C. R., HENDERSON, C. J. & PHILLIPS, D. H. 2011. Effect of hepatic cytochrome P450 (P450) oxidoreductase deficiency on 2-amino-1-methyl-6-phenylimidazo[4,5-b]pyridine-DNA adduct formation in P450 reductase conditional null mice. *Drug Metab Dispos,* 39**,** 2169-73.

ARLT, V. M., STIBOROVA, M., HENDERSON, C. J., THIEMANN, M., FREI, E., AIMOVA, D., SINGH, R., GAMBOA DA COSTA, G., SCHMITZ, O. J., FARMER, P. B., WOLF, C. R. & PHILLIPS, D. H. 2008. Metabolic activation

of benzo[a]pyrene in vitro by hepatic cytochrome P450 contrasts with detoxification in vivo: experiments with hepatic cytochrome P450 reductase null mice. *Carcinogenesis,* 29**,** 656-65.

ARLT, V. M., STIBOROVA, M., HEWER, A., SCHMEISER, H. H. & PHILLIPS, D. H. 2003. Human enzymes involved in the metabolic activation of the environmental contaminant 3-nitrobenzanthrone: evidence for reductive activation by human NADPH:cytochrome p450 reductase. *Cancer Res,* 63**,** 2752-61.

ARLT, V. M., STIBOROVA, M. & SCHMEISER, H. H. 2002. Aristolochic acid as a probable human cancer hazard in herbal remedies: a review. *Mutagenesis,* 17**,** 265-277.

ASHA, S. & VIDYAVATHI, M. 2010. Role of human liver microsomes in in vitro metabolism of drugs-a review. *Appl Biochem Biotechnol,* 160**,** 1699-722.

BAHARVAND, H., HASHEMI, S. M., KAZEMI ASHTIANI, S. & FARROKHI, A. 2006. Differentiation of human embryonic stem cells into hepatocytes in 2D and 3D culture systems in vitro. *Int J Dev Biol,* 50**,** 645-52.

BAILLIE, T. A. & RETTIE, A. E. 2011. Role of biotransformation in drug-induced toxicity: influence of intra- and inter-species differences in drug metabolism. *Drug Metab Pharmacokinet,* 26**,** 15-29.

BAIRD, W. M., HOOVEN, L. A. & MAHADEVAN, B. 2005. Carcinogenic polycyclic aromatic hydrocarbon-DNA adducts and mechanism of action. *Environ Mol Mutagen,* 45**,** 106-14.

BANERJEE, A., SANYAL, S., MAJUMDER, P., CHAKRABORTY, P., JANA, K., DAS, C. & DASGUPTA, D. 2015. Recognition of chromatin by the plant alkaloid, ellipticine as a dual binder. *Biochem Biophys Res Commun,* 462**,** 352-357.

BARKER, N., HUCH, M., KUJALA, P., VAN DE WETERING, M., SNIPPERT, H. J., VAN ES, J. H., SATO, T., STANGE, D. E., BEGTHEL, H., VAN DEN BORN, M., DANENBERG, E., VAN DEN BRINK, S., KORVING, J., ABO, A., PETERS, P. J., WRIGHT, N., POULSOM, R. & CLEVERS, H. 2010. Lgr5(+ve) stem cells drive self-renewal in the stomach and build long-lived gastric units in vitro. *Cell Stem Cell,* 6**,** 25-36.

BERNHARD, H. P., DARLINGTON, G. J. & RUDDLE, F. H. 1973. Expression of liver phenotypes in cultured mouse hepatoma cells: Synthesis and secretion of serum albumin. *Developmental Biology,* 35**,** 83-96.

BESARATINIA, A. & TOMMASI, S. 2013. Genotoxicity of tobacco smoke-derived aromatic amines and bladder cancer: current state of knowledge and future research directions. *Faseb j,* 27**,** 2090-100.

BRANDON, E. F. A., RAAP, C. D., MEIJERMAN, I., BEIJNEN, J. H. & SCHELLENS, J. H. M. 2003. An update on in vitro test methods in human hepatic drug biotransformation research: pros and cons. *Toxicol Appl Pharmacol,* 189**,** 233-246.

BRODIE, B. B., AXELROD, J., COOPER, J. R., GAUDETTE, L., LA DU, B. N., MITOMA, C. & UDENFRIEND, S. 1955. Detoxication of drugs and other foreign compounds by liver microsomes. *Science,* 121**,** 603-4.

BROOKES, P. & LAWLEY, P. D. 1964. Evidence for the binding of polynuclear aromatic hydrocarbons to the nucleic acids of mouse skin: relation between carcinogenic power of hydrocarbons and their binding to deoxyribonucleic acid. *Nature,* 202**,** 781-4.

BROUNS, S. J., JORE, M. M., LUNDGREN, M., WESTRA, E. R., SLIJKHUIS, R. J., SNIJDERS, A. P., DICKMAN, M. J., MAKAROVA, K. S., KOONIN, E. V. & VAN DER OOST, J. 2008. Small CRISPR RNAs guide antiviral defense in prokaryotes. *Science,* 321**,** 960-4.

BUTERS, J. T. M., SAKAI, S., RICHTER, T., PINEAU, T., ALEXANDER, D. L., SAVAS, U., DOEHMER, J., WARD, J. M., JEFCOATE, C. R. & GONZALEZ, F. J. 1999. Cytochrome P450 CYP1B1 determines susceptibility to 7,12-dimethylbenz[a]anthracene-induced lymphomas. *Proc Natl Acad Sci U S A,* 96**,** 1977-82.

BUTLER, M. A., GUENGERICH, F. P. & KADLUBAR, F. F. 1989a. Metabolic oxidation of the carcinogens 4-aminobiphenyl and 4,4'-methylene-bis(2-chloroaniline) by human hepatic microsomes and by purified rat hepatic cytochrome P-450 monooxygenases. *Cancer Res,* 49**,** 25-31.

BUTLER, M. A., IWASAKI, M., GUENGERICH, F. P. & KADLUBAR, F. F. 1989b. Human cytochrome P-450PA (P-450IA2), the phenacetin O-deethylase, is primarily responsible for the hepatic 3-demethylation of caffeine and N-oxidation of carcinogenic arylamines. *Proc Natl Acad Sci U S A,* 86**,** 7696-700.

CAMPBELL, J. J., DAVIDENKO, N., CAFFAREL, M. M., CAMERON, R. E. & WATSON, C. J. 2011. A multifunctional 3D co-culture system for studies of mammary tissue morphogenesis and stem cell biology. *PloS one,* 6**,** e25661.

CANOVA-DAVIS, E., CHIANG, J. Y. L. & WASKELL, L. 1985. Obligatory role of cytochrome b5 in the microsomal metabolism of methoxyflurane. *Biochem Pharmacol,* 34**,** 1907-1912.

CAPECCHI, M. R. 1989. Altering the genome by homologous recombination. *Science,* 244**,** 1288-92.

CHEAH, S. S. & BEHRINGER, R. R. 2000. Gene-targeting strategies. *Methods Mol Biol,* 136**,** 455-63.

CHEN, L., BUTERS, J. T., HARDWICK, J. P., TAMURA, S., PENMAN, B. W., GONZALEZ, F. J. & CRESPI, C. L. 1997. Coexpression of cytochrome P4502A6 and human NADPH-P450 oxidoreductase in the baculovirus system. *Drug metab dispos,* 25**,** 399-405.

CHEN, Y., TANG, Y., GUO, C., WANG, J., BORAL, D. & NIE, D. 2012. Nuclear receptors in the multidrug resistance through the regulation of drug-metabolizing enzymes and drug transporters. *Biochem Pharmacol,* 83**,** 1112-26.

CHUNG, J.-Y., KIM, J. Y., KIM, W. R., LEE, S. G., KIM, Y.-J., PARK, J.-E., HONG, Y.-P., CHUN, Y.-J., PARK, Y. C., OH, S., YOO, K. S., YOO, Y. H. & KIM, J.-M. 2007. Abundance of aryl hydrocarbon receptor potentiates benzo[a]pyrene-induced apoptosis in Hepa1c1c7 cells via CYP1A1 activation. *Toxicology,* 235**,** 62-72.

CLAYSON, D. B. 1981. Specific aromatic amines as occupational bladder carcinogens. *Natl Cancer Inst Monogr***,** 15-9.

COLEMAN, M. D. 2010. *Human Drug Metabolism: An Introduction*, Wiley.

COLLINS, A. R., OSCOZ, A. A., BRUNBORG, G., GAIVAO, I., GIOVANNELLI, L., KRUSZEWSKI, M., SMITH, C. C. & STETINA, R. 2008. The comet assay: topical issues. *Mutagenesis,* 23**,** 143-51.

CONROY, J. L., FANG, C., GU, J., ZEITLIN, S. O., YANG, W., YANG, J., VANALSTINE, M. A., NALWALK, J. W., ALBRECHT, P. J., MAZURKIEWICZ, J. E., SNYDER-KELLER, A., SHAN, Z., ZHANG, S. Z., WENTLAND, M. P., BEHR, M., KNAPP, B. I., BIDLACK, J. M.,

ZUIDERVELD, O. P., LEURS, R., DING, X. & HOUGH, L. B. 2010. Opioids activate brain analgesic circuits through cytochrome P450/epoxygenase signaling. *Nat Neurosci,* 13**,** 284-6.
COOK, J., HASLEWOOD, G., HEWETT, C., HIEGER, I., KENNAWAY, E. & MAYNEORD, W. 1937. Chemical compounds as carcinogenic agents. *The Amn J Cancer,* 29**,** 219-259.
COOK, J. W., HEWETT, C. & HIEGER, I. 1933. 106. The isolation of a cancer-producing hydrocarbon from coal tar. Parts I, II, and III. *JChem Soc***,** 395-405.
CROOM, E. 2012. Chapter Three - Metabolism of xenobiotics of human environments. *In:* HODGSON, E. (ed.) *Prog Mol Bio Transl Sci.* Academic Press.
DALTON, T. P., DIETER, M. Z., MATLIB, R. S., CHILDS, N. L., SHERTZER, H. G., GENTER, M. B. & NEBERT, D. W. 2000. Targeted knockout of Cyp1a1 gene does not alter hepatic constitutive expression of other genes in the mouse [Ah] battery. *Biochem Biophys Res Commun,* 267**,** 184-9.
DARLINGTON, G. J., BERNHARD, H. P., MILLER, R. A. & RUDDLE, F. H. 1980. Expression of liver phenotypes in cultured mouse hepatoma cells. *J Natl Cancer Inst,* 64**,** 809-19.
DAUJAT, M., CLAIR, P., ASTIER, C., FABRE, I., PINEAU, T., YERLE, M., GELLIN, J. & MAUREL, P. 1991. Induction, regulation and messenger half-life of cytochromes P450 IA1, IA2 and IIIA6 in primary cultures of rabbit hepatocytes. CYP 1A1, 1A2 and 3A6 chromosome location in the rabbit and evidence that post-transcriptional control of gene IA2 does not involve mRNA stabilization. *Eur J Biochem,* 200**,** 501-10.
DEBELLE, F. D., VANHERWEGHEM, J. L. & NORTIER, J. L. 2008. Aristolochic acid nephropathy: a worldwide problem. *Kidney Int,* 74**,** 158-69.
DONATO, M. T., TOLOSA, L. & GOMEZ-LECHON, M. J. 2015. Culture and functional characterization of human hepatoma HepG2 cells. *Methods Mol Biol,* 1250**,** 77-93.
DOOLEY, T. P., GADWOOD, R. C., KILGORE, K. & THOMASCO, L. M. 1994. Development of an in vitro primary screen for skin depigmentation and antimelanoma agents. *Skin Pharmacol,* 7**,** 188-200.
DOUKI, T., KOSCHEMBAHR, A. & CADET, J. 2017. Insight in DNA repair of UV-induced pyrimidine dimers by chromatographic methods. *Photochem Photobiol,* 93**,** 207-215.
DRAGIN, N., SHI, Z., MADAN, R., KARP, C. L., SARTOR, M. A., CHEN, C., GONZALEZ, F. J. & NEBERT, D. W. 2008. Phenotype of the Cyp1a1/1a2/1b1-/- triple-knockout mouse. *Mol Pharmacol,* 73**,** 1844-56.
DUSINSKA, M. & COLLINS, A. R. 2008. The comet assay in human biomonitoring: gene-environment interactions. *Mutagenesis,* 23**,** 191-205.
EDWARDS, R. J., MURRAY, B. P., MURRAY, S., SCHULZ, T., NEUBERT, D., GANT, T. W., THORGEIRSSON, S. S., BOOBIS, A. R. & DAVIES, D. S. 1994. Contribution of CYP1A1 and CYP1A2 to the activation of heterocyclic amines in monkeys and human. *Carcinogenesis,* 15**,** 829-36.
EIRAKU, M., TAKATA, N., ISHIBASHI, H., KAWADA, M., SAKAKURA, E., OKUDA, S., SEKIGUCHI, K., ADACHI, T. & SASAI, Y. 2011. Self-organizing optic-cup morphogenesis in three-dimensional culture. *Nature,* 472**,** 51-6.
ENOIU, M., JIRICNY, J. & SCHÄRER, O. D. 2012. Repair of cisplatin-induced DNA interstrand crosslinks by a replication-independent pathway involving

transcription-coupled repair and translesion synthesis. *Nucleic Acids Res,* 40**,** 8953-64.

EVANS, W. E. & RELLING, M. V. 1999. Pharmacogenomics: translating functional genomics into rational therapeutics. *Science,* 286**,** 487-91.

FANG, C., GU, J., XIE, F., BEHR, M., YANG, W., ABEL, E. D. & DING, X. 2008. Deletion of the NADPH-cytochrome P450 reductase gene in cardiomyocytes does not protect mice against doxorubicin-mediated acute cardiac toxicity. *Drug Metab Dispos,* 36**,** 1722-8.

FELICIA, N. D., REKHA, G. K. & MURPHY, S. E. 2000. Characterization of cytochrome P450 2A4 and 2A5-catalyzed 4-(methylnitrosamino)-1-(3-pyridyl)-1-butanone (NNK) metabolism. *Arch Biochem Biophys,* 384**,** 418-24.

FINN, R. D. 2008. Defining the in Vivo Role for Cytochrome b(5). 283**,** 31385-93.

FINN, R. D., MCLAREN, A. W., CARRIE, D., HENDERSON, C. J. & WOLF, C. R. 2007. Conditional deletion of cytochrome P450 oxidoreductase in the liver and gastrointestinal tract: a new model for studying the functions of the P450 system. *J Pharmacol Exp Ther,* 322**,** 40-7.

FINN, R. D., MCLAUGHLIN, L. A., HUGHES, C., SONG, C., HENDERSON, C. J. & ROLAND WOLF, C. 2011. Cytochrome b5 null mouse: a new model for studying inherited skin disorders and the role of unsaturated fatty acids in normal homeostasis. *Transgenic Res,* 20**,** 491-502.

FINN, R. D., MCLAUGHLIN, L. A., RONSEAUX, S., ROSEWELL, I., HOUSTON, J. B., HENDERSON, C. J. & WOLF, C. R. 2008. Defining the in Vivo Role for cytochrome b5 in cytochrome P450 function through the conditional hepatic deletion of microsomal cytochrome b5. *J Biol Chem,* 283**,** 31385-93.

FONG, C. J., BURGOON, L. D. & ZACHAREWSKI, T. R. 2005. Comparative microarray analysis of basal gene expression in mouse Hepa-1c1c7 wild-type and mutant cell lines. *Toxicol Sci,* 86**,** 342-53.

GARBETT, N. C. & GRAVES, D. E. 2004. Extending nature's leads: the anticancer agent ellipticine. *Curr Med Chem Anticancer Agents,* 4**,** 149-72.

GAUTIER, J. C., LECOEUR, S., COSME, J., PERRET, A., URBAN, P., BEAUNE, P. & POMPON, D. 1996. Contribution of human cytochrome P450 to benzo[a]pyrene and benzo[a]pyrene-7,8-dihydrodiol metabolism, as predicted from heterologous expression in yeast. *Pharmacogenetics,* 6**,** 489-99.

GERLAI, R. 2016. Gene targeting using homologous recombination in embryonic stem cells: the future for behavior genetics? *Front Genet,* 7.

GINSBERG, G. L. & ATHERHOLT, T. B. 1989. Transport of DNA-adducting metabolites in mouse serum following benzo[a]pyrene administration. *Carcinogenesis,* 10**,** 673-9.

GOKMEN, M. R., COSYNS, J. P., ARLT, V. M., STIBOROVA, M., PHILLIPS, D. H., SCHMEISER, H. H., SIMMONDS, M. S., COOK, H. T., VANHERWEGHEM, J. L., NORTIER, J. L. & LORD, G. M. 2013. The epidemiology, diagnosis, and management of aristolochic acid nephropathy: a narrative review. *Ann Intern Med,* 158**,** 469-77.

GONZALEZ, F. J. 2003. Role of gene knockout and transgenic mice in the study of xenobiotic metabolism. *Drug Metab Rev,* 35**,** 319-35.

GOODERHAM, N. J. & CARMICHAEL, P. L. 2007. Mechanisms of chemical carcinogenesis. *The Cancer Handbook.* M. R. Alison.

GOODERHAM, N. J., ZHU, H., LAUBER, S., BOYCE, A. & CRETON, S. 2002. Molecular and genetic toxicology of 2-amino-1-methyl-6-phenylimidazo[4,5-b]pyridine (PhIP). *Mutat Res,* 506-507**,** 91-9.

GRECO, K. V., IQBAL, A. J., RATTAZZI, L., NALESSO, G., MORADI-BIDHENDI, N., MOORE, A. R., GOLDRING, M. B., DELL'ACCIO, F. & PERRETTI, M. 2011. High density micromass cultures of a human chondrocyte cell line: a reliable assay system to reveal the modulatory functions of pharmacological agents. *Biochem Pharmacol,* 82**,** 1919-29.

GSUR, A., HAIDINGER, G., HOLLAUS, P., HERBACEK, I., MADERSBACHER, S., TRIEB, K., PRIDUN, N., MOHN-STAUDNER, A., VETTER, N., VUTUC, C. & MICKSCHE, M. 2001. Genetic polymorphisms of CYP1A1 and GSTM1 and lung cancer risk. *Anticancer Res,* 21**,** 2237-42.

GU, J., WENG, Y., ZHANG, Q. Y., CUI, H., BEHR, M., WU, L., YANG, W., ZHANG, L. & DING, X. 2003. Liver-specific deletion of the NADPH-cytochrome P450 reductase gene: impact on plasma cholesterol homeostasis and the function and regulation of microsomal cytochrome P450 and heme oxygenase. *J Biol Chem,* 278**,** 25895-901.

GUENGERICH, F. P. 2001. Common and uncommon cytochrome P450 reactions related to metabolism and chemical toxicity. *Chem Res Toxicol,* 14**,** 611-650.

GUENGERICH, F. P. 2008. Cytochrome p450 and chemical toxicology. *Chem Res Toxicol,* 21**,** 70-83.

GUENGERICH, F. P. 2010. Mechanisms of Drug Toxicity and Relevance to Pharmaceutical Development. *Drug Metab Pharmacokinet,* advpub**,** 1010210090-1010210090.

GUENGERICH, F. P. & JOHNSON, W. W. 1997. Kinetics of ferric cytochrome P450 reduction by NADPH-cytochrome P450 reductase: rapid reduction in the absence of substrate and variations among cytochrome P450 systems. *Biochemistry,* 36**,** 14741-50.

GUENGERICH, F. P., PARIKH, A., JOHNSON, E. F., RICHARDSON, T. H., VON WACHENFELDT, C., COSME, J., JUNG, F., STRASSBURG, C. P., MANNS, M. P., TUKEY, R. H., PRITCHARD, M., FOURNEL-GIGLEUX, S. & BURCHELL, B. 1997. Heterologous expression of human drug-metabolizing enzymes. *Drug Metab Dispos,* 25**,** 1234-41.

GUENGERICH, F. P. & SHIMADA, T. 1991. Oxidation of toxic and carcinogenic chemicals by human cytochrome P-450 enzymes. *Chem Res Toxicol,* 4**,** 391-407.

HAKURA, A., SONODA, J., TSUTSUI, Y., MIKAMI, T., IMADE, T., SHIMADA, M., YAGUCHI, S., YAMANAKA, M., TOMIMATSU, M. & TSUKIDATE, K. 1998. Toxicity profile of benzo[a]pyrene in the male LacZ transgenic mouse (MutaMouse) following oral administration for 5 consecutive days. *Regul Toxicol Pharmacol,* 27**,** 273-9.

HAMMONS, G. J., DOOLEY, K. L. & KADLUBAR, F. F. 1991. 4-Aminobiphenyl-hemoglobin adduct formation as an index of in vivo N-oxidation by hepatic cytochrome P-450IA2. *Chem Res Toxicol,* 4**,** 144-7.

HAMOUCHENE, H., ARLT, V. M., GIDDINGS, I. & PHILLIPS, D. H. 2011. Influence of cell cycle on responses of MCF-7 cells to benzo[a]pyrene. *BMC Genomics,* 12**,** 333.

HANKINSON, O. 1979. Single-step selection of clones of a mouse hepatoma line deficient in aryl hydrocarbon hydroxylase. *Proc Natl Acad Sci U S A,* 76**,** 373-6.

HANKINSON, O. 1995. The aryl hydrocarbon receptor complex. *Annual review of pharmacology and toxicology,* 35**,** 307-340.

HARA, M., HORITA, M., TANAKA, K., IMAIZUMI, T., KUDO, S., HIGAKI, Y., SAKAMOTO, T., OZAKI, I., YAMAMOTO, K., MIZUTA, T., YASUTAKE, T., EGUCHI, Y., SHIGEMATSU, H., KAWAZOE, S., ONOHARA, S. & KOIZUMI, S. 2009. Interaction between cytochrome P450 1A2 genetic polymorphism and cigarette smoking on the risk of hepatocellular carcinoma in a Japanese population. *Carcinogenesis,* 30**,** 1729-1734.

HECHT, S. S. 1998. Biochemistry, biology, and carcinogenicity of tobacco-specific N-nitrosamines. *Chem Res Toxicol,* 11**,** 559-603.

HECHT, S. S., TRUSHIN, N., RIGOTTY, J., CARMELLA, S. G., BORUKHOVA, A., AKERKAR, S. & RIVENSON, A. 1996. Complete inhibition of 4-(methylnitrosamino)-1-(3-pyridyl)-1-butanone-induced rat lung tumorigenesis and favorable modification of biomarkers by phenethyl isothiocyanate. *Cancer Epidemiol Biomarkers Prev,* 5**,** 645-52.

HEFFNER, C. S., HERBERT PRATT, C., BABIUK, R. P., SHARMA, Y., ROCKWOOD, S. F., DONAHUE, L. R., EPPIG, J. T. & MURRAY, S. A. 2012. Supporting conditional mouse mutagenesis with a comprehensive cre characterization resource. *Nature Communications,* 3**,** 1218.

HEILMANN, S., KUCHLER, S. & SCHAFER-KORTING, M. 2012. Morphine metabolism in human skin microsomes. *Skin Pharmacol Physiol,* 25**,** 319-22.

HENDERSON, C. J., MCLAUGHLIN, L. A. & WOLF, C. R. 2013. Evidence that cytochrome b5 and cytochrome b5 reductase can act as sole electron donors to the hepatic cytochrome P450 system. *Mol Pharmacol,* 83**,** 1209-17.

HENDERSON, C. J., OTTO, D. M., CARRIE, D., MAGNUSON, M. A., MCLAREN, A. W., ROSEWELL, I. & WOLF, C. R. 2003. Inactivation of the hepatic cytochrome P450 system by conditional deletion of hepatic cytochrome P450 reductase. *J Biol Chem,* 278**,** 13480-6.

HENDERSON, C. J., PASS, G. J. & WOLF, C. R. 2006. The hepatic cytochrome P450 reductase null mouse as a tool to identify a successful candidate entity. *Toxicol Lett,* 162**,** 111-7.

HILDEBRANDT, A. & ESTABROOK, R. W. 1971. Evidence for the participation of cytochrome b5 in hepatic microsomal mixed-function oxidation reactions. *Arch Biochem Biophys,* 143**,** 66-79.

HOCKLEY, S. L., ARLT, V. M., BREWER, D., GIDDINGS, I. & PHILLIPS, D. H. 2006. Time- and concentration-dependent changes in gene expression induced by benzo(a)pyrene in two human cell lines, MCF-7 and HepG2. *BMC Genomics,* 7**,** 260.

HOLME, J. A., GORRIA, M., ARLT, V. M., OVREBO, S., SOLHAUG, A., TEKPLI, X., LANDVIK, N. E., HUC, L., FARDEL, O. & LAGADIC-GOSSMANN, D. 2007. Different mechanisms involved in apoptosis following exposure to benzo[a]pyrene in F258 and Hepa1c1c7 cells. *Chem Biol Interact,* 167**,** 41-55.

HORTON, J. K., ROSENIOR, J. C., BEND, J. R. & ANDERSON, M. W. 1985. Quantitation of benzo(a)pyrene metabolite: DNA adducts in selected hepatic and pulmonary cell types isolated from [3H]benzo(a)pyrene-treated rabbits. *Cancer Res,* 45**,** 3477-81.

HUANG, M., BLAIR, I. A. & PENNING, T. M. 2013. Identification of stable benzo[a]pyrene-7,8-dione-DNA adducts in human lung cells. *Chem Res Toxicol,* 26**,** 685-92.

HUANG, Y. & LI, L. 2013. DNA crosslinking damage and cancer - a tale of friend and foe. *Transl cancer res,* 2**,** 144-154.

HUANG, Z., ROY, P. & WAXMAN, D. J. 2000. Role of human liver microsomal CYP3A4 and CYP2B6 in catalyzing N-dechloroethylation of cyclophosphamide and ifosfamide. *Biochem pharmacol,* 59**,** 961-972.

HUCH, M., BONFANTI, P., BOJ, S. F., SATO, T., LOOMANS, C. J., VAN DE WETERING, M., SOJOODI, M., LI, V. S., SCHUIJERS, J., GRACANIN, A., RINGNALDA, F., BEGTHEL, H., HAMER, K., MULDER, J., VAN ES, J. H., DE KONING, E., VRIES, R. G., HEIMBERG, H. & CLEVERS, H. 2013. Unlimited in vitro expansion of adult bi-potent pancreas progenitors through the Lgr5/R-spondin axis. *Embo j,* 32**,** 2708-21.

HUNG, R. J., BOFFETTA, P., BROCKMOLLER, J., BUTKIEWICZ, D., CASCORBI, I., CLAPPER, M. L., GARTE, S., HAUGEN, A., HIRVONEN, A., ANTTILA, S., KALINA, I., LE MARCHAND, L., LONDON, S. J., RANNUG, A., ROMKES, M., SALAGOVIC, J., SCHOKET, B., GASPARI, L. & TAIOLI, E. 2003. CYP1A1 and GSTM1 genetic polymorphisms and lung cancer risk in Caucasian non-smokers: a pooled analysis. *Carcinogenesis,* 24**,** 875-82.

IARC 2010a. Some aromatic amines, organic dyes, and related exposures. *IARC monographs on the evaluation of carcinogenic risks to humans,* 99**,** 1-678.

IARC 2010b. Some non-heterocyclic polycyclic aromatic hydrocarbons and some related occupational exposures. *IARC monographs on the evaluation of carcinogenic risks to humans,* 92.

IARC 2012. Pharmaceuticals: A review of human carcinogens. *IARC monographs on the evaluation of carcinogenic risks to humans,* 100**,** 1.

IARC 2015. Mycotoxin control in low- and middle-income countries. *In:* WILD, C. P., MILLER, J. D. & GROOPMAN, J. D. (eds.). Lyon (FR).

IARC 2016. Outdoor Air Pollution. *IARC monographs on the evaluation of carcinogenic risks to humans,* 109.

INCHEM, W.-I. 2003. Selected nitro-and nitro-oxy-polycyclic aromatic hydrocarbons. *Environmental Health Criteria (EHC) Monograph,* 229.

JAISSER, F. 2000. Inducible Gene Expression and Gene Modification in Transgenic Mice. *J Am Soc Nephrol,* 11**,** S95-S100.

JALAS, J. R., DING, X. & MURPHY, S. E. 2003. Comparative metabolism of the tobacco-specific nitrosamines 4-(methylnitrosamino)-1-(3-pyridyl)-1-butanone and 4-(methylnitrosamino)-1-(3-pyridyl)-1-butanol by rat cytochrome P450 2A3 and human cytochrome P450 2A13. *Drug Metab Dispos,* 31**,** 1199-1202.

JALAS, J. R., HECHT, S. S. & MURPHY, S. E. 2005. Cytochrome P450 enzymes as catalysts of metabolism of 4-(methylnitrosamino)-1-(3-pyridyl)-1-butanone, a tobacco specific carcinogen. *Chem Res Toxicol,* 18**,** 95-110.

JENNEN, D. G. J., MAGKOUFOPOULOU, C., KETELSLEGERS, H. B., VAN HERWIJNEN, M. H. M., KLEINJANS, J. C. S. & VAN DELFT, J. H. M. 2010. Comparison of HepG2 and HepaRG by whole-genome gene expression analysis for the purpose of chemical hazard identification. *Toxicol Sci,* 115**,** 66-79.

JENNINGS, P. 2015. The future of in vitro toxicology. *Toxicol in Vitro,* 29**,** 1217-1221.

JIANG, H., SHEN, Y. M., QUINN, A. M. & PENNING, T. M. 2005. Competing roles of cytochrome P450 1A1/1B1 and aldo-keto reductase 1A1 in the metabolic activation of (+/-)-7,8-dihydroxy-7,8-dihydro-benzo[a]pyrene in human bronchoalveolar cell extracts. *Chem Res Toxicol,* 18**,** 365-74.

JIANG, H., VUDATHALA, D. K., BLAIR, I. A. & PENNING, T. M. 2006. Competing roles of aldo-keto reductase 1A1 and cytochrome P4501B1 in benzo[a]pyrene-7,8-diol activation in human bronchoalveolar H358 cells: role of AKRs in P4501B1 induction. *Chem Res Toxicol,* 19**,** 68-78.

JOSEPHY, D. P., GUENGERICH, P. F. & MINERS, J. O. 2005. "Phase I and Phase II" Drug metabolism: terminology that we should phase out? *Drug Metab Rev,* 37**,** 575-580.

JUNG, C. 2011. The mystery of cytochrome P450 Compound I: A mini-review dedicated to Klaus Ruckpaul. *Biochimica et Biophysica Acta (BBA) - Proteins Proteom,* 1814**,** 46-57.

KATAOKA, H. 1997. Methods for the determination of mutagenic heterocyclic amines and their applications in environmental analysis. *J Chromatogr A,* 774**,** 121-42.

KENNAWAY, E. & HIEGER, I. 1930. Carcinogenic substances and their fluorescence spectra. *BMJ,* 1**,** 1044.

KEW, M. C. 2013. Aflatoxins as a cause of hepatocellular carcinoma. *J Gastrointestin Liver Dis,* 22**,** 305-10.

KEWLEY, R. J., WHITELAW, M. L. & CHAPMAN-SMITH, A. 2004. The mammalian basic helix–loop–helix/PAS family of transcriptional regulators. *Int J Biochem Cell Biol,* 36**,** 189-204.

KIM, K., OHASHI, K., UTOH, R., KANO, K. & OKANO, T. 2012. Preserved liver-specific functions of hepatocytes in 3D co-culture with endothelial cell sheets. *Biomaterials,* 33**,** 1406-1413.

KIMURA, S., KAWABE, M., WARD, J. M., MORISHIMA, H., KADLUBAR, F. F., HAMMONS, G. J., FERNANDEZ-SALGUERO, P. & GONZALEZ, F. J. 1999. CYP1A2 is not the primary enzyme responsible for 4-aminobiphenyl-induced hepatocarcinogenesis in mice. *Carcinogenesis,* 20**,** 1825-1830.

KIMURA, S., KAWABE, M., YU, A., MORISHIMA, H., FERNANDEZ-SALGUERO, P., HAMMONS, G. J., WARD, J. M., KADLUBAR, F. F. & GONZALEZ, F. J. 2003. Carcinogenesis of the food mutagen PhIP in mice is independent of CYP1A2. *Carcinogenesis,* 24**,** 583-7.

KING, R. S., TEITEL, C. H. & KADLUBAR, F. F. 2000. In vitro bioactivation of N-hydroxy-2-amino-alpha-carboline. *Carcinogenesis,* 21**,** 1347-54.

KIZEK, R., ADAM, V., HRABETA, J., ECKSCHLAGER, T., SMUTNY, S., BURDA, J. V., FREI, E. & STIBOROVA, M. 2012. Anthracyclines and ellipticines as DNA-damaging anticancer drugs: recent advances. *Pharmacol Ther,* 133**,** 26-39.

KLIEWER, S. A. 2003. The nuclear pregnane X receptor regulates xenobiotic detoxification. *J Nutr,* 133**,** 2444s-2447s.

KNASMULLER, S., PARZEFALL, W., SANYAL, R., ECKER, S., SCHWAB, C., UHL, M., MERSCH-SUNDERMANN, V., WILLIAMSON, G., HIETSCH, G., LANGER, T., DARROUDI, F. & NATARAJAN, A. T. 1998. Use of metabolically competent human hepatoma cells for the detection of mutagens and antimutagens. *Mutat Res,* 402**,** 185-202.

KONDRAGANTI, S. R., FERNANDEZ-SALGUERO, P., GONZALEZ, F. J., RAMOS, K. S., JIANG, W. & MOORTHY, B. 2003. Polycyclic aromatic hydrocarbon-inducible DNA adducts: evidence by 32P-postlabeling and use of knockout mice for Ah receptor-independent mechanisms of metabolic activation in vivo. *Int J Cancer,* 103**,** 5-11.

KOTRBOVA, V., AIMOVA, D., BREZINOVA, A., JANOUCHOVA, K., POLJAKOVA, J., FREI, E. & STIBOROVA, M. 2006. Cytochromes P450 reconstituted with NADPH: P450 reductase mimic the activating and detoxicating metabolism of the anticancer drug ellipticine in microsomes. *Neuro Endocrinol Lett,* 27 Suppl 2**,** 18-22.

KOTRBOVA, V., MRAZOVA, B., MOSEROVA, M., MARTINEK, V., HODEK, P., HUDECEK, J., FREI, E. & STIBOROVA, M. 2011. Cytochrome b(5) shifts oxidation of the anticancer drug ellipticine by cytochromes P450 1A1 and 1A2 from its detoxication to activation, thereby modulating its pharmacological efficacy. *Biochem Pharmacol,* 82**,** 669-80.

KRAIS, A. M., SPEKSNIJDER, E. N., MELIS, J. P., INDRA, R., MOSEROVA, M., GODSCHALK, R. W., VAN SCHOOTEN, F. J., SEIDEL, A., KOPKA, K., SCHMEISER, H. H., STIBOROVA, M., PHILLIPS, D. H., LUIJTEN, M. & ARLT, V. M. 2016. The impact of p53 on DNA damage and metabolic activation of the environmental carcinogen benzo[a]pyrene: effects in Trp53(+/+), Trp53(+/-) and Trp53(-/-) mice. *Arch Toxicol,* 90**,** 839-51.

KRETSCHMER, X. C. & BALDWIN, W. S. 2005. CAR and PXR: xenosensors of endocrine disrupters? *Chem Biol Interact,* 155**,** 111-28.

KRIEK, E. 1992. Fifty years of research on N-acetyl-2-aminofluorene, one of the most versatile compounds in experimental cancer research. *J Cancer Res Clin Oncol,* 118**,** 481-9.

KUCAB, J. E., VAN STEEG, H., LUIJTEN, M., SCHMEISER, H. H., WHITE, P. A., PHILLIPS, D. H. & ARLT, V. M. 2015. TP53 mutations induced by BPDE in Xpa-WT and Xpa-Null human TP53 knock-in (Hupki) mouse embryo fibroblasts. *Mutat Res,* 773**,** 48-62.

KUNZ-SCHUGHART, L. A., FREYER, J. P., HOFSTAEDTER, F. & EBNER, R. 2004. The use of 3-D cultures for high-throughput screening: the multicellular spheroid model. *JBS,* 9**,** 273-285.

LABIB, S., WILLIAMS, A., GUO, C. H., LEINGARTNER, K., ARLT, V. M., SCHMEISER, H. H., YAUK, C. L., WHITE, P. A. & HALAPPANAVAR, S. 2016. Comparative transcriptomic analyses to scrutinize the assumption that genotoxic PAHs exert effects via a common mode of action. *Arch Toxicol,* 90**,** 2461-80.

LABIB, S., YAUK, C., WILLIAMS, A., ARLT, V. M., PHILLIPS, D. H., WHITE, P. A. & HALAPPANAVAR, S. 2012. Subchronic oral exposure to benzo(a)pyrene leads to distinct transcriptomic changes in the lungs that are related to carcinogenesis. *Toxicol Sci,* 129**,** 213-24.

LANCASTER, M. A. & KNOBLICH, J. A. 2014. Organogenesis in a dish: modeling development and disease using organoid technologies. *Science,* 345**,** 1247125.

LANCASTER, M. A., RENNER, M., MARTIN, C. A., WENZEL, D., BICKNELL, L. S., HURLES, M. E., HOMFRAY, T., PENNINGER, J. M., JACKSON, A. P. & KNOBLICH, J. A. 2013. Cerebral organoids model human brain development and microcephaly. *Nature,* 501**,** 373-9.

LANDI, M. T., ZOCCHETTI, C., BERNUCCI, I., KADLUBAR, F. F., TANNENBAUM, S., SKIPPER, P., BARTSCH, H., MALAVEILLE, C., SHIELDS, P., CAPORASO, N. E. & VINEIS, P. 1996. Cytochrome P4501A2: enzyme induction and genetic control in determining 4-aminobiphenyl-hemoglobin adduct levels. *Cancer Epidemiol Biomarkers Prev,* 5**,** 693-698.

LAO, Y., VILLALTA, P. W., STURLA, S. J., WANG, M. & HECHT, S. S. 2006. Quantitation of pyridyloxobutyl DNA adducts of tobacco-specific

nitrosamines in rat tissue DNA by high-performance liquid chromatography-electrospray ionization-tandem mass spectrometry. *Chem Res Toxicol,* 19**,** 674-82.

LAURSEN, T., JENSEN, K. & MØLLER, B. L. 2011. Conformational changes of the NADPH-dependent cytochrome P450 reductase in the course of electron transfer to cytochromes P450. *Biochimica et Biophysica Acta (BBA) - Proteins and Proteomics,* 1814**,** 132-138.

LE, Y. & SAUER, B. 2001. Conditional gene knockout using cre recombinase. *Mol Biotech,* 17**,** 269-275.

LEISTEN, I., KRAMANN, R., VENTURA FERREIRA, M. S., BOVI, M., NEUSS, S., ZIEGLER, P., WAGNER, W., KNÜCHEL, R. & SCHNEIDER, R. K. 2012. 3D co-culture of hematopoietic stem and progenitor cells and mesenchymal stem cells in collagen scaffolds as a model of the hematopoietic niche. *Biomaterials,* 33**,** 1736-1747.

LI, L., MEGARAJ, V., WEI, Y. & DING, X. 2014. Identification of cytochrome P450 enzymes critical for lung tumorigenesis by the tobacco-specific carcinogen 4-(methylnitrosamino)-1-(3-pyridyl)-1-butanone (NNK): insights from a novel Cyp2abfgs-null mouse. *Carcinogenesis,* 35**,** 2584-91.

LIANG, H. C., LI, H., MCKINNON, R. A., DUFFY, J. J., POTTER, S. S., PUGA, A. & NEBERT, D. W. 1996. Cyp1a2(-/-) null mutant mice develop normally but show deficient drug metabolism. *PNAS,* 93**,** 1671-1676.

LIGUORI, I., RUSSO, G., CURCIO, F., BULLI, G., ARAN, L., DELLA-MORTE, D., GARGIULO, G., TESTA, G., CACCIATORE, F., BONADUCE, D. & ABETE, P. 2018. Oxidative stress, aging, and diseases. *Clin Interv Aging,* 13**,** 757-772.

LIN, R. Z. & CHANG, H. Y. 2008. Recent advances in three-dimensional multicellular spheroid culture for biomedical research. *Biotechnol J,* 3**,** 1172-84.

LIN, Y., YAO, Y., LIU, S., WANG, L., MOORTHY, B., XIONG, D., CHENG, T., DING, X. & GU, J. 2012. Role of mammary epithelial and stromal P450 enzymes in the clearance and metabolic activation of 7,12-dimethylbenz(a)anthracene in mice. *Toxicol Lett,* 212**,** 97-105.

LIU, S., TAYLOR, L. T., BORGERDING, M. F., COLEMAN, W. M. & BOMBICK, B. R. 2013. Trace analysis of mutagenic heterocyclic aromatic amines in cigarette smoke condensate and its base fractions via silylation-GC-MS. *Beiträge zur Tabakforschung International/Contributions to Tobacco Research.*

LONG, A. S., WILLS, J. W., KROLAK, D., GUO, M., DERTINGER, S. D., ARLT, V. M. & WHITE, P. A. 2017. Benchmark dose analyses of multiple genetic toxicity endpoints permit robust, cross-tissue comparisons of MutaMouse responses to orally delivered benzo[a]pyrene. *Arch Toxicol*.

LONG, D. J., WAIKEL, R. L., WANG, X. J., PERLAKY, L., ROOP, D. R. & JAISWAL, A. K. 2000. NAD(P)H:quinone oxidoreductase 1 deficiency increases susceptibility to benzo(a)pyrene-induced mouse skin carcinogenesis. *Cancer Res,* 60**,** 5913-5.

LUAN, Y., XING, G., QI, X., WU, M., LI, C., YAO, J., GONG, L., NOHMI, T., GU, J., ZHOU, W., ZHENG, S. & REN, J. 2012. The application of hepatic P450 reductase null gpt delta mice in studying the role of hepatic P450 in genotoxic carcinogen 4-(methylnitrosamino)-1-(3-pyridyl)-1-butanone-induced mutagenesis. *Arch Toxicol,* 86**,** 1753-61.

LUCH, A. 2005. Nature and nurture - lessons from chemical carcinogenesis. *Nat Rev Cancer,* 5**,** 113-25.

LUCH, A. & BAIRD, W. M. 2005. Metabolic activation and detoxification of polycyclic aromatic hydrocarbons. *In:* LUCH, A. (ed.) *The Carcinogenic Effects of Polycyclic Aromatic Hydrocarbons.* London: Imperial College Press.

MA, Q. & WHITLOCK, J. P., JR. 1996. The aromatic hydrocarbon receptor modulates the Hepa 1c1c7 cell cycle and differentiated state independently of dioxin. *Mol Cell Biol,* 16**,** 2144-50.

MAKAROVA, K. S., HAFT, D. H., BARRANGOU, R., BROUNS, S. J., CHARPENTIER, E., HORVATH, P., MOINEAU, S., MOJICA, F. J., WOLF, Y. I., YAKUNIN, A. F., VAN DER OOST, J. & KOONIN, E. V. 2011. Evolution and classification of the CRISPR-Cas systems. *Nat Rev Microbiol,* 9**,** 467-77.

MANSOUR, S. L., THOMAS, K. R. & CAPECCHI, M. R. 1988. Disruption of the proto-oncogene int-2 in mouse embryo-derived stem cells: a general strategy for targeting mutations to non-selectable genes. *Nature,* 336**,** 348-52.

MARNETT, L. J. 1990. Prostaglandin synthase-mediated metabolism of carcinogens and a potential role for peroxyl radicals as reactive intermediates. *Environ health perspect,* 88**,** 5.

MARTINKOVA, E., MAGLOTT, A., LEGER, D. Y., BONNET, D., STIBOROVA, M., TAKEDA, K., MARTIN, S. & DONTENWILL, M. 2010. alpha5beta1 integrin antagonists reduce chemotherapy-induced premature senescence and facilitate apoptosis in human glioblastoma cells. *Int J Cancer,* 127**,** 1240-8.

MAZZOLENI, G., DI LORENZO, D. & STEIMBERG, N. 2009. Modelling tissues in 3D: the next future of pharmaco-toxicology and food research? *Genes Nutr,* 4**,** 13-22.

MCLAUGHLIN, L. A., RONSEAUX, S., FINN, R. D., HENDERSON, C. J. & ROLAND WOLF, C. 2010. Deletion of microsomal cytochrome b5 profoundly affects hepatic and extrahepatic drug metabolism. *Mol Pharmacol,* 78**,** 269-78.

MCMILLAN, A., RENAUD, J. B., BURGESS, K. M. N., ORIMADEGUN, A. E., AKINYINKA, O. O., ALLEN, S. J., MILLER, J. D., REID, G. & SUMARAH, M. W. 2018. Aflatoxin exposure in Nigerian children with severe acute malnutrition. *FCT,* 111**,** 356-362.

MELTON, D. W. 1994. Gene targeting in the mouse. *Bioessays,* 16**,** 633-8.

METZGER, D. & FEIL, R. 1999. Engineering the mouse genome by site-specific recombination. *Curr opin biotechnol,* 10**,** 470-476.

MEUNIER, B., DE VISSER, S. P. & SHAIK, S. 2004. Mechanism of oxidation reactions catalyzed by cytochrome p450 enzymes. *Chem Rev,* 104**,** 3947-80.

MILLER, C. M. & MCCARTHY, F. O. 2012. Isolation, biological activity and synthesis of the natural product ellipticine and related pyridocarbazoles. *RSC Advances,* 2**,** 8883-8918.

MILLER, E. C. & MILLER, J. A. 1947. The presence and significance of bound aminoazo dyes in the livers of rats fed p-Dimethylaminoazobenzene. *Cancer Res,* 7**,** 468-480.

MIMURA, J. & FUJII-KURIYAMA, Y. 2003. Functional role of AhR in the expression of toxic effects by TCDD. *Biochimica et Biophysica Acta (BBA) - General Subjects,* 1619**,** 263-268.

MIYAMOTO, S., HIRATA, K., SUGIMOTO, S., HARADA, K. & MITAKA, T. 2005. Expression of cytochrome P450 enzymes in hepatic organoid reconstructed by rat small hepatocytes. *J Gastroenterol Hepatol,* 20**,** 865-72.

MIYAZAKI, M., YAMAZAKI, H., TAKEUCHI, H., SAOO, K., YOKOHIRA, M., MASUMURA, K.-I., NOHMI, T., FUNAE, Y., IMAIDA, K. & KAMATAKI, T. 2005. Mechanisms of chemopreventive effects of 8-methoxypsoralen against 4-(methylnitrosamino)-1-(3-pyridyl)-1-butanone-induced mouse lung adenomas. *Carcinogenesis,* 26**,** 1947-1955.

MOHUTSKY, M. A., ROMEIKE, A., MEADOR, V., LEE, W. M., FOWLER, J. & FRANCKE-CARROLL, S. 2010. Hepatic Drug-Metabolizing Enzyme Induction and Implications for Preclinical and Clinical Risk Assessment. *Toxicologic Pathology,* 38**,** 799-809.

MOJICA, F. J., DIEZ-VILLASENOR, C., GARCIA-MARTINEZ, J. & ALMENDROS, C. 2009. Short motif sequences determine the targets of the prokaryotic CRISPR defence system. *Microbiology,* 155**,** 733-40.

MÖLLER, L. 1994. In vivo metabolism and genotoxic effects of nitrated polycyclic aromatic hydrocarbons. *Environ health perspect,* 102**,** 139.

MOLLERUP, S., BERGE, G., BÆRA, R., SKAUG, V., HEWER, A., PHILLIPS, D. H., STANGELAND, L. & HAUGEN, A. 2006. Sex differences in risk of lung cancer: Expression of genes in the PAH bioactivation pathway in relation to smoking and bulky DNA adducts. *Int J Cancer,* 119**,** 741-744.

MORGAN, E. T. & COON, M. J. 1984. Effects of cytochrome b5 on cytochrome P-450-catalyzed reactions. Studies with manganese-substituted cytochrome b5. *Drug Metab Dispos,* 12**,** 358-64.

MORONI, L., DE WIJN, J. R. & VAN BLITTERSWIJK, C. A. 2008. Integrating novel technologies to fabricate smart scaffolds. *J Biomater Sci Polym Ed,* 19**,** 543-72.

MUELLER, G. & MILLER, J. A. 1948. The metabolism of 4-dimethylaminoazobenzene by rat liver homogenates. *J. biol. Chem,* 176**,** 535-544.

MURATALIEV, M. B., FEYEREISEN, R. & WALKER, F. A. 2004. Electron transfer by diflavin reductases. *Biochimica et Biophysica Acta (BBA) - Proteins and Proteomics,* 1698**,** 1-26.

NASPINSKI, C., GU, X., ZHOU, G. D., MERTENS-TALCOTT, S. U., DONNELLY, K. C. & TIAN, Y. 2008. Pregnane X receptor protects HepG2 cells from BaP-induced DNA damage. *Toxicol Sci,* 104**,** 67-73.

NEBERT, D. W. & DALTON, T. P. 2006. The role of cytochrome P450 enzymes in endogenous signalling pathways and environmental carcinogenesis. *Nat Rev Cancer,* 6**,** 947-60.

NEBERT, D. W. & KARP, C. L. 2008. Endogenous functions of the aryl hydrocarbon receptor (AHR): intersection of cytochrome P450 1 (CYP1)-metabolized eicosanoids and AHR biology. *J Biol Chem,* 283**,** 36061-5.

NEBERT, D. W., SHI, Z., GALVEZ-PERALTA, M., UNO, S. & DRAGIN, N. 2013. Oral benzo[a]pyrene: understanding pharmacokinetics, detoxication, and consequences--Cyp1 knockout mouse lines as a paradigm. *Mol Pharmacol,* 84**,** 304-13.

NEMOTO, N. & TAKAYAMA, S. 1984. Arachidonic acid-dependent activation of benzo[a]pyrene to bind to proteins with cytosolic and microsomal fractions from rat liver and lung. *Carcinogenesis,* 5**,** 961-4.

NIROGI, R., PALACHARLA, R. C., UTHUKAM, V., MANOHARAN, A., SRIKAKOLAPU, S. R., KALAIKADHIBAN, I., BOGGAVARAPU, R. K., PONNAMANENI, R. K., AJJALA, D. R. & BHYRAPUNENI, G. 2015. Chemical inhibitors of CYP450 enzymes in liver microsomes: combining selectivity and unbound fractions to guide selection of appropriate concentration in phenotyping assays. *Xenobiotica,* 45**,** 95-106.

NISHIMASU, H., RAN, F. A., HSU, P. D., KONERMANN, S., SHEHATA, S. I., DOHMAE, N., ISHITANI, R., ZHANG, F. & NUREKI, O. 2014. Crystal structure of Cas9 in complex with guide RNA and target DNA. *Cell,* 156**,** 935-49.

NIWA, T., YAMAZOE, Y. & KATO, R. 1982. Metabolic activation of 2-amino-9H-pyrido[2,3-b]indole by rat-liver microsomes. *Mutat Res,* 95**,** 159-70.

NORTIER, J. L., MARTINEZ, M. C., SCHMEISER, H. H., ARLT, V. M., BIELER, C. A., PETEIN, M., DEPIERREUX, M. F., DE PAUW, L., ABRAMOWICZ, D., VEREERSTRAETEN, P. & VANHERWEGHEM, J. L. 2000. Urothelial carcinoma associated with the use of a Chinese herb (Aristolochia fangchi). *N Engl J Med,* 342**,** 1686-92.

O'BRIEN, J. M., BEAL, M. A., YAUK, C. L. & MARCHETTI, F. 2016. Next generation sequencing of benzo(a)pyrene-induced lacZ mutants identifies a germ cell-specific mutation spectrum. *Sci Rep,* 6.

OMIECINSKI, C. J., VANDEN HEUVEL, J. P., PERDEW, G. H. & PETERS, J. M. 2011. Xenobiotic metabolism, disposition, and regulation by receptors: from biochemical phenomenon to predictors of major toxicities. *Toxicol Sci,* 120 Suppl 1**,** S49-75.

OMURA, T. & SATO, R. 1962. A new cytochrome in liver microsomes. *J Biol Chem,* 237**,** 1375-6.

OTTO, D. M., HENDERSON, C. J., CARRIE, D., DAVEY, M., GUNDERSEN, T. E., BLOMHOFF, R., ADAMS, R. H., TICKLE, C. & WOLF, C. R. 2003. Identification of novel roles of the cytochrome p450 system in early embryogenesis: effects on vasculogenesis and retinoic Acid homeostasis. *Mol Cell Biol,* 23**,** 6103-16.

PANDA, S. P., GUNTUR, A. R., KAR, R., TANG, K. & MASTERS, B. S. 2012. Conditional deletion of cytochrome P450 reductase in mouse bone results in Antley-Bixler Syndrome-like craniofacial and bone mass defects. *The FASEB Journal,* 26**,** 784.8-784.8.

PARIKH, A., GILLAM, E. M. & GUENGERICH, F. P. 1997. Drug metabolism by Escherichia coli expressing human cytochromes P450. *Nat Biotechnol,* 15**,** 784-8.

PENNING, T. M. 2014. Human Aldo-Keto Reductases. *Chem Res Toxicol,* 27**,** 1901-17.

PHILLIPS, D. H. 1999. Polycyclic aromatic hydrocarbons in the diet. *Mutat Res,* 443**,** 139-47.

PHILLIPS, D. H. 2005. Macromolecular adducts as biomarkers of human exposure to polycyclic aromatic hydrocarbons. *In:* LUCH, A. (ed.) *The Carcinogenic Effects of Polycyclic Aromatic Hydrocarbons.* London: Imperial College Press.

PHILLIPS, D. H. 2007. The Formation of DNA Adducts. *In:* ALLISON, M. R. (ed.) *The Cancer Handbook.* Chichester: Wiley.

PHILLIPS, D. H. & ARLT, V. M. 2007. The 32P-postlabeling assay for DNA adducts. *Nature Protocols,* 2**,** 2772.

PHILLIPS, D. H. & ARLT, V. M. 2008. Genotoxicity: damage to DNA and its consequences. *In:* LUCH, A. (ed.) *Molecular, Clinical and Environmental Toxicology: Volume 1: Molecular Toxicology.* Basel: Birkhäuser Basel.

PHILLIPS, D. H. & VENITT, S. 2012. DNA and protein adducts in human tissues resulting from exposure to tobacco smoke. *International Journal of Cancer,* 131**,** 2733-2753.

POIRIER, M. C. 2016. Linking DNA adduct formation and human cancer risk in chemical carcinogenesis. *Environ Mol Mutagen,* 57**,** 499-507.

POLJAKOVA, J., FORSTEROVA, K., SULC, M., FREI, E. & STIBOROVA, M. 2005. Oxidation of an antitumor drug ellipticine by peroxidases. *Biomed Pap Med Fac Univ Palacky Olomouc Czech Repub,* 149**,** 449-53.

POON, S. L., MCPHERSON, J. R., TAN, P., TEH, B. T. & ROZEN, S. G. 2014. Mutation signatures of carcinogen exposure: genome-wide detection and new opportunities for cancer prevention. *Genome Med,* 6**,** 24.

PORTER, T. D. 2002. The roles of cytochrome b5 in cytochrome P450 reactions. *J Biochem Mol Toxicol,* 16**,** 311-6.

POSTIC, C., SHIOTA, M., NISWENDER, K. D., JETTON, T. L., CHEN, Y., MOATES, J. M., SHELTON, K. D., LINDNER, J., CHERRINGTON, A. D. & MAGNUSON, M. A. 1999. Dual roles for glucokinase in glucose homeostasis as determined by liver and pancreatic beta cell-specific gene knock-outs using Cre recombinase. *J Biol Chem,* 274**,** 305-15.

POULOS, T. L., FINZEL, B. C. & HOWARD, A. J. 1987. High-resolution crystal structure of cytochrome P450cam. *J Mol Biol,* 195**,** 687-700.

PROBST-HENSCH, N. M., BELL, D. A., WATSON, M. A., SKIPPER, P. L., TANNENBAUM, S. R., CHAN, K. K., ROSS, R. K. & YU, M. C. 2000. N-Acetyltransferase 2 phenotype but not NAT1*10 genotype affects aminobiphenyl-hemoglobin adduct levels. *Cancer Epidemiol Biomarkers Prev,* 9**,** 619-623.

PUGA, A., HOFFER, A., ZHOU, S., BOHM, J. M., LEIKAUF, G. D. & SHERTZER, H. G. 1997. Sustained increase in intracellular free calcium and activation of cyclooxygenase-2 expression in mouse hepatoma cells treated with dioxin. *Biochem Pharmacol,* 54**,** 1287-1296.

PUROHIT, V. & BASU, A. K. 2000. Mutagenicity of nitroaromatic compounds. *Chem res toxicol,* 13**,** 673-692.

RAN, F. A., HSU, P. D., LIN, C. Y., GOOTENBERG, J. S., KONERMANN, S., TREVINO, A. E., SCOTT, D. A., INOUE, A., MATOBA, S., ZHANG, Y. & ZHANG, F. 2013a. Double nicking by RNA-guided CRISPR Cas9 for enhanced genome editing specificity. *Cell,* 154**,** 1380-9.

RAN, F. A., HSU, P. D., WRIGHT, J., AGARWALA, V., SCOTT, D. A. & ZHANG, F. 2013b. Genome engineering using the CRISPR-Cas9 system. *Nature Protocols,* 8**,** 2281.

RAVI, M., PARAMESH, V., KAVIYA, S. R., ANURADHA, E. & SOLOMON, F. D. P. 2015. 3D cell culture systems: advantages and applications. *J Cellr Physiol,* 230**,** 16-26.

RAZA, H., KING, R. S., SQUIRES, R. B., GUENGERICH, F. P., MILLER, D. W., FREEMAN, J. P., LANG, N. P. & KADLUBAR, F. F. 1996. Metabolism of 2-amino-alpha-carboline. A food-borne heterocyclic amine mutagen and carcinogen by human and rodent liver microsomes and by human cytochrome P4501A2. *Drug Metab Dispos,* 24**,** 395-400.

REDDY, M. V. & RANDERATH, K. 1986. Nuclease P1-mediated enhancement of sensitivity of 32P-postlabeling test for structurally diverse DNA adducts. *Carcinogenesis,* 7**,** 1543-51.

REED, L., ARLT, V. M. & PHILLIPS, D. H. 2018a. The role of cytochrome P450 enzymes in carcinogen activation and detoxication: an in vivo-in vitro paradox. *Carcinogenesis,* 39**,** 851-859.

REED, L., MRIZOVA, I., BARTA, F., INDRA, R., MOSEROVA, M., KOPKA, K., SCHMEISER, H. H., WOLF, C. R., HENDERSON, C. J., STIBOROVA, M., PHILLIPS, D. H. & ARLT, V. M. 2018b. Cytochrome b 5 impacts on cytochrome P450-mediated metabolism of benzo[a]pyrene and its DNA adduct formation: studies in hepatic cytochrome b 5 /P450 reductase null (HBRN) mice. *Arch Toxicol,* 92**,** 1625-1638.

RENDIC, S. & GUENGERICH, F. P. 2012. Contributions of human enzymes in carcinogen metabolism. *Chem Res Toxicol,* 25**,** 1316-83.

RENDIC, S., NOLTEERNSTING, E. & SCHÄNZER, W. 1999. Metabolism of anabolic steroids by recombinant human cytochrome P450 enzymes: Gas chromatographic–mass spectrometric determination of metabolites. *JChromatog B: Biomedical Sciences and Applications,* 735**,** 73-83.

RIDDICK, D. S., DING, X., WOLF, C. R., PORTER, T. D., PANDEY, A. V., ZHANG, Q. Y., GU, J., FINN, R. D., RONSEAUX, S., MCLAUGHLIN, L. A., HENDERSON, C. J., ZOU, L. & FLUCK, C. E. 2013. NADPH-cytochrome P450 oxidoreductase: roles in physiology, pharmacology, and toxicology. *Drug Metab Dispos,* 41**,** 12-23.

RITTLE, J. & GREEN, M. T. 2010. Cytochrome P450 compound I: capture, characterization, and C-H bond activation kinetics. *Science,* 330**,** 933-7.

RIVRON, N. C., ROUWKEMA, J., TRUCKENMULLER, R., KARPERIEN, M., DE BOER, J. & VAN BLITTERSWIJK, C. A. 2009. Tissue assembly and organization: developmental mechanisms in microfabricated tissues. *Biomaterials,* 30**,** 4851-8.

RIZWAN, A., SASKIA, T., IRINA, L. & THOMAS, H. 2015. Live cell imaging of the intracellular compartmentalization of the contaminate benzo[a]pyrene. *J Biophoton,* 8**,** 361-371.

ROSANO, G. L. & CECCARELLI, E. A. 2014. Recombinant protein expression in Escherichia coli: advances and challenges. *Front Microbiol,* 5.

RUAN, Q., GELHAUS, S. L., PENNING, T. M., HARVEY, R. G. & BLAIR, I. A. 2007. Aldo-keto reductase- and cytochrome P450-dependent formation of benzo[a]pyrene-derived DNA adducts in human bronchoalveolar cells. *Chem Res Toxicol,* 20**,** 424-31.

SAGREDO, C., MOLLERUP, S., COLE, K. J., PHILLIPS, D. H., UPPSTAD, H. & OVREBO, S. 2009. Biotransformation of benzo[a]pyrene in Ahr knockout mice is dependent on time and route of exposure. *Chem Res Toxicol,* 22**,** 584-91.

SAGREDO, C., OVREBO, S., HAUGEN, A., FUJII-KURIYAMA, Y., BAERA, R., BOTNEN, I. V. & MOLLERUP, S. 2006. Quantitative analysis of benzo[a]pyrene biotransformation and adduct formation in Ahr knockout mice. *Toxicol Lett,* 167**,** 173-82.

SATO, T., VRIES, R. G., SNIPPERT, H. J., VAN DE WETERING, M., BARKER, N., STANGE, D. E., VAN ES, J. H., ABO, A., KUJALA, P., PETERS, P. J. & CLEVERS, H. 2009. Single Lgr5 stem cells build crypt-villus structures in vitro without a mesenchymal niche. *Nature,* 459**,** 262-5.

SAUER, B. 1998. Inducible Gene Targeting in Mice Using the Cre/loxSystem. *Methods,* 14**,** 381-392.

SCOTCHER, D., BILLINGTON, S., BROWN, J., JONES, C. R., BROWN, C. D. A., ROSTAMI-HODJEGAN, A. & GALETIN, A. 2017. Microsomal and cytosolic scaling factors in dog and human kidney cortex and application for in vitro-in vivo extrapolation of renal metabolic clearance. *Drug Metab Dispos,* 45**,** 556-568.

SEBTI, S. M., BAIRD, W. M., KNOWLES, B. B. & DIAMOND, L. 1982. Benzo[a]pyrene--DNA adduct formation in target cells in a cell-mediated mutation assay. *Carcinogenesis,* 3**,** 1317-20.

SERGEEV, G. V., GILEP, A. A. & USANOV, S. A. 2014. The role of cytochrome b5 structural domains in interaction with cytochromes P450. *Biochemistry (Mosc),* 79**,** 406-16.

SHEN, A. L., O'LEARY, K. A. & KASPER, C. B. 2002. Association of multiple developmental defects and embryonic lethality with loss of microsomal NADPH-cytochrome P450 oxidoreductase. *J Biol Chem,* 277**,** 6536-41.

SHERTZER, H. G., DALTON, T. P., TALASKA, G. & NEBERT, D. W. 2002. Decrease in 4-aminobiphenyl-induced methemoglobinemia in Cyp1a2(-/-) knockout mice. *Toxicol Appl Pharmacol,* 181**,** 32-7.

SHI, Z., DRAGIN, N., GALVEZ-PERALTA, M., JORGE-NEBERT, L. F., MILLER, M. L., WANG, B. & NEBERT, D. W. 2010. Organ-specific roles of CYP1A1 during detoxication of dietary benzo[a]pyrene. *Mol Pharmacol,* 78**,** 46-57.

SHIIZAKI, K., KAWANISHI, M. & YAGI, T. 2013. Dioxin suppresses benzo[a]pyrene-induced mutations and DNA adduct formation through cytochrome P450 1A1 induction and (+/-)-anti-benzo[a]pyrene-7,8-diol-9,10-epoxide inactivation in human hepatoma cells. *Mutat Res,* 750**,** 77-85.

SHIIZAKI, K., KAWANISHI, M. & YAGI, T. 2017. Modulation of benzo[a]pyrene–DNA adduct formation by CYP1 inducer and inhibitor. *Genes and Environment,* 39**,** 14.

SHIMADA, T. & FUJII-KURIYAMA, Y. 2004. Metabolic activation of polycyclic aromatic hydrocarbons to carcinogens by cytochromes P450 1A1 and 1B1. *Cancer Sci,* 95**,** 1-6.

SHIMADA, T., HAYES, C. L., YAMAZAKI, H., AMIN, S., HECHT, S. S., GUENGERICH, F. P. & SUTTER, T. R. 1996. Activation of chemically diverse procarcinogens by human cytochrome P-450 1B1. *Cancer Res,* 56**,** 2979-84.

SIDDENS, L. K., LARKIN, A., KRUEGER, S. K., BRADFIELD, C. A., WATERS, K. M., TILTON, S. C., PEREIRA, C. B., LÖHR, C. V., ARLT, V. M., PHILLIPS, D. H., WILLIAMS, D. E. & BAIRD, W. M. 2012. Polycyclic aromatic hydrocarbons as skin carcinogens: Comparison of benzo[a]pyrene, dibenzo[def,p]chrysene and three environmental mixtures in the FVB/N mouse. *Toxicol Appl Pharmacol,* 264**,** 377-86.

SIM, S. C. & INGELMAN-SUNDBERG, M. 2010. The Human Cytochrome P450 (CYP) Allele Nomenclature website: a peer-reviewed database of CYP variants and their associated effects. *Hum Genomics,* 4**,** 278-81.

SKOG, K. I., JOHANSSON, M. A. & JAGERSTAD, M. I. 1998. Carcinogenic heterocyclic amines in model systems and cooked foods: a review on formation, occurrence and intake. *Food Chem Toxicol,* 36**,** 879-96.

SLAUGHTER, B. V., KHURSHID, S. S., FISHER, O. Z., KHADEMHOSSEINI, A. & PEPPAS, N. A. 2009. Hydrogels in regenerative medicine. *Adv Mater,* 21**,** 3307-29.

SLIGAR, S. G., CINTI, D. L., GIBSON, G. G. & SCHENKMAN, J. B. 1979. Spin state control of the hepatic cytochrome P450 redox potential. *Biochem Biophys Res Commun,* 90**,** 925-32.

SMITHIES, O., GREGG, R. G., BOGGS, S. S., KORALEWSKI, M. A. & KUCHERLAPATI, R. S. 1985. Insertion of DNA sequences into the human chromosomal beta-globin locus by homologous recombination. *Nature,* 317**,** 230-4.

SNYDERWINE, E. G., YU, M., SCHUT, H. A., KNIGHT-JONES, L. & KIMURA, S. 2002. Effect of CYP1A2 deficiency on heterocyclic amine DNA adduct levels in mice. *Food Chem Toxicol,* 40**,** 1529-33.

SOLHAUG, A., ØVREBØ, S., MOLLERUP, S., LÅG, M., SCHWARZE, P. E., NESNOW, S. & HOLME, J. A. 2005. Role of cell signaling in B[a]P-induced apoptosis: Characterization of unspecific effects of cell signaling inhibitors and apoptotic effects of B[a]P metabolites. *Chemico-Biological Interactions,* 151**,** 101-119.

SOLHAUG, A., REFSNES, M. & HOLME, J. A. 2004a. Role of cell signalling involved in induction of apoptosis by benzo[a]pyrene and cyclopenta[c,d]pyrene in hepa1c1c7 cells. *J Cell Biochem,* 93**,** 1143-1154.

SOLHAUG, A., REFSNES, M., LÅG, M., SCHWARZE, P. E., HUSØY, T. & HOLME, J. A. 2004b. Polycyclic aromatic hydrocarbons induce both apoptotic and anti-apoptotic signals in Hepa1c1c7 cells. *Carcinogenesis,* 25**,** 809-819.

SPENCE, J. R., MAYHEW, C. N., RANKIN, S. A., KUHAR, M. F., VALLANCE, J. E., TOLLE, K., HOSKINS, E. E., KALINICHENKO, V. V., WELLS, S. I., ZORN, A. M., SHROYER, N. F. & WELLS, J. M. 2011. Directed differentiation of human pluripotent stem cells into intestinal tissue in vitro. *Nature,* 470**,** 105-9.

SQUIRES, E. J., SUEYOSHI, T. & NEGISHI, M. 2004. Cytoplasmic localization of pregnane X receptor and ligand-dependent nuclear translocation in mouse liver. *J Biol Chem,* 279**,** 49307-14.

STERNBERG, S. H., REDDING, S., JINEK, M., GREENE, E. C. & DOUDNA, J. A. 2014. DNA interrogation by the CRISPR RNA-guided endonuclease Cas9. *Nature,* 507**,** 62-7.

STIBOROVA, M., ARLT, V. M., HENDERSON, C. J., WOLF, C. R., KOTRBOVA, V., MOSEROVA, M., HUDECEK, J., PHILLIPS, D. H. & FREI, E. 2008. Role of hepatic cytochromes P450 in bioactivation of the anticancer drug ellipticine: studies with the hepatic NADPH:cytochrome P450 reductase null mouse. *Toxicol Appl Pharmacol,* 226**,** 318-27.

STIBOROVA, M., BARTA, F., LEVOVA, K., HODEK, P., FREI, E., ARLT, V. M. & SCHMEISER, H. H. 2015. The influence of ochratoxin A on DNA adduct formation by the carcinogen aristolochic acid in rats. *Arch Toxicol,* 89**,** 2141-58.

STIBOROVÁ, M., BIELER, C. A., WIESSLER, M. & FREI, E. 2001. The anticancer agent ellipticine on activation by cytochrome P450 forms covalent DNA adducts. *Biochem Pharmacol,* 62**,** 1675-1684.

STIBOROVA, M., BREUER, A., AIMOVA, D., STIBOROVA-RUPERTOVA, M., WIESSLER, M. & FREI, E. 2003a. DNA adduct formation by the anticancer

drug ellipticine in rats determined by 32P postlabeling. *Int J Cancer,* 107**,** 885-90.

STIBOROVA, M., CERNA, V., MOSEROVA, M., ARLT, V. M. & FREI, E. 2013a. The effect of benzo[a]pyrene on metabolic activation of anticancer drug ellipticine in mice. *Neuro Endocrinol Lett,* 34 Suppl 2**,** 43-54.

STIBOROVA, M., CERNA, V., MOSEROVA, M., MRIZOVA, I., ARLT, V. M. & FREI, E. 2014a. The anticancer drug ellipticine activated with cytochrome P450 mediates DNA damage determining its pharmacological efficiencies: studies with rats, Hepatic Cytochrome P450 Reductase Null (HRN) mice and pure enzymes. *Int J Mol Sci,* 16**,** 284-306.

STIBOROVA, M. & FREI, E. 2014. Ellipticines as DNA-targeted chemotherapeutics. *Curr Med Chem,* 21**,** 575-91.

STIBOROVA, M., FREI, E., ARLT, V. M. & SCHMEISER, H. H. 2014b. Knockout and humanized mice as suitable tools to identify enzymes metabolizing the human carcinogen aristolochic acid. *Xenobiotica,* 44**,** 135-45.

STIBOROVÁ, M., INDRA, R., FREI, E., KOPEČKOVÁ, K., SCHMEISER, H. H., ECKSCHLAGER, T., ADAM, V., HEGER, Z., ARLT, V. M. & MARTÍNEK, V. 2017. Cytochrome b 5 plays a dual role in the reaction cycle of cytochrome P450 3A4 during oxidation of the anticancer drug ellipticine. *Monatsh Chem*.

STIBOROVA, M., INDRA, R., MOSEROVA, M., BOREK-DOHALSKA, L., HODEK, P., FREI, E., KOPKA, K., SCHMEISER, H. H. & ARLT, V. M. 2017. Comparison of human cytochrome P450 1A1-catalysed oxidation of benzo[a]pyrene in prokaryotic and eukaryotic expression systems. *Monatsh Chem,* 148**,** 1959-1969.

STIBOROVA, M., INDRA, R., MOSEROVA, M., CERNA, V., RUPERTOVA, M., MARTINEK, V., ECKSCHLAGER, T., KIZEK, R. & FREI, E. 2012a. Cytochrome b5 increases cytochrome P450 3A4-mediated activation of anticancer drug ellipticine to 13-hydroxyellipticine whose covalent binding to DNA is elevated by sulfotransferases and N,O-acetyltransferases. *Chem Res Toxicol,* 25**,** 1075-85.

STIBOROVA, M., INDRA, R., MOSEROVA, M., FREI, E., SCHMEISER, H. H., KOPKA, K., PHILLIPS, D. H. & ARLT, V. M. 2016a. NADH:Cytochrome b5 Reductase and Cytochrome b5 Can Act as Sole Electron Donors to Human Cytochrome P450 1A1-Mediated Oxidation and DNA Adduct Formation by Benzo[a]pyrene. *Chem Res Toxicol,* 29**,** 1325-34.

STIBOROVA, M., INDRA, R., MOSEROVA, M., SULC, M., HODEK, P., FREI, E., SCHMEISER, H. H. & ARLT, V. M. 2016b. NADPH- and NADH-dependent metabolism of and DNA adduct formation by benzo[a]pyrene catalyzed with rat hepatic microsomes and cytochrome P450 1A1. *Monatsh Chem,* 147**,** 847-855.

STIBOROVA, M., MARTINEK, V., FREI, E., M. ARLT, V. & H. SCHMEISER, H. 2013b. Enzymes metabolizing aristolochic acid and their contribution to the development of aristolochic acid nephropathy and urothelial cancer. *Curr Drug Metab,* 14**,** 695-705.

STIBOROVA, M., MOSEROVA, M., CERNA, V., INDRA, R., DRACINSKY, M., SULC, M., HENDERSON, C. J., WOLF, C. R., SCHMEISER, H. H., PHILLIPS, D. H., FREI, E. & ARLT, V. M. 2014c. Cytochrome b5 and epoxide hydrolase contribute to benzo[a]pyrene-DNA adduct formation catalyzed by cytochrome P450 1A1 under low NADPH:P450 oxidoreductase conditions. *Toxicology,* 318**,** 1-12.

STIBOROVA, M., MOSEROVA, M., MRIZOVA, I., DRACINSKA, H., MARTINEK, V., INDRA, R., FREI, E., ADAM, V., KIZEK, R., SCHMEISER, H. H., KUBACKOVA, K. & ARLT, V. M. 2016c. Induced expression of microsomal cytochrome b5 determined at mRNA and protein levels in rats exposed to ellipticine, benzo[a]pyrene, and 1-phenylazo-2-naphthol (Sudan I). *Monatsh Chem,* 147**,** 897-904.

STIBOROVA, M., POLJAKOVA, J., ECKSCHLAGER, T., KIZEK, R. & FREI, E. 2012b. Analysis of covalent ellipticine- and doxorubicin-derived adducts in DNA of neuroblastoma cells by the (3)(2)P-postlabeling technique. *Biomed Pap Med Fac Univ Palacky Olomouc Czech Repub,* 156**,** 115-21.

STIBOROVÁ, M., POLJAKOVÁ, J., MARTÍNKOVÁ, E., BOŘEK-DOHALSKÁ, L., ECKSCHLAGER, T., KIZEK, R. & FREI, E. 2011. Ellipticine cytotoxicity to cancer cell lines — a comparative study. *Interdiscip Toxicol,* 4**,** 98-105.

STIBOROVÁ, M., POLJAKOVÁ, J., MARTÍNKOVÁ, E., ULRICHOVÁ, J., ŠIMÁNEK, V., DVOŘÁK, Z. & FREI, E. 2012. Ellipticine oxidation and DNA adduct formation in human hepatocytes is catalyzed by human cytochromes P450 and enhanced by cytochrome b5. *Toxicology,* 302**,** 233-241.

STIBOROVA, M., POLJAKOVA, J., RYSLAVA, H., DRACINSKY, M., ECKSCHLAGER, T. & FREI, E. 2007. Mammalian peroxidases activate anticancer drug ellipticine to intermediates forming deoxyguanosine adducts in DNA identical to those found in vivo and generated from 12-hydroxyellipticine and 13-hydroxyellipticine. *Int J Cancer,* 120**,** 243-51.

STIBOROVÁ, M., RUPERTOVÁ, M., AIMOVÁ, D., RYŠLAVÁ, H. & FREI, E. 2007. Formation and persistence of DNA adducts of anticancer drug ellipticine in rats. *Toxicology,* 236**,** 50-60.

STIBOROVA, M., RUPERTOVA, M. & FREI, E. 2011. Cytochrome P450- and peroxidase-mediated oxidation of anticancer alkaloid ellipticine dictates its anti-tumor efficiency. *Biochim Biophys Acta,* 1814**,** 175-85.

STIBOROVA, M., SEJBAL, J., BOREK-DOHALSKA, L., AIMOVA, D., POLJAKOVA, J., FORSTEROVA, K., RUPERTOVA, M., WIESNER, J., HUDECEK, J., WIESSLER, M. & FREI, E. 2004. The anticancer drug ellipticine forms covalent DNA adducts, mediated by human cytochromes P450, through metabolism to 13-hydroxyellipticine and ellipticine N2-oxide. *Cancer Res,* 64**,** 8374-80.

STIBOROVA, M., STIBOROVA-RUPERTOVA, M., BOREK-DOHALSKA, L., WIESSLER, M. & FREI, E. 2003b. Rat microsomes activating the anticancer drug ellipticine to species covalently binding to deoxyguanosine in DNA are a suitable model mimicking ellipticine bioactivation in humans. *Chem Res Toxicol,* 16**,** 38-47.

STRINGER, R. A., STRAIN-DAMERELL, C., NICKLIN, P. & HOUSTON, J. B. 2009. Evaluation of recombinant cytochrome P450 enzymes as an in vitro system for metabolic clearance predictions. *Drug Metab Dispos,* 37**,** 1025-34.

SUGIYAMA, T., MIKI, N., MIYAKE, Y. & YAMANO, T. 1982. Interaction and Electron Transfer between Cytochrome b5 and Cytochrome P-450 in the Reconstituted p-Nitroanisole O-Demethylase System1. *JBiochem,* 92**,** 1793-1803.

SUGIYAMA, T., MIKI, N. & YAMANO, T. 1980. NADH- and NADPH-Dependent Reconstituted p-Nitroanisole O-Demethylation System Containing Cytochrome P-450 with High Affinity for Cytochrome b51. *J Biochem,* 87**,** 1457-1467.

SUSEWIND, J., DE SOUZA CARVALHO-WODARZ, C., REPNIK, U., COLLNOT, E.-M., SCHNEIDER-DAUM, N., GRIFFITHS, G. W. & LEHR, C.-M. 2016. A 3D co-culture of three human cell lines to model the inflamed intestinal mucosa for safety testing of nanomaterials. *Nanotoxicology,* 10**,** 53-62.

TAKASATO, M., ER, P. X., BECROFT, M., VANSLAMBROUCK, J. M., STANLEY, E. G., ELEFANTY, A. G. & LITTLE, M. H. 2014. Directing human embryonic stem cell differentiation towards a renal lineage generates a self-organizing kidney. *Nat Cell Biol,* 16**,** 118-26.

TAKEBE, T., SEKINE, K., ENOMURA, M., KOIKE, H., KIMURA, M., OGAERI, T., ZHANG, R. R., UENO, Y., ZHENG, Y. W., KOIKE, N., AOYAMA, S., ADACHI, Y. & TANIGUCHI, H. 2013. Vascularized and functional human liver from an iPSC-derived organ bud transplant. *Nature,* 499**,** 481-4.

TAKEUCHI, H., SAOO, K., YOKOHIRA, M., IKEDA, M., MAETA, H., MIYAZAKI, M., YAMAZAKI, H., KAMATAKI, T. & IMAIDA, K. 2003. Pretreatment with 8-methoxypsoralen, a potent human CYP2A6 inhibitor, strongly inhibits lung tumorigenesis induced by 4-(methylnitrosamino)-1-(3-pyridyl)-1-butanone in female A/J mice. *Cancer Res,* 63**,** 7581-3.

TIMSIT, Y. E. & NEGISHI, M. 2007. CAR and PXR: The xenobiotic-sensing receptors. *Steroids,* 72**,** 231-246.

TMEJOVA, K., KREJCOVA, L., HYNEK, D., ADAM, V., BABULA, P., TRNKOVA, L., STIBOROVA, M., ECKSCHLAGER, T. & KIZEK, R. 2014. Electrochemical study of ellipticine interaction with single and double stranded oligonucleotides. *Anticancer Agents Med Chem,* 14**,** 331-40.

TOKIWA, H., OHNISHI, Y. & ROSENKRANZ, H. S. 1986. Mutagenicity and carcinogenicity of nitroarenes and their sources in the environment. *CRC Crit Rev Toxicol,* 17**,** 23-58.

TOKIWA, H., SERA, N., HORIKAWA, K., NAKANISHI, Y. & SHIGEMATU, N. 1993. The presence of mutagens/carcinogens in the excised lung and analysis of lung cancer induction. *Carcinogenesis,* 14**,** 1933-1938.

TOMPKINS, L. M. & WALLACE, A. D. 2007. Mechanisms of cytochrome P450 induction. *JBiochemMol Toxicol,* 21**,** 176-181.

TSUJI, N., FUKUDA, K., NAGATA, Y., OKADA, H., HAGA, A., HATAKEYAMA, S., YOSHIDA, S., OKAMOTO, T., HOSAKA, M., SEKINE, K., OHTAKA, K., YAMAMOTO, S., OTAKA, M., GRAVE, E. & ITOH, H. 2014. The activation mechanism of the aryl hydrocarbon receptor (AhR) by molecular chaperone HSP90. *FEBS Open Bio,* 4**,** 796-803.

TSUNEOKA, Y., DALTON, T. P., MILLER, M. L., CLAY, C. D., SHERTZER, H. G., TALASKA, G., MEDVEDOVIC, M. & NEBERT, D. W. 2003. 4-aminobiphenyl-induced liver and urinary bladder DNA adduct formation in Cyp1a2(-/-) and Cyp1a2(+/+) mice. *J Natl Cancer Inst,* 95**,** 1227-37.

TURESKY, R. J., KONOREV, D., FAN, X., TANG, Y., YAO, L., DING, X., XIE, F., ZHU, Y. & ZHANG, Q.-Y. 2015. Effect of cytochrome P450 reductase deficiency on 2-Amino-9H-pyrido[2,3-b]indole metabolism and DNA adduct formation in liver and extrahepatic tissues of mice. *Chem Res Toxicol,* 28**,** 2400-2410.

TURESKY, R. J., LANG, N. P., BUTLER, M. A., TEITEL, C. H. & KADLUBAR, F. F. 1991. Metabolic activation of carcinogenic heterocyclic aromatic amines by human liver and colon. *Carcinogenesis,* 12**,** 1839-45.

TURESKY, R. J. & LE MARCHAND, L. 2011. Metabolism and Biomarkers of Heterocyclic Aromatic Amines in Molecular Epidemiology Studies: Lessons Learned from Aromatic Amines. *Chem Res Toxicol,* 24**,** 1169-214.

UNO, S., DALTON, T. P., DERKENNE, S., CURRAN, C. P., MILLER, M. L., SHERTZER, H. G. & NEBERT, D. W. 2004. Oral exposure to benzo[a]pyrene in the mouse: detoxication by inducible cytochrome P450 is more important than metabolic activation. *Mol Pharmacol,* 65**,** 1225-37.

UNO, S., DALTON, T. P., DRAGIN, N., CURRAN, C. P., DERKENNE, S., MILLER, M. L., SHERTZER, H. G., GONZALEZ, F. J. & NEBERT, D. W. 2006. Oral benzo[a]pyrene in Cyp1 knockout mouse lines: CYP1A1 important in detoxication, CYP1B1 metabolism required for immune damage independent of total-body burden and clearance rate. *Mol Pharmacol,* 69**,** 1103-14.

UNO, S., DALTON, T. P., SHERTZER, H. G., GENTER, M. B., WARSHAWSKY, D., TALASKA, G. & NEBERT, D. W. 2001. Benzo[a]pyrene-induced toxicity: paradoxical protection in Cyp1a1(-/-) knockout mice having increased hepatic BaP-DNA adduct levels. *Biochem Biophys Res Commun,* 289**,** 1049-56.

VAN DER OOST, J., WESTRA, E. R., JACKSON, R. N. & WIEDENHEFT, B. 2014. Unravelling the structural and mechanistic basis of CRISPR-Cas systems. *Nat Rev Microbiol,* 12**,** 479-92.

VAN HERWAARDEN, A. E. 2007. Knockout of cytochrome P450 3A yields new mouse models for understanding xenobiotic metabolism. 117**,** 3583-92.

VANHERWEGHEM, J. L., DEPIERREUX, M., TIELEMANS, C., ABRAMOWICZ, D., DRATWA, M., JADOUL, M., RICHARD, C., VANDERVELDE, D., VERBEELEN, D., VANHAELEN-FASTRE, R. & ET AL. 1993. Rapidly progressive interstitial renal fibrosis in young women: association with slimming regimen including Chinese herbs. *Lancet,* 341**,** 387-91.

VANN, K. R., ERGÜN, Y., ZENCIR, S., ONCUOGLU, S., OSHEROFF, N. & TOPCU, Z. 2016. Inhibition of human DNA topoisomerase IIα by two novel ellipticine derivatives. *Bioorganic & Medicinal Chemistry Letters,* 26**,** 1809-1812.

WANG, L., XU, W., MA, L., ZHANG, S., ZHANG, K., YE, P., XING, G., ZHANG, X., CAO, Y., XI, J., GU, J. & LUAN, Y. 2017. Detoxification of benzo[a]pyrene primarily depends on cytochrome P450, while bioactivation involves additional oxidoreductases including 5-lipoxygenase, cyclooxygenase, and aldo-keto reductase in the liver. *J Biochem Mol Toxicol*.

WANG, M., ROBERTS, D. L., PASCHKE, R., SHEA, T. M., MASTERS, B. S. & KIM, J. J. 1997. Three-dimensional structure of NADPH-cytochrome P450 reductase: prototype for FMN- and FAD-containing enzymes. *Proc Natl Acad Sci U S A,* 94**,** 8411-6.

WANG, S., BOTT, D., TUNG, A., SUGAMORI, K. S. & GRANT, D. M. 2015. Relative Contributions of CYP1A2 and CYP2E1 to the Bioactivation and Clearance of 4-Aminobiphenyl in Adult Mice. *Drug Metab Dispos,* 43**,** 916-21.

WENG, Y., FANG, C., TURESKY, R. J., BEHR, M., KAMINSKY, L. S. & DING, X. 2007. Determination of the role of target tissue metabolism in lung carcinogenesis using conditional cytochrome P450 reductase-null mice. *Cancer Res,* 67**,** 7825-32.

WHITE, R. E. 2000. High-throughput screening in drug metabolism and pharmacokinetic support of drug discovery. *Annu Rev Pharmacol Toxicol,* 40**,** 133-57.

WIECHELMAN, K. J., BRAUN, R. D. & FITZPATRICK, J. D. 1988. Investigation of the bicinchoninic acid protein assay: identification of the groups responsible for color formation. *Anal Biochem,* 175**,** 231-7.

WILKENING, S., STAHL, F. & BADER, A. 2003. Comparison of primary human hepatocytes and hepatoma cell line Hepg2 with regard to their biotransformation properties. *Drug Metab Dispos,* 31**,** 1035-42.

WOGAN, G. N., HECHT, S. S., FELTON, J. S., CONNEY, A. H. & LOEB, L. A. 2004. Environmental and chemical carcinogenesis. *Semin Cancer Biol,* 14**,** 473-86.

WOHAK, L. E., KRAIS, A. M., KUCAB, J. E., STERTMANN, J., OVREBO, S., SEIDEL, A., PHILLIPS, D. H. & ARLT, V. M. 2016. Carcinogenic polycyclic aromatic hydrocarbons induce CYP1A1 in human cells via a p53-dependent mechanism. *Arch Toxicol,* 90**,** 291-304.

WOODCROFT, K. J. & NOVAK, R. F. 1998. Xenobiotic-enhanced expression of cytochromes P450 2E1 and 2B in primary cultured rat hepatocytes. *Drug Metab Dispos,* 26**,** 372-8.

WU, L., GU, J., WENG, Y., KLUETZMAN, K., SWIATEK, P., BEHR, M., ZHANG, Q. Y., ZHUO, X., XIE, Q. & DING, X. 2003. Conditional knockout of the mouse NADPH-cytochrome p450 reductase gene. *Genesis,* 36**,** 177-81.

YAMAGIWA, K. & ICHIKAWA, K. 1915. Experimentelle studie über die pathogenese der epithelialgeschwülste. *Mitt. Med. Fak. Tokio,* 15**,** 295-344.

YAMAZAKI, H., NAKAMURA, M., KOMATSU, T., OHYAMA, K., HATANAKA, N., ASAHI, S., SHIMADA, N., GUENGERICH, F. P., SHIMADA, T., NAKAJIMA, M. & YOKOI, T. 2002. Roles of NADPH-P450 reductase and apo- and holo-cytochrome b5 on xenobiotic oxidations catalyzed by 12 recombinant human cytochrome P450s expressed in membranes of Escherichia coli. *Protein Expr Purif,* 24**,** 329-37.

YAMAZAKI, H., NAKANO, M., GILLAM, E. M., BELL, L. C., GUENGERICH, F. P. & SHIMADA, T. 1996a. Requirements for cytochrome b5 in the oxidation of 7-ethoxycoumarin, chlorzoxazone, aniline, and N-nitrosodimethylamine by recombinant cytochrome P450 2E1 and by human liver microsomes. *Biochem Pharmacol,* 52**,** 301-9.

YAMAZAKI, H., NAKANO, M., GILLAM, E. M. J., BELL, L. C., GUENGERICH, F. P. & SHIMADA, T. 1996b. Requirements for cytochrome b5 in the oxidation of 7-ethoxycoumarin, chlorzoxazone, aniline, and N-nitrosodimethylamine by recombinant cytochrome P450 2E1 and by human liver microsomes. *Biochem Pharmacol,* 52**,** 301-309.

YAMAZAKI, H., NAKANO, M., IMAI, Y., UENG, Y. F., GUENGERICH, F. P. & SHIMADA, T. 1996c. Roles of cytochrome b5 in the oxidation of testosterone and nifedipine by recombinant cytochrome P450 3A4 and by human liver microsomes. *Arch Biochem Biophys,* 325**,** 174-82.

YIN, X., MEAD, B. E., SAFAEE, H., LANGER, R., KARP, J. M. & LEVY, O. 2016. Stem cell organoid engineering. *Cell Stem Cell,* 18**,** 25-38.

YOSHIHARA, S. & TATSUMI, K. 1995. Metabolism of 4-aminobiphenyl and 4-acetylaminobiphenyl in perfused guinea pig liver. *Biol Pharm Bull,* 18**,** 872-5.

ZANGER, U. M. & SCHWAB, M. 2013. Cytochrome P450 enzymes in drug metabolism: Regulation of gene expression, enzyme activities, and impact of genetic variation. *PharmacolTher,* 138**,** 103-141.

ZHANG, L., ASHLEY, D. L. & WATSON, C. H. 2011. Quantitative analysis of six heterocyclic aromatic amines in mainstream cigarette smoke condensate using isotope dilution liquid chromatography-electrospray ionization tandem mass spectrometry. *Nicotine Tob Res,* 13**,** 120-6.

ZHANG, Q. Y., FANG, C., ZHANG, J., DUNBAR, D., KAMINSKY, L. & DING, X. 2009. An intestinal epithelium-specific cytochrome P450 (P450) reductase-knockout mouse model: direct evidence for a role of intestinal p450s in first-pass clearance of oral nifedipine. *Drug Metab Dispos,* 37**,** 651-7.

ZHOU, X., D'AGOSTINO, J., XIE, F. & DING, X. 2012. Role of CYP2A5 in the bioactivation of the lung carcinogen 4-(methylnitrosamino)-1-(3-pyridyl)-1-butanone in mice. *J Pharmacol Exp Ther,* 341**,** 233-41.

Awards and publications

MRC-PHE Annual Postgraduate Training Day 2015: Oral presentation award

AES Postgraduate Symposium: Poster award

UKEMS 2016: Poster award

NUKEMS 2018: Poster pitch 3rd place

REED, L., MRIZOVA, I., BARTA, F., INDRA, R., MOSEROVA, M., KOPKA, K., SCHMEISER, H. H., WOLF, C. R., HENDERSON, C. J., STIBOROVA, M., PHILLIPS, D. H. & ARLT, V. M. (2018). Cytochrome b5 impacts on cytochrome P450-mediated metabolism of benzo[a]pyrene and its DNA adduct formation: studies in hepatic cytochrome b5 /P450 reductase null (HBRN) mice. Arch Toxicol, 92, 1625-1638.

REED, L., ARLT, V. M. & PHILLIPS, D. H. (2018). The role of cytochrome P450 enzymes in carcinogen activation and detoxication: an in vivo-in vitro paradox. Carcinogenesis, 39, 851-859.

REED, L., INDRA, R., MRIZOVA, I., MOSEROVA, M., SCHMEISER, H. H., WOLF, C. R., HENDERSON, C. J., STIBOROVA, M., PHILLIPS, D. H. & ARLT, V. M. (2019). Application of hepatic cytochrome b5/P450 reductase null (HBRN) mice to study the role of cytochrome b5 in the cytochrome P450-mediated bioactivation of the anticancer drug ellipticine. Toxicol Appl Pharmacol, 366, 64-74.